Radiation Sources and electron-photon QED interactions beyond Synchrotron Light Sources (see C. Biscari lecture): Free Electron Lasers - Inverse Compton Sources - Secondary/Tertiary Beams (muons, positrons) - something special for fundamental physics …

Luca Serafini – INFN-Milan and University of Milan
with important contributions from Vittoria Petrillo and Sanae Samsam

Lecture Outline (leit motiv):

A journey from
Undulatory Radiation Sources
towards
Collisional Radiation Sources

8th African School of Physics - Marrakech (MO) - July 2024

Schematic recap of X/γ Radiation Sources (keV, MeV, GeV…)

Spontaneous undulatory radiation (synchrotron, wiggler, *betatron*, *channeling*, *bremsstrahlung*)

$$E_X = f(\gamma^2\vartheta^2)$$

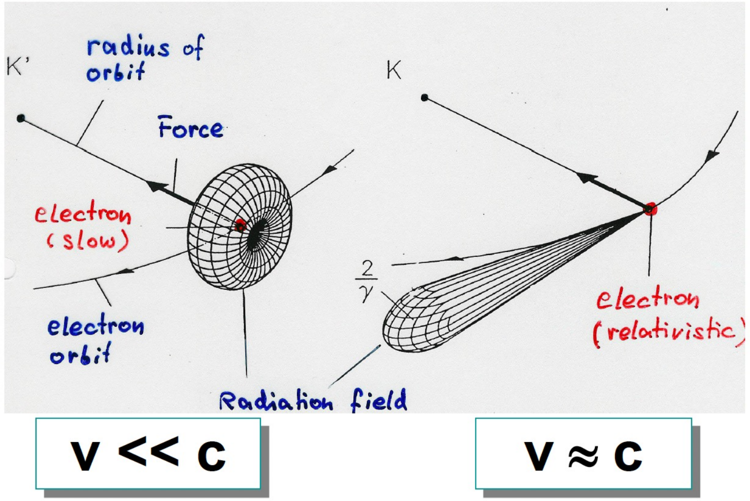

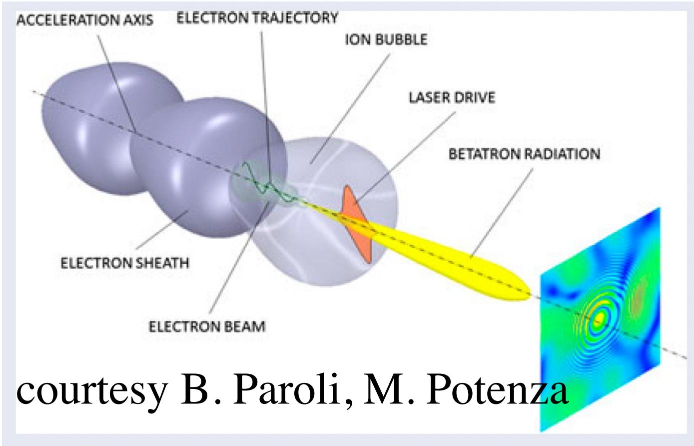

Rotating Anode Tube

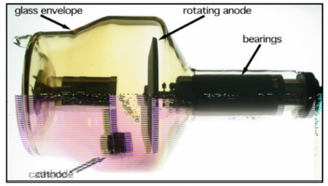

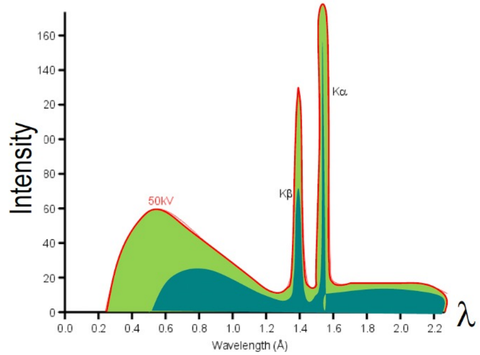

Resonant/amplified undulatory radiation (undulator, FEL)

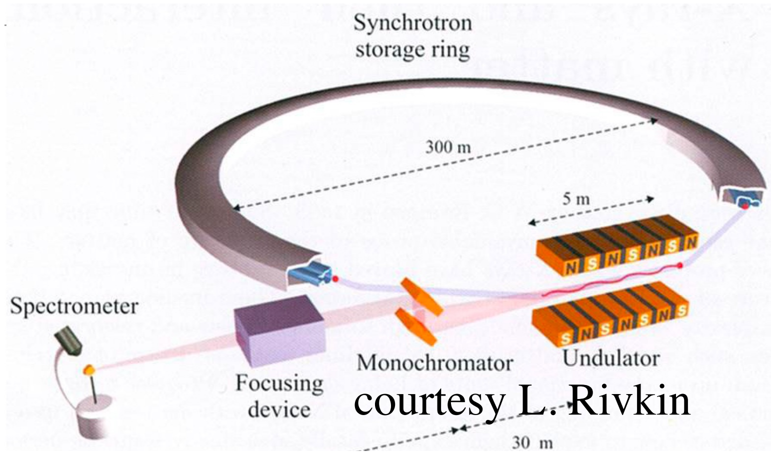

ELSEVIER

Optics Communications

Volume 50, Issue 6, 15 July 1984, Pages 373-378

Collective instabilities and high-gain regime in a free electron laser

R. Bonifacio *, C. Pellegrini, L.M. Narducci

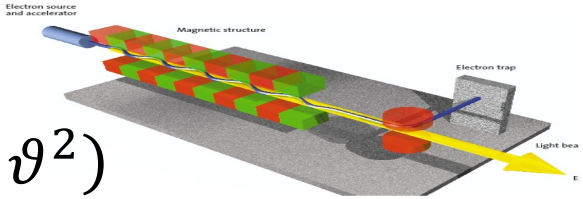

$$E_X \neq f(\gamma^2\vartheta^2)$$

Collisional radiation

(Relativistic Rayleigh Scattering aka Gamma Factory, Inverse Compton Scattering, Large Recoil ICS, Symmetric Compton Scattering)

Gamma Factory

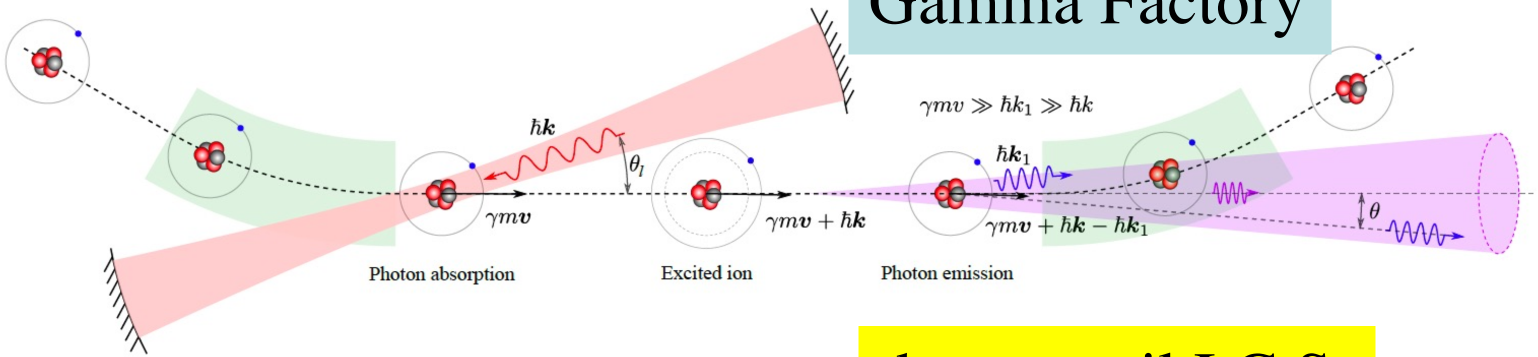

I.C.S.

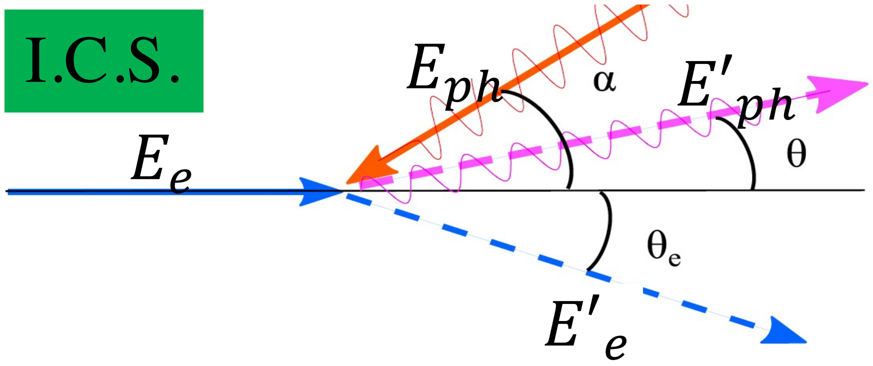

deep recoil I.C.S.

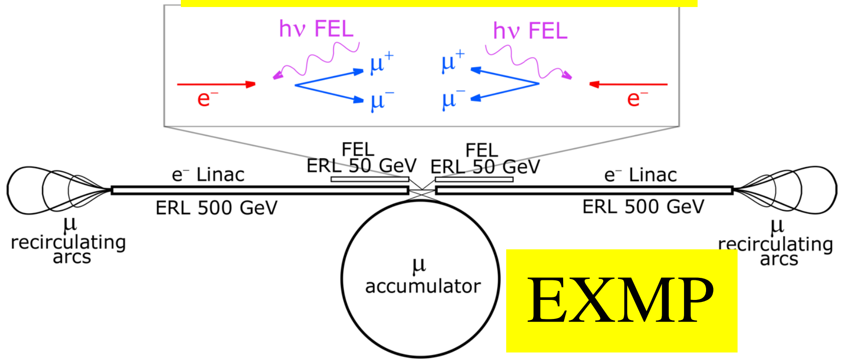

EXMP

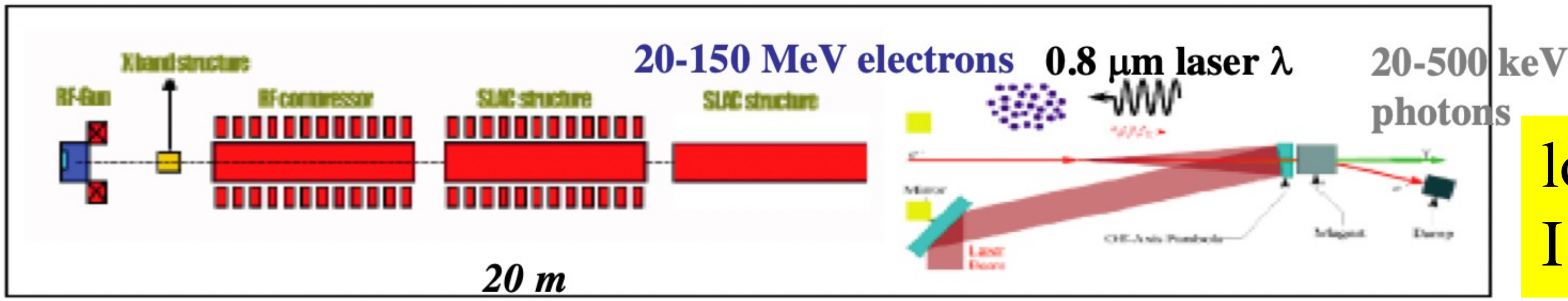

low recoil I.C.S. - STAR

how to collide bright beams of electrons and photons to generate advanced secondary beams

Lecture Outline – second view

Classical Electro-Magnetism prevalent

Classical Electro-Dynamics easier

Quantum Electro-Dynamics necessary

- Electro… undulators – from spontaneous incoherent emission towards coherent cooperat… emission via Free Electron Laser instability
- Inverse Compton Scattering sources of photon beams: electro… ematics
- Increasing E_{cm} , the center of mass available energy, towards generation of extreme positron or muon beams

Istituto Nazionale di Fisica Nucleare

Mini-Course on
Compact radiation sources of X/γ rays for medical/cultural heritage/industrial applications

1 - Today

16:00 → 16:30 **Break** 30m

16:30 → 18:30 **High performance computing**
Convener: Horst Severini (University of Oklahoma (US))
Computing Tutorial ...

16:30 → 18:30 **Light sources**
16:30 **Radiation Sources - FEL's, ICS, and Photo-Muons** 2h
Speaker: Luca Serafini (INFN-Milan)

16:30 → 18:30 **Small detector labs**
16:30 **Internet of Things** 2h
Speaker: Uli Raich (retired)

18:30 → 20:00 **Accelerators: EuPRAXIA**
Convener: Massimo Ferrario

Mini-Course on Compact radiation sources of X/γ rays for medical/cultural heritage/industrial applications

2 - Tomorrow

16:00 → 16:30 **Break** 30m

16:30 → 18:30 **Astrophysics and cosmology**

Convener: Mathieu JACOBE DE NAUROIS (Ecole Polytechnique, France)

deNaurois_Cosmol... deNaurois_Cosmol...

16:30 → 18:30 **High performance computing**

Convener: Horst Severini (University of Oklahoma (US))

Computing Tutorial ...

16:30 → 18:30 **Light sources**

16:30 **Applications of Compact Light Sources for X-Ray Technologies** 2h

Speaker: Luca Serafini (INFN-Milan)

16:30 → 18:30 **Medical physics**

Convener: Rajaa Sebihi (MOhammed V University, Morocco)

16:30 **Radioactivity, X-rays and radiation protection** 2h

Speaker: Rajaa Sebihi (MOhammed V University, Morocco)

Mini-Course on Compact radiation sources of X/γ rays for medical/cultural heritage/industrial applications

3 - Friday

14:30 → 16:00 **High Energy Physics**

14:30 **Neutrino physics** — 1h 30m
Speaker: Mary Bishai (Brookhaven National Laboratory (US))

14:30 → 16:00 **Light sources**

14:30 **High Brightness Electron Beams for Radiation Sources** — 1h 30m
Speaker: Alberto Bacci (INFN-Milan)

14:30 → 16:00 **Small detector labs**

14:30 **Internet of Things** — 1h 30m
Speaker: Uli Raich (retired)

16:00 → 16:30 **Survey** — 30m

16:30 → 18:30 **Light sources**

16:30 **Applications and Practical Implementations of Advancements in Compact Light Sources for X-ray Technologies** — 2h
Speakers: Alberto Bacci (INFN-Milan), Dr Sanae SAMSAM (INFN Milano)

★ ASP-2016 (Rwanda-Kigali) Alumna

8th African School of Physics - Marrakech (MO) - July 2024

Radiation Sources from relativistic electron beams: Synchrotron radiation, Compton Back-scattering, Free Electron Lasers

- **When Quantum description (Q.E.D.) is necessary: electron recoil affecting the characteristics of the radiation beam (electron energy loss during radiation emission non-negligible, momentum-energy conservation requested)**
- **When Classical Electro-Magnetism is more adequate (easier): phase effects (self-organization, cooperation) in the radiation beam are dominant (FEL's, amplified stimulated emission of radiation vs. spontaneous incoherent one like in Synchrotrons and I.C.S.)**
- **2 Relevant Examples follow**

Electron Recoil effect in γ-ray I.C.S. for Nuclear Photonics: C.E.D. fails to evaluate the correct red-shift in the spectrum

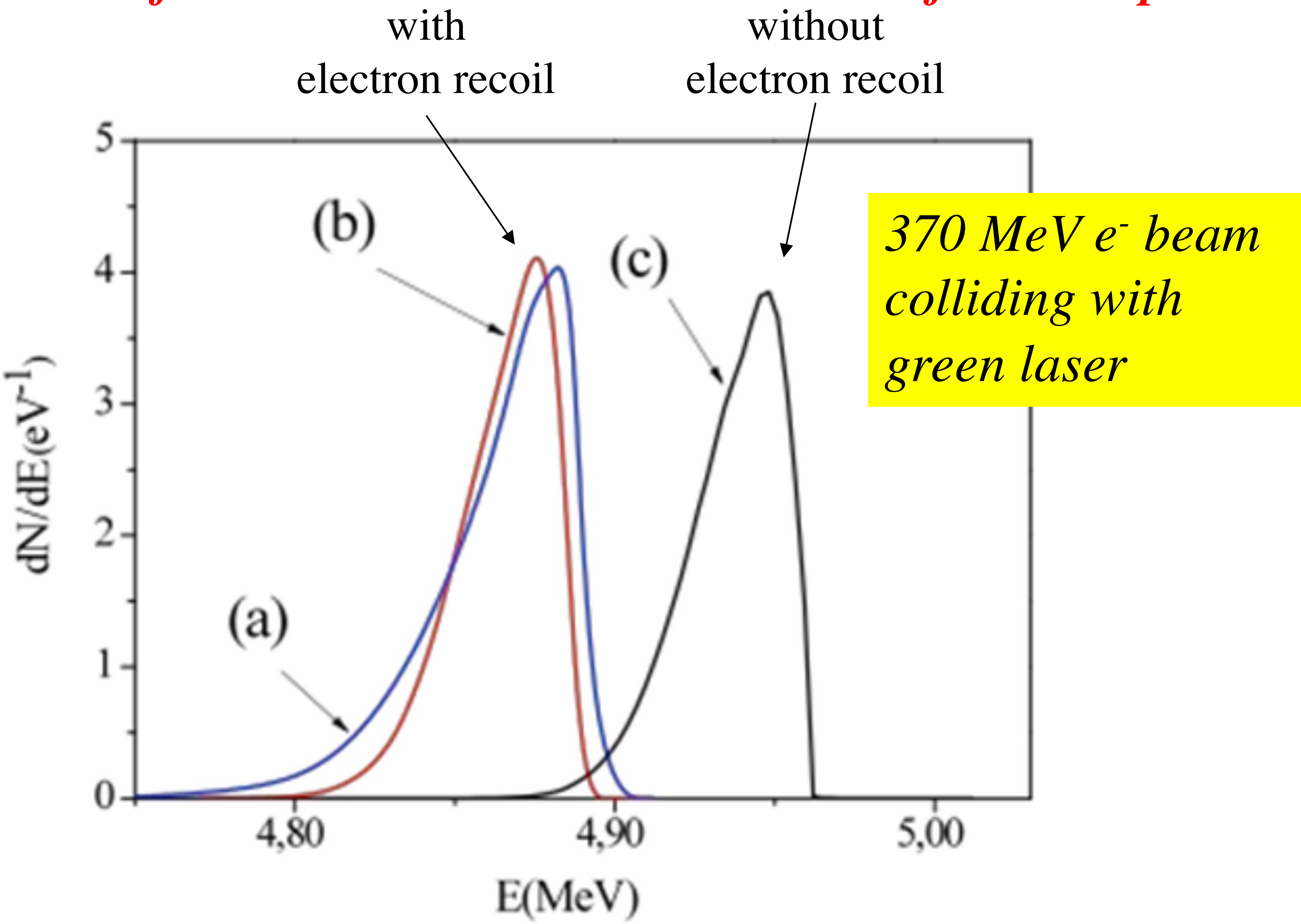

Fig. 5. Spectra of the rays. (a) CAIN (b) Quantum model (c) Classical treatment in the case of beam (A) and for the laser parameter of Table 1 and interaction angle α=π ; rms acceptance angle θ_{rms} = 25μrad

Cooperation among electrons in the beam, driven by the emitted radiation field in SASE (Self-Amplified Spontaneous Emission). FEL's cannot be explained by linear (single photon) Q.E.D. because its instability is driven by phase effects and (quasi)coherence

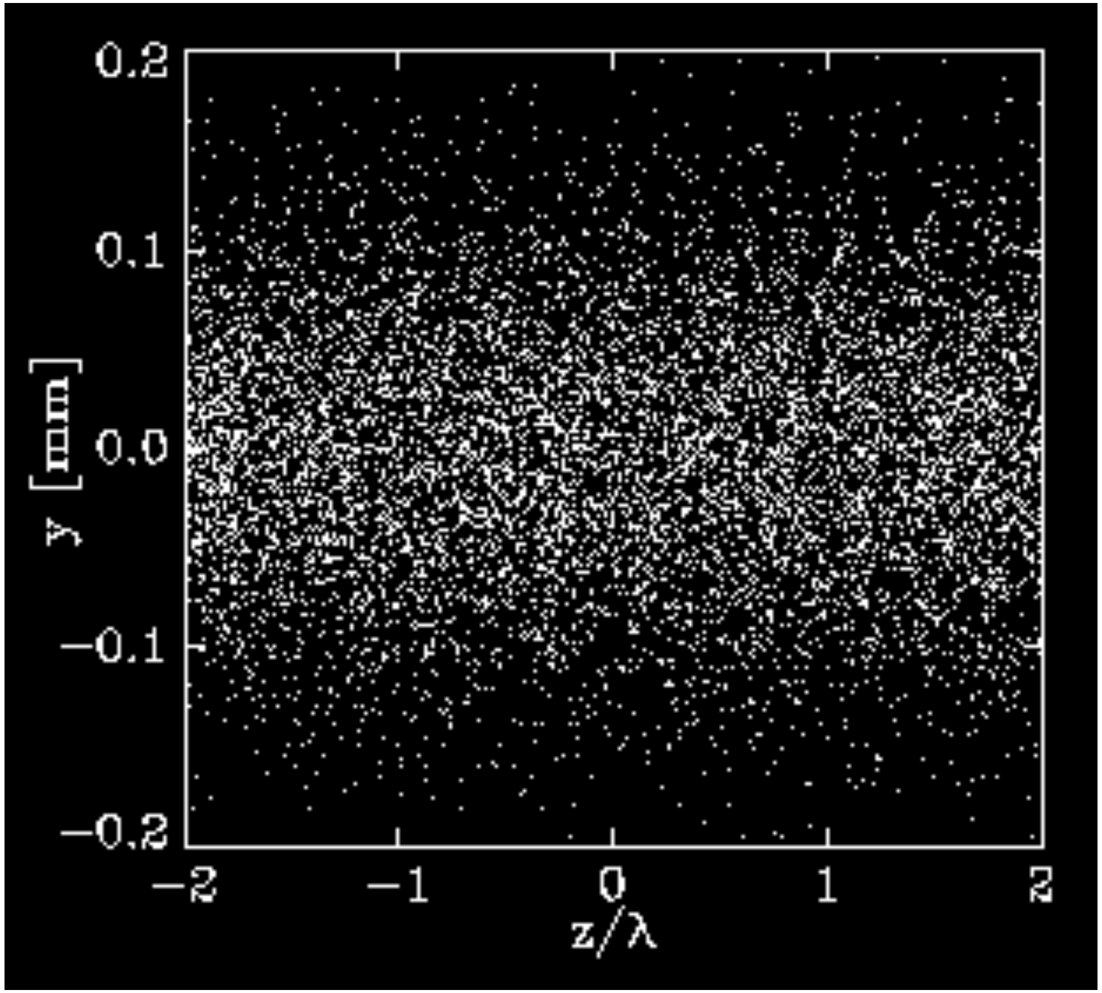

FEL is a laser (light amplification by stimulated emission of radiation)

At the border between C.E.D. and Q.E.D.

explaining why an isolated electron (or any other charged particle) propagating in vacuum DOES NOT RADIATE, i.e. does not emit radiation

Uniformly moving charge does not radiate

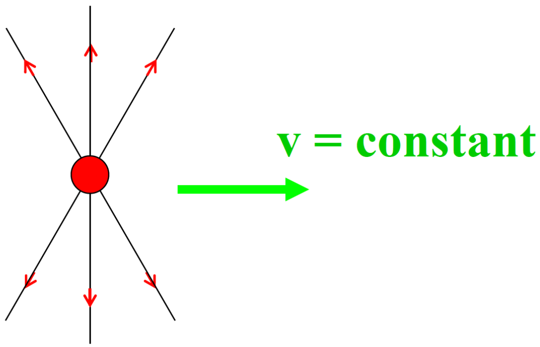

We need to separate the field from charge

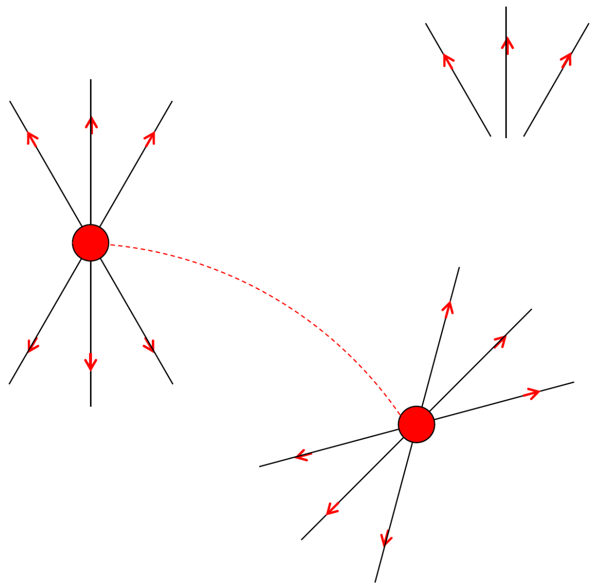

The C.E.D. vision

The em self-fields are calculated directly (*i.e.* without calculating first the em potentials) in terms of the values of the charge density $\rho(\mathbf{x},t)$ at time t and at all preceding times, through the following equations that can be readily obtained by an easy manipulation of the usual retarded forms

$$\mathbf{E}(\mathbf{x},t) = \int d\mathbf{x}' \rho(\mathbf{x}',\tau) \mathbf{Q}_E(\mathbf{x}-\mathbf{x}',\tau) \tag{1}$$

$$\mathbf{B}(\mathbf{x},t) = \int d\mathbf{x}' \rho(\mathbf{x}',\tau) \mathbf{Q}_B(\mathbf{x}-\mathbf{x}',\tau) \tag{2}$$

where $\tau = t - \frac{1}{c}|\mathbf{x}-\mathbf{x}'|$ and

Radiation - propagating field   Coulomb, quasi-static field

$$\mathbf{Q}_E = \frac{\mathbf{n}\times((\mathbf{n}-\beta)\times\dot{\beta})}{c|\mathbf{x}-\mathbf{x}'|(1-\mathbf{n}\cdot\beta)^2} + \frac{(\mathbf{n}-\beta)(1-\mathbf{n}\cdot\beta)^{-2}}{\gamma^2|\mathbf{x}-\mathbf{x}'|^2} \quad (3)$$

$$\mathbf{Q}_B = -\frac{\mathbf{n}\times(\dot{\beta}(1-\mathbf{n}\cdot\beta)+\beta(\mathbf{n}\cdot\dot{\beta}))}{c|\mathbf{x}-\mathbf{x}'|(1-\mathbf{n}\cdot\beta)^2} - \frac{(\mathbf{n}\times\beta)(1-\mathbf{n}\cdot\beta)^{-2}}{\gamma^2|\mathbf{x}-\mathbf{x}'|^2} \quad (4)$$

In addition, $\mathbf{n} = (\mathbf{x}-\mathbf{x}')/|x-x'|$, $\boldsymbol{\beta} = \mathbf{v}(t)/c$, and all time dependent quantities in (3) and (4) are calculated at the retarded time τ.

$$\gamma \equiv \frac{1}{\sqrt{1-\beta^2}}$$

momentum $p = \gamma m v$

total energy $E = \gamma m c^2$

kinetic energy $K = E - mc^2$

$$E = \sqrt{(mc^2)^2 + (pc)^2}$$

PHYSICAL REVIEW SPECIAL TOPICS - ACCELERATORS AND BEAMS **12**, 104202 (2009)

Numerical treatment of retarded radiation effects from high brightness electron beams

A. R. Rossi, A. Bacci, and L. Serafini
INFN-MI, via Celoria 16, I-20133 Milano, Italy

C. Maroli and V. Petrillo
Dipartimento di Fisica, Università degli Studi di Milano, via Celoria 16, I-20133 Milano, Italy
(Received 21 April 2009; published 20 October 2009)

A form is given of the retarded electric field and magnetic induction generated by the motion of a charged particle that expresses these fields as integrals of the retarded charge density only, with kernels depending on the charge velocity and acceleration fields. In the case of a single pointlike charge, the usual Liénard-Wiechert fields follow very easily. The set of equations for the dynamics of particles in assigned electromagnetic fields with the self-consistent field is written and integrated. The code RETAR for the dynamics of charged particles in external and self-consistent fields is described and a few examples of benchmark are proposed. As a physical application, the case of an electron beam moving in a bending magnetic dipole is examined, and the radiation produced analyzed, in order to characterize a therahertz radiation source.

DOI: 10.1103/PhysRevSTAB.12.104202 PACS numbers: 41.60.−m, 41.75.−i, 41.20.−q

And, of course… Chapt. 14th Jackson – Classical Electro-Dynamics

The Q.E.D. vision: relativistic kinematics and energy/momentum conservation of electron-photon system

$$electron\ 4-vector\ \mathbf{P}_e = \left[E_e/c, p_{ex}=0, p_{ey}=0, p_{ez}=p_e=\sqrt{E_e^2/c^2-m_e^2c^2}\right]$$

$$photon\ 4-vector\ \mathbf{P}_{h\nu} = \left[h\nu_L/c, \hbar k_x=0, \hbar k_y=0, \hbar k_z=-h\nu_L/c\right]$$

if no photon in the initial state (only an electron freely propagating in vacuum)

$$\mathbf{P}_{tot} = \mathbf{P}_e$$

$$Invariant\ Mass\ s \equiv c\mathbf{P}_{tot} \bullet c\mathbf{P}_{tot} = E_{tot}^{2*} = E_{cm}^2$$

$$\left(4-vector\ product\ \mathbf{P}_1 \bullet \mathbf{P}_2 \equiv \left[E_1E_2/c^2 - \vec{p}_1 \cdot \vec{p}_2\right]\right)$$

So in this case we have $E_{cm} = m_ec^2$. Therefore there is no energy available in the final state to generate another particle, or a photon. The electron will keep propagating in vacuum unperturbed and no photon emission is possible

Side comment: a free electron cannot absorb a photon, it can only scatter an incident photon. Demonstration: time-reversal of the previous statement.

Non-relativistic Coulomb Field

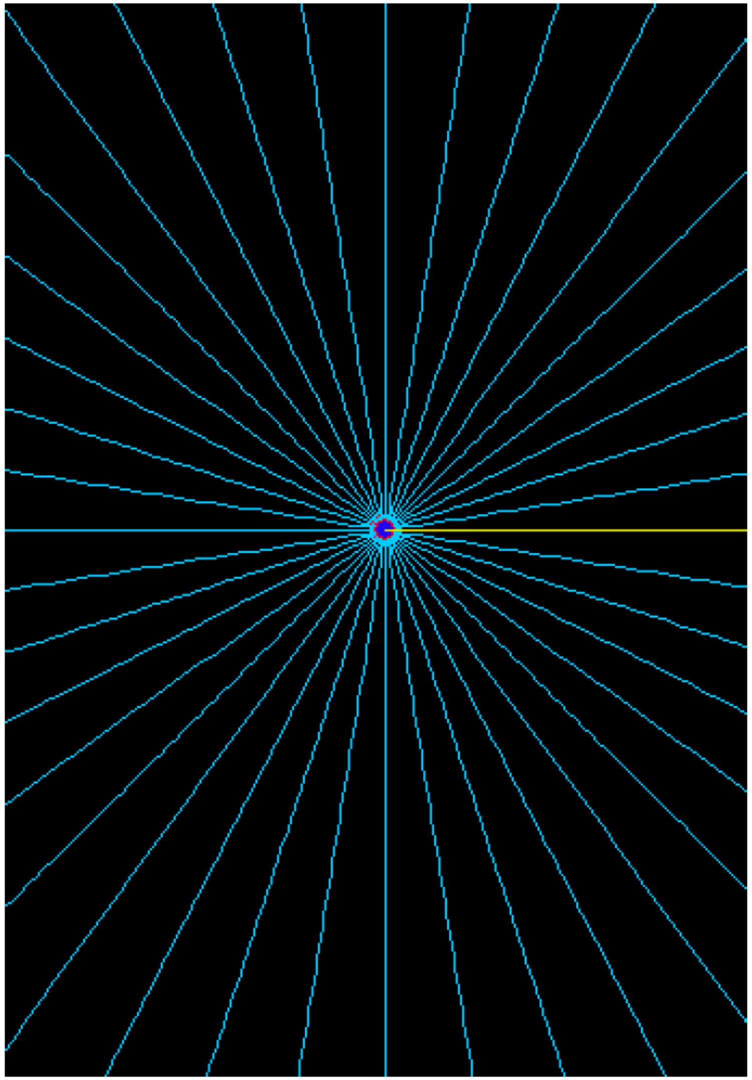

Relativistic (3 MeV) Coulomb Field

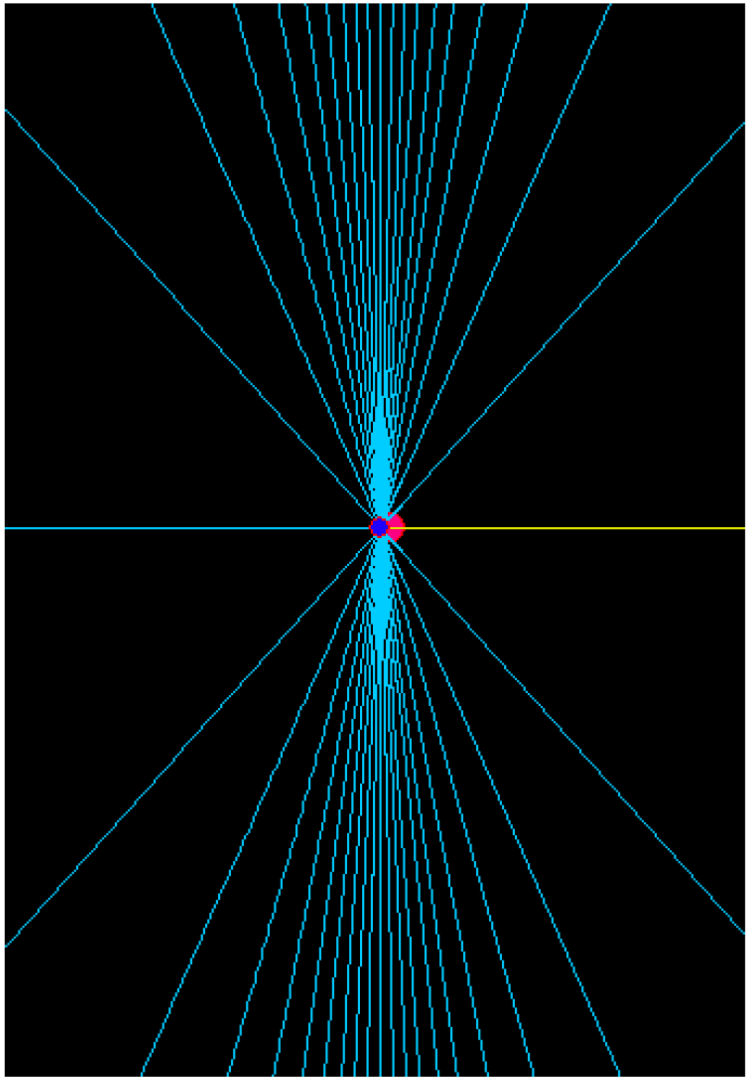

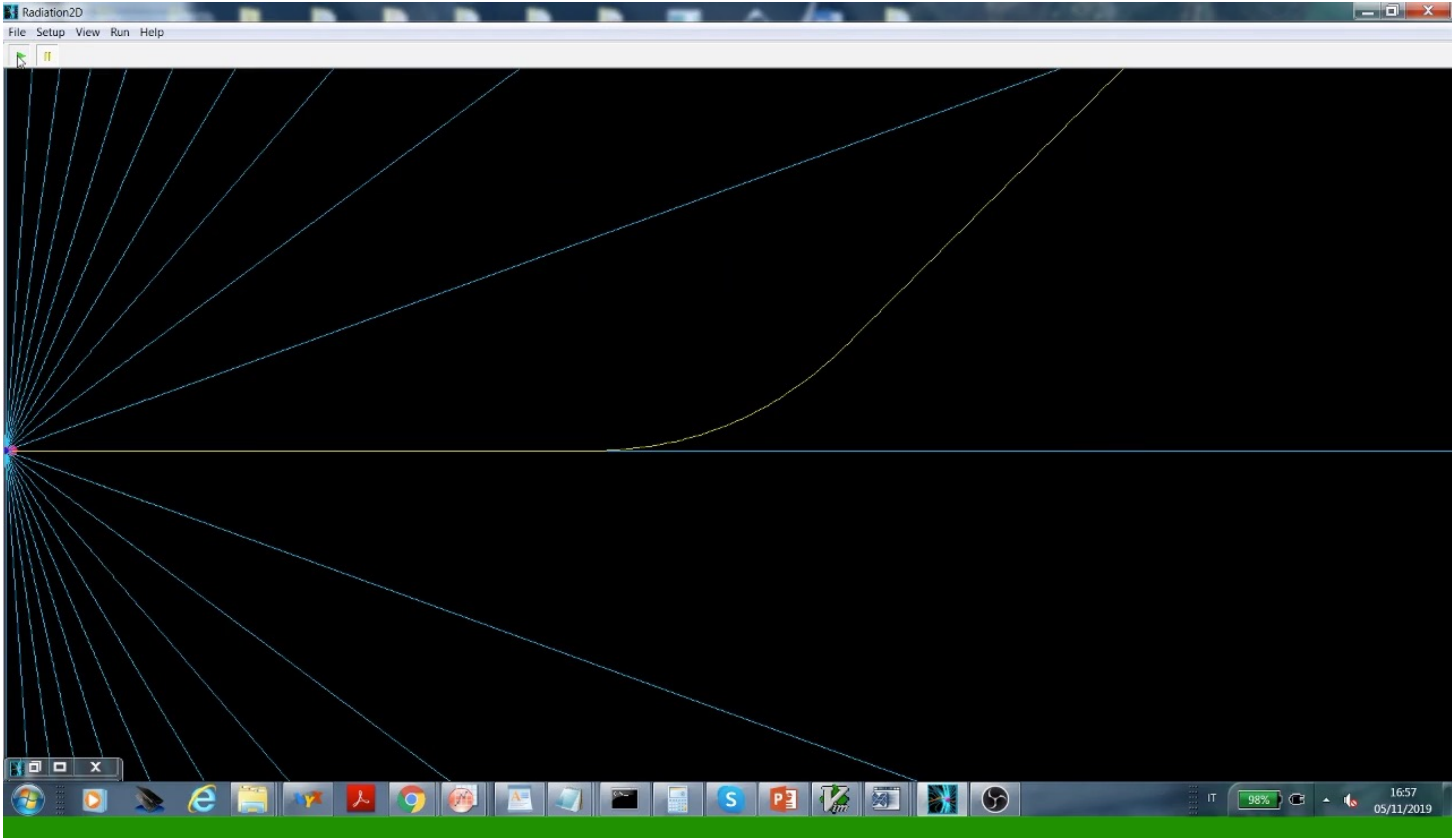
Radiation2D
File Setup View Run Help
IT
98%
16:57
05/11/2019

NEW MATHEMATICAL METHOD FOR RADIATION FIELD OF MOVING CHARGE

T. Shintake
RIKEN: The Institute of Physical and Chemical Research
Hyogo, 679-5143, Japan

Abstract

New mathematical method has been developed to compute radiation field from a moving charge in free space. It is not based on the retarded potential and its derivation. It uses the following two facts: (1) once a wave is emitted from a particle, it propagates as a spherical wave. It's wavelet (a part of the wavefront) runs with speed of the light, and does not change its direction, (2) the initial direction of the wavelet is determined by the Lorentz transformation from electron rest frame to the laboratory frame by taking into account the light aberration. 2D radiation simulator has been developed with this method, which simulates synchrotron, undulator and dipole radiation in time domain.

1 INTRODUCTIONS

In various experimental applications of radiation, such as, the synchrotron, undulator and FEL radiations, discussions are made in terms of the angular and frequency spectrum of these radiations. These field properties are historically analysed by solving retarded potential for specified trajectory. Usually only the far-field radiation proportional to r^{-1} is considered, and the Coulomb field is omitted since it decays quickly as r^{-2}. The results from this approximation have been widely used to evaluate the experimental data and well confirmed.

However, today's advanced accelerator uses extreme beam parameters, for example, ultra-short and high-current beams, where both of the space charge field and radiation field affect beam kinematics at the same time.

Back to 1972, R. Y. Tsien[1] firstly computed electric field of a point charge moving at relativistic velocities. He numerically integrated parametric equations for the field lines, using IBM 360/65 computer and visualize the lines by California Computer Products model 665 11-in. drum plotter. His method was based on the retarded potential, and it was very time consuming process.

The method reported in this paper is totally different from these retarded potential methods, which was originally made by the author in 1974 [2]. It is quite simple and suitable to numerical simulation.

2 MATHMATICAL MODEL

2.1 Basic Equation

The Maxwell equation with field source is

$$\begin{aligned} \nabla\times\boldsymbol{H} &= \boldsymbol{J}+\frac{\partial\boldsymbol{D}}{\partial t} \\ \nabla\times\boldsymbol{E} &= -\frac{\partial\boldsymbol{B}}{\partial t} \\ \nabla\cdot\boldsymbol{B} &= 0 \\ \nabla\cdot\boldsymbol{D} &= \rho \end{aligned} \qquad (1)$$

Here we consider radiation field from a single charge in free space. In the Maxwell equation, there are two driving terms, ρ and $\boldsymbol{J}$, which are related by the following continues equation,

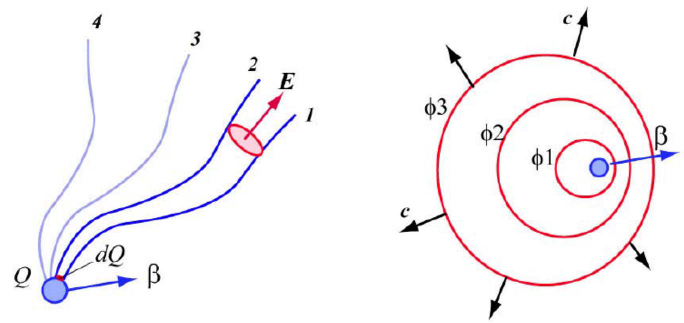

(a) Electric Field Lines (b) Wavefronts

Fig. 1 Electric field lines of moving charge, and wavefronts.

INFN
Istituto Nazionale di Fisica Nucleare

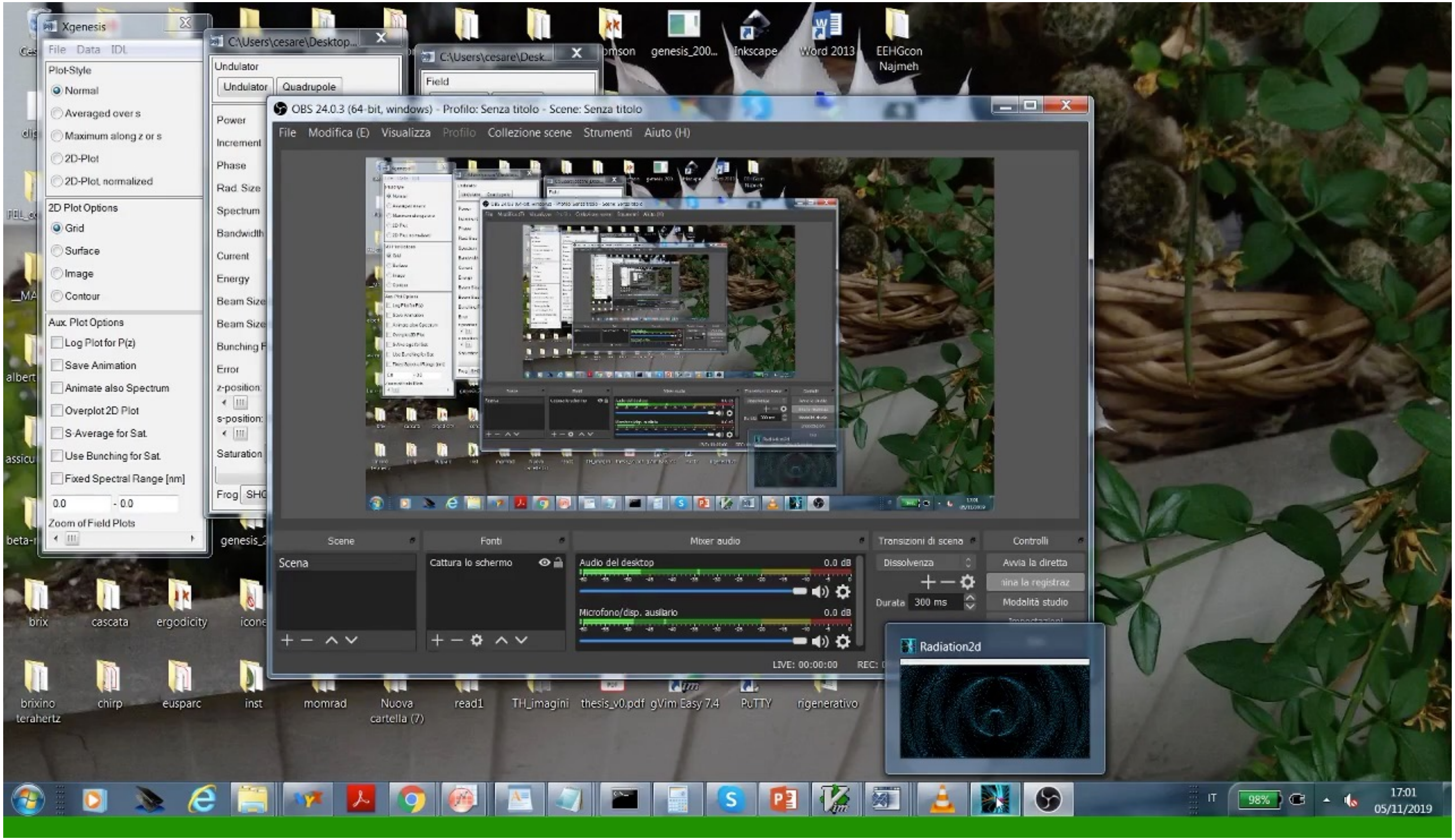

The Classical E.M. view (Maxwell eq.): Thomson Sources as synchrotron radiation sources with electro-magnetic undulator

FEL's and Thomson/Compton Sources common mechanism:
collision between a relativistic electron and a (pseudo)electromagnetic wave

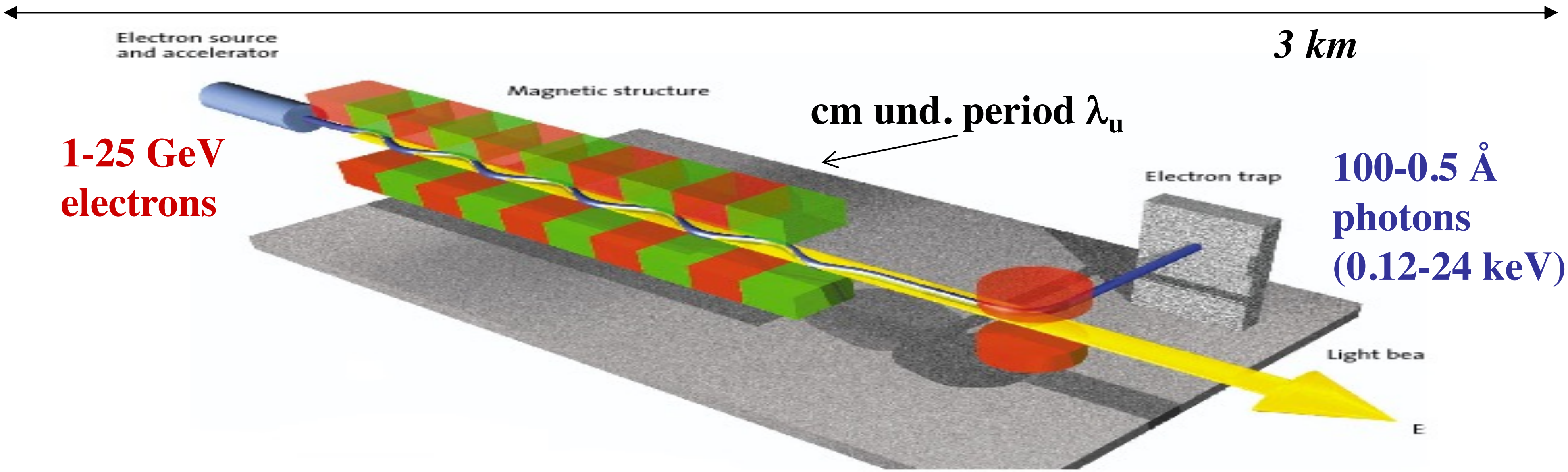

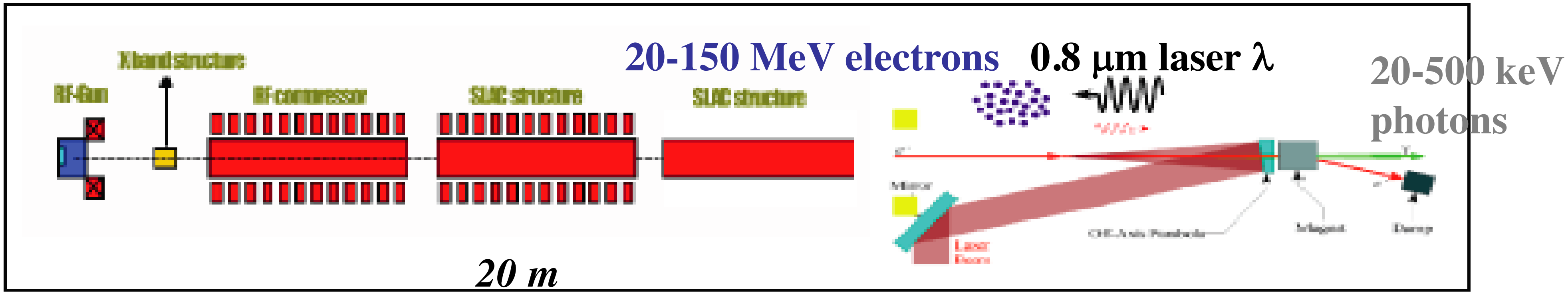

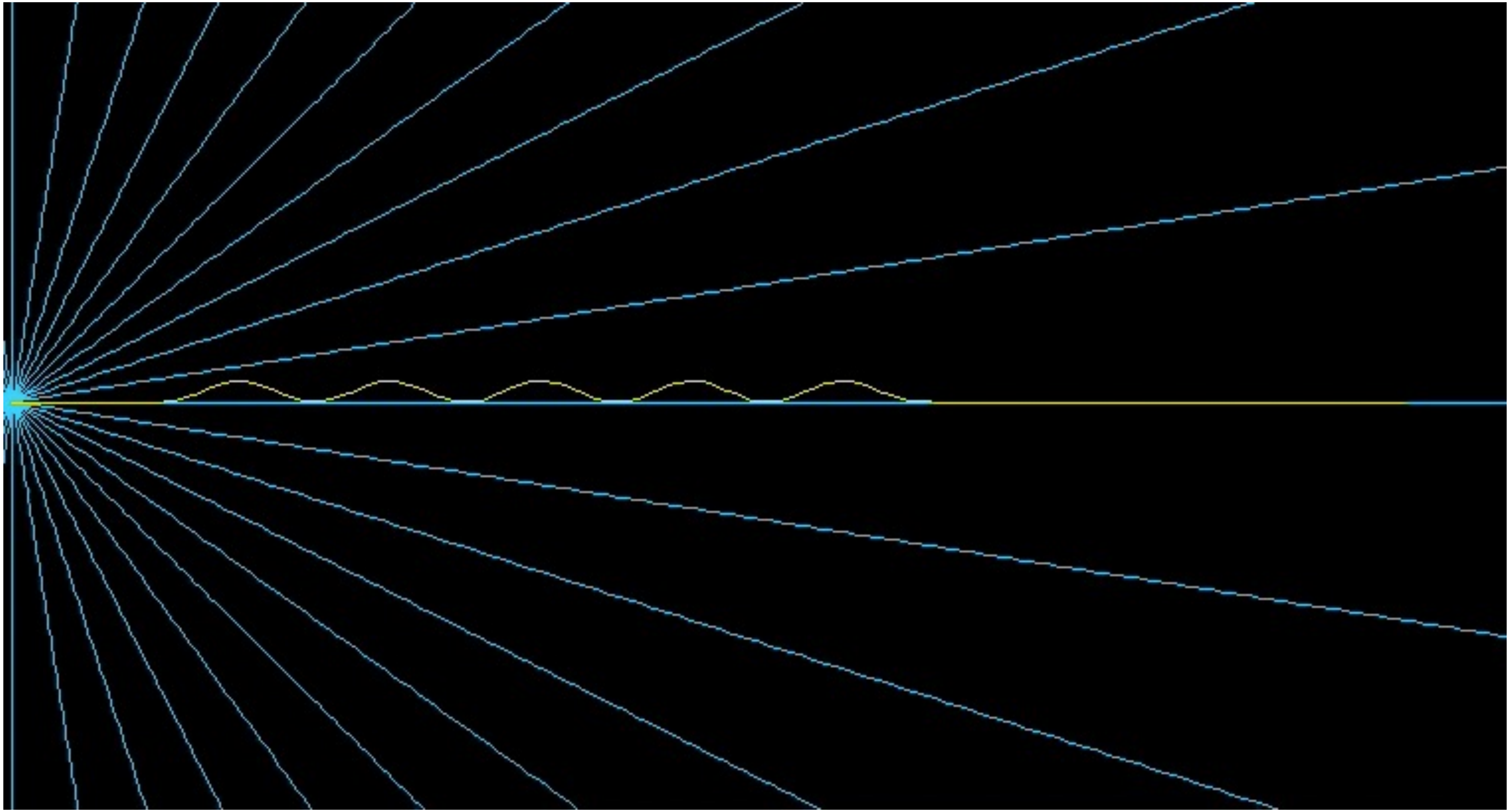

From single-electron radiation to Particle Beams emitting Photon Beams

Particle beams diffract like radiation: emittance of particle beams is equivalent to wavelength of coherent e.m. fields

Diffraction limit: ideal overlap of charged particle beam and generated photon beam while co-propagating over distances much longer than diffraction length

Such a condition assures not only maximum brilliance of the radiation beam in synchrotrons but also the onset of FEL instability with high-gain exponential growth, as well as maximum luminosity in I.C.S. e-γ colliders

electron beam with large emittance: tight focus implies large diffraction (divergence) angles, therefore a largely diverging beam envelope

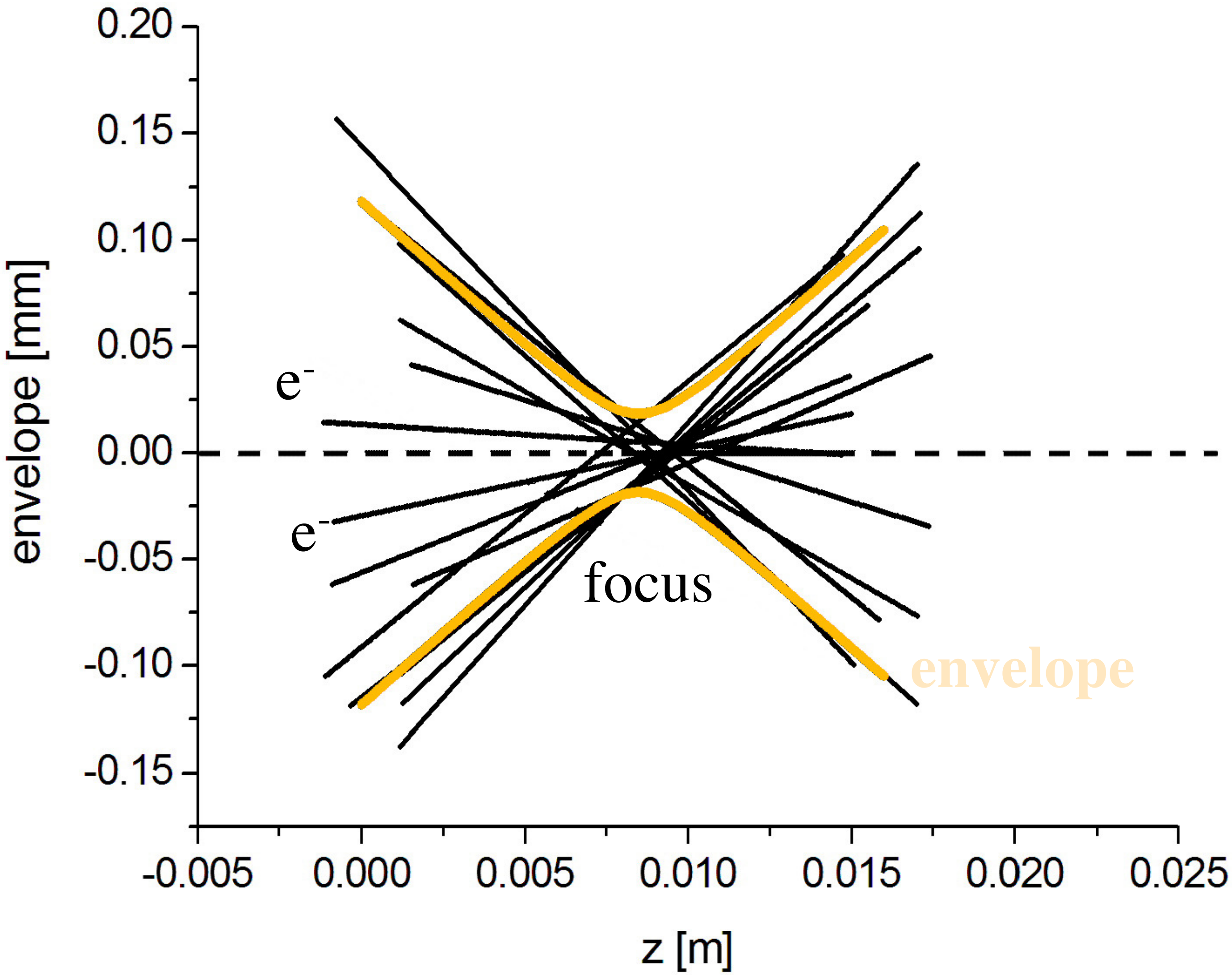

Emittance and beam dimensions

- The emittance is the area of the phase space occupied by the particles Knowing the emittance and the Twiss parameters in a point of the accelerator, the beam dimensions are obtained : $\sigma_{x,y}$ e $\sigma'_{x,y}$

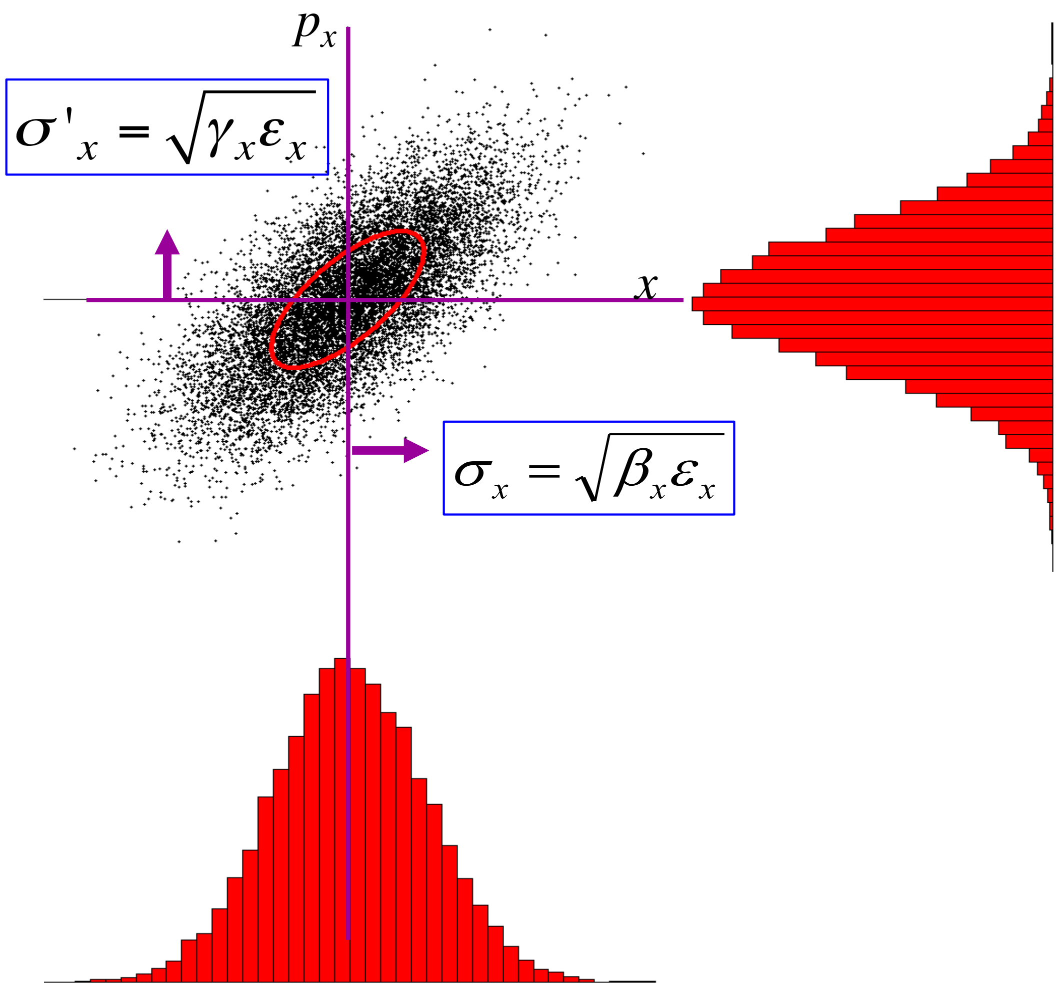

$$\varepsilon_x = \sqrt{\langle x^2 \rangle \langle x'^2 \rangle - \langle x x' \rangle^2}$$

Ellipse area= $\pi\varepsilon_x$

$$\langle x^2 \rangle = \beta_x \varepsilon_x$$

$$\langle x'^2 \rangle = \gamma_x \varepsilon_x$$

$$\langle x x' \rangle = -\alpha_x \varepsilon_x$$

$$\beta_x \gamma_x - \alpha_x^2 = 1$$

Photon / Particle Beams: diffraction, envelope, matching, co-propagation.
Example: TEM_{00} Gaussian Laser mode (circ. pol. M^2=1 diffr. limited)

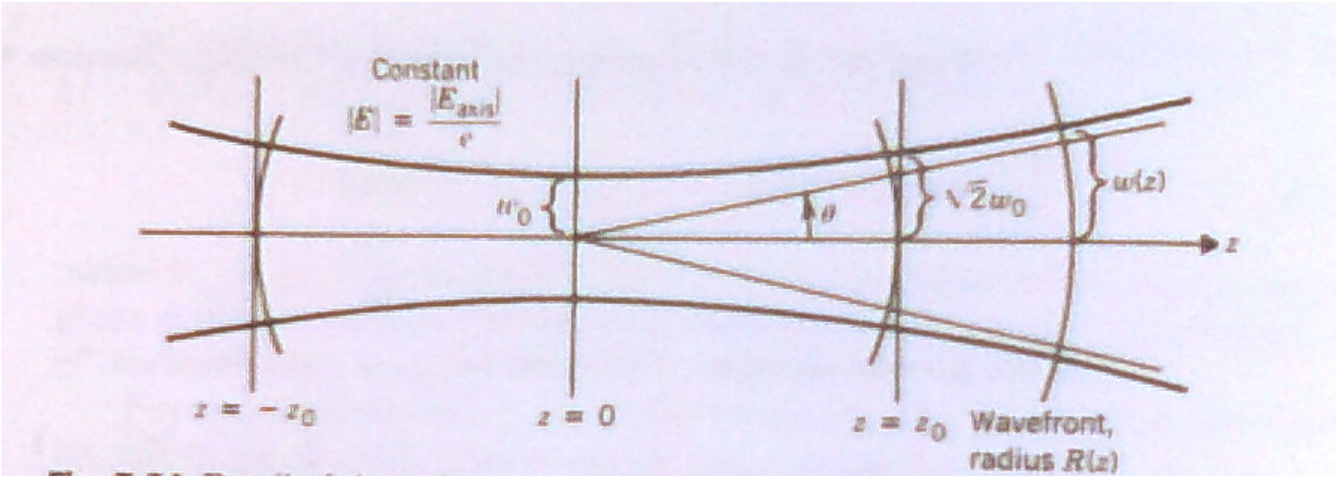

$$E_0(x,y,z,t) = A_0 e^{i\omega t} e^{-ikz} \frac{Z_0}{Z_0 - iz} \exp\left[-\frac{k\left(x^2+y^2\right)}{2}\frac{1}{Z_0 - iz}\right] \quad k = 2\pi/\lambda$$

$$\left|E_0(x,y,z,t)\right| = E_0 \frac{w_0}{w} e^{-\frac{x^2+y^2}{w^2}}$$

$$w = w_0\sqrt{1+\frac{z^2}{Z_0^2}} \qquad Z_0 = \frac{\pi w_0^2}{\lambda} \qquad \vartheta = \frac{w_0}{Z_0} = \frac{\lambda}{\pi w_0}$$

INFN Istituto Nazionale di Fisica Nucleare

$$I \propto \left| E_0(x,y,z,t) \right|^2$$

LASER | **PARTICLE BEAM**

$$Z_0 = \frac{4\pi \left(\frac{w_0}{2} \right)^2}{\lambda} \quad \Longleftrightarrow \quad \beta^* = \frac{\sigma_0^2}{\varepsilon_n / \gamma}$$

$$\frac{w}{2} = \frac{w_0}{2} \sqrt{1 + \frac{z^2}{Z_0^2}} \quad \Longleftrightarrow \quad \sigma(z) = \sigma_0 \sqrt{1 + \frac{z^2}{\beta^{*2}}}$$

DIFFRACTION LIMIT

$$\frac{\lambda}{4\pi} = \frac{\varepsilon_n}{\gamma} \quad and \quad w_0 = 2\sigma_0$$

$$\varepsilon_n \leq \frac{\lambda_{FEL} \gamma}{4\pi}$$

$$w(z) = 2\sigma(z) \quad and \quad \vartheta(z) = 2\sigma'(z)$$

$$\varepsilon = \frac{\varepsilon_n}{\gamma} < \frac{\lambda}{4\pi}$$

Niels Bohr's derivation of Heisenberg's uncertainty principle and its analogy with the concept of Diffraction Limited Photon Beam

$$\Delta x \cdot \Delta p_x \geq \frac{h}{4\pi}$$

se fotone $p_x = x' p = x' \frac{h\nu}{c} = \frac{x' h}{\lambda}$

se $\Delta x \sim \sigma_x$

$\Delta x' \sim \sigma_{x'}$

$\varepsilon_x \equiv \sigma_x \sigma_{x'}$

$$\Downarrow$$

$$\sigma_x \sigma_{x'} \geq \frac{\lambda}{4\pi}$$

$$\Downarrow$$

$\varepsilon_x = \frac{\lambda}{4\pi}$ diffraction limited

$\varepsilon_x > \frac{\lambda}{4\pi}$ any photon beam

Coherent/Collective propagation of radiation and particle beams
i.e. phase space matching of particle beam and photon beam

Synchrotrons: diffraction limit

$\varepsilon < \lambda$

ESRF 100 pm (10^{-10}) to be compared to
12 keV X-rays *i.e.* 10^{-10} m wavelength

I.C.S. bandwidth scaling as $\gamma^2\varepsilon^2/\sigma^2$
Petrillo-Serafini criterion

$$S_d \propto \frac{\langle I_e \rangle U_{las}}{\varepsilon_n^2 E_x}$$

Pellegrini-Kim criterion on SASE FEL:

$$\varepsilon = \frac{\varepsilon_n}{\gamma}$$

$$\varepsilon_n \leq \frac{\lambda_{FEL}\gamma}{4\pi}$$

Brilliance of Lasers and X-ray sources

$$N_{ph} = 10^{19} - 10^{20}$$

$$\sigma_t = 10 - 20 \quad fs$$

ELI

BELLA

$$B = \frac{N_{ph}}{\sqrt{2\pi}\sigma_t \left(M^2\lambda\right)^2 \frac{\Delta\lambda}{\lambda}}$$

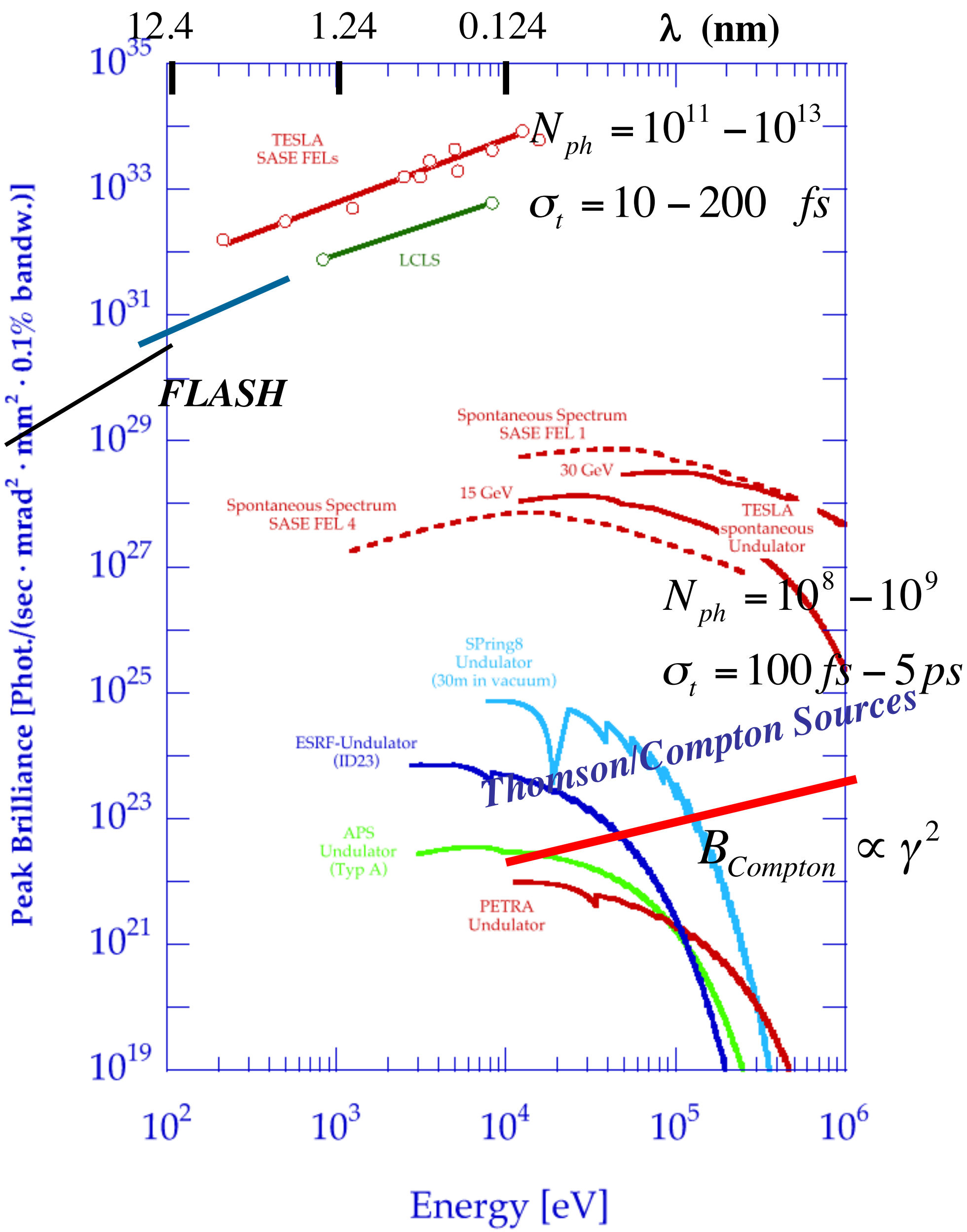

$$B_{peak} = \frac{N_{ph}}{\sqrt{2\pi}\sigma_t \varepsilon_x^2 \frac{\Delta E_X}{E_X}}$$

$$B_{av} = \frac{N_{ph} f}{\varepsilon_x^2 \frac{\Delta E_X}{E_X}}$$

2 Approaches to describe the Physics of I.C.S.
A) (linear) Quantum B) Classical

- **A) Quantum: linear QED of electron-photon 2-body kinematics and Klein-Nishina cross section**

Limitation of (linear) quantum description: does not take into account the coherent organization of photons in the e.m. field of the laser pulse (intensity field, no phase)

- **Effect of electron recoil on *X/γ* ray bean (spectral density, bandwidth broadenin beam (emittance dilution in multiple scattering and incoherent energy spread due to scattering stochasticity)**

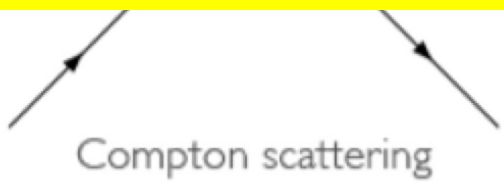

- **B) Classical:**
- **No Energy/M collective effe absorption/er**

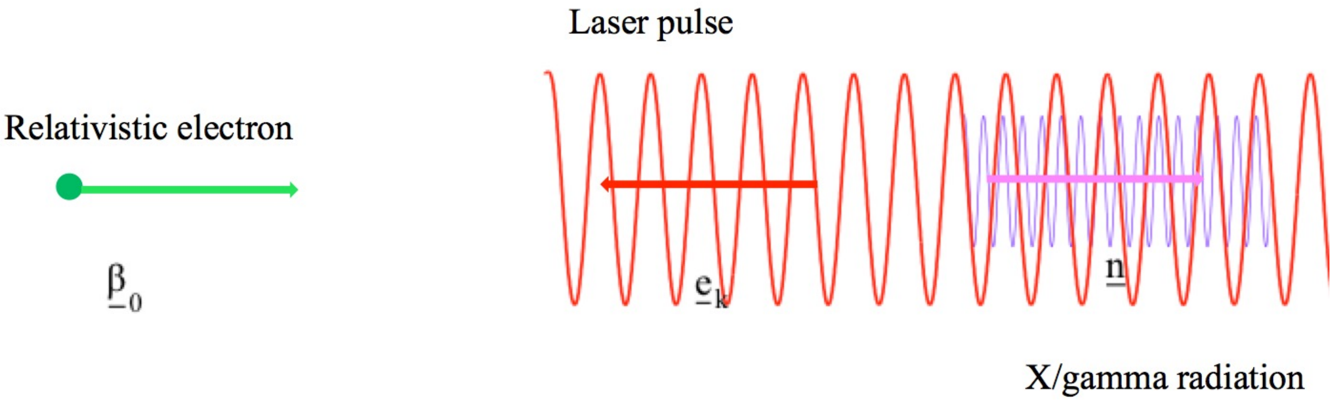

Classical model

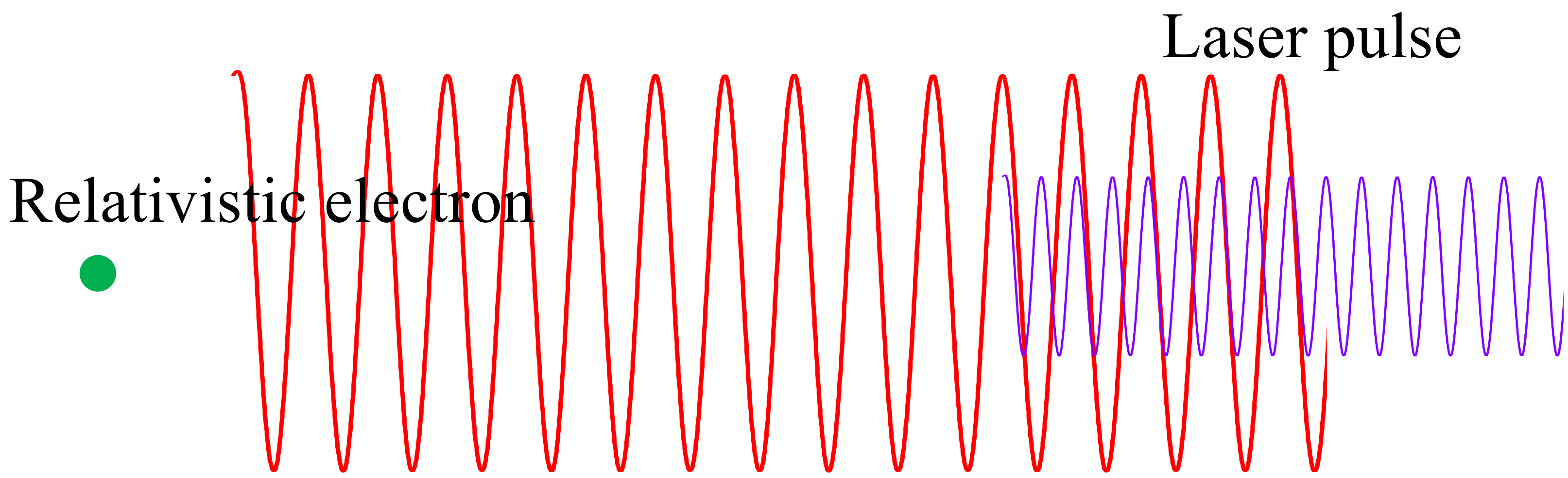

Courtesy V. Petrillo

Let us analyze in details similarities and differences between otpical and magnetic undulators (see also ref.1): the field on axis of a magnetostatic undulator is given by $B_w = B_{0w} e^{ik_w z}$, associated to a vector potential of normalized amplitude $a_w = \frac{eB_{0w}}{mck_w}$.

The field on axis of an optical undulator (under the approximation of a plane wave) is $B_L = B_{0L} e^{i(k_L z + \omega_L t)}$, $E_L = E_{0L} e^{i(k_L z + \omega_L t)}$, with $E_{0L} = cB_{0L}$: the associated normalized vector potential is $a_0 = \frac{eB_{0L}}{m\omega_L}$ with $\omega_L = ck_L = \frac{2\pi c}{\lambda}$. The two undulators apply, to a relativistic electron traveling on axis with $z = \beta_{//} ct$, a transverse force given by

$$F_\perp^L = mca_0 \omega_L \left(1 + \beta_{//}\right) e^{i(1+\beta_{//})\omega_L t} \tag{1a}$$

and

$$F_\perp^w = mc^2 a_w \beta_{//} k_w e^{i\beta_{//} k_w ct} \tag{1b}$$

respectively. From $\dot{p}_\perp = F_\perp$ and $p_\perp = mc\beta_\perp \gamma$ we derive $\beta_\perp^L = \frac{a_0}{\gamma} e^{i\omega_L (1+\beta_{//})t}$ and $\beta_\perp^w = \frac{a_w}{\gamma} e^{i\beta_{//} k_w ct}$.

In case of a helical magnetic undulator, as well as for a cicrcularly polarized laser pulse acting as an optical undulator, we are in a simple situation of constant transverse and longitudinal momentum components, so that we can write $\beta_\perp^L = \frac{a_0}{\gamma}$ and $\beta_\perp^w = \frac{a_w}{\gamma}$, while $\beta_{//}^w = \sqrt{1 - \frac{1 + a_w^2}{\gamma^2}}$ and $\beta_{//}^L = \sqrt{1 - \frac{1 + a_0^2}{\gamma^2}}$.

In case of a helical magnetic undulator, as well as for a cicrcularly polarized laser pulse acting as an optical undulator, we are in a simple situation of constant transverse and longitudinal momentum components, so that we can write $\beta_\perp^L = \frac{a_0}{\gamma}$ and $\beta_\perp^w = \frac{a_w}{\gamma}$, while $\beta_{//}^w = \sqrt{1 - \frac{1 + a_w^2}{\gamma^2}}$ and $\beta_{//}^L = \sqrt{1 - \frac{1 + a_0^2}{\gamma^2}}$.

In order to derive the resonance expression for the radiation emitted in the forward direction on axis, we note that the angular frequency ω_e of the oscillating electron in the field of the optical undulator (see Eq.1a) is $\omega_e = \left(1 + \beta_{//}^L\right)\omega_L$, *i.e.* almost double than the laser frequency. The typical FEL slippage condition will therefore set the resonance frequency for the radiation emitted by the electron at: $n\lambda_R = cT_e - \beta_{//}^L cT_e$ ($\omega_R = ck_R = \frac{2\pi c}{\lambda_R}$), which can be trasformed into

$$\lambda_R = \frac{\lambda}{n}\frac{1 - \beta_{//}^L}{1 + \beta_{//}^L} \tag{2a}$$

This expression comes out to be equal (for *n=1*) to the expression of a Thomson backscattered radiation of a laser of wavelength λ by an electron travelling on axis at speed $\beta_{//}^L c$. Expanding uo to second order in the small value $\delta = \frac{1 + a_0^2}{\gamma^2}$ we obtain

$$\lambda_R = \frac{\lambda}{4n\gamma^2}\left(1 + a_0^2\right)\left(1 + \frac{1 + a_0^2}{2\gamma^2}\right) \tag{2b}$$

In the case of a magnetic undulator the resonance condition is derived considering that the angular frequency of the oscillating electron in the field of the undulator (see Eq.1b) is $\omega_e = \beta_{//} c k_w$, so the resonance condition $n\lambda_R = cT_e - \beta_{//}^w cT_e$ now becomes

$$\lambda_R = \frac{\lambda_w}{n} \frac{1-\beta_{//}^w}{\beta_{//}^w} \tag{3a}$$

which is equivalent to

$$\lambda_R = \frac{\lambda_w}{2n\gamma^2}\left(1+a_w^2\right)\left(1+3\frac{1+a_w^2}{4\gamma^2}\right) \tag{3b}$$

It is well known[1] that there is an equivalence between a magnetic and an optical undulator: if the conditions

$$\left(1+\beta_{//}^L\right)\omega_L = c\beta_{//}^w k_w \quad ; \quad a_0 = a_w \tag{4}$$

are satisfied, the two undulators apply the same force on any electron travelling on axis and, furthermore, the emitted radiation in the forward direction on axis has the same frequency as far as we neglect the small red-shift ($\delta/2$ for the optical and $3\delta/4$ for the magnetic undulator). For an ultrarelativistic beam $\beta_{//} \approx 1$, the equivalence principle can be cast in the much simpler form

$$\lambda_w = \lambda/2 \quad ; \quad a_0 = a_w \tag{4b}$$

Therefore, we can say that if two undulators are equivalent, *i.e.* apply the same force and produce the same radiation, the two are undistinguishable by the electron beam.

Optics Communications

Volume 50, Issue 6, 15 July 1984, Pages 373-378

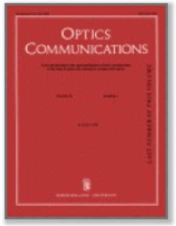

Collective instabilities and high-gain regime in a free electron laser

R. Bonifacio *, C. Pellegrini, L.M. Narducci

Show more

https://doi.org/10.1016/0030-4018(84)90105-6

Abstract

We study the behavior of a free electron laser in the high gain regime, and the conditions for the emergence of a collective instability in the electron beam-undulator-field system. Our equations, in the appropriate limit, yield the traditional small gain formula. In the nonlinear regime, numerical solutions of the coupled equations of motion support the correctness of our proposed empirical estimator for the build-up time of the pulses, and indicate the existence of optimum parameters for the production of high peak-power radiation.

969 citations

The emitted radiation wavelength is given by

$$\lambda = \frac{\lambda_w(1 + a_w^2)}{2\gamma^2}$$

The Pierce parameter is

$$\rho = \sqrt[3]{\frac{I}{I_A}\left(\frac{\lambda_w a_w}{2\pi\sigma_x}\right)^2\left(\frac{1}{2\gamma}\right)^3}$$

where λ_w is the wiggler period and, for a planar wiggler of magnetic field B_0, the wiggler paramter a_w is

$$a_w = \frac{K}{\sqrt{2}} = \frac{93.4\lambda_w B_0}{\sqrt{2}}$$

$$\Gamma = \rho$$
$$L_G = \lambda_L/(4\sqrt{3}\pi\rho)$$

$$\Gamma = \rho$$
$$L_G = \lambda_L/(4\sqrt{3}\pi\rho)$$

a. Beam emittance of the order of or smaller than the wavelength:

$$\varepsilon \leq \frac{\lambda}{4\pi}$$

b. Beam relative energy spread smaller than the FEL parameter:

$$\sigma_E / E < \rho$$

The SASE regime with exponential growth of radiation power

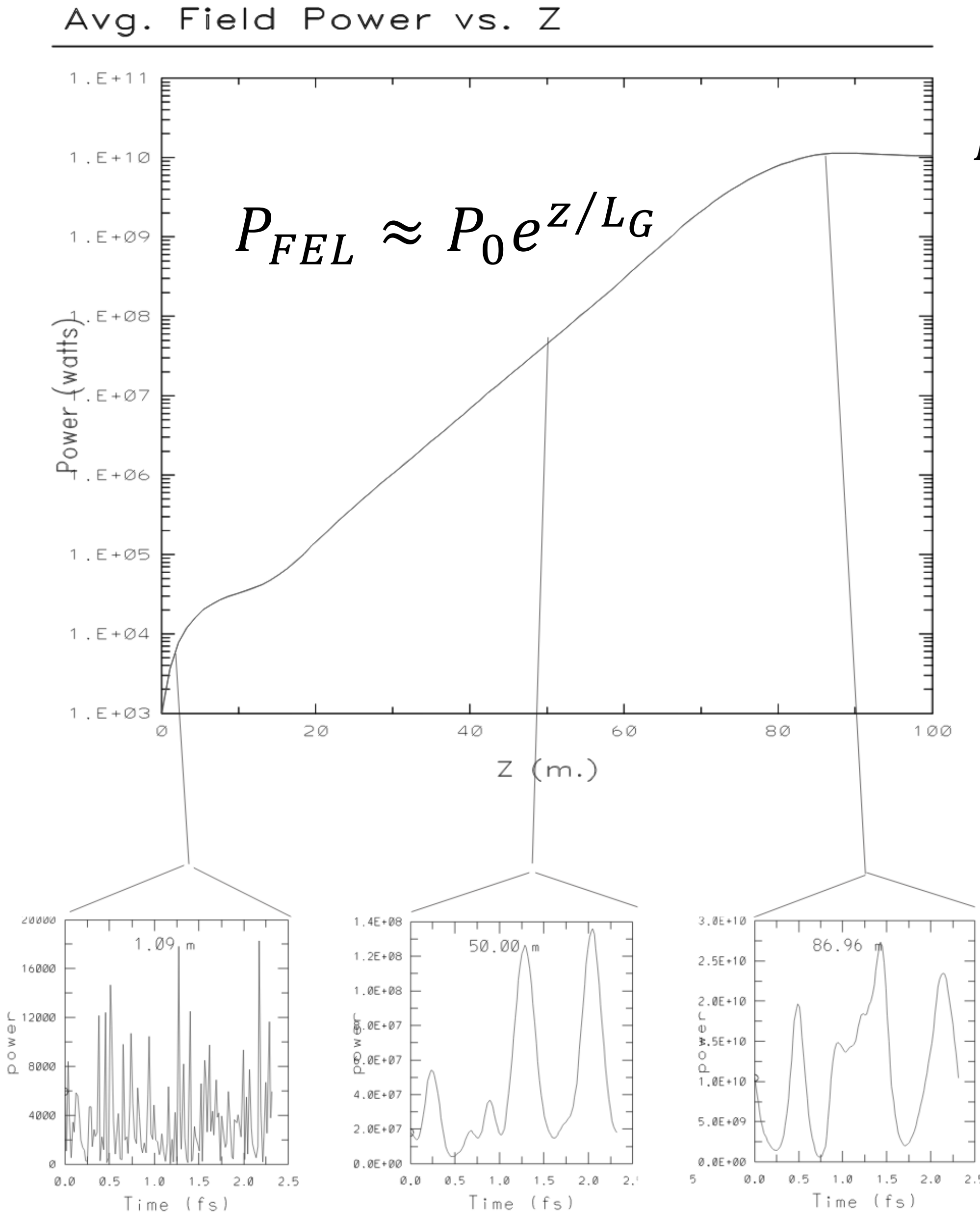

$$P_{FEL} \approx P_0 e^{z/L_G}$$

Figure 5.17 FEL output power pattern along the bunch for different position along the gain process.

$$P_{sat} \approx \rho P_{e-beam} \approx \rho I_e T_e$$

$$N_{FEL-photons} \approx N_e^{4/3}$$

Spontaneous Radiation
(Synchrotron, I.C.S.)

$$N_{photons} \approx N_e$$

Coherent emission

$$N_{photons} \approx N_e^2$$

when $L_{e\text{-}bunch} << \lambda_{rad}$

Modern X-ray FEL (LCLS)

- Linac Coherent Light Source is powered by 14 GeV beam from SLAC linear accelerator
- 2 mile long linear accelerator is followed by 130 m long undulator
- Self Amplified Spontaneous Emission FEL lases down to 10 keV photon energy
- Free Electron Laser is commissioned in 2009
- Six instruments are in operations in 0.25-2 keV and 5-9 keV energy ranges
- LCLS-II project is under way!

https://portal.slac.stanford.edu/sites/lcls_public/Pages/status.aspx

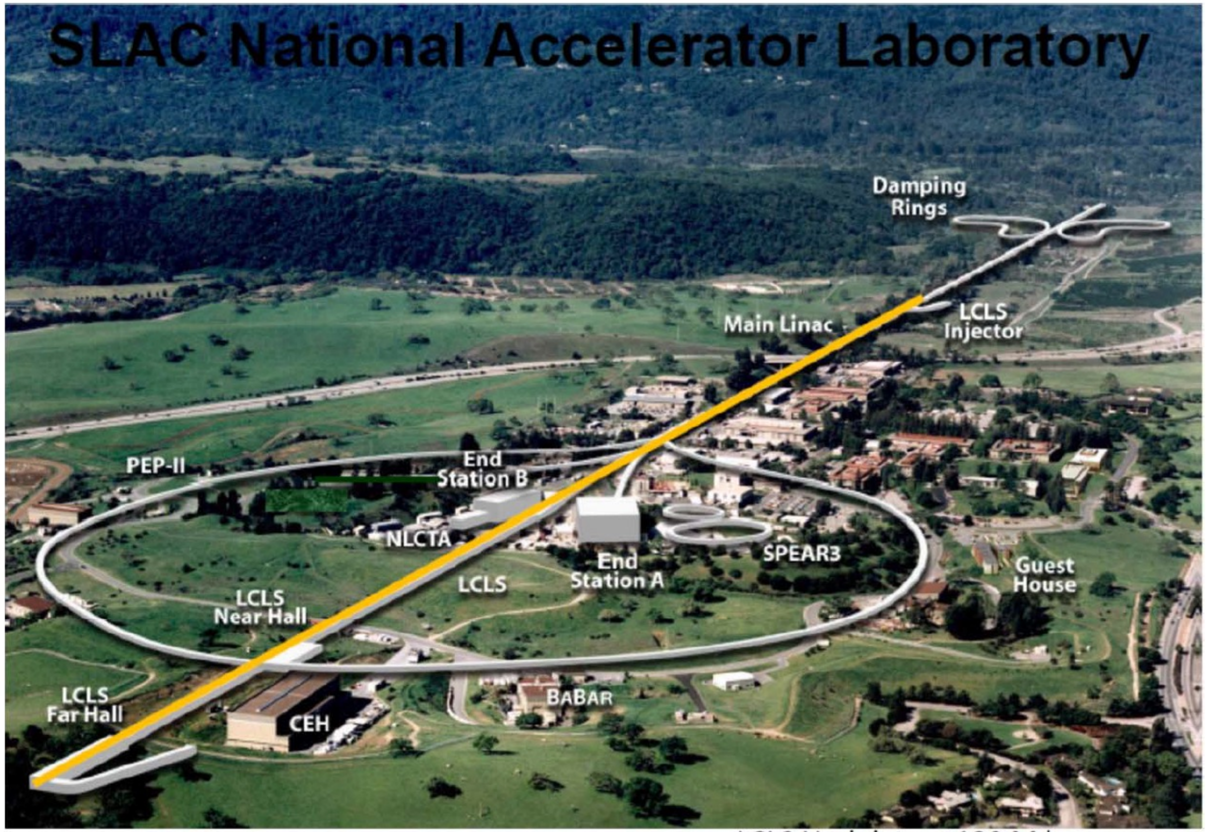

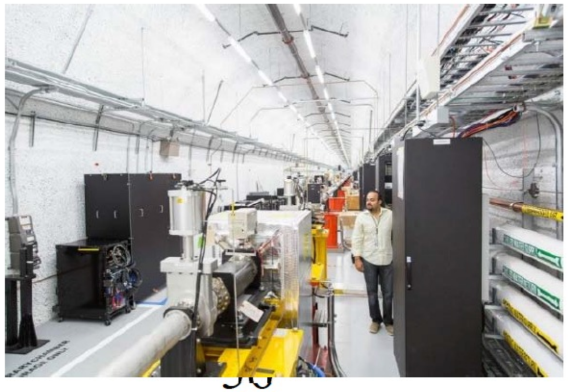

LCLS Undulator ~130 M long

U.S. DEPARTMENT OF ENERGY | Office of Science

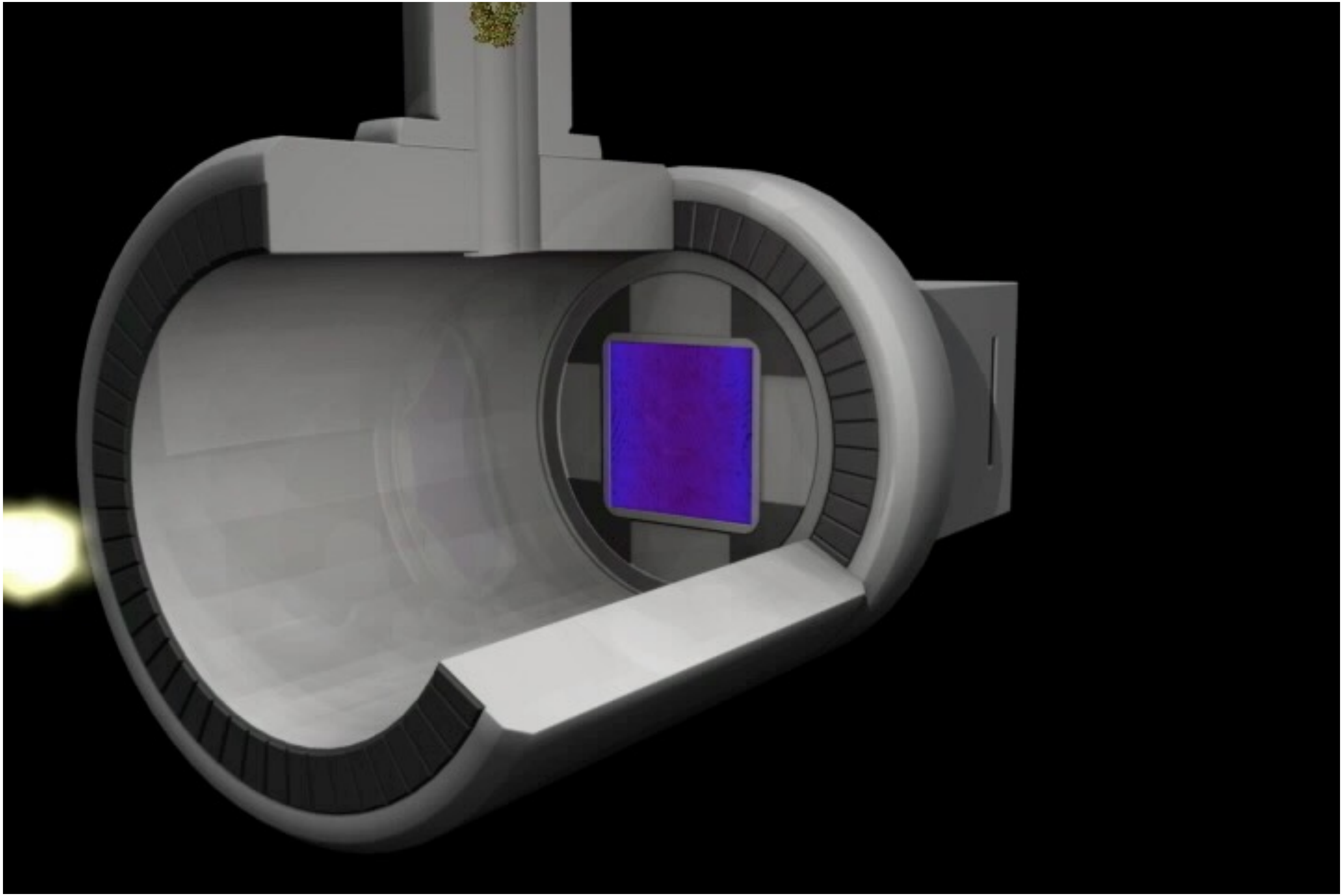

FEL resonance condition

$$\lambda_R = \lambda_w \frac{\left(1 + a_w{}^2\right)}{2\gamma^2}$$

(magnetostatic undulator)

Example : for λ_R=*1A*, λ_w=*2cm, E=7 GeV*

Violation of Energy-Momentum Conservation !!

$$\lambda_R = \lambda \frac{\left(1 + a_0^2/2\right)}{4\gamma^2}$$

(electromagnetic undulator)

Example : for λ_R=*1A, h*ν*=12 keV,* λ*=0.8*μ*m, E=25MeV*

Example : for *h*ν*=10 MeV,* λ*=0.4*μ*m, E=530 MeV*

Paradox : for E=100 GeV , λ*=0.4*μ*m , h*ν*=368 GeV !**wrong!***

$$\nu_X = \frac{4\gamma^2 \nu_L}{1+\Delta}\left(1 - \frac{\gamma^2 \vartheta^2}{1+\Delta}\right) + \textit{collective effects} \Rightarrow$$

$$\nu_X = \frac{4\gamma^2 \nu_L}{1+\Delta}\left(1 - \frac{\gamma^2 \vartheta^2}{1+\Delta} - \frac{a_0^2}{2}\right)$$

$$\Delta = \frac{4\gamma h \nu_L}{m_e c^2}$$

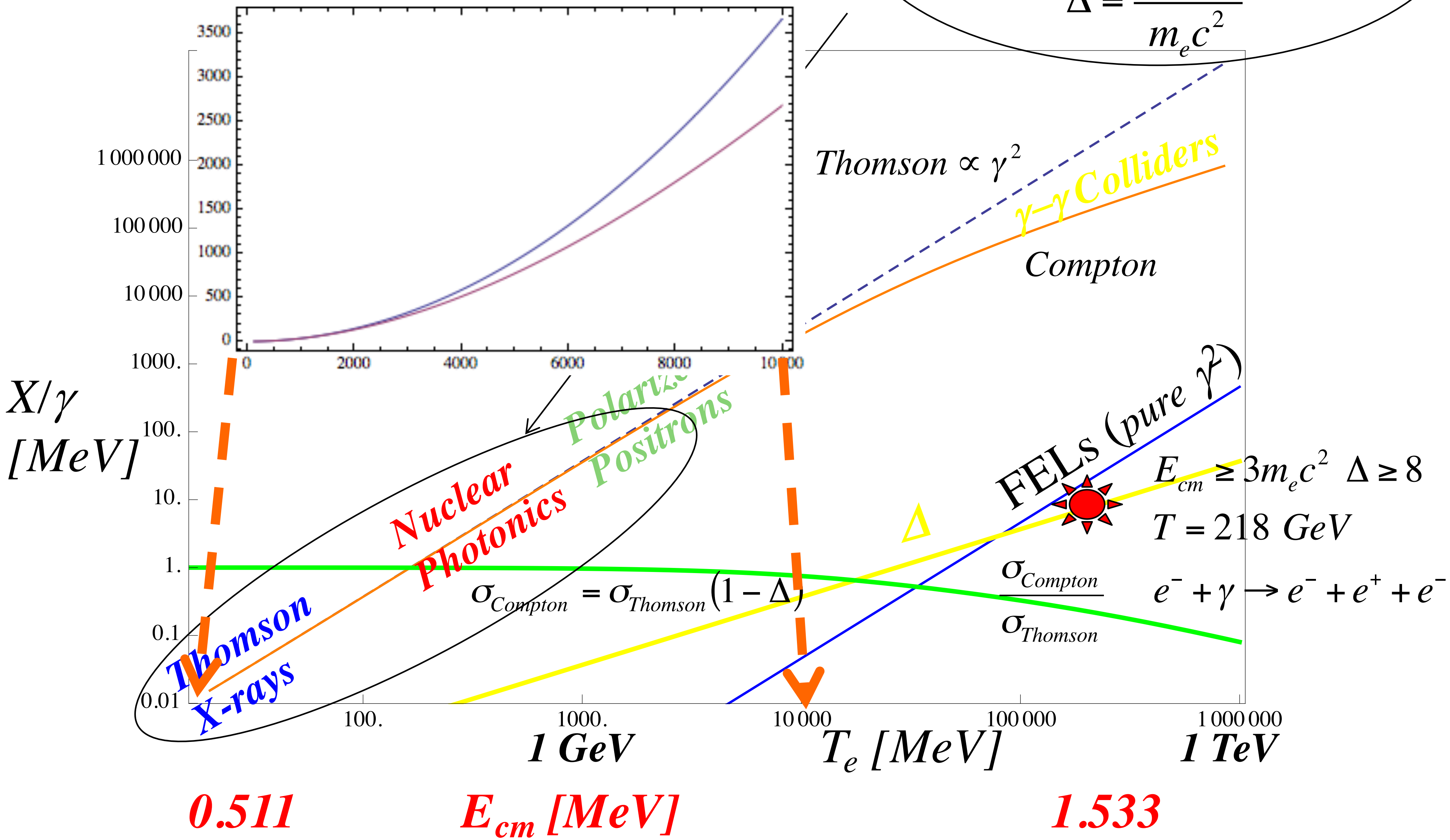

Electron Recoil effect in γ-ray I.C.S. for Nuclear Photonics: C.E.D. fails to evaluate the correct red-shift in the spectrum

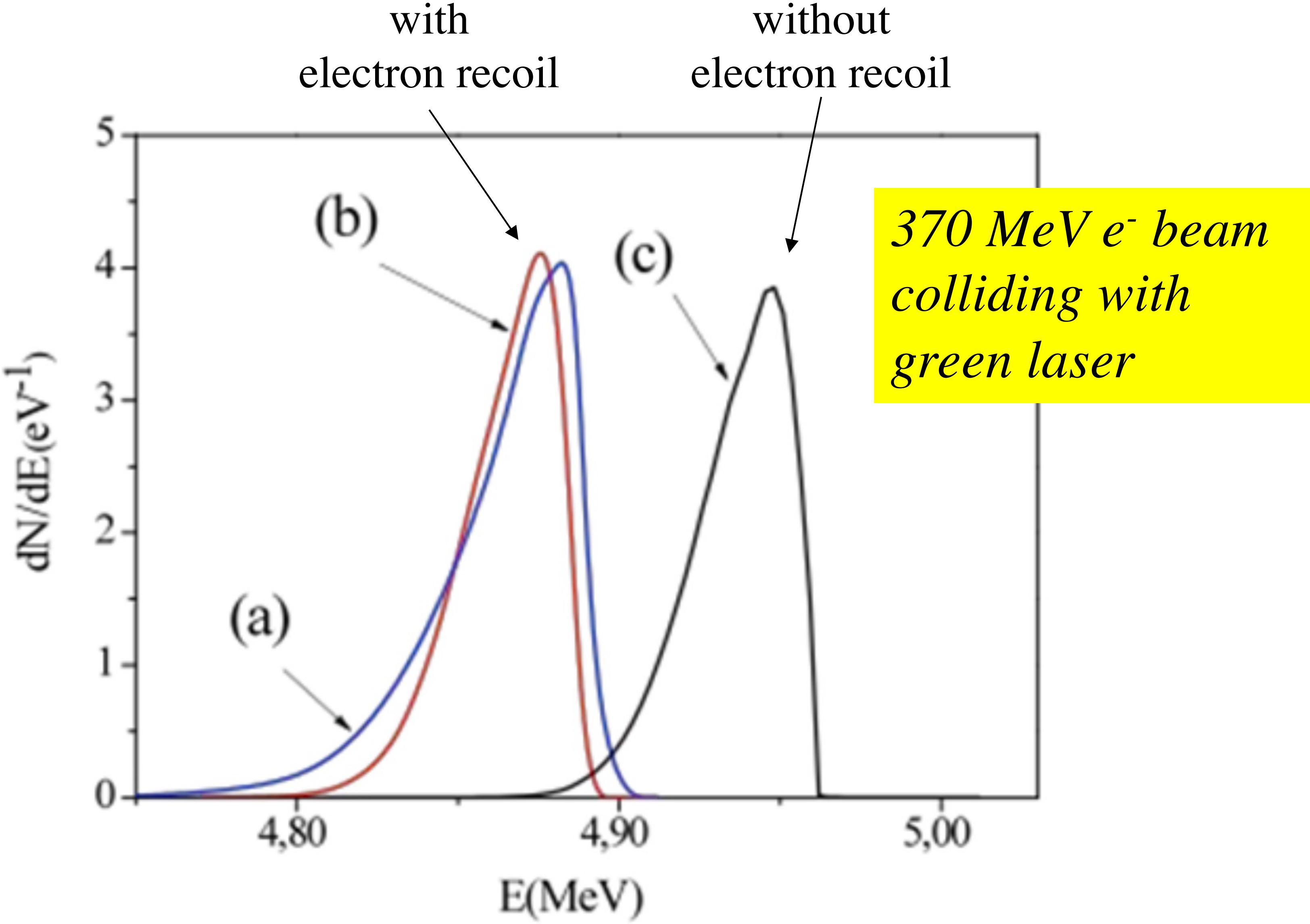

Fig. 5. **Spectra of the rays. (a) CAIN (b) Quantum model (c) Classical treatment in the case of beam (A) and for the laser parameter of Table 1 and interaction angle α=π ; rms acceptance angle θ_{rms} = 25μrad**

Istituto Nazionale di Fisica Nucleare

A journey into (Inverse) Compton Scattering

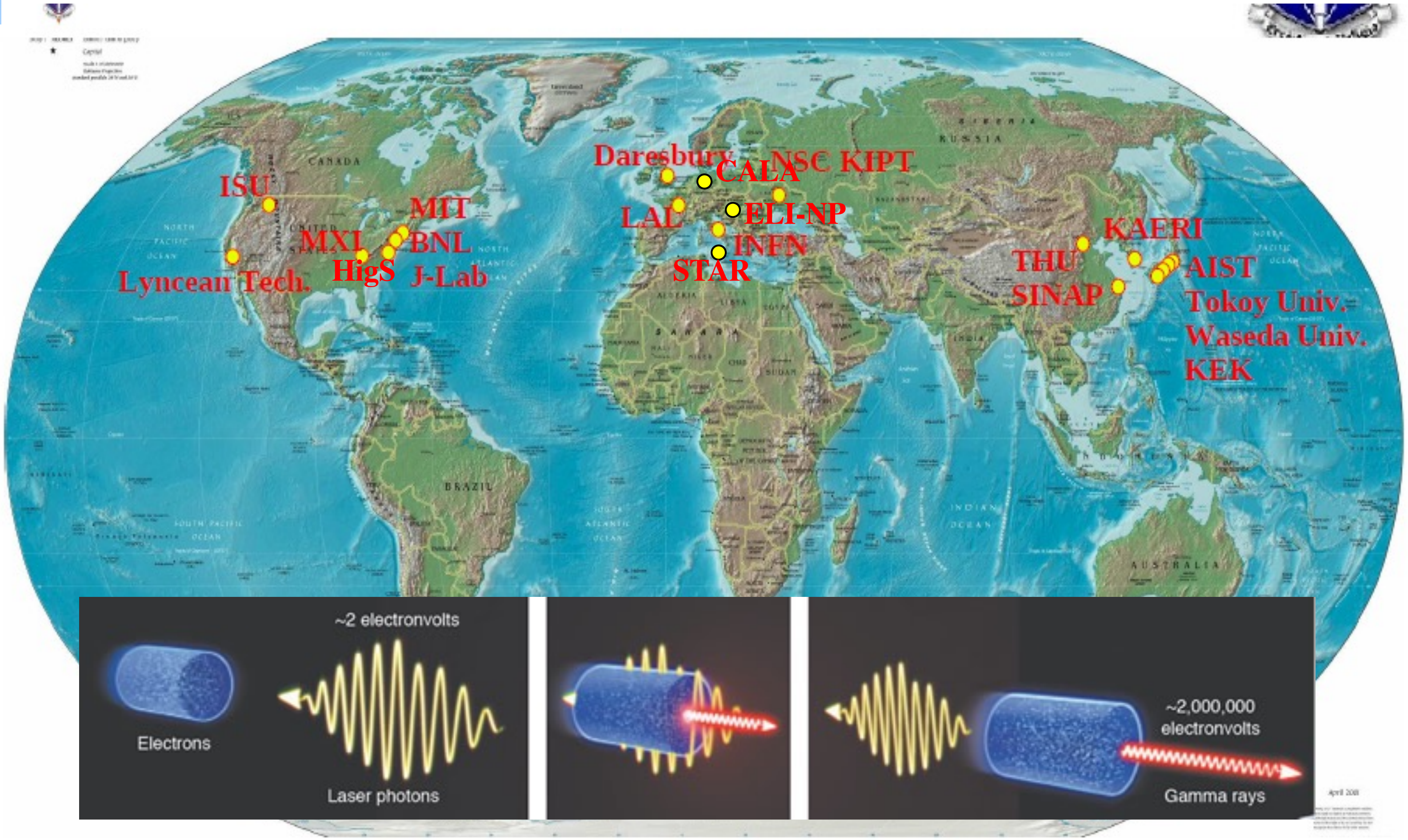

ICS are the most effective "photon accelerators" **(boost twice than FELs)**

"$4\gamma^2$ boost effect" $E_{X/\gamma} = 4\gamma^2 E_{laser}$ $T = (\gamma - 1) m_0 c^2$ m_0=511 keV

$$with\ T = 100\,MeV\ (\gamma = 197)\ E_{laser} = 1.2\ eV \Rightarrow E_{X/\gamma} = 186\ keV$$

incident electron

$E_e = \gamma mc^2$

incident photon E_{ph}

Lab Reference Frame

Kinematics of Inverse Compton Scattering a Cartoon

Lorentz transformation ($\gamma_{cm} = \gamma$)

$$
\begin{cases}
E_{ph} = p^*_{ph}\gamma_{cm}\left(1+\sqrt{1-\frac{1}{\gamma^2_{cm}}}\cos\theta^*\right)\\
p_{phx} = p^*_{ph}\sin\theta^*\cos\phi^*\\
p_{phy} = p^*_{ph}\sin\theta^*\sin\phi^*\\
p_{phz} = p^*_{ph}\gamma_{cm}\left(\sqrt{1-\frac{1}{\gamma^2_{cm}}}+\cos\theta^*\right)
\end{cases}
$$

Electron res

$E^*_e = m$

$E^*_{ph} = 2\gamma E_{ph}$

red photon at

$\gamma \quad E'_{ph} = E'_0/2$

$=1/\gamma$

θ

Lab Referen

after Sca

scattered electron

$E'_e = \gamma mc^2 + E_{ph} - E'_{ph}$

energy of scattered photon at $\theta=0$ $\quad E'_0 = 2\gamma E^*_{ph} = 4\gamma^2 E_{ph}$

Rivaling with Synchr. Light Sources for energies above 50 keV

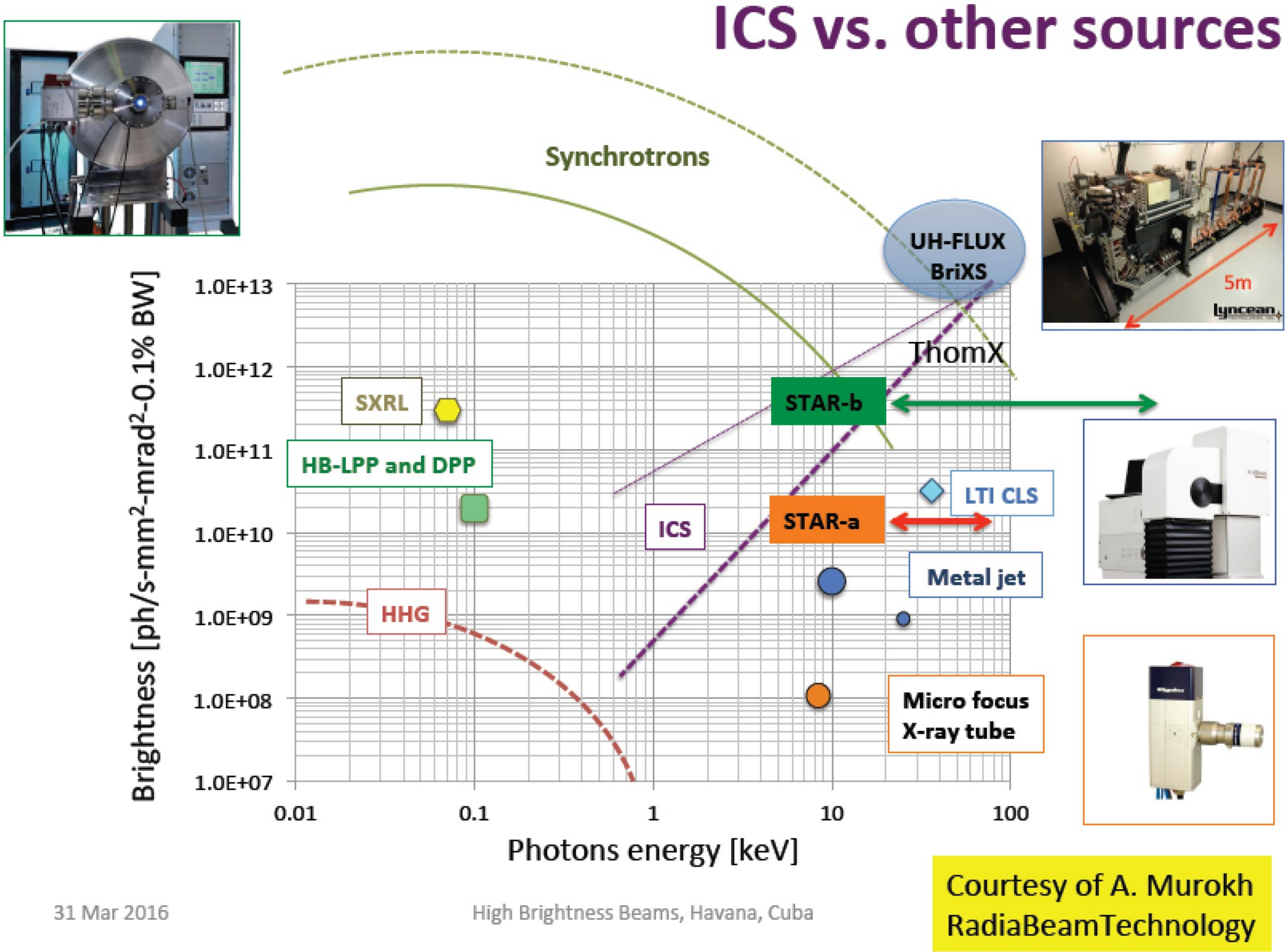

Inverse Compton Sources rivaling/overcoming Synchrotron Light Sources at photon energies above 80-100 keV

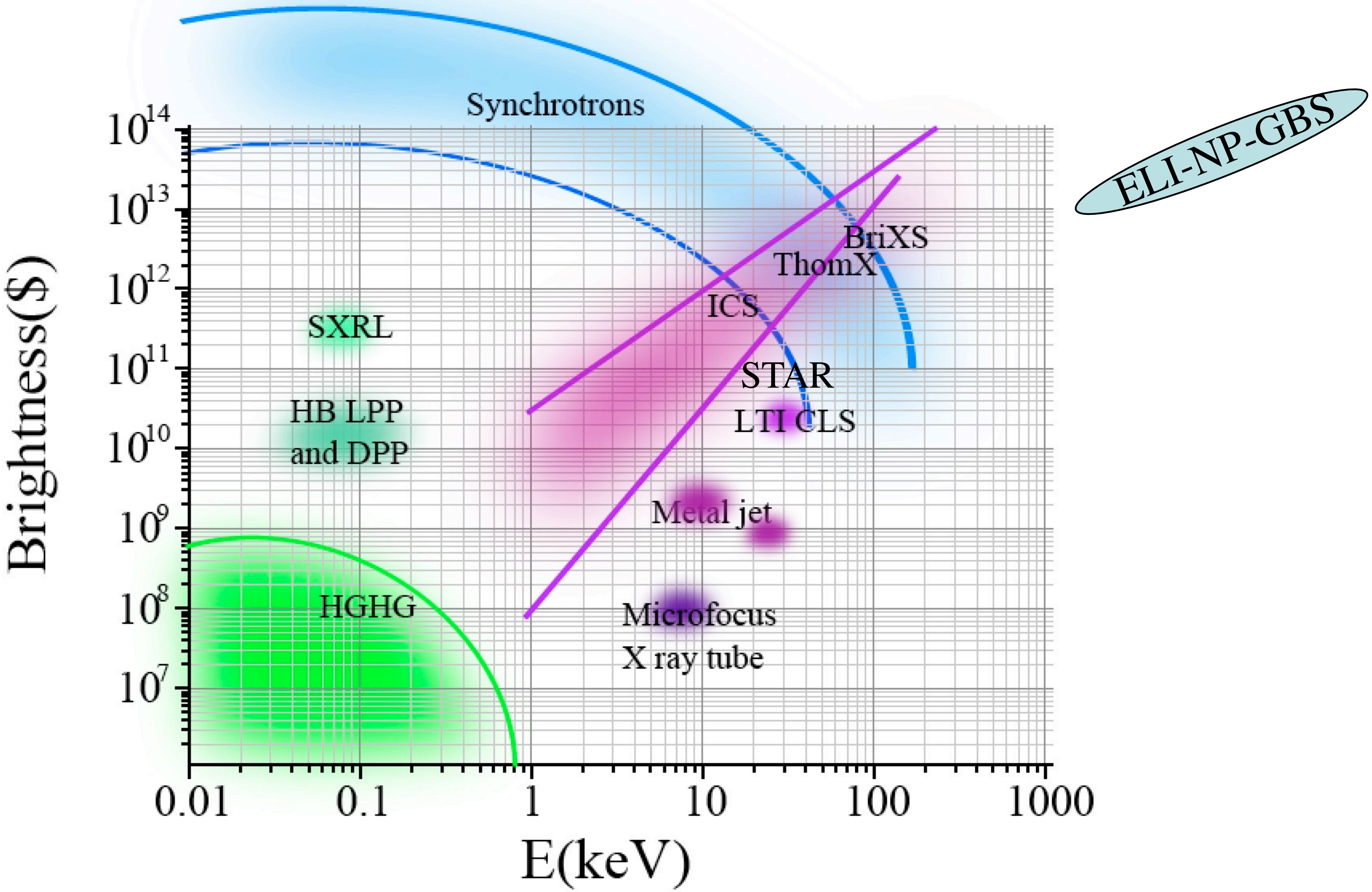

Figure 1: Brightness of several radiation sources as a function of the photon energy. $: Photon $number/s/mm^2/mrad^2/(0.1\%$.
I.C.S. Sources (LTI-CLS,ThomX, STAR, UH-FLUX and BriXS) are compared to Synchrotron Light Sources and the most performing X-ray tube so far (Metal Jet).

An ICS based *X*-ray User Facility in operation in Germany

E17 Lehrstuhl für Biomedizinische Physik

Technische Universität München

Biomedical imaging with the lab-sized laser-driven synchrotron source Munich Compact Light Source

Klaus Achterhold

Biomedical Physics, Physics-Department E17, Technische Universität München

Compact machine
10x10 m^2
In operation since early 2015

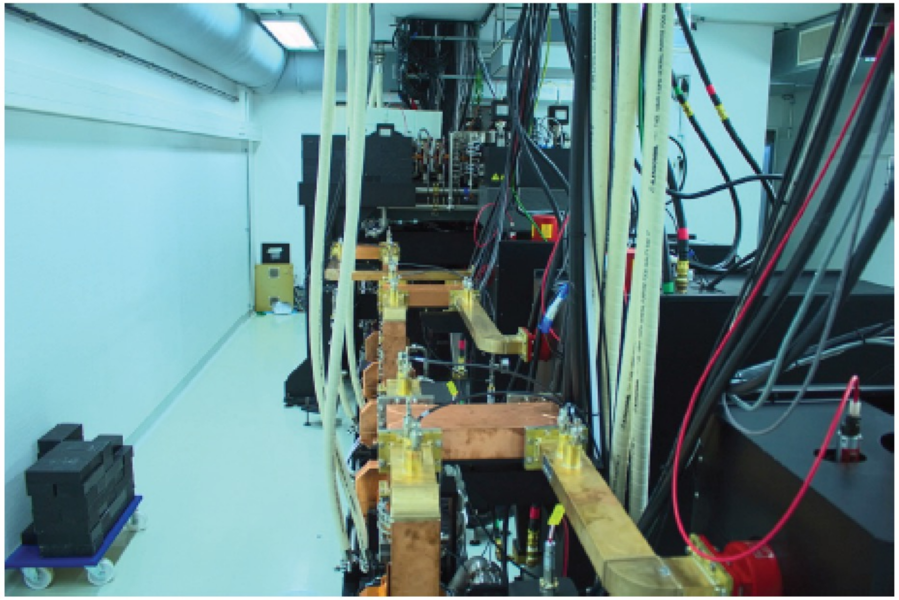

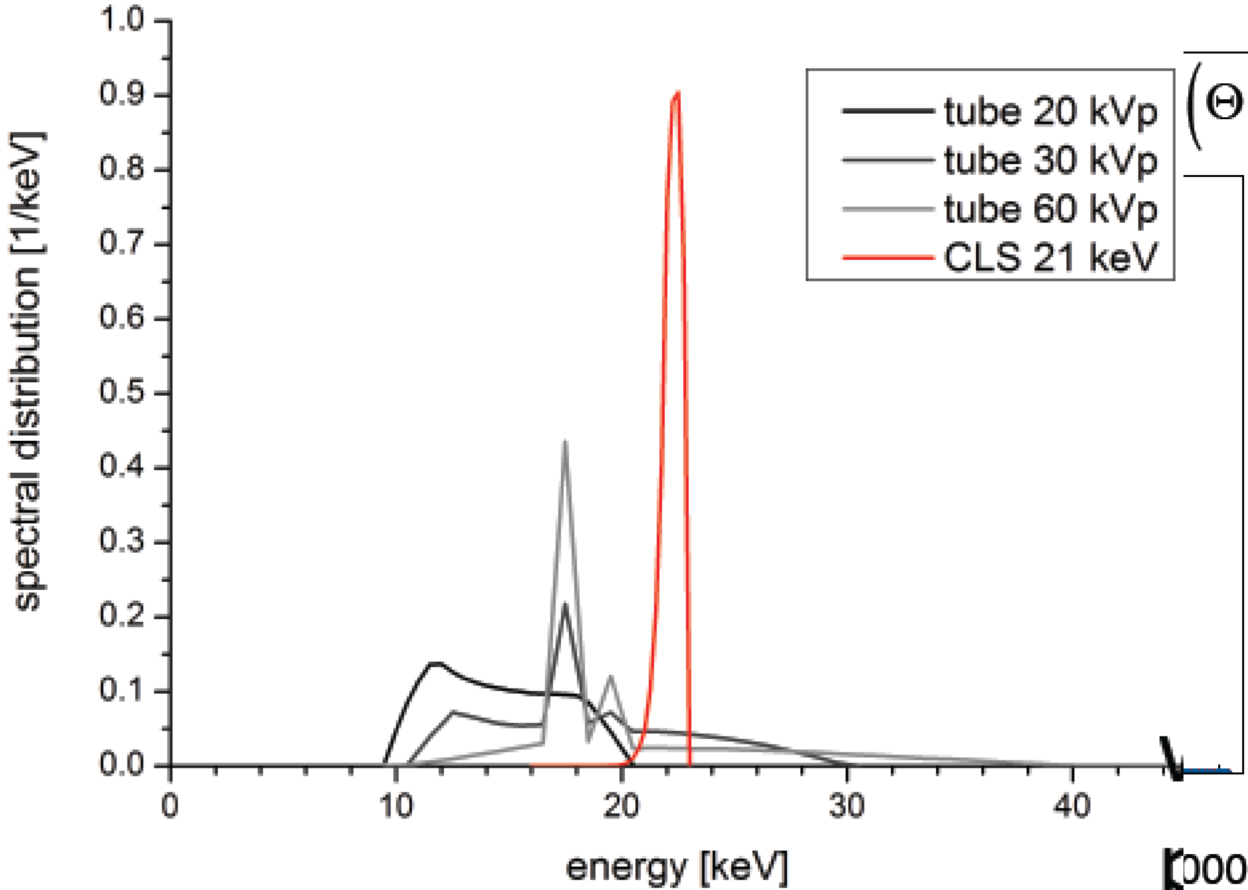

$(\Theta+\alpha))$

measured
Spectrum of X-rays
into +/- 2 mrad

Bandwidth

000+0.0016 · ΔT with ΔT/T=0.3%

35000+30000 · ΔE_L with $\Delta E_L/E_L=10^{-12}$

35000-9000 · $\Delta\alpha^2$ with Δα=0.03

Measured $5{\cdot}10^{10}$ ph/sec with 20 mA

$$E_x\left(\Theta,\alpha,E_L,T\right)=\frac{\left(1+\beta\cos\alpha\right)E_L}{1-\beta\cos\Theta+\left(E_L/mc2\right)\left(1+\cos\left(\Theta+\alpha\right)\right)}$$

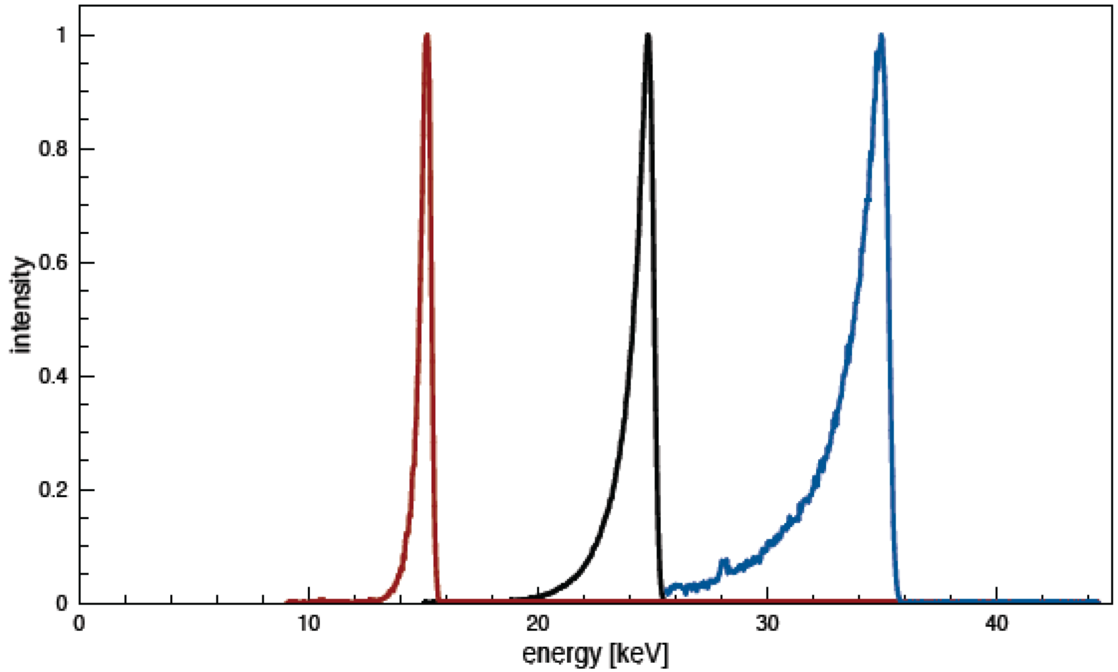

measured
Spectrum of X-rays
into +/- 2 mrad

Bandwidth

$35000+0.0016\cdot\Delta T$ with $\Delta T/T=0.3\%$
$35000+30000\cdot\Delta E_L$ with $\Delta E_L/E_L=10^{-12}$

$35000-9000\cdot\Delta\alpha^2$ with $\Delta\alpha=0.03$

Measured $5\cdot10^{10}$ ph/sec with 20 mA

Great example of Radio-logical imaging applied to mass screening over population: mammography

Conventional X-ray tube for mammography

Spatial resolution ~100 μm

High Flux ~10^7 γ/(mm^{2}s) equivalent to ~$5 \cdot 10^{11}$ γ/s over 20x20 cm^2 area.

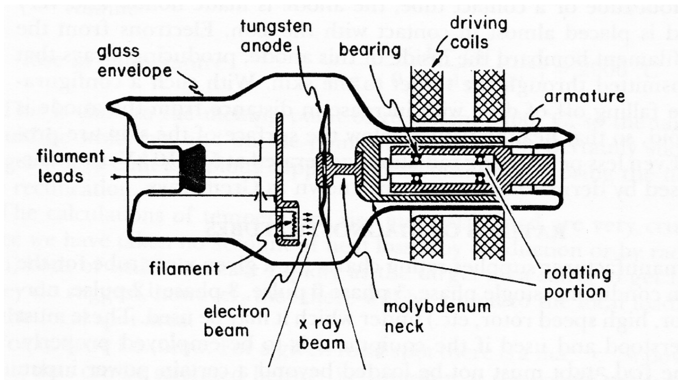

Anode Material	Molybdenum
Anode Angle	12?
Anodic Voltage	28 kV
Filtrations	1 mm Be 0.03 mm Mo 600 mm Air

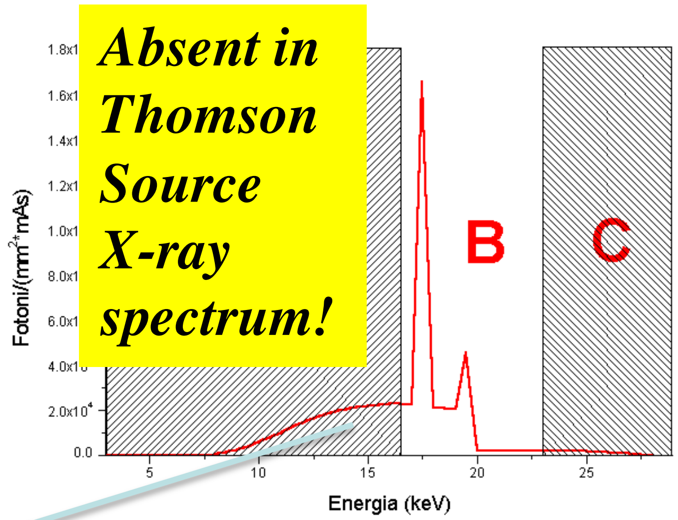

Low energy photons in the spectrum are absorbed by tissue, delivering radiation dose without bringing informations to detector. Risk of inducing secondary tumors increases without increasing the benefit of detecting early tumors

Mammography with Mono-chromatic X-rays at 20 keV has been proven far superior in Signal-to-Noise-Ratio w.r.t. conventional mammographic tubes, with a considerably lower radiation dose to the tissue

Conventional
X-ray tube 26 kVp
MGD 1 mGy

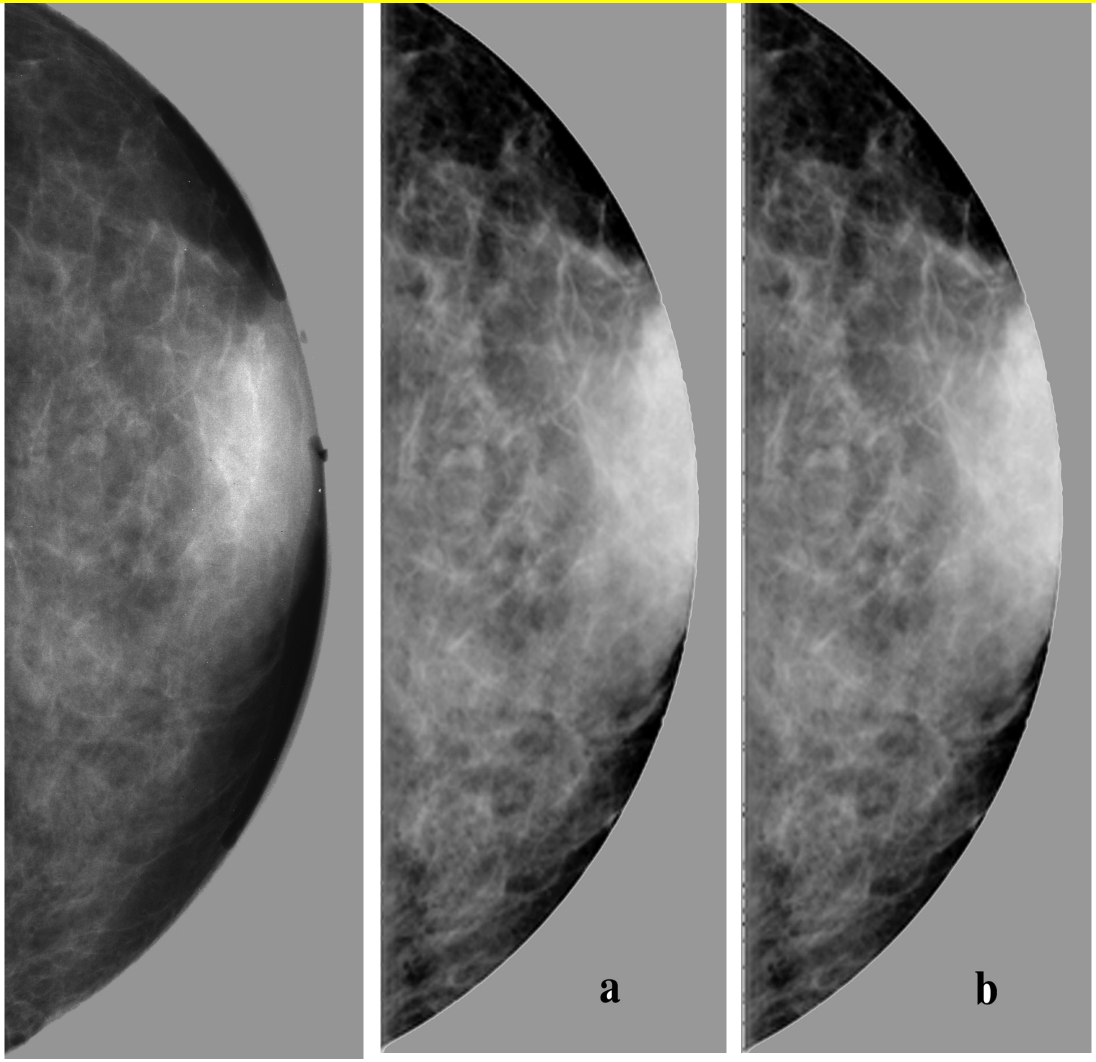

a) SR digital image
Energy 17 keV
Scan step 100 mm
MGD 1 mGy

b) SR digital image
Energy 20 keV
Scan step 100 mm
MGD 0.33 mGy

3 cm thick in vitro human breast tissue

Compact Thomson X-ray Sources could be located inside hospitals to diagnose and treat patients directly at the hospital site (unlike Synchrotrons…)

IOP Publishing | Institute of Physics and Engineering in Medicine Physics in Medicine & Biology

Phys. Med. Biol. 61 (2016) 1634–1649 doi:10.1088/0031-9155/61/4/1634

Towards breast tomography with synchrotron radiation at Elettra: first images

R Longo[1,2], F Arfelli[1,2], R Bellazzini[3,4], U Bottigli[5], A Brez[3,4], F Brun[2,6], A Brunetti[7], P Delogu[4,8], F Di Lillo[9], D Dreossi[10], V Fanti[11], C Fedon[1,2], B Golosio[7], N Lanconelli[12], G Mettivier[9], M Minuti[3,4], P Oliva[7], M Pinchera[3,4], L Rigon[1,2], P Russo[9], A Sarno[9], G Spandre[3,4], G Tromba[10] and F Zanconati[13]

Istituto Nazionale di Fisica Nucleare

E17 Lehrstuhl für Biomedizinische Physik

Technische Universität München

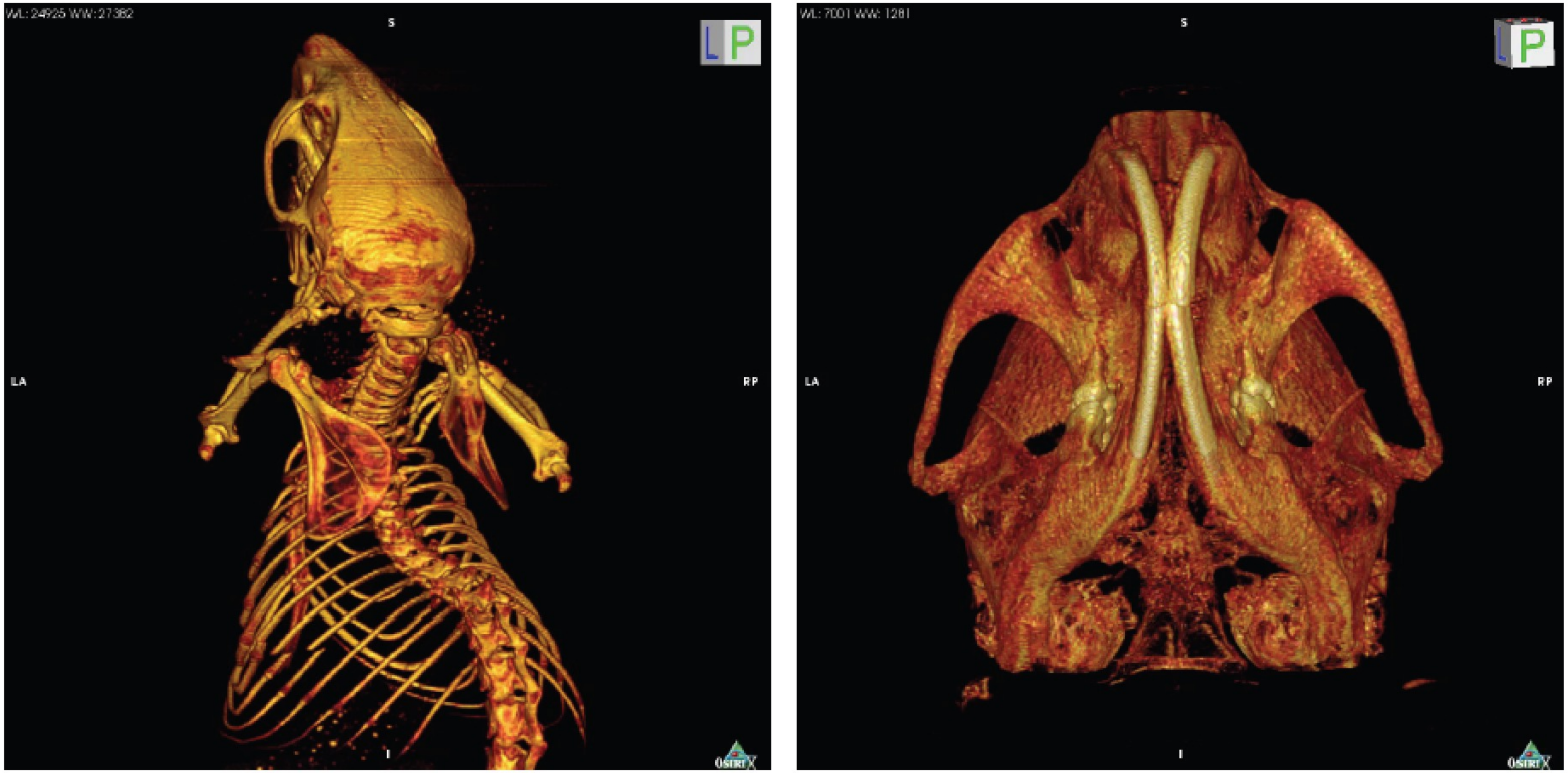

small source size → high resolution (81 μm)
monochromatic → no beam hardening artefacts

Klaus.Achterhold@tum.de

Phase Contrast Imaging made possible by small round source spot size (< 20 μm)

SCIENTIFIC REPORTS

OPEN

Mono-Energy Coronary Angiography with a Compact Synchrotron Source

Received: 05 October 2016
Accepted: 06 January 2017
Published: 09 February 2017

Elena Eggl[1,2], Korbinian Mechlem[1,2,3], Eva Braig[1,2,3], Stephanie Kulpe[1,2], Martin Dierolf[1,2], Benedikt Günther[1,2,4], Klaus Achterhold[1,2], Julia Herzen[1,2], Bernhard Gleich[2], Ernst Rummeny[3], Peter B. Noël[1,3], Franz Pfeiffer[1,2,3] & Daniela Muenzel[3]

X-ray coronary angiography is an invaluable tool for the diagnosis of coronary artery disease. However, the use of iodine-based contrast media can be contraindicated for patients who present with chronic renal insufficiency or with severe iodine allergy. These patients could benefit from a reduced contrast agent concentration, possibly achieved through application of a mono-energetic x-ray beam. While large-scale synchrotrons are impractical for daily clinical use, the technology of compact synchrotron sources strongly advanced during the last decade. Here we present a quantitative analysis of the benefits a compact synchrotron source can offer in coronary angiography. Simulated projection data from quasi-mono-energetic and conventional x-ray tube spectra is used for a CNR comparison. Results show that compact synchrotron spectra would allow for a significant reduction of contrast media. Experimentally, we demonstrate the feasibility of coronary angiography at the Munich Compact Light Source, the first commercial installation of a compact synchrotron source.

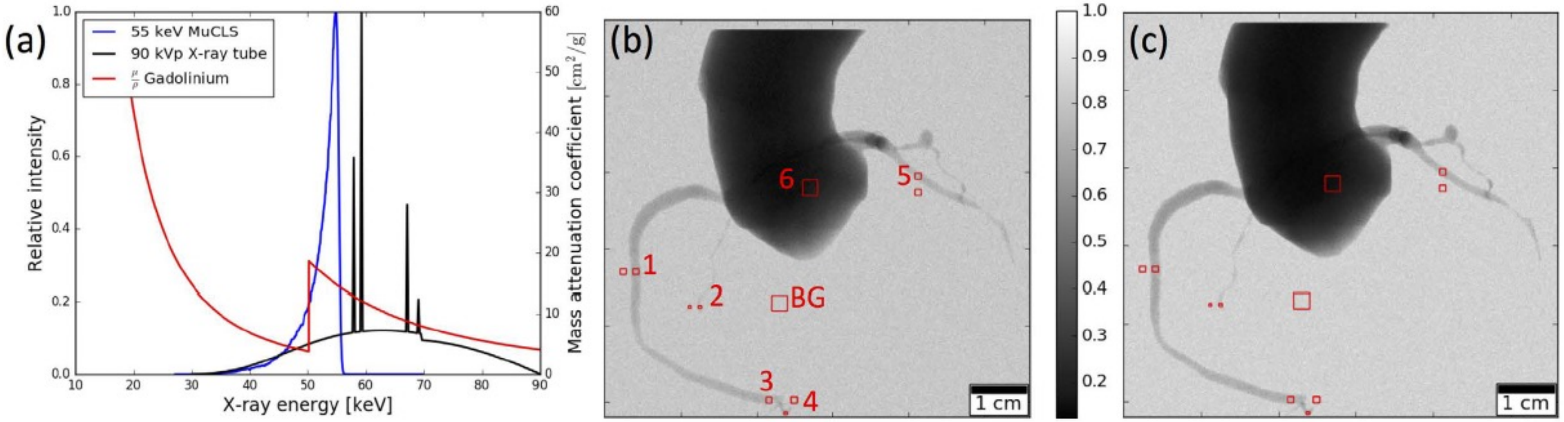

Figure 2. (**a**) MuCLS spectrum rescaled at 55.8 keV peak energy, x-ray tube spectrum at 90 kVp and mass attenuation coefficient of gadolinium. (**b**) Simulated gadolinium-based angiography image for the 90 kVp x-ray tube spectrum. (**c**) Simulated gadolinium-based angiography image for the 55 keV MuCLS spectrum.

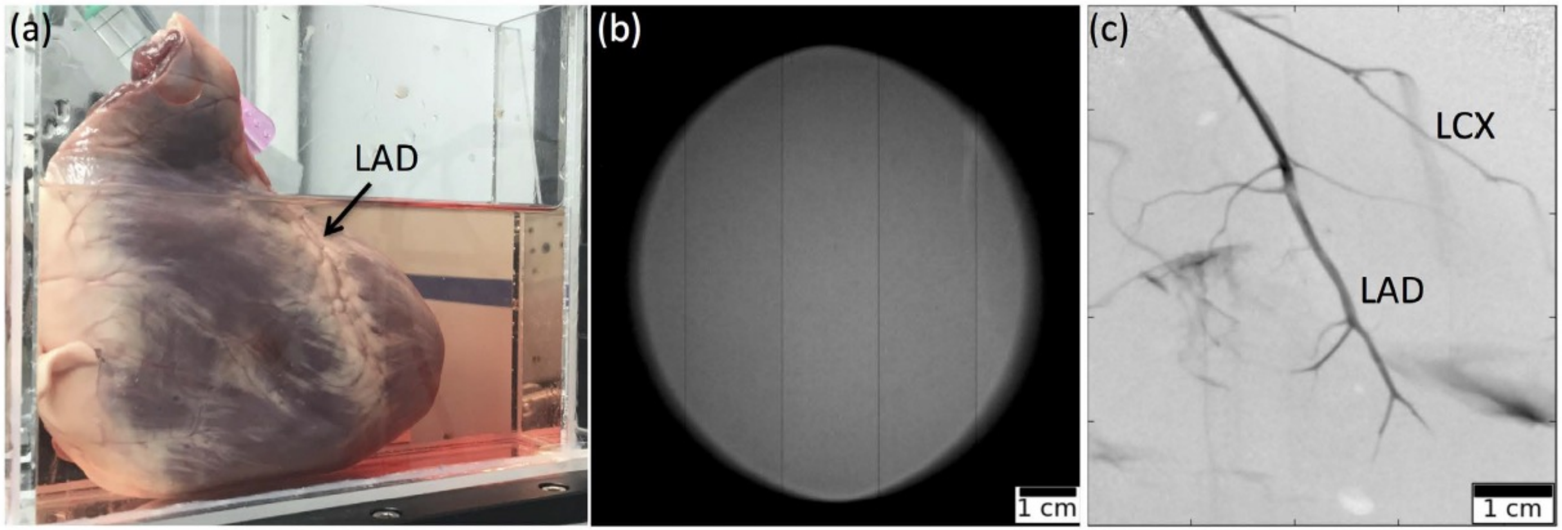

Figure 3. MuCLS angiography image. (**a**) Photograph of the sample in waterbath. (**b**) Empty image of full MuCLS beam. (**c**) Quasi-mono-energetic angiography image of a porcine heart acquired at the MuCLS, with iodine-based contrast agent injected into the left coronary artery. Visible are the left anterior descending artery (LAD) and the left circumflex artery (LCX).

SCIENTIFIC REPORTS

OPEN

Trabecular bone anisotropy imaging with a compact laser-undulator synchrotron x-ray source

Received: 9 March 2017
Accepted: 18 October 2017
Published online: 03 November 2017

Christoph Jud[1], Eva Braig[1,2], Martin Dierolf[1], Elena Eggl[1], Benedikt Günther[1,3], Klaus Achterhold[1], Bernhard Gleich[1], Ernst Rummeny[2], Peter Noël[2], Franz Pfeiffer[1,2,4] & Daniela Muenzel[2]

Figure 2. Attenuation and XVR images of a human hand, showing the radius, ulna, carpals and metacarpals. In (**A**) the integrated attenuation coefficient is depicted. (**B**) Depicts the mean scattering strength. (**C**) Illustrates the degree of anisotropy, i.e. the difference of maximum and minimum scattering divided by its sum. The mean values in the colored ROI's are $da_{cyan} = 0.27$, $da_{purple} = 0.08$ and $da_{green} = 0.41$. In (**D**) the orientation of scattering structures is color-coded according to the color wheel shown in the bottom left. Brightness once again corresponds to the degree of anisotropy.

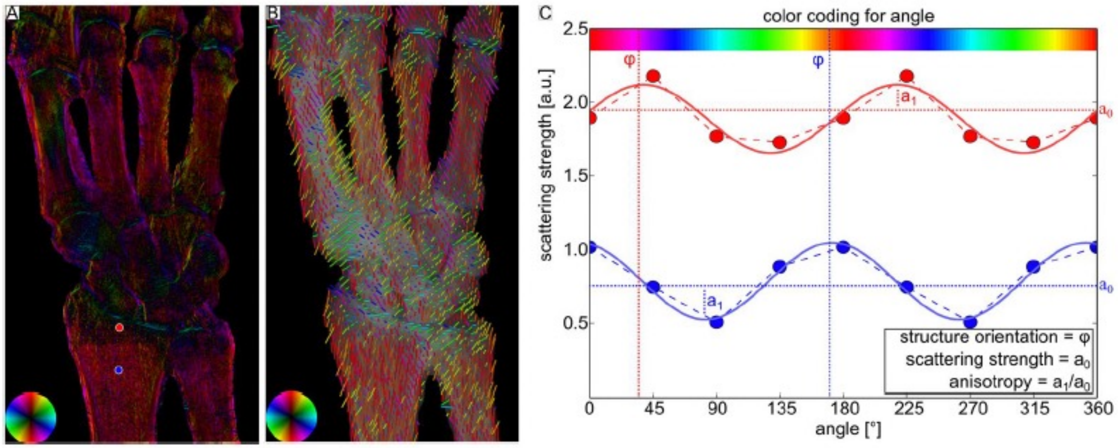

Figure 3. Illustration of how the XVR-data is extracted from different dark-field contrast (DFC) images. In (**A**) the orientation of scattering structures is shown color-coded, the brightness corresponds to the degree of anisotropy. (**B**) Illustrates an alternative representation using a vector field. Their color emphasizes the direction, the degree of anisotropy is encoded by the length. (**C**) Depicts the scattering strength versus the sample orientation relative to the grating interferometer for two pixels marked by a red dot and a blue dot in A. From the sinusoidal fit, a_0 corresponds to the mean scattering, the phase ϕ corresponds to the angle of maximal scattering and the ratio a_1/a_0 to the degree of anisotropy.

Journal of
Synchrotron Radiation
ISSN 0909-0495

Received 6 September 2008
Accepted 23 October 2008

Hard X-ray phase-contrast imaging with the Compact Light Source based on inverse Compton X-rays

Martin Bech,[a]* Oliver Bunk,[b] Christian David,[b] Ronald Ruth,[c,d] Jeff Rifkin,[c] Rod Loewen,[c] Robert Feidenhans'l[a] and Franz Pfeiffer[b,e]*

[a]University of Copenhagen, Universitetsparken 5, DK-2100 Copenhagen, Denmark, [b]Paul Scherrer Institut, CH-5232 Villigen PSI, Switzerland, [c]Lyncean Technologies Inc., 370 Portage Avenue, Palo Alto, CA 94306, USA, [d]Stanford Linear Accelerator Center, 2575 Sand Hill Road, Menlo Park, CA 94025, USA, and [e]École Polytechnique Fédérale de Lausanne, CH-1015 Lausanne, Switzerland. E-mail: bech@fys.ku.dk, franz.pfeiffer@psi.ch

The first imaging results obtained from a small-size synchrotron are reported. The newly developed Compact Light Source produces inverse Compton X-rays at the intersection point of the counter propagating laser and electron beam. The small size of the intersection point gives a highly coherent cone beam with a few milliradian angular divergence and a few percent energy spread. These specifications make the Compact Light Source ideal for a recently developed grating-based differential phase-contrast imaging method.

Keywords: medical X-ray imaging; phase contrast; inverse Compton X-rays.

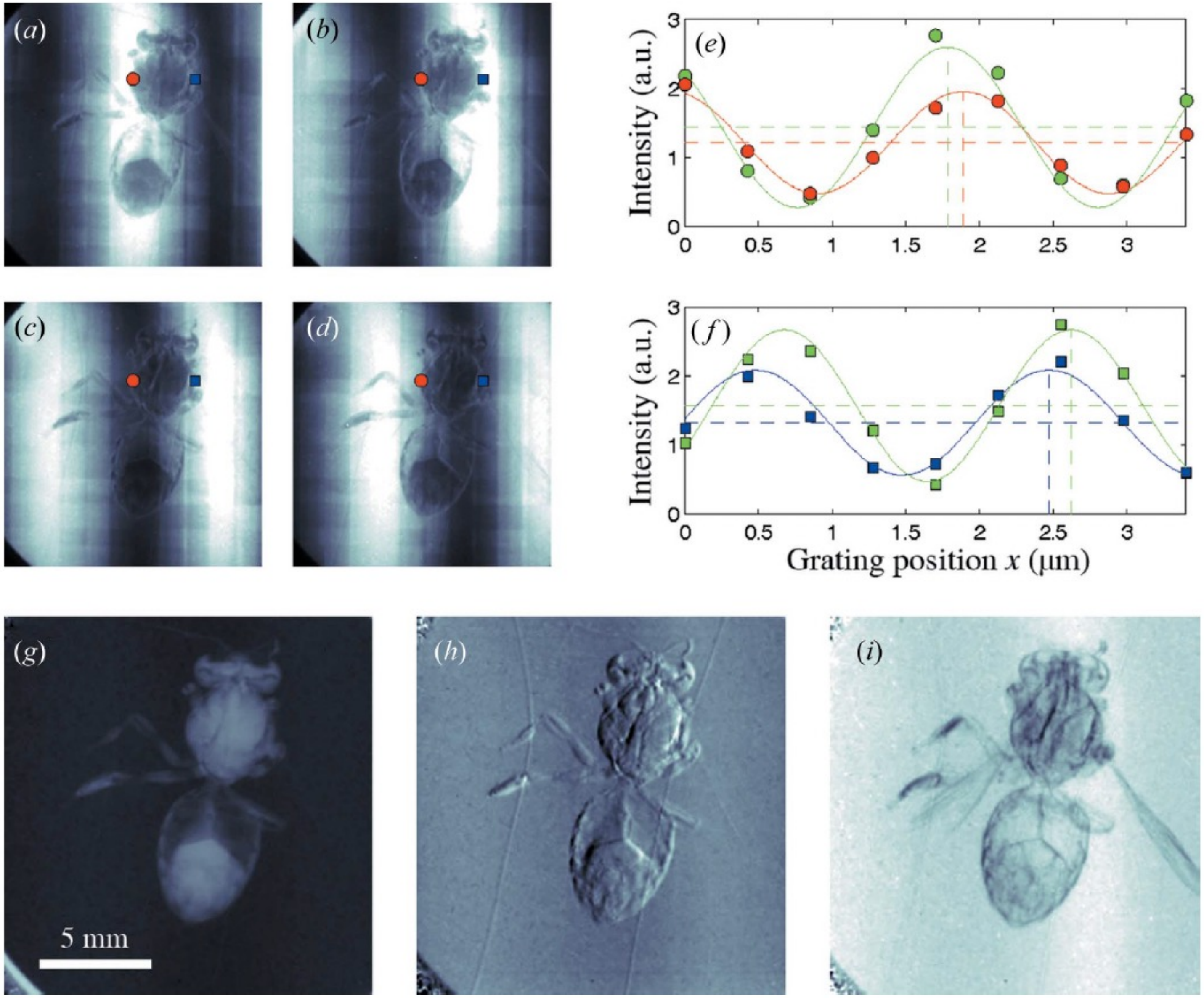

Figure 2

X-ray images of a bee and pixel intensity variations. (*a*)–(*d*) Raw images during phase stepping. (*e*)–(*f*) Intensity plot of two detector pixels during phase stepping. The green plot is from the flat-field data (without sample present), red and blue plots are with sample present corresponding to the intensity in the red and blue pixels in (*a*)–(*d*). Panels (*g*)–(*i*) show the three types of contrast obtained from data processing: (*g*) standard absorption image, (*h*) differential phase-contrast image, (*i*) dark-field image.

Istituto Nazionale di Fisica Nucleare

Advancing Thomson X Ray Sources for Bio/Medical Imaging Applications and Matter Science

NUCLEAR INSTRUMENTS & METHODS IN PHYSICS RESEARCH

Section A: accelerators, spectrometers, detectors and associated equipment

Volume 608 (2009), Issue 1S
Supplement

COMPTON 2008

Compton sources for X/γ rays:
Physics and applications
Alghero, Sardinia, Italy, September 7–12, 2008

Edited by Massimo Carpinelli, Luca Serafini

Abstracted/Indexed in: Current Contents: Engineering, Computing and Technology; Current Contents: Physical, Chemical and Earth Sciences; EI Compendex Plus; Engineering Index; INSPEC. Also covered in the abstract and citation database SCOPUS®. Full text available on ScienceDirect®.

0168-9002(20090901)608:1s;1-V

608 1S

NUCLEAR INSTRUMENTS AND METHODS IN PHYSICS RESEARCH (SECTION A)—VOL. 608/1S (2009) S1–S120

ELSEVIER

ELSEVIER

Volume 608, Issue 1S
Supplement

September 1, 2009

ISSN 0168-9002

COMPTON 2008

Compton sources for X/γ rays:
Physics and applications

Alghero, Sardinia, Italy
September 7–12, 2008

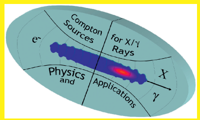

Guest Editors

Massimo Carpinelli
Luca Serafini

Advanced Medical Imaging with Synchrotron and Compton X-ray Sources

21-22 November 2019
Bologna
Europe/Rome timezone

- Overview
- Organizing Commitee
- Scientific Commitee
- Invited Speaker
- Scientific Programme
- Timetable
- Contribution List
- Registration
- Participant List
- Travel Information
- Help to reach the Conference Sites

Conctat

armando.bazzani@bo.in...

New X rays sources based on the inverse Compton scattering process are under development or already operational. Their beam quality is comparable to that available at modern synchrotron light sources. The moderate footprint and financial involvment makes them suitable for clinical use.

The first session will compare some of them with an emphasis on their possible use for medical applications. Location: sala Ulisse, Accademia delle Scienze, Via Zamboni 31.

The second session will present results obtained on preclinical and clinical images with ELETTRA synchrotron light source and the compact CLS source at Munich and techniques developed to improve the image quality, in particular for soft tissues and cartilages. This session is specially addressed to physicians whose expectations are crucial to the development of future sources. Location: Aula Anfiteatro, Centro di Ricerca Codivilla Putti, IRCCS Istituto Ortopedico Rizzoli, Via di Barbiano 1/10.

Accelerator and Equipments
in ELI-NP Building
100 m, 100 M$ scale

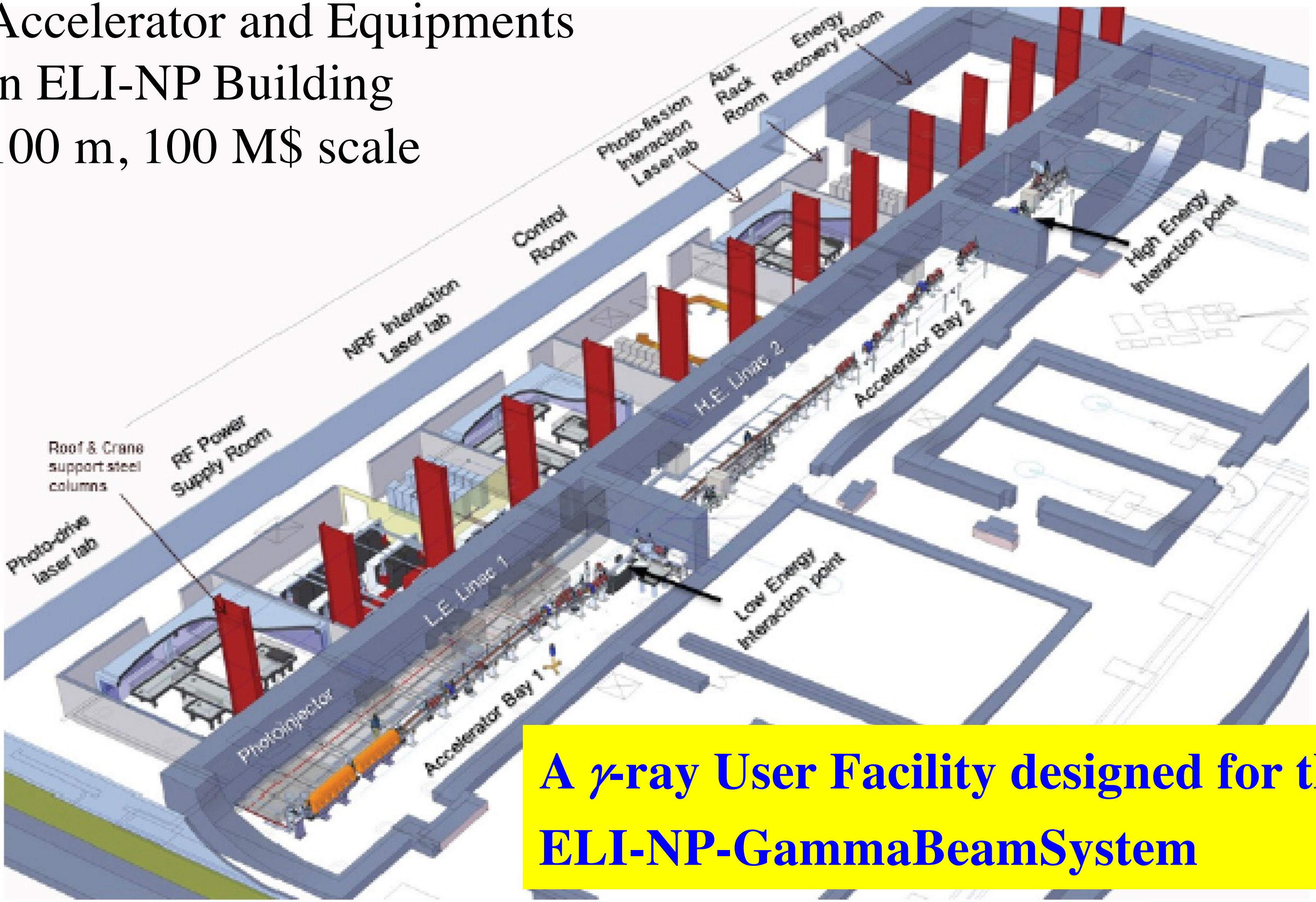

A γ-ray User Facility designed for the ELI-NP-GammaBeamSystem

Fig. 197. Isometric 3D view of Building Layout of the Accelerator Hall & Experimental Areas

Photonuclear Reactions

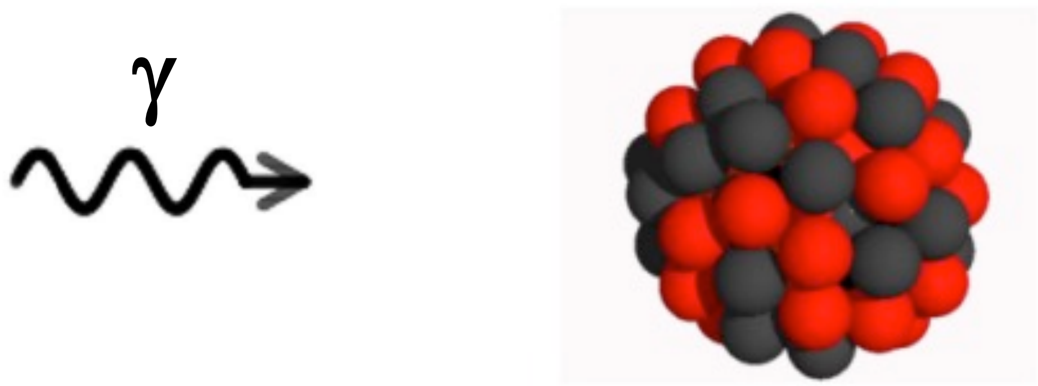

What happens?

Narrowband gamma-ray absorption and re-radiation by the nucleus is an "isotope-specific" signature

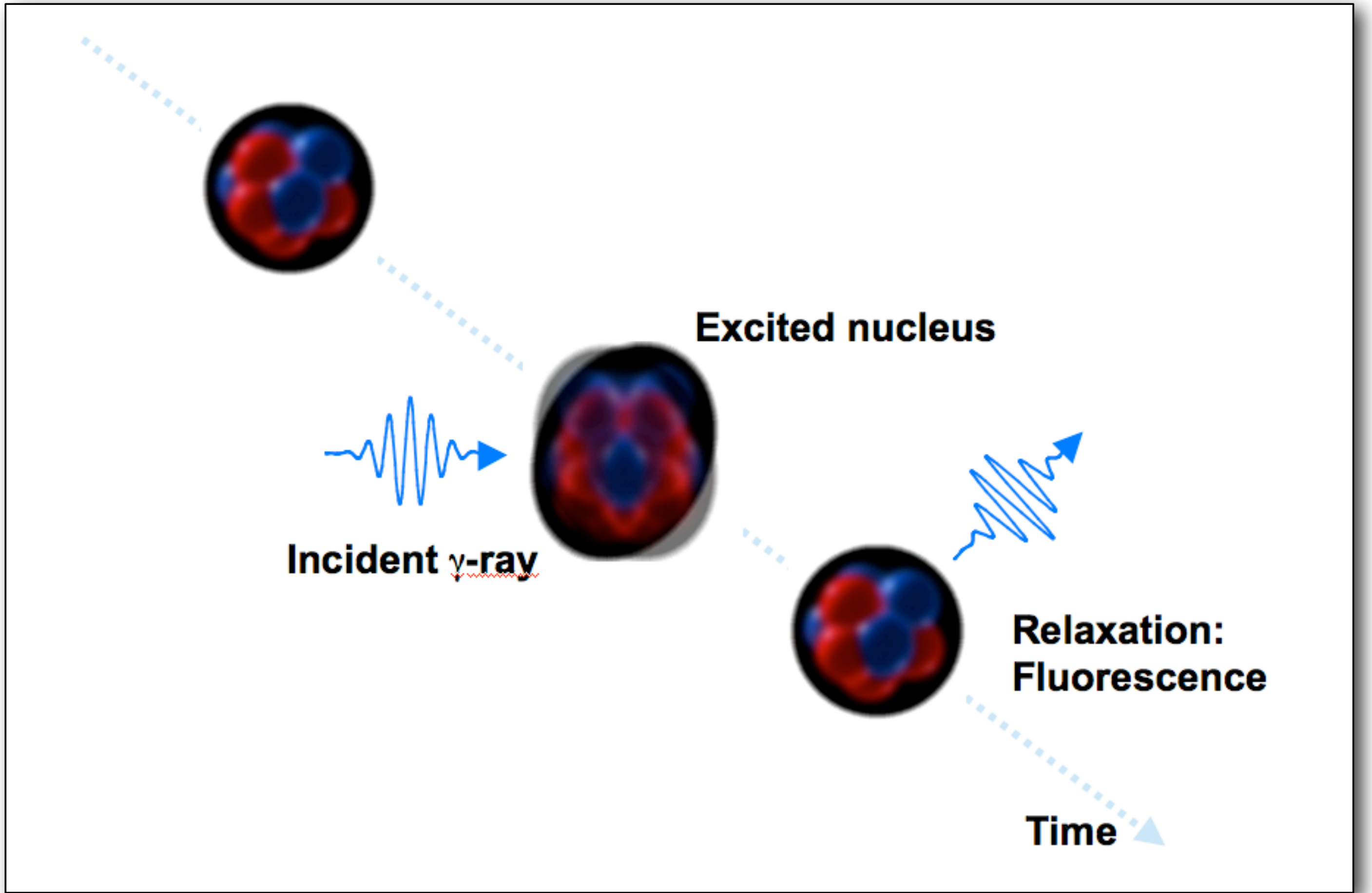

Nuclear Resonance Fluorescence (NRF) is analogous to atomic resonance fluorescence but depends upon the number of protons AND the number of neutrons in the nucleus

Courtesy C. Barty - LLNL

Photonuclear Reactions

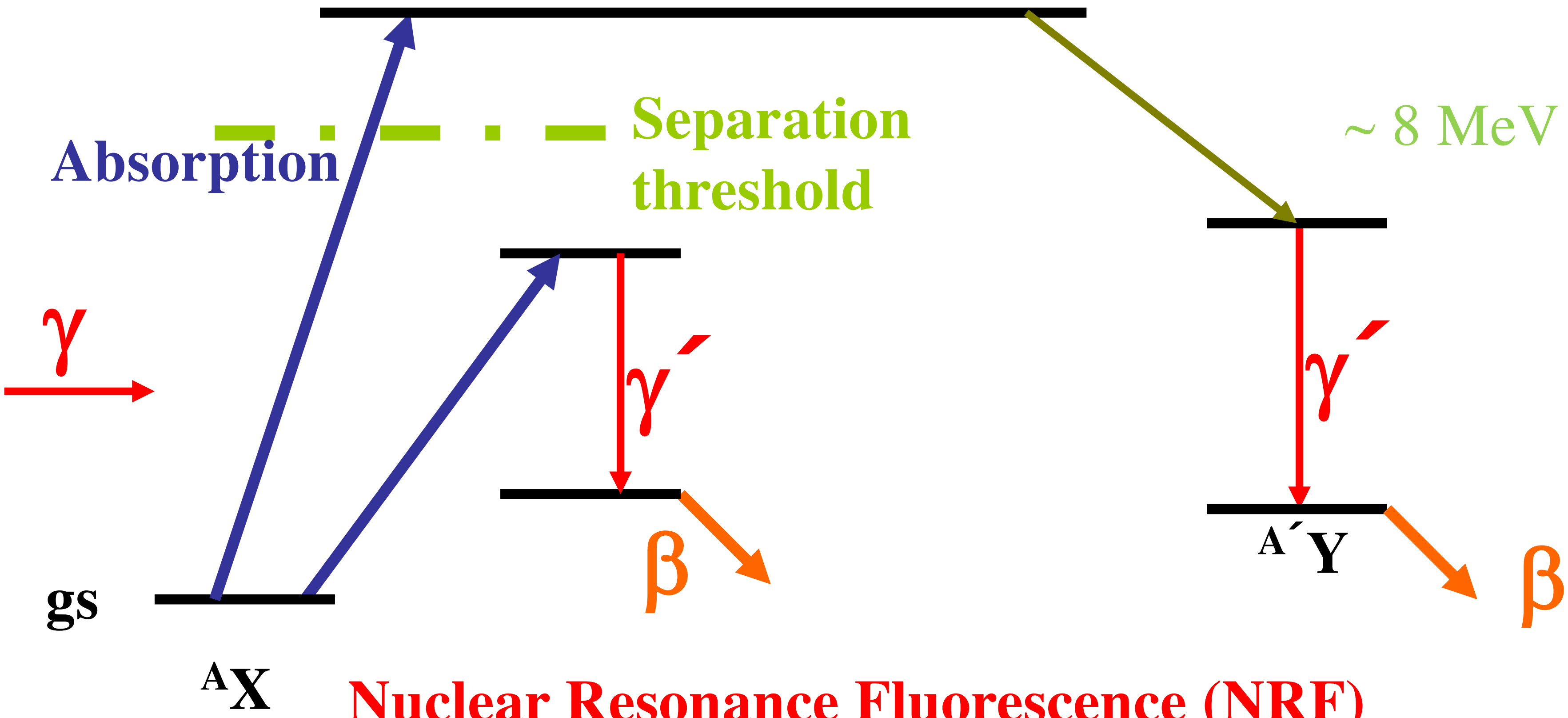

Nuclear Resonance Fluorescence (NRF)

Photoactivation

Photodisintegration **(-activation)**

Nondestructive Assay by Nuclear Resonant Fluorescence

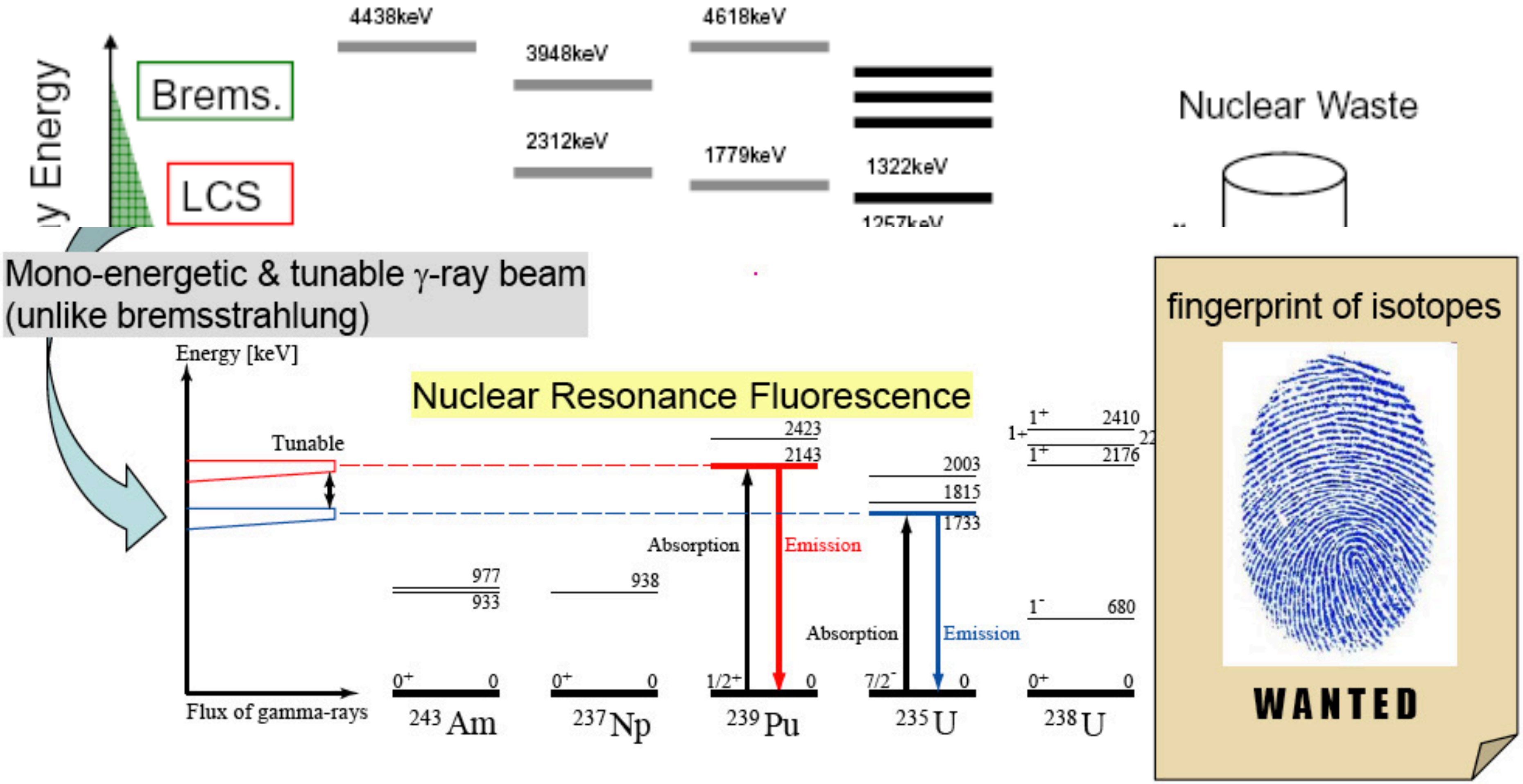

R. Hajima et al., J. Nuclear Science and Technology, 45, 441-451 (2008).

Simulation 2: 2-D Mapping of Shielded Isotopes

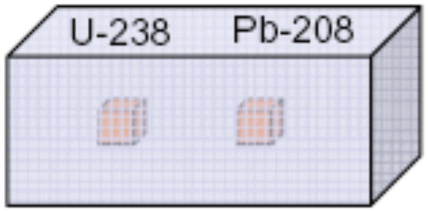

Metal objects
in a concrete block

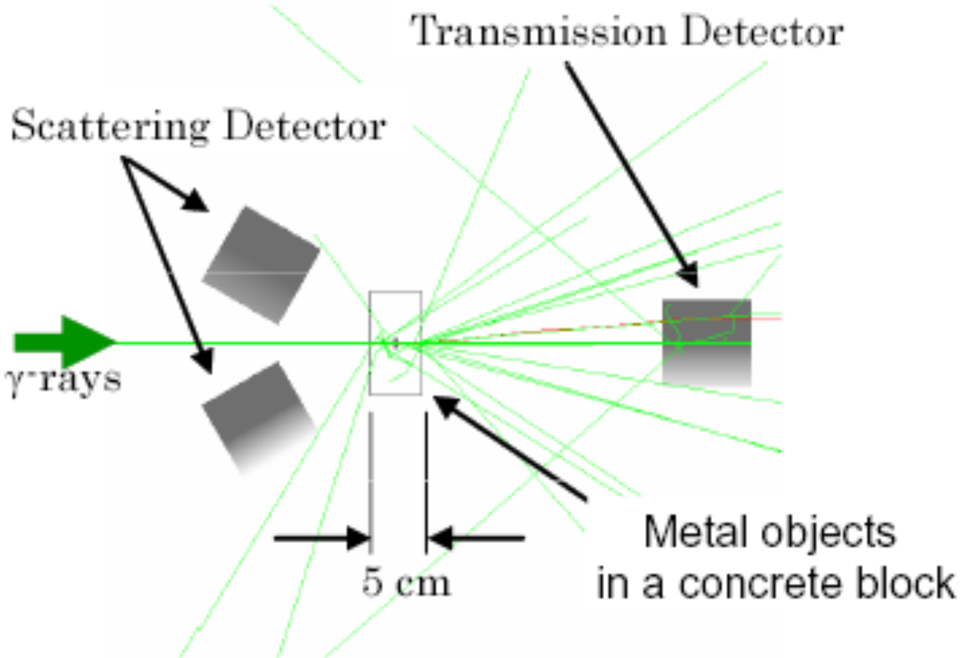

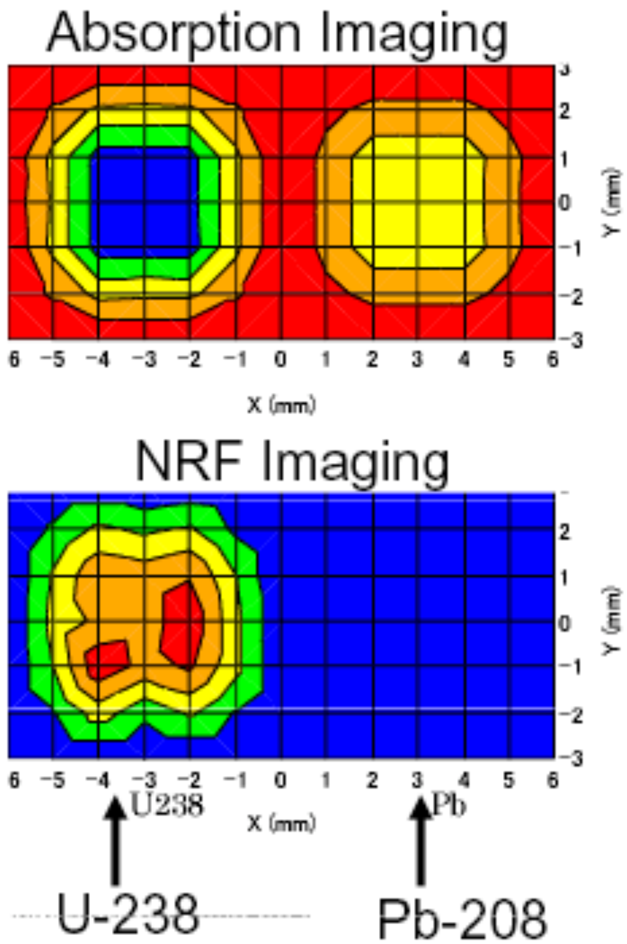

STAR

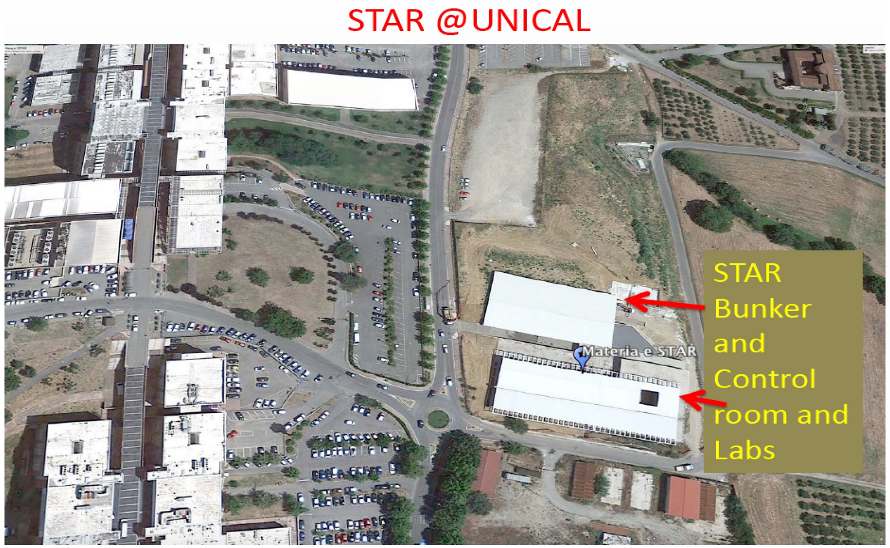

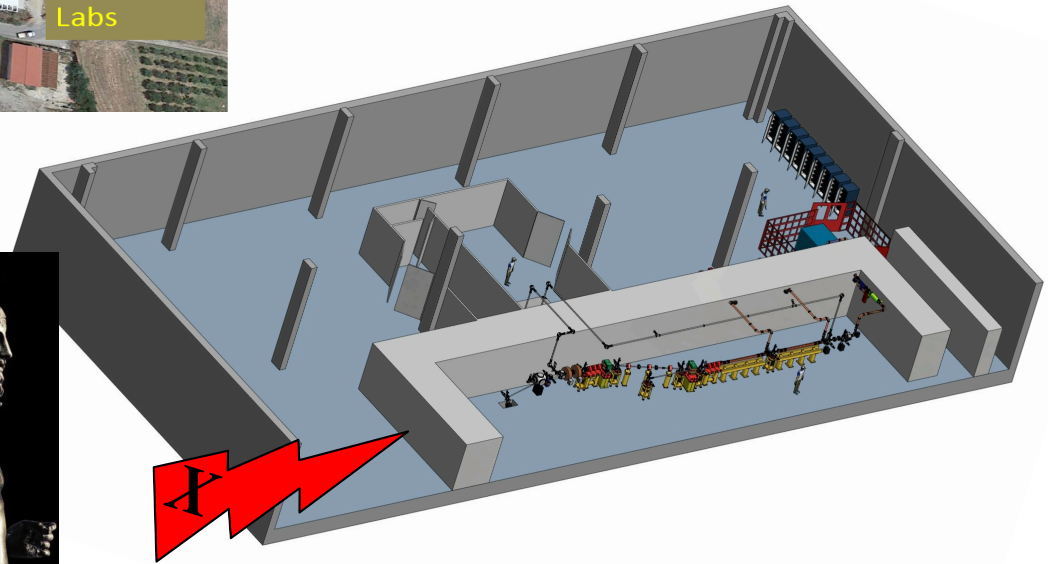

- **STAR (Southern europe Thomson source for Applied Research) is a Compton Source of mono-chromatic X-rays tunable in the range 20-350 keV, devoted to advanced non-invasive diagnostics of cultural heritage/archeological samples.**

Calabria

Convergency regions

Funds for development from the European Community, including research infrastructures

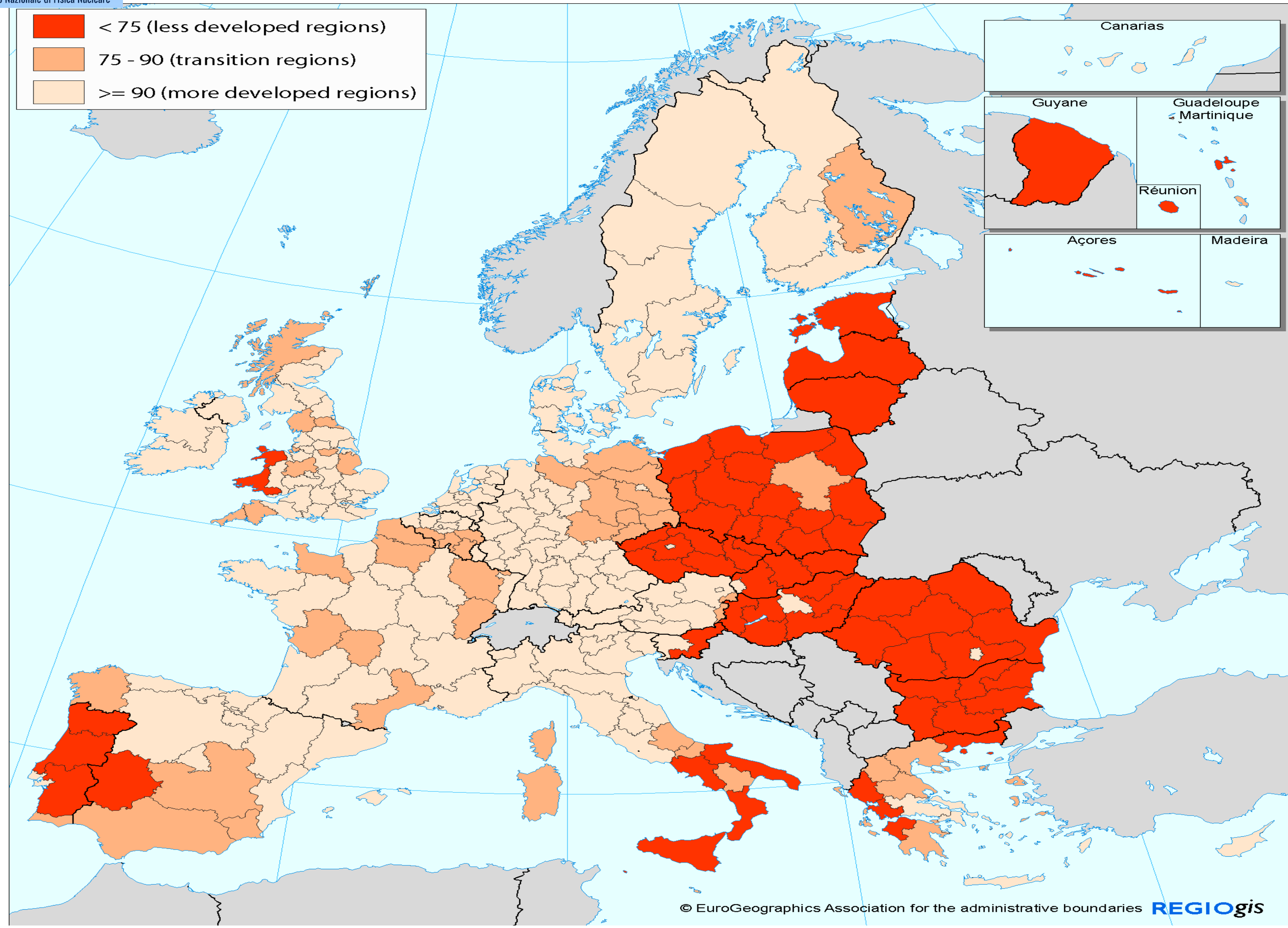

<u>2014-2020</u>

(<u>indicativa</u>)

Regioni meno sviluppate

Regioni in transizione

Regioni piú sviluppate

3^{rd}-4^{th} Generation Light Sources

- Synchrotron light sources: < 50 keV, > 50 ps (100 m, 300 M$)

- X-ray FEL (LCLS): energy ≤25 (50?) keV, 1-100 fs (1 km, 1 G$)

- **New approach: inverse Compton scattering (ICS) 20-200 keV , sub-ps, (10 m , 10 M$) – sometimes called Laser Synchrotron since a laser pulse substitutes the magnetic undulators**

STAR X-ray beamlines foreseen applications

Calabria: rich in archaeological sites and findings

List of Calabrian's museumes:
1)
2)
3)
4)
5)
6)
7)
8)
9)
10)
11)

List of archaeological sites or area
1) Area archeologica di Casignana
2) Area archeologica di Monasterace
3) Sito archeologico di Castiglione di Paludi
4) Sito archeologico di Francavilla Marittima
5) Sito archeologico di Punta Alice
6) Area archeologica di Vibo Valentia
7) Area archeologica di Capo Colonna
8) Area archeologica di Locri Epizefiri
9) Area archeologica di Sibari
10) Area archeologica di Scolacium

PEACE SYMBOLS IN CALABRIA BEFORE GREEK COLONIZATION (A preliminary study @ STAR µTomo)

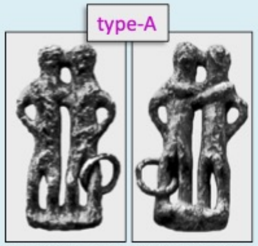

1. - Pendaglio a coppia antropomorfa da Francavilla Marittima tipo A (lato 1 e 2).

2. - Pendaglio a coppia antropomorfa da Francavilla Marittima tipo B (lato 1 e 2).

- Bronze anthropomorphic couples as pendants.
- Burial goods in calabrian area (VIII sec B.C.)
- Two sets: type-A (30 findings);type-B (2 findings)

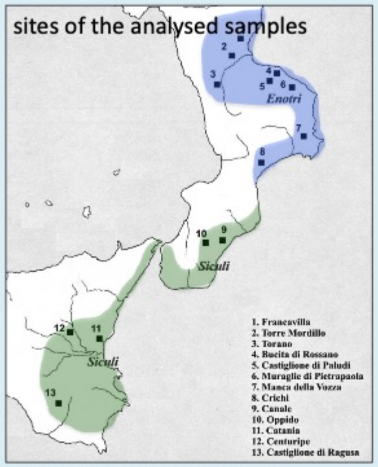

6. - Carta di distribuzione dei pendagli a coppia antropomorfa.

STAR — Thanks to R. G. Agostino on behalf of STAR-UNICAL team

La microtomografia è sfruttata in modo ottimale in indagini **archeometriche** e **paleontologiche**. Inoltre, la sua applicazione può supportare **restauratori** e conservatori a comprendere le tecniche di costruzione di un'opera d'arte o individuare restauri di scarsa qualità o, ancora, **contraffazioni**.

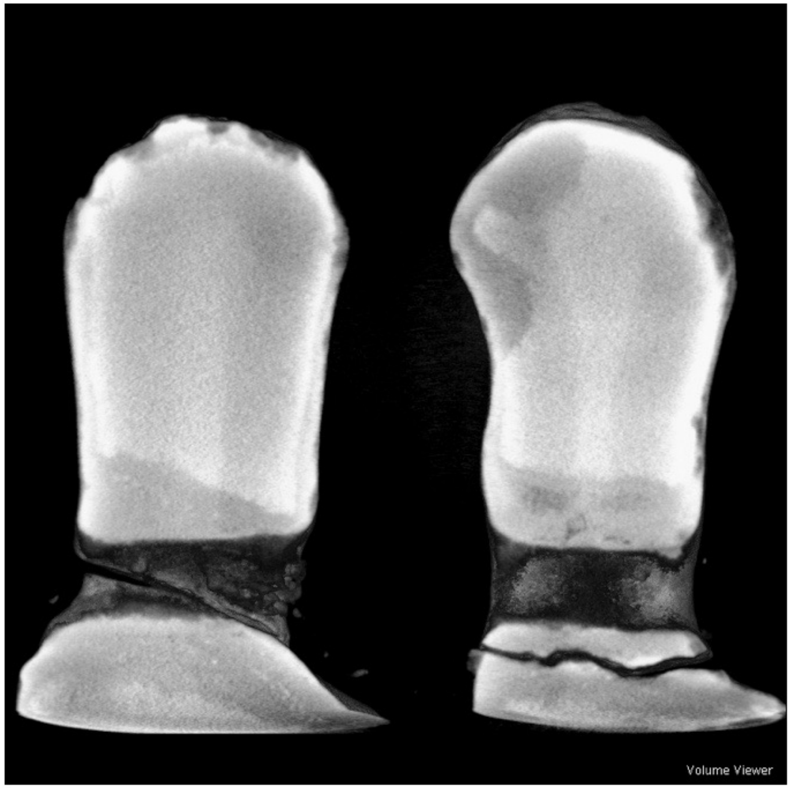

Courtesy R. Agostino

Abbiamo sottoposto a microtomografia una coppietta in bronzo dell'VIII sec. a.C. (*). Le sezioni mostrano una serie di elementi che permettono di ipotizzare tecniche di realizzazione e stabilire quale sia lo stato di conservazione del reperto. Nella sezione tomografica a destra, un particolare delle teste in cui si individua un foro passante alla base delle stesse e una frattura restaurata attraverso l'utilizzo di resine.

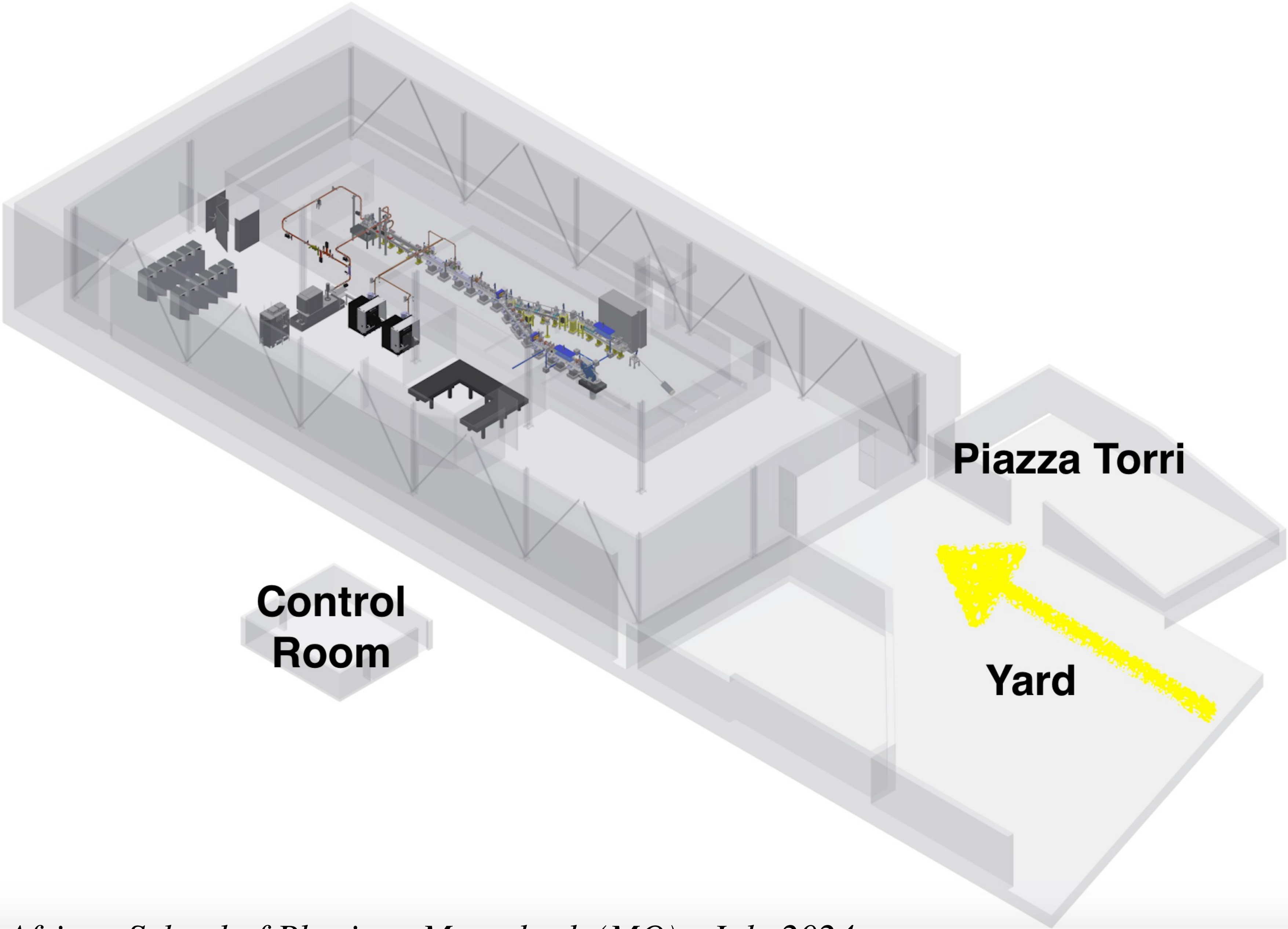
Piazza Torri
Control
Room
Yard

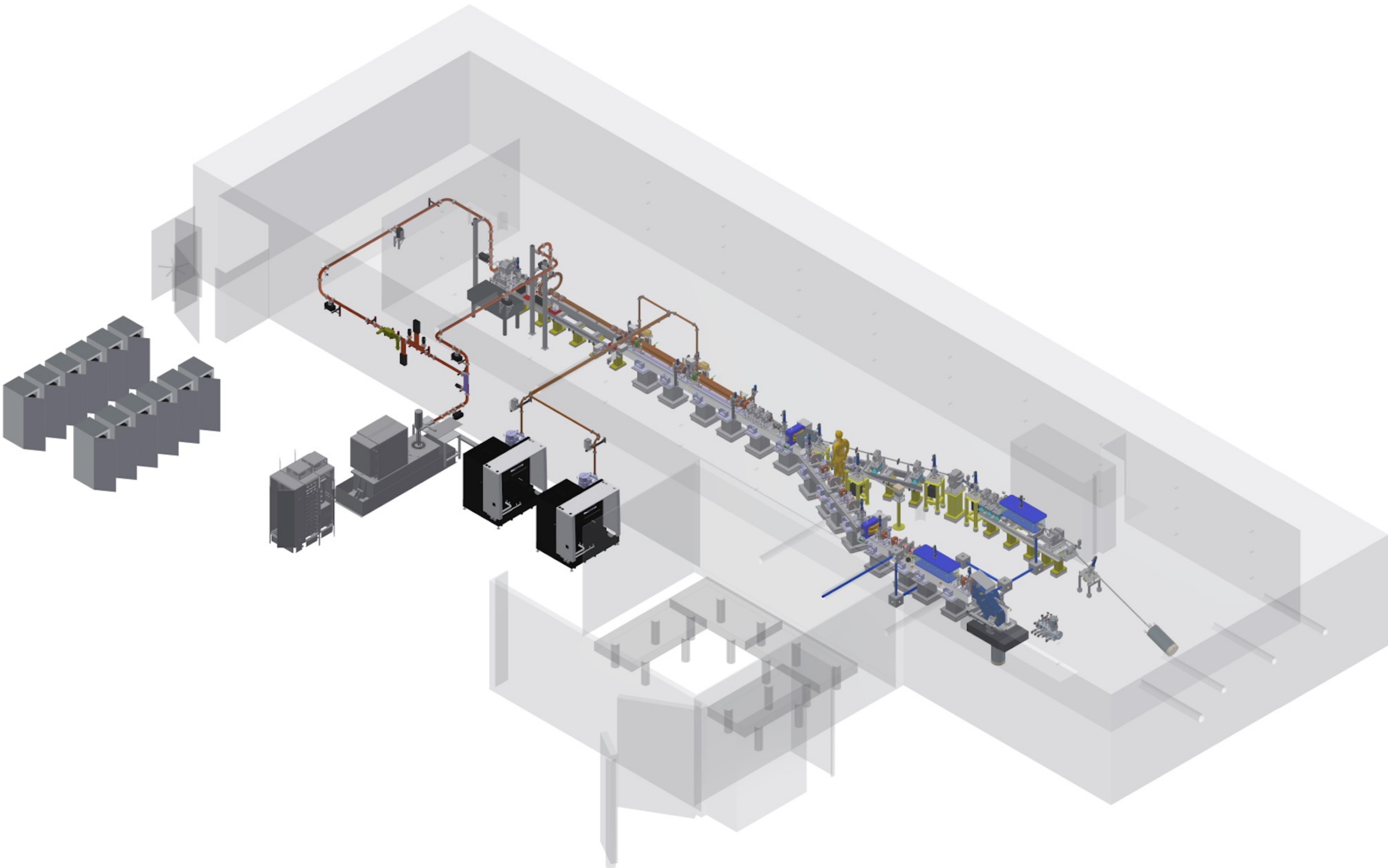

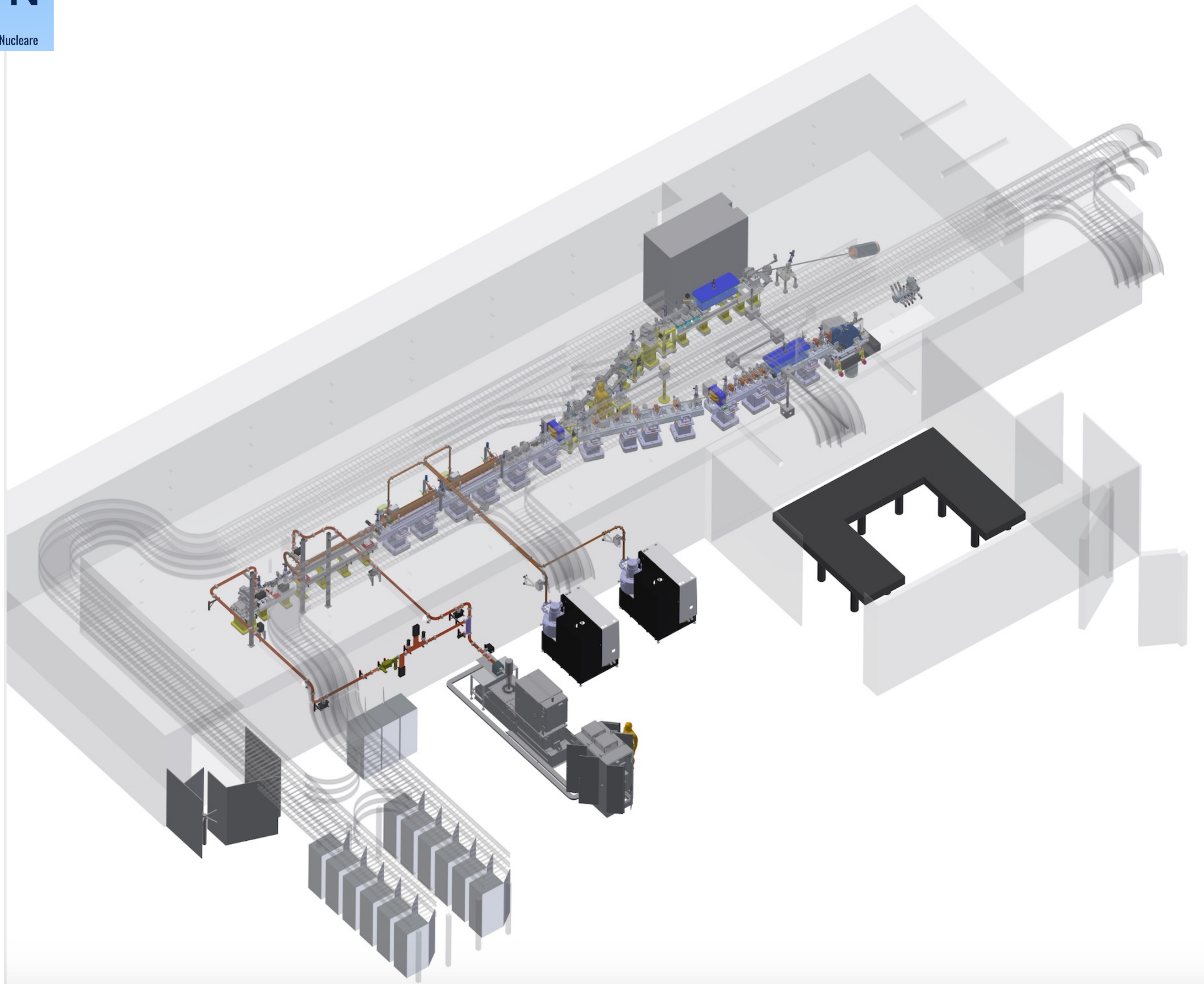

Main components position in the STAR accelerator (upgrade version)

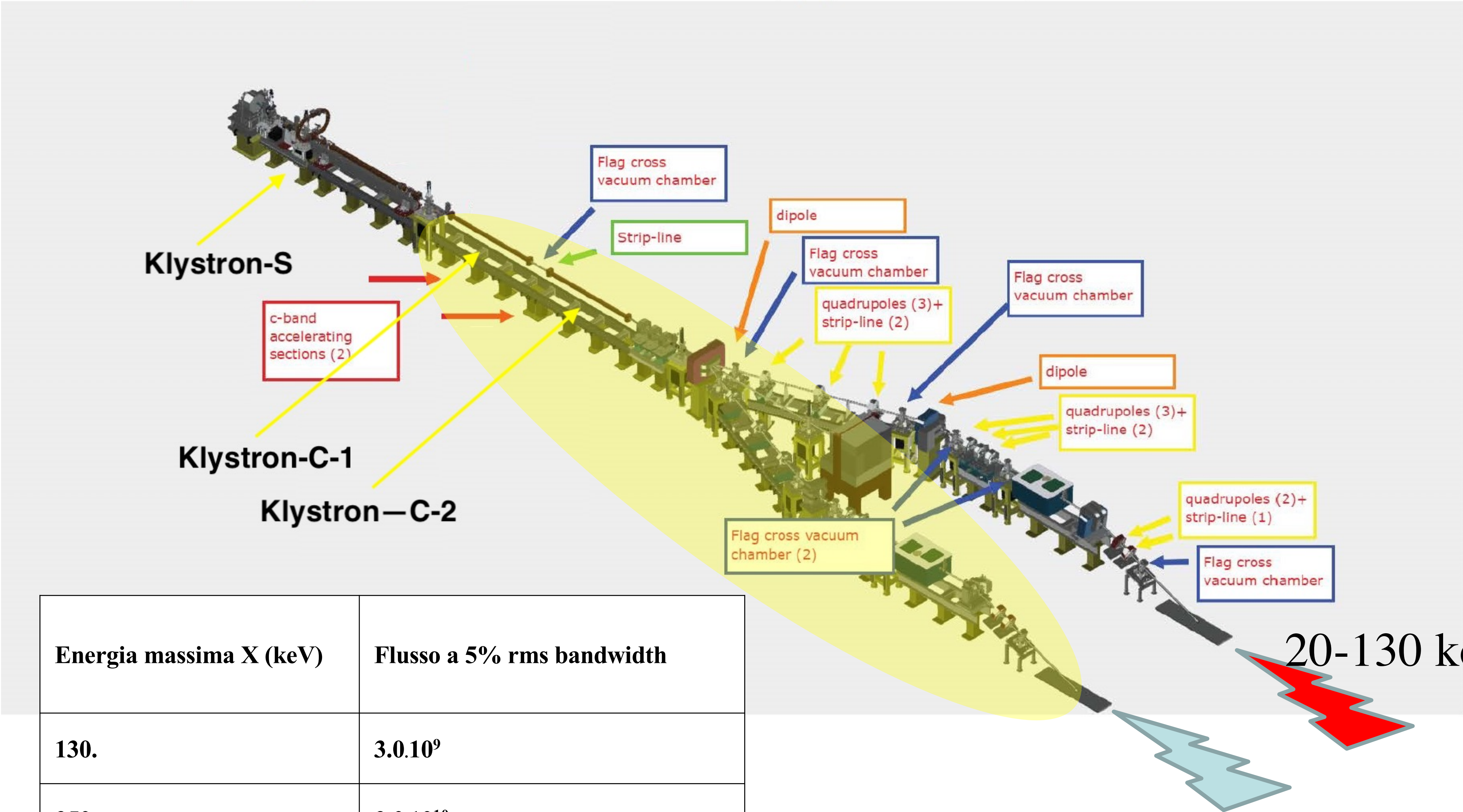

Energia massima X (keV)	Flusso a 5% rms bandwidth
130.	$3.0.10^{9}$
350.	$3.0.10^{10}$

Commissioning the STAR Inverse Thomson Scattering X-ray source: progress report

Marcel Ruijter[1], Adolfo Esposito[2], Alberto Bacci[1], Luigi Faillace[2], Alessandro Gallo[2], Alessandro Vannozzi[2], Andrea Ghigo[2], Angelo Stella[2], Dario Giannotti[1], Alesini David[2], Ezio Puppin[3], Fabio Cardelli[2], Francesco Prelz[1], Gaetano Catuscelli[2], Gianluca Luminati[2], Giorgio Scarselletta[2], Illya Drebot[1], Luca Piersanti[2], Luca Serafini[1], Luigi Pellegrino[2], Marcello Rossetti Conti[1], Marco Bellaveglia[2], Sanae Samsam[1], Sandro Vescovi[2], Simone Bini[2], Simone Tocci[2], Vittoria Petrillo[4]

[1] INFN – Sezione di Milano, Italy
[2] INFN – Laboratori Nazionale di Frascati, Italy
[3] Politecnico di Milano, Italy
[4] Università degli Studi di Milano, Italy

Abstract

The Southern European Thomson back-scattering source for Applied Research (STAR) is a high energy photon facility located on the campus of the University of Calabria (UniCal). The facility was designed for its first phase to operate with an electron and photon energy up to 85MeV and 140keV respectively. For the second phase of the project the energy of the electrons, and thereby the photons, would be increased up to 150MeV and 300keV respectively. The Italian Institute for Nuclear Physics (INFN) was awarded the project for installing, testing and commissioning the energy upgrade of the electron beamline. Here we will outline the progress made regarding the RF system and the Control System Software (CSS). The former consists out of two C-band linacs connected to their individual RF power stations for which the site acceptence test has recently been performed. For the latter the network of the STAR site has been extended to allow the EPICS based CSS to be further developed, including top level GUIs and IT security infrastructure.

Upgrade to High Energy Line

Upgrade to High Energy line (HE-line) consist out of:

- Installation of soilenoid (8 cm) in front of S-band cavity for emittance control
- Installation of two C-band RF cavities incl. powerstations, for higher beam energy
- Cooling system upgrade
- Electric system upgrade, incl. backup power, power supplies and cabeling
- IT infrastructure & control system software

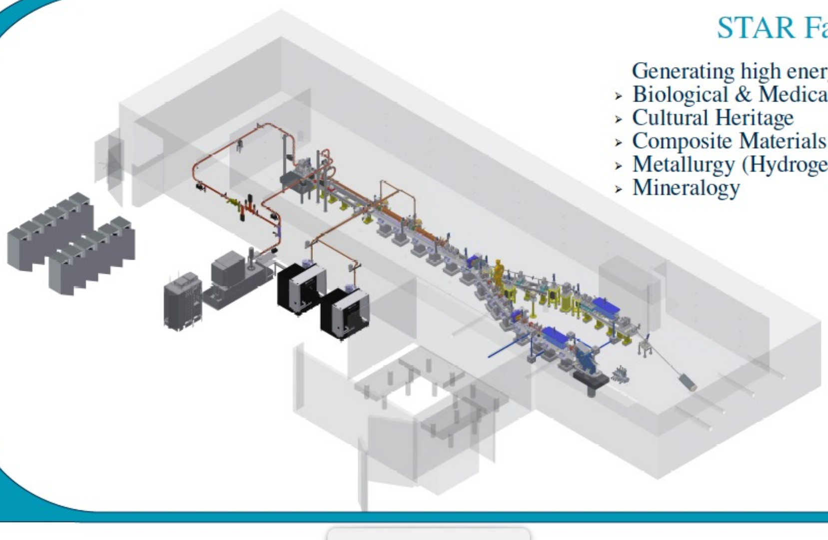

STAR Facility

Generating high energy radiation for

- Biological & Medical Imaging
- Cultural Heritage
- Composite Materials
- Metallurgy (Hydrogen embrittlement)
- Mineralogy

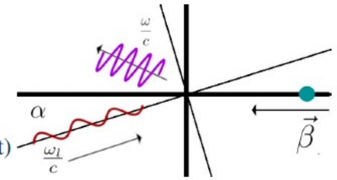

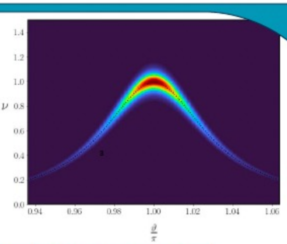

	Electron [Mev]	Photon [keV]
LE – line	23 -65	40 - 150
HE – line	40-150	25 - 350

Electrons

- Emittance : 1 [mm mrad]
- Charge : 100 – 500 [pC]
- Bunch length : < 0.7 [mm]
- Energy spread : 0.1 %, 0.05%

(CPA) Laser

- Energy : > 0.5 [Joule]
- Wavelength : 1030 [nm]
- Bandwidth : 1 [nm]

Istituto Nazionale di Fisica Nucleare

Mission of African Light Source initiative and Compact Light Source based on STAR model

Courtesy S. Connell

Istituto Nazionale di Fisica Nucleare

THE AFRICAN PHYSICS NEWSLETTER

APS

The First African Light Source Project Roundtable Discussion at the African Conference of Physics (ACP2023)

Led by accelerator physics experts, a collaborative roundtable unveiled the African Light Source Project (AfLS), attracting a global audience.

AfLS discussion at the ACP2023 in George, South Africa.

(Photo Credits: The Authors)

AUTHOR

Sanae Samsam,
Istituto Nazionale di Fisica Nucleare (INFN), Milano, Italy

Luca Serafini,
INFN-Section of Milan, Italy

Simon Connell,
University of Johannesburg, South Africa

CONTRIBUTING EDITOR

Mounia Laassiri

JANUARY 2024

INFN
Istituto Nazionale di Fisica Nucleare

The African Light Source Foundation

Towards a Lightsource for the African Continent

AfLS Website https://www.africanlightsource.org

Institute of Physics
Learned society
IOP
Institute of Physics

Debating the Societal Impact of Big Science in the 21st Century

Recent Progress Towards an African Light Source

Simon Connell[1,*], Katharina C. Cramer[2], Ed Mitchell[3,‡], Sekazi K. Mtingwa[4], Prosper Ngabonziza[5,6,#]

To appear soon .....

Modern Physics Letters A
Vol. 33, No. 9 (2018) 1830003 (19 pages)
© World Scientific Publishing Company
DOI: 10.1142/S0217732318300033
https://www.worldscientific.com/doi/abs/10.1142/S0217732318300033

World Scientific
www.worldscientific.com

Synchrotron light sources in developing countries

Sekazi K. Mtingwa Herman Winick*

SCIENCE AND PUBLIC POLICY

2023-06-14 Science and Public Policy 00 (2023) 1-12 "Science diplomacy from the Global South: the case of intergovernmental science organizations"

ResearchProfessional News

African Light Source aims for science with ubuntu

By Katharina Cramer et al

Share

https://www.researchprofessionalnews.com/rr-news-europe-views-of-europe-2022-5-african-light-source-aims-for-science-with-ubuntu/

http://lamp.ictp.it/index.php/aphysrev/article/view/1610/586

The African Review of Physics

The African Review of Physics (2018) **13**: 0019

Proceedings of the first African Conference on Fundamental Physics and Applications 2018, Namibia.
Guest Editors: K. A. Assamagan, M. Backes, D. Charlton, S. Muanza, D. Sahu, and D. Singh

The African Light Source Project

nature reviews physics

Explore content About the journal Publish with us

https://i0.wp.com/www.africanlightsource.org/wp-content/uploads/2022/12/Nature-Review-Physics.png?ssl=1

Comment | Published: 19 October 2022

Building a brighter future for Africa with the African Light Source

BIOPHYSICAL REVIEWS

Biophysical Reviews
pp 1–9 | Cite as

Towards an African Light Source

https://link.springer.com/article/10.1007/s12551-019-00578-3

Authors Authors and affiliations

World Scientific
Connecting Great Minds

Subject Journals Books E-Products Partner With

Modern Physics Letters A | Vol. 33, No. 09, 1830003 (2018)
| Brief Review No Access

Synchrotron light sources in developing countries

Sekazi K. Mtingwa and Herman Winick

https://www.worldscientific.com/doi/abs/10.1142/S0217732318300033

Let's try to understand the budget of energy/momentum exchange between electrons and (radiated/scattered) photons

General Compton Scattering geometry
between an incident eletron E_e and a photon E_{ph}
at a collision angle α, photon E'_{ph} scattering angle θ
and electron E'_e scattering angle θ_e

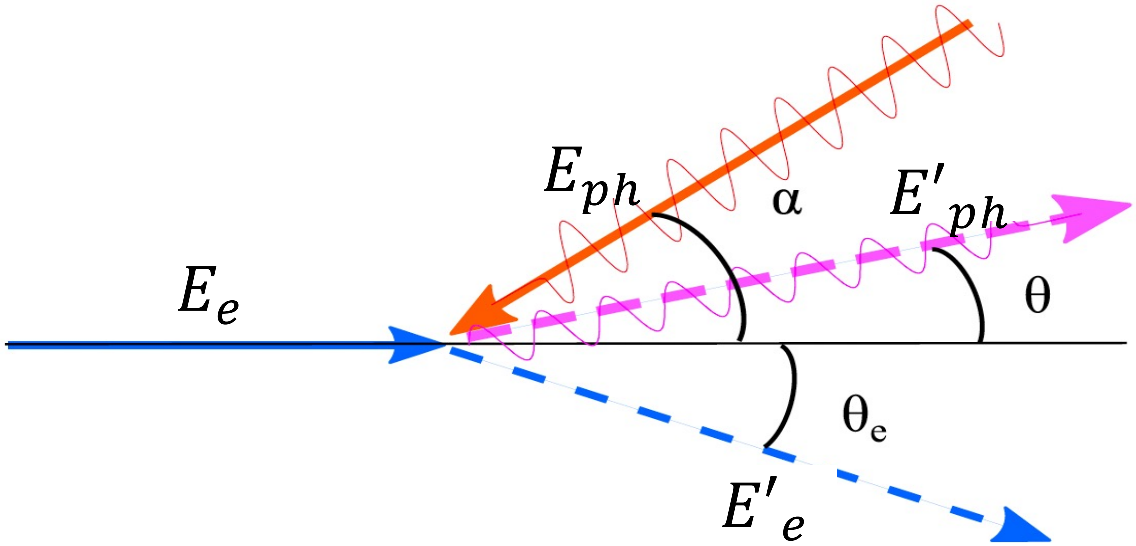

To be continued on File b

Slides following on this file are additional slides

Quantu… ens in the Center … nematics)

… ref.

A…

… m. ref.

$$\ldots \vec{p}_e^{\,*} + \hbar \vec{k}_{h\nu}^{\,*} = \vec{0}$$

$electron\ 4-vec\ldots \sqrt{E_e^2/c^2 - m_e^2c^2}\,]$

$photon\ 4-vect\ldots \nu_L/c\,]$

Analytical description of photon beam phase spaces in Inverse Compton Scattering sources

C. Curatolo,[1] I. Drebot,[1] V. Petrillo,[1,2] and L. Serafini[1]

[1] *INFN-Milan, via Celoria 16, 20133 Milano, Italy*
[2] *Università degli Studi di Milano, via Celoria 16, 20133 Milano, Italy*

(Dated: 22 May 2017)

We revisit the description of inverse Compton scattering sources and the photon beams generated therein, emphasizing the behavior of their phase space density distributions and how they depend upon those of the two colliding beams of electrons and photons. Main objective is to provide practical formulas for bandwidth, spectral density, brilliance, which are valid in general for any value of the recoil factor, i.e. both in the Thomson regime of negligible electron recoil, and in the deep Compton recoil dominated region, which is of interest for gamma-gamma colliders and Compton Sources for the production of multi-GeV photon beams. We adopt a description based on the center of mass reference system of the electron-photon collision, in order to underline the role of the electron recoil and how it controls the relativistic Doppler/boost effect in various regimes. Using the center of mass reference frame greatly simplifies the treatment, allowing to derive simple formulas expressed in terms of rms momenta of the two colliding beams (emittance, energy spread, etc.) and the collimation angle in the laboratory system. Comparisons with Monte Carlo simulations of inverse Compton scattering in various scenarios are presented, showing very good agreement with the analytical formulas: in particular we find that the bandwidth dependence on the electron beam emittance, of paramount importance in Thomson regime, as it limits the amount of focusing imparted to the electron beam, becomes much less sensitive in deep Compton regime, allowing a stronger focusing of the electron beam to enhance luminosity without loss of mono-chromaticity. A similar effect occurs concerning the bandwidth dependence on the frequency spread of the incident photons: in deep recoil regime the bandwidth comes out to be much less dependent on the frequency spread. The set of formulas here derived are very helpful in designing inverse Compton sources in diverse regimes, giving a quite accurate first estimate in typical operational conditions for number of photons, bandwidth, spectral density and brilliance values - the typical figures of merit of such radiation sources.

I. INTRODUCTION

Inverse Compton Scattering sources (ICSs) are becoming increasingly attractive as radiation sources in photon energy regions either not covered by other high brilliance sources (FEL's, synchrotron light sources) or where compactness becomes an important figure of merit, like for advanced X-ray imaging applications to be implemented in university campus, hospitals, museums, etc., i.e. outside of research centers or large scale laboratories [1]. ICSs are becoming the γ-ray sources of reference in nuclear photonics, photo-nuclear [2, 3] and fundamental physics [4], thanks to superior performances in spectral densities achievable. Eventually they will be considered for very high energy photon generation (in the GeV to TeV range) since there are no other competing techniques at present, neither on the horizon, based on artificial tools at this high photon energy [5]. As a consequence, a flourishing of design activities is presently occurring in several laboratories [6–15] and companies [16–19], where ICSs are being conceived, designed and built to enable several domains of applications, and ranging from a few keV photon energy up to GeV's and beyond. Designs of ICSs are carried out considering several diverse schemes, ranging from high gradient room temperature pulsed RF Linacs [3, 20, 21] to CW ERL Super-conducting Linacs [22, 23] or storage rings [2, 24–27], as far as the electron beam generation is concerned, and from single pulse J-class amplified laser systems running at 100 Hz to optical cavities (e.g. Fabry-Perot) running at 100 MHz acting as photon storage rings for the optical photon beams, not to mention schemes based on FEL's to provide the colliding photon beam [22, 28, 29].

In order to assess the performances of a specific ICSs under design, detailed simulations of the electron-photon beam collision are typically carried out using Monte Carlo codes [30–32] able to model the linear and non-linear electron-photon quantum interaction leading to Compton back-scattering events, taking into account in a complete fashion the space-time propagation of the two colliding beams through the interaction point region, including possible multiple scattering events occurring during the overlap of the two pulses. Only in case of negligible electron recoil, i.e. in the so called Thomson regime typical of low energy X-ray ICSs, classical electromagnetic numerical codes (e.g. TSST [33]), modelling the equivalent undulator radiation emitted by electrons wiggling in the electromagnetic field of the incoming laser pulse, allow to analyze particular situations such as the use of chirped [34], tilted [35] and twisted [36] lasers.

In the recent past some efforts have been developed to carry out analytical treatments of the beam-beam collision physics, embedding the single electron-photon collision from a quantum point of view within a rms distribution of the scattered photon beam [27, 37–43], or,

Invariant Mass, Lorentz transformation from Lab to c.m. ref. system

$$Total\ \ 4-vector\ \ \mathbf{P}\ \ = \mathbf{P}_e + \mathbf{P}_{h\nu} = \left[E_e/c + h\nu_L/c, 0, 0, \sqrt{\frac{E_e^2}{c^2} - m_e^2 c^2} - h\nu_L/c \right]$$

$$Invariant\ \ Mass\ \ s \equiv c\mathbf{P} \bullet c\mathbf{P} = E_{tot}^{2*} = E_{cm}^2$$

$$\left(4-vector\ \ product\ \ \mathbf{P}_1 \bullet \mathbf{P}_2 \equiv \left[E_1 E_2 / c^2 - \vec{p}_1 \cdot \vec{p}_2 \right] \right)$$

$$E_{cm} \cong \sqrt{4E_e h\nu_L + m_e^2 c^4} = m_e c^2 \sqrt{1 + \frac{4\gamma h\nu_L}{m_e c^2}} = m_e c^2 \sqrt{1+\Delta}$$

$$e^-\ \ recoil\ \ factor\ \ \Delta \equiv \frac{4\gamma h\nu_L}{m_e c^2}$$

To transform to the Lab ref. system we need to compute γ_{cm}

$$\gamma_{cm} = \frac{E_{lab}}{E_{cm}} = \frac{E_e + h\nu_L}{m_e c^2 \sqrt{1+\Delta}} \cong \frac{\gamma}{\sqrt{1+\Delta}}$$

Then apply a Lorentz transformation

$$\begin{cases} E_{ph} = p^*_{ph}\gamma_{cm}\left(1 + \sqrt{1 - \frac{1}{\gamma_{cm}^2}}\cos\theta^*\right) \\ p_{phx} = p^*_{ph}\sin\theta^*\cos\phi^* \\ p_{phy} = p^*_{ph}\sin\theta^*\sin\phi^* \\ p_{phz} = p^*_{ph}\gamma_{cm}\left(\sqrt{1 - \frac{1}{\gamma_{cm}^2}} + \cos\theta^*\right) \end{cases}$$

Recap
(exact analytical formula, no approximations)

$$\Delta = \frac{4\gamma h\nu_L}{m_e c^2} \qquad \gamma_{cm} = \frac{\gamma}{\sqrt{1+\Delta}}$$

$$E_{ph} = \frac{2\gamma^2 h\nu_L}{1+\Delta}\left[1 + \sqrt{1 - \frac{1+\Delta}{\gamma^2}}\cos\vartheta^*\right]$$

$$\cos\vartheta^* = \frac{\sqrt{1+tan^2\vartheta} - \gamma_{cm} tan^2\vartheta\sqrt{\gamma_{cm}^2 - 1}}{1+\gamma_{cm}^2 tan^2\vartheta} \qquad if \quad \vartheta < \frac{\pi}{2}$$

$$\cos\vartheta^* = \frac{-\sqrt{1+tan^2\vartheta} - \gamma_{cm} tan^2\vartheta\sqrt{\gamma_{cm}^2 - 1}}{1+\gamma_{cm}^2 tan^2\vartheta} \qquad if \quad \vartheta > \frac{\pi}{2}$$

$$E_{ph} = \frac{4\gamma^2 h\nu_L}{1+\Delta+\gamma_{cm}^2\vartheta^2} \qquad E_{ph-max} = \frac{4\gamma^2 h\nu_L}{1+\Delta} = 4\gamma_{cm}^2 h\nu_L$$

Recap
(exact analytical formula, example 250 MeV electrons against $h\nu_L$=1.2 eV photons)

$\gamma = 490. \quad \Delta = 0.0046 \quad \gamma_{cm} = 488.88$

$$E_{ph}(MeV) = \frac{1.1472}{2}\left[1 + \sqrt{1 - \frac{1+\Delta}{\gamma^2}\cos\vartheta^*}\right]$$

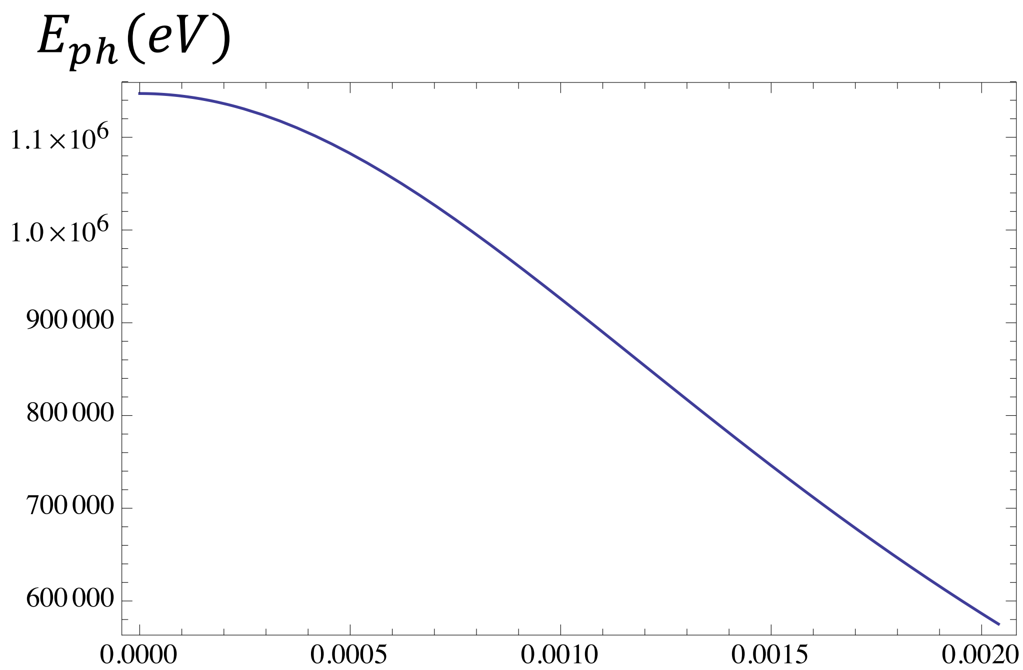

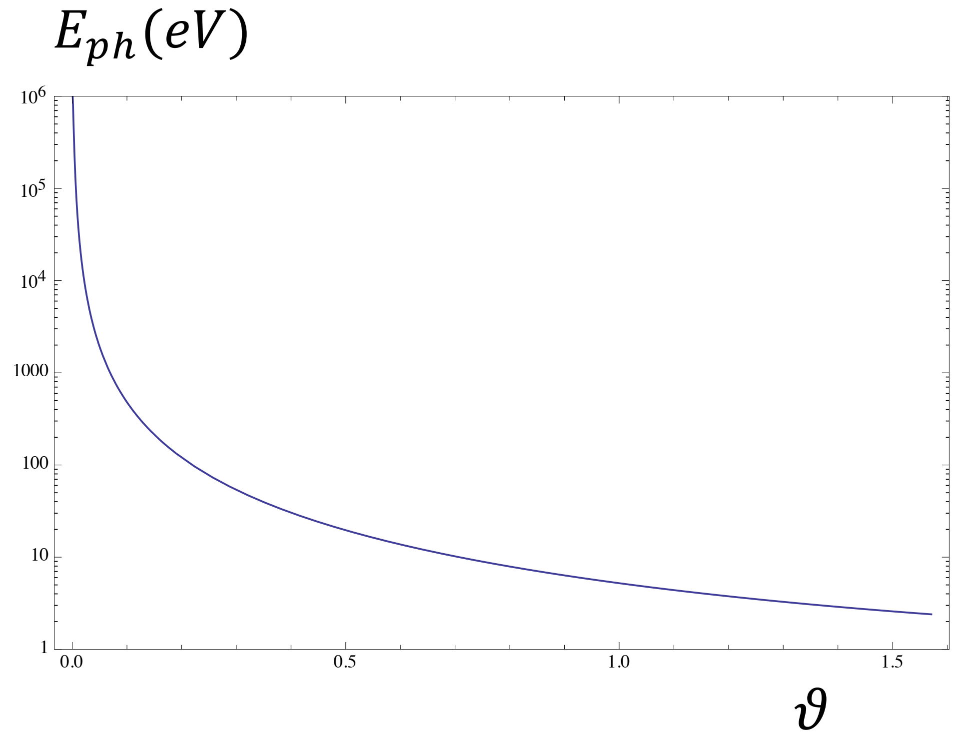

$\vartheta = 1/\gamma$

Recap (exact analytical formula, example 250 MeV electrons against $h\nu_L$=1.2 eV photons)

$$\gamma = 490. \quad \Delta = 0.0046 \quad \gamma_{cm} = 488.88 \qquad E_{ph}(MeV) = \frac{1.1472}{2}\left[1 + \sqrt{1 - \frac{1+\Delta}{\gamma^2}\cos\vartheta^*}\right]$$

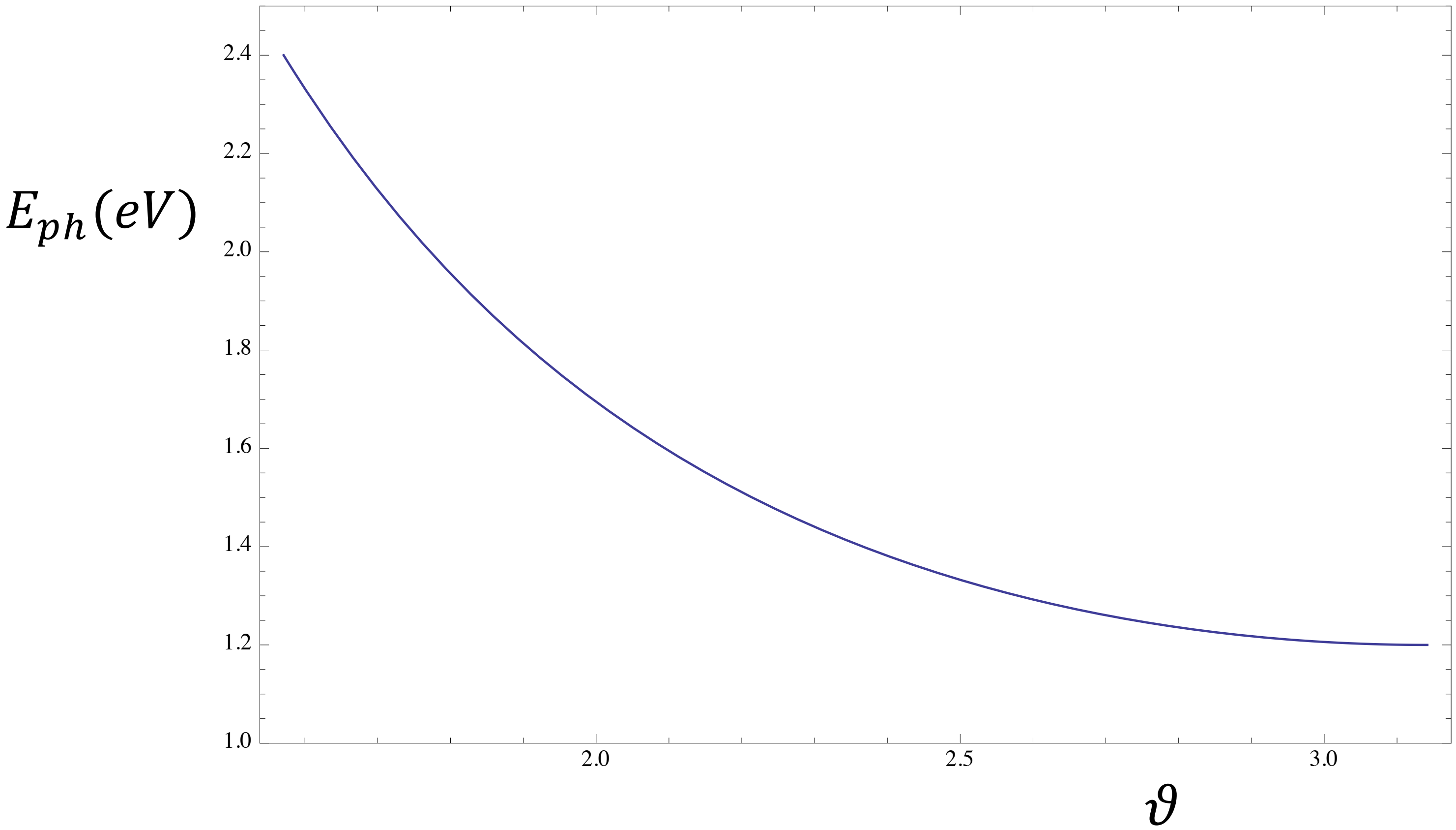

Analogy with Synchrotron radiation emission and its angular cone 1/γ

Radiation is emitted into a narrow cone

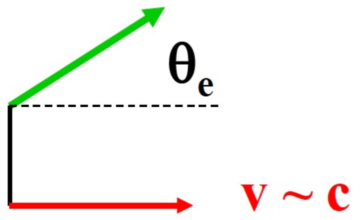

$$\theta = \frac{1}{\gamma} \cdot \theta_e$$

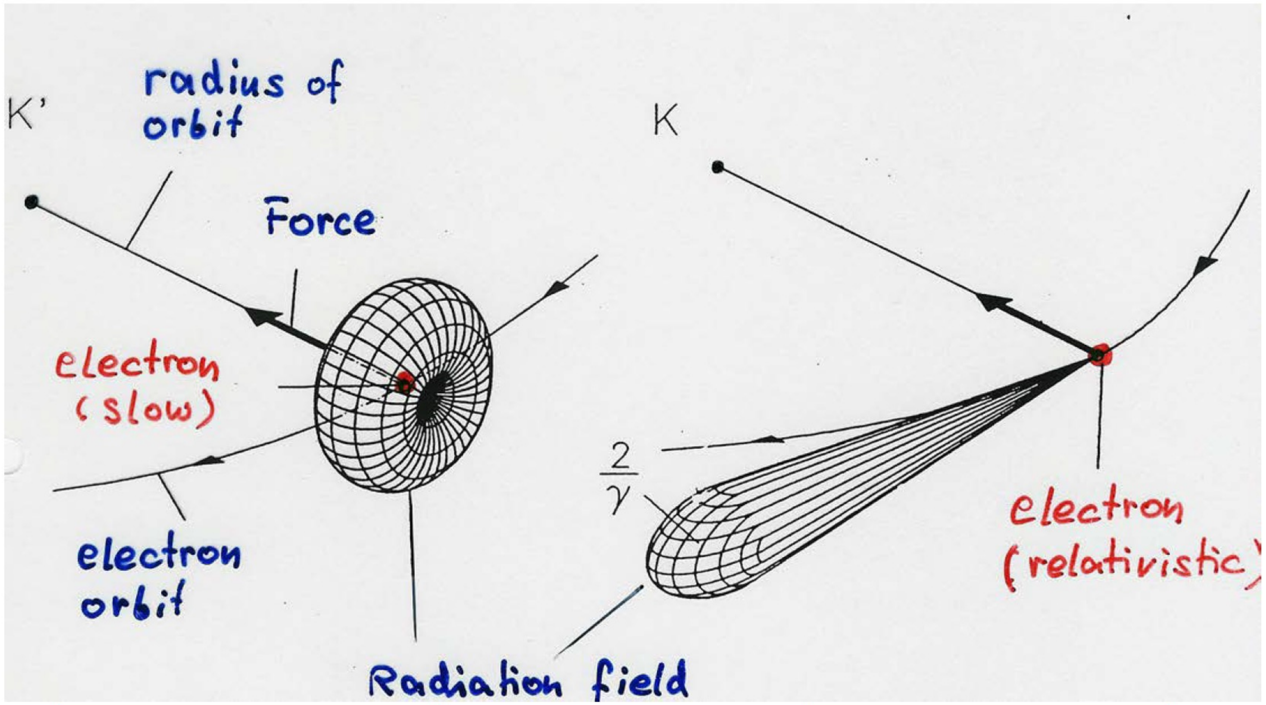

v << c

v ≈ c

courtesy of L. Rivkin - PSI

Single electron-photon spectra

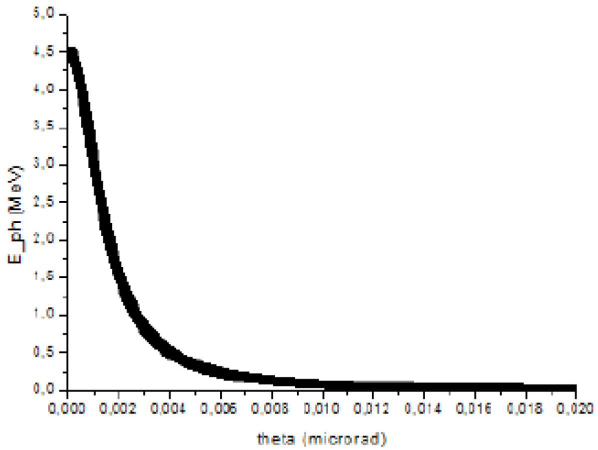

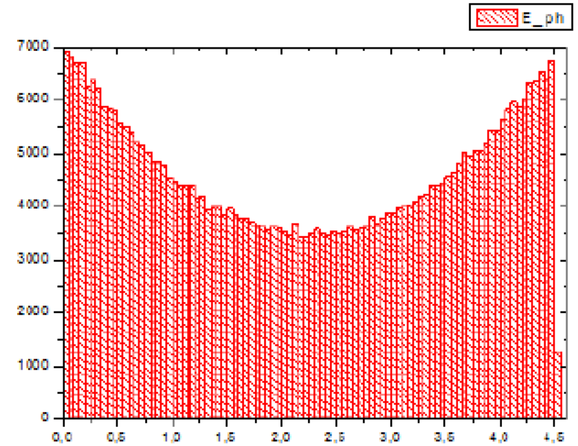

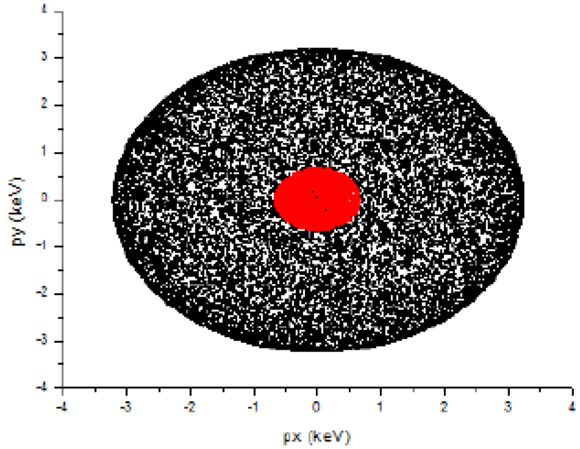

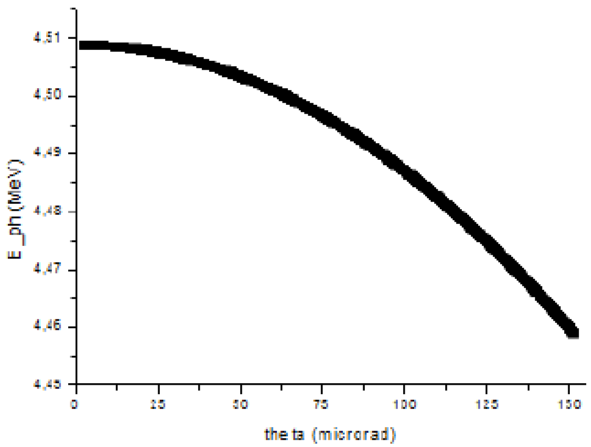

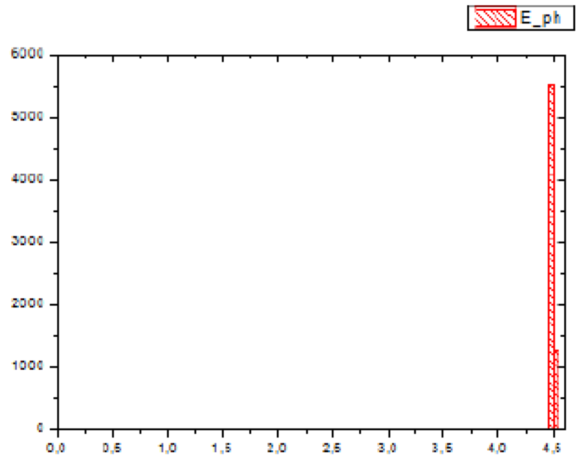

Energia elettroni 360 MeV
Energia fotoni 2.3 eV
Angolo alpha 0 gradi
Theta collimazione 151 microrad
Banda relativa 0.003

$$\gamma\vartheta = 0.11$$

What happens when we scatter beams of electron against beams of photons?

Electron beam emittance and energy spread spread out the c.m. propagation so to generate a "beam" of c.m. ref. frames

If the electron has not null transverse components respect to the z axis, the Lorentz transformations in a generic direction have to be used:

$$
\begin{cases}
E_{ph} = p^*_{ph}\gamma_{cm} + p^*_{phx}\gamma_{cm}\beta_x + p^*_{phy}\gamma_{cm}\beta_y + p^*_{phz}\gamma_{cm}\beta_z \\
p_{phx} = p^*_{ph}\gamma_{cm}\beta_x + p^*_{phx}\dfrac{1+\gamma^2_{cm}\beta^2_x}{1+\gamma_{cm}} + p^*_{phy}\dfrac{\gamma^2_{cm}\beta_x\beta_y}{1+\gamma_{cm}} + p^*_{phz}\dfrac{\gamma^2_{cm}\beta_x\beta_z}{1+\gamma_{cm}} \\
p_{phy} = p^*_{ph}\gamma_{cm}\beta_y + p^*_{phx}\dfrac{\gamma^2_{cm}\beta_x\beta_y}{1+\gamma_{cm}} + p^*_{phy}\dfrac{1+\gamma^2_{cm}\beta^2_y}{1+\gamma_{cm}} + p^*_{phz}\dfrac{\gamma^2_{cm}\beta_y\beta_z}{1+\gamma_{cm}} \\
p_{phz} = p^*_{ph}\gamma_{cm}\beta_z + p^*_{phx}\dfrac{\gamma^2_{cm}\beta_x\beta_z}{1+\gamma_{cm}} + p^*_{phy}\dfrac{\gamma^2_{cm}\beta_y\beta_z}{1+\gamma_{cm}} + p^*_{phz}\dfrac{1+\gamma^2_{cm}\beta^2_z}{1+\gamma_{cm}}
\end{cases}
$$

See C. Curatolo, PhD Thesis, Univ. of Milan, 2016 (and references therein)

Electron-photon Collider Spectra

The transverse momentum of the incoming electron beam is linked to the emittance by the relation

$$\sigma_{p_x} = \frac{\epsilon_{n,x} M_e}{\sigma_x}$$

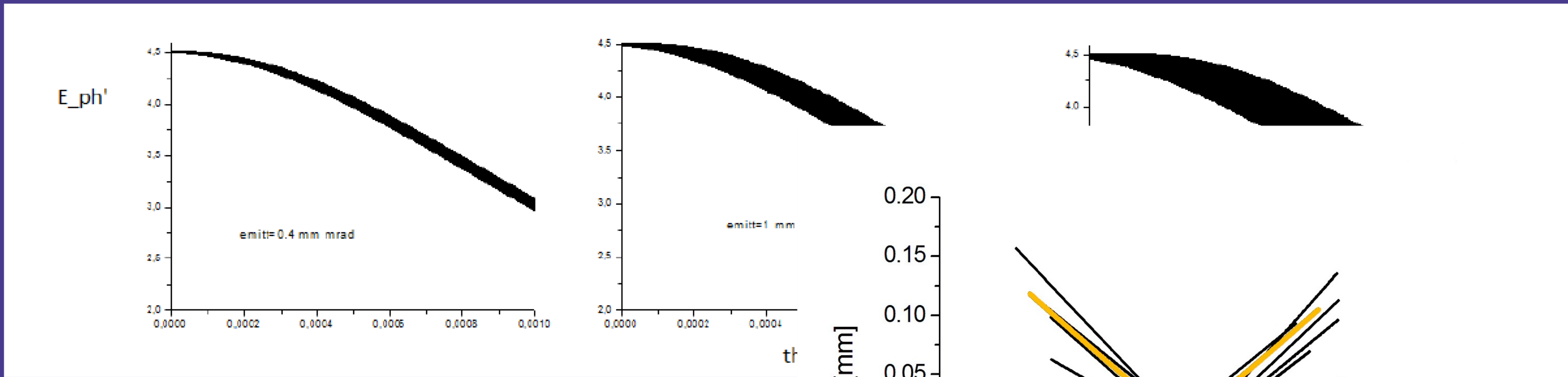

FIGURA : Energy of the emitted photons as a fun
different values of the electron beam emittance.

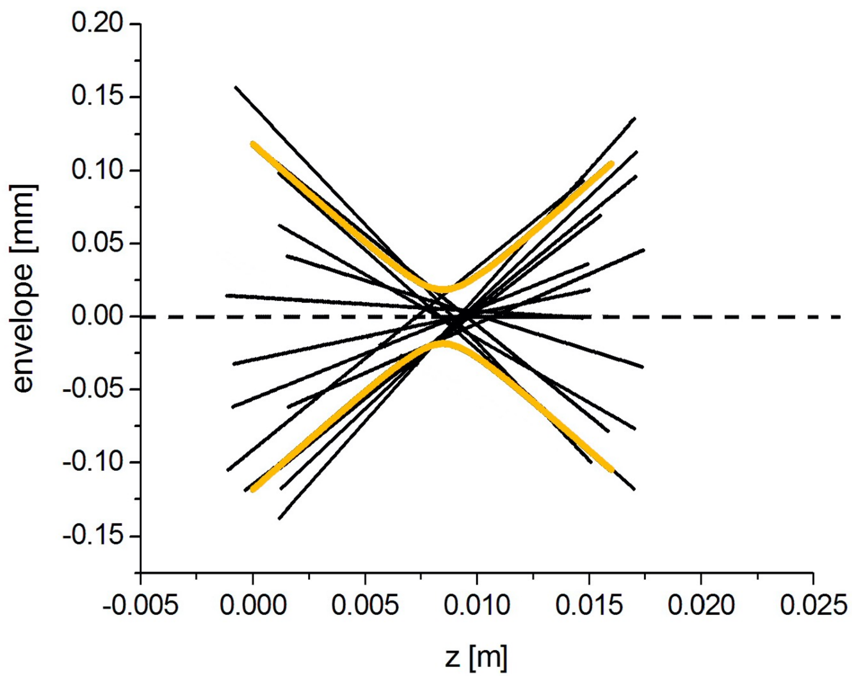

We ... ollider,
tha ... nosity,

KEK-76-3

GENERAL FORMULAE OF LUMINOSITY
FOR VARIOUS TYPES OF COLLIDING
BEAM MACHINES

Toshio SUZUKI

JULY 1976

NATIONAL LABORATORY FOR
HIGH ENERGY PHYSICS
OHO-MACHI, TSUKUBA-GUN
IBARAKI, JAPAN

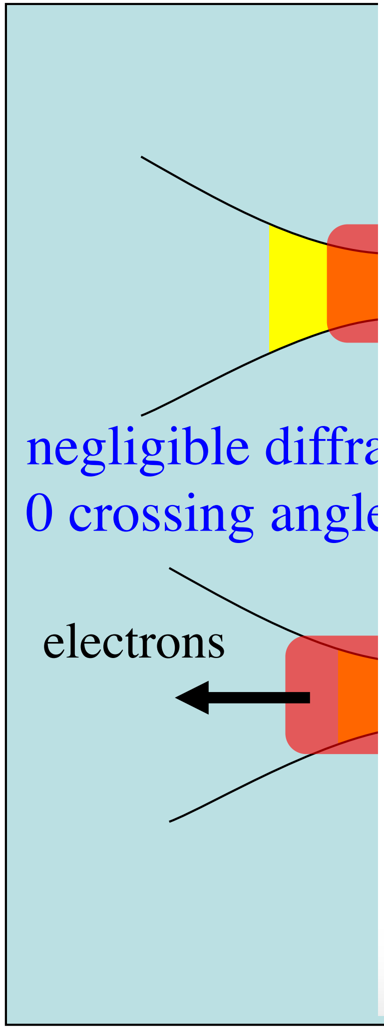

$...7 \cdot 10^{-24}\,cm^2 = 0.67\ barn$

$= \mathbf{L}\sigma_T$ $\qquad \sigma_T = \frac{8\pi}{3} r_e^2$

...HEP collisions

...ectrons

$= \frac{N_L N_{e-}}{4\pi\sigma_x^2} f$

$L_S \equiv \frac{L}{\Delta\nu_\gamma}$

$...^{1}) = 2.5 \cdot 10^{35}\,cm^{-2}s^{-1}$

cf.: LHC 10..., Hi-Lumi LHC 10^{35}

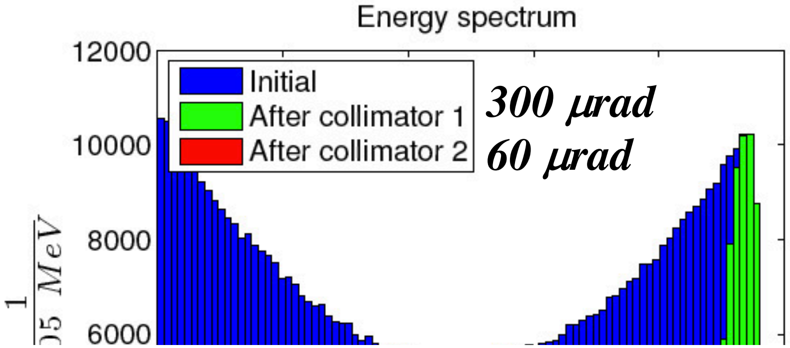

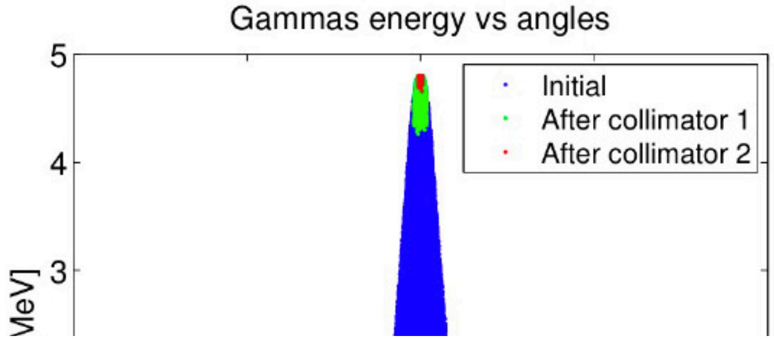

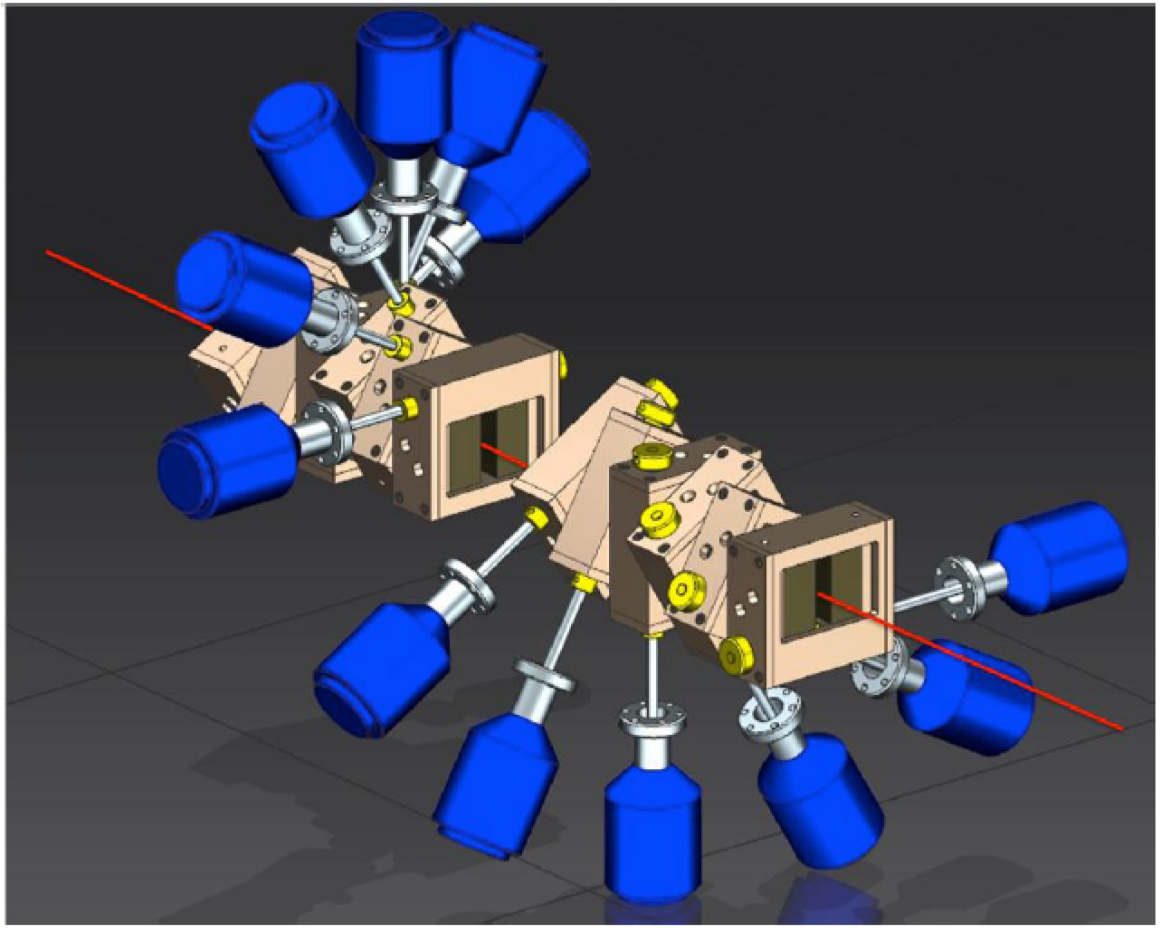

Fig. 184. Drawing of the configuration of low energy collimator made up of 12 tungsten adjustable slits with a relative 30° rotation each

Courtesy M. Gambaccini

STAR was designed by INFN in 2013-2014 adopting a common paradigm with ELI-NP-GBS: both are e-γ linear collider based on 100 Hz amplified J-class lasers interacting with high brightness RF photo-injector. The design strategy applies Petrillo-Serafini criterion for maximum spectral density.

$$E_{X/\gamma} = 4\gamma^2 E_{laser}$$

$$with\ T = 100\,MeV\ (\gamma = 197)\ E_{laser} = 1.2\ eV \Rightarrow E_{X/\gamma} = 186\ keV$$

strong focusing of high brightness (peak & average) to maximize Luminosity According to Petrillo-Serafini criterion

$$S_d \propto \frac{\langle I_e \rangle U_{las}}{\varepsilon_n^2 E_x}$$

30-150 MeV e⁻
20-350 keV X

Fig.2 – STAR machine as an example of Paradigm A. Overall length about 12 m.

250-750 MeV e⁻
1-19.5 MeV γ

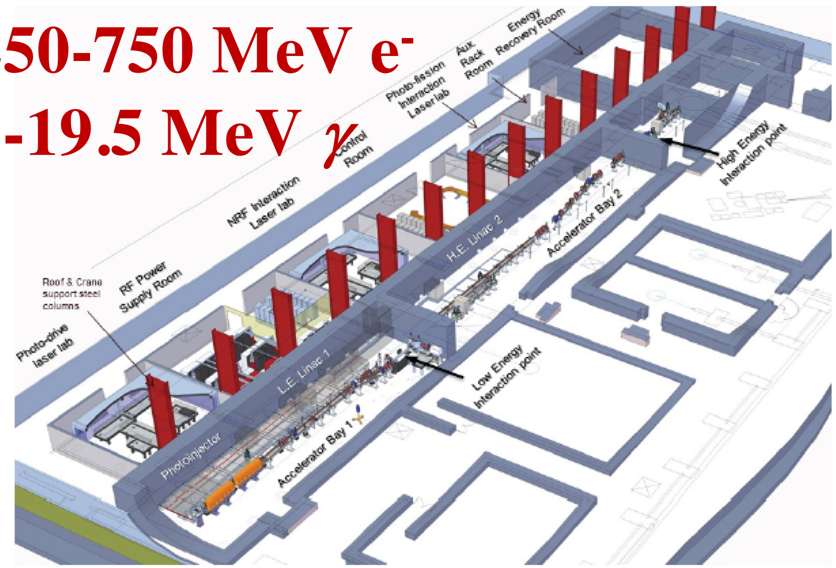

Fig. 197. Isometric 3D view of Building Layout of the Accelerator Hall & Experimental Areas

Visita Ministra C. Messa a STAR, 7 giugno 2022

https://acceleratori.infn.it/it/

Extra-Slides (optional)

Luca.Serafini@mi.infn.it

Inverse Compton Sources, Overview, Theory, Main Technological Challenges – Photonic Colliders

- **New Generation of *X*/γ ray beams via electron-photon beam collisions for advanced applications in medicine/biology-material science/cultural heritage/national security *and* fundamental research in nuclear physics and high energy physics (*e*-γ, γ-γ colliders, pol. e^+ beams, hadron. physics, etc)**
- **Inverse Compton Sources (ICS) are e^-/photon colliders aimed at producing secondary beams of photons**
- **Several Test-Facilities world-wide: after a decade of machine test&development we are entering the era of User Facilities in *X*-ray imaging and γ-ray Nuclear Physics and Photonics**

I.C.S. in operation or under-construction

	Type	Energy [KeV]	Flux (@ 10% bandwidth)	Source size (µm)
*PLEIADES (LLNL) [11,12]	Linac	10-100	10^{7} (10 Hz)	18
*Vanderbilt [13,14]	Linac	15-50	10^{8} (few Hz)	30
*SLAC [15]	Linac	20-85		
*Waseda University [16,17]	Linac	0.25-0.5	2.5 10^{4} (5 Hz)	
*AIST, Japan [18]	Linac	10-40	10^{6}	30
*Tsinguha University [19]	Linac	4.6	1.7 10^{4}	
*LUCX (KEK) [20]	Linac	33	5 10^{4} (12.5 Hz)	80
+ UTNL, Japan [21,22]	Linac	10-40	10^{9}	
MIT project [23]	Linac	3-30	3 10^{12} (100 MHz)	2
MXI systems [24]	Linac	8-100	10^{9} (10Hz)	
SPARC –PLASMONX [25]	Linac	20-380	2 10^{8} -2 10^{10}	0.5-13
Quantum Beam (KEK) [26,27]	Linac		10^{13}	3
*TERAS (AIST) [28]	Storage ring	1-40	5 10^{4}	2
*Lyncean Tech [29,30,31]	Storage ring	7-35	~ 10^{12}	30
Kharkov (SNC KIPT) [32]	Storage ring	10-500	2.6 10^{13} (25 MHz)	35
TTX (THU China) [33,34]	Storage ring	20-80	2 10^{12}	35
ThomX France [35]	Storage ring	50	10^{13} (25 MHz)	70

Table 3: Compact Compton X ray sources. Symbols * and + refers respectively to machines in operation and to machines in construction.

STAR (Calabria) Linac 20-100 10^{11} (100 Hz) 18

From **THOMX** Conceptual Design Report, A.Variola, A.Loulergue, F.Zomer, LAL RT 09/28, SOLEIL/SOU-RA-2678, 2010 highly asymmetric compact*

electron-photon colliders

*10 m, 10 M$

secondary photon beams via large

lorentz boost of c.m. reference frame

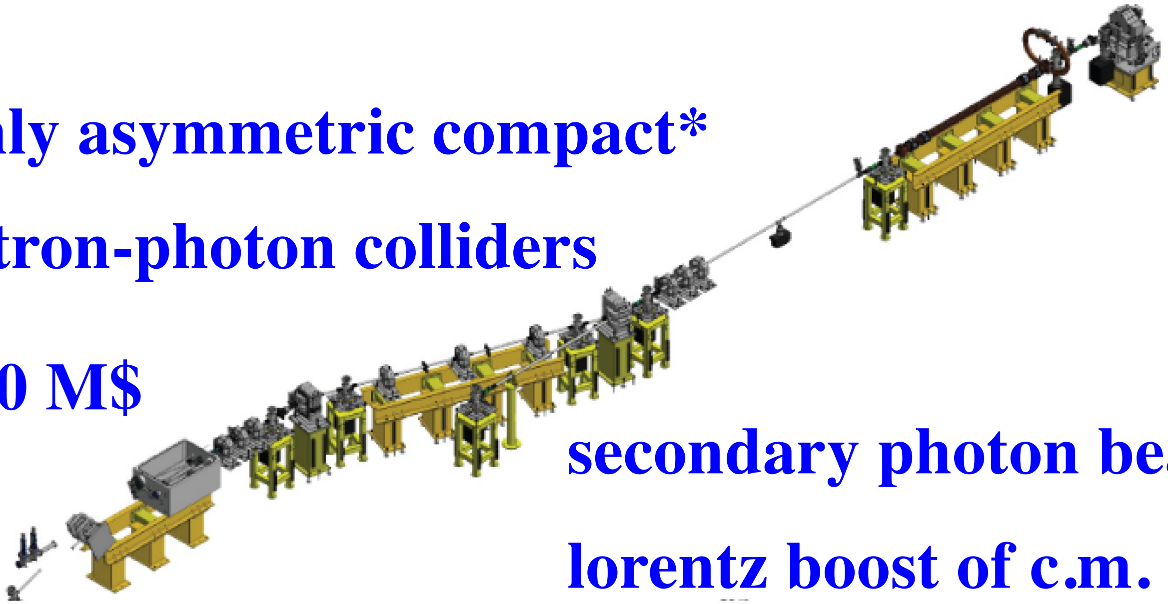

Fig.2 – *STAR machine as an example of Paradigm A. Overall length about 12 m.*

MeV/GeV's electrons

eV's photons

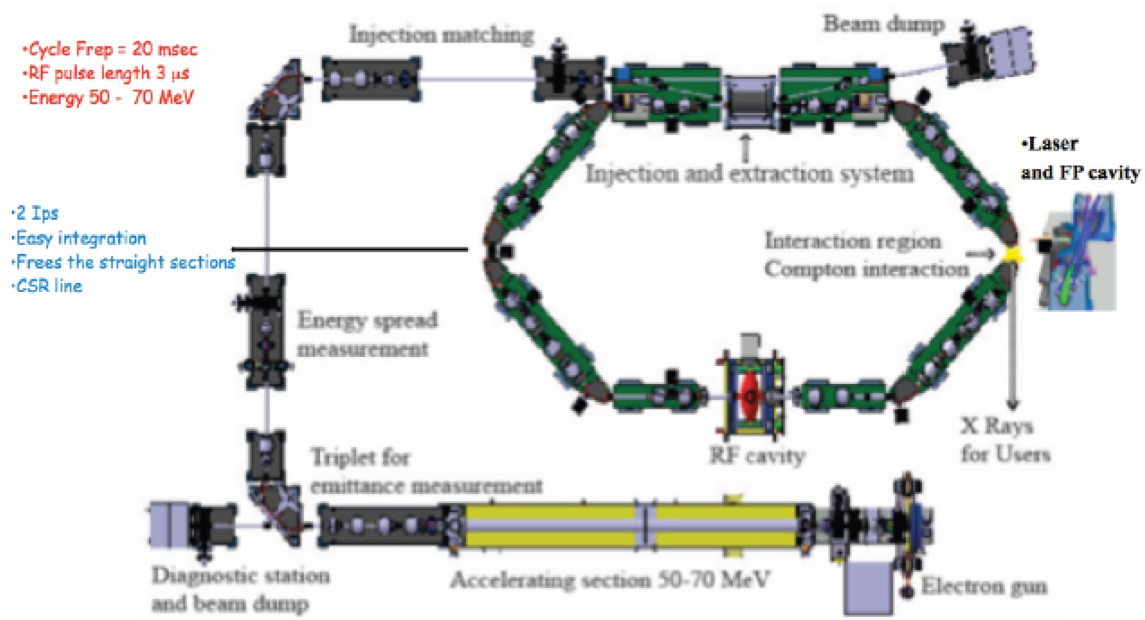

Fig.3 – *ThomX as an example of Paradigm B. Size is about 10x10 m^2.*

BriXS: an example of high sustainability. High power 2 MW beam delivered to user with only 200 kW power consumption/dissipation with outstanding beam quality (larger than storage rings, same current)

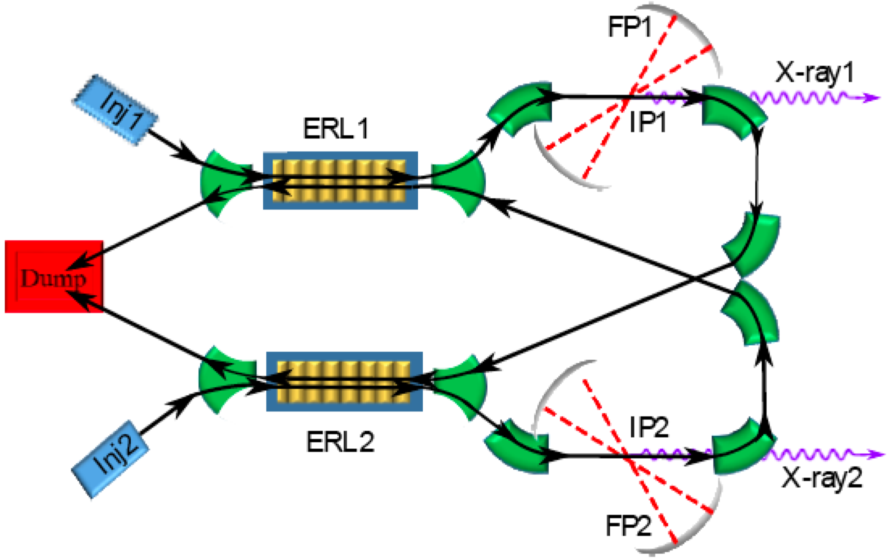

Energy (MeV)	30 - 100
Bunch charge (pC)	100 - 200
Repetition rate (for CW operation) (MHz)	100
Average Current (mA)	10 - 20
Nominal beam power (MW)	0.3 - 2.0
Energy recovered beam power (kW)	60 - 120
rms bunch length (μm)	400 - 900
$\varepsilon_{x,y}$ (mm mrad)	< 1.0
Bunch Energy spread (%)	< 0.05
Focal spot size (μm)	15 - 40
Bunch separation (ns)	10
Energy jitter shot-to-shot (%)	0.2
Time arrival jitter (ps)	< 0.15
Pointing jitter (μm)	3

Photon energy (keV)	20 - 180
Bandwidth (%)	1 - 10
# photons per shot within FWHM bw	0.05×10^5 - 1.0×10^5
# photons/sec within FWHM bw	0.05×10^{13} - 1.0×10^{13}
Source size (μm)	≤ 20
Source divergence (mrad)	6 - 1
Photon beam spot size (FWHM at z = 100 m) (cm)	40 - 4
Peak Brilliance†	10^{18} - 10^{19}
Radiation pulse length (ps)	0.7 - 1.5
Linear/Circular Polarization (%)	> 99
Repetition rate (MHz)	100
Pulse-to-pulse separation (ns)	10

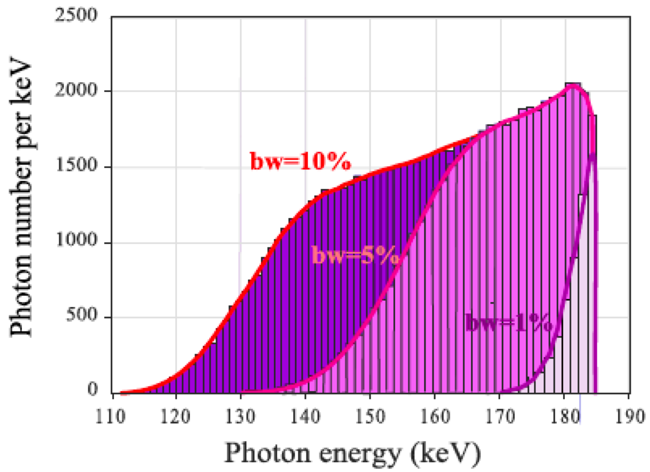

BriXSino: MariX Demonstrator at LASA/Milano

UNIVERSITÀ DEGLI STUDI DI MILANO

5 mA, 100 MHz, 45 MeV
> 90% energy recovery

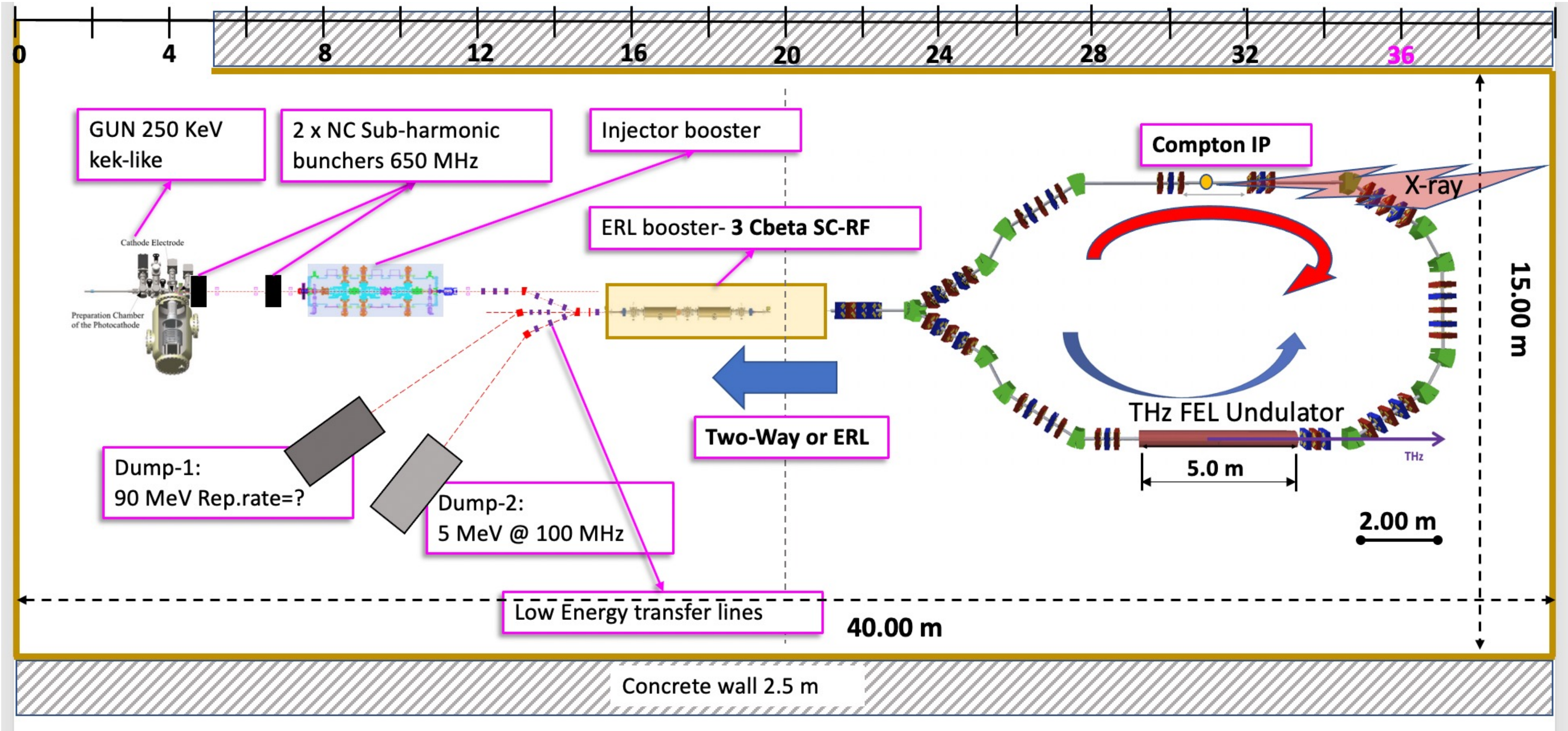

≈ 6 M€, TDR preparation approved by INFN, due by March 2021

Nuclear Inst. and Methods in Physics Research, A 930 (2019) 167–172

UNIVERSITÀ DEGLI STUDI DI MILANO

Contents lists available at ScienceDirect

Nuclear Inst. and Methods in Physics Research, A

journal homepage: www.elsevier.com/locate/nima

ELSEVIER

MariX, an advanced MHz-class repetition rate X-ray source for linear regime time-resolved spectroscopy and photon scattering

L. Serafini [1], A. Bacci [1], A. Bellandi [2], M. Bertucci [1], M. Bolognesi [3], A. Bosotti [1], F. Broggi [1], R. Calandrino [4], F. Camera [3,1], F. Canella [3], S. Capra [3,1], P. Cardarelli [5,6], M. Carrara [7], K. Cassou [8], A. Castoldi [9,1], R. Castriconi [4], G.M. Cattaneo [4], S. Cialdi [3,1], A. Cianchi [10], N. Coluccelli [9,11], C. Curatolo [12], A. Del Vecchio [4], S. Di Mitri [13], I. Drebot [1], K. Dupraz [8], A. Esposito [14], L. Faillace [1], M. Ferrario [14], C. Fiorini [9,1], G. Galzerano [11,9], M. Gambaccini [5,6], G. Ghiringhelli [9], D. Giannotti [1], D. Giove [1], F. Groppi [3,1], C. Guazzoni [9,1], P. Laporta [9,11], S. Leoni [3,1], A. Loria [4], P. Mangili [4], A. Martens [8], T. Mazza [15], Z. Mazzotta [16], C. Meroni [1], G Mettivier [17], P. Michelato [1], L. Monaco [1], S. Morante [10], M. Moretti Sala [9], D. Nutarelli [8], S. Olivares [3,1], G. Onida [3], M. Opromolla [3,1], C. Pagani [3,1], R. Paparella [1], M.G.A. Paris [3,1], B. Paroli [3,1], G. Paternò [6], C. Paulin [3], L. Perini [3,1], M. Petrarca [18], V. Petrillo [3,1,*], E. Pinotti [9], P. Piseri [3,1], M.A.C. Potenza [3], F. Prelz [1], A. Pullia [3,1], E. Puppin [9,1], F. Ragusa [3,1], R. Ramponi [9,11,1], M. Romè [3,1], M. Rossetti Conti [1], A.R. Rossi [1], L. Rossi [19], M. Ruijter [18,1], P. Russo [17], S. Samsam [20,1], A. Sarno [17], D. Sertore [1], M. Sorbi [3,1], B. Spataro [14], M. Statera [1], F. Stellato [10], E. Suerra [3,1], A. Tagliaferri [9], A. Taibi [5,6], V. Torri [1], G. Turchetti [21], C. Vaccarezza [14], R. Valdagni [22], A. Vanzulli [3,23], F. Zomer [8], G. Rossi [3]

[1] INFN - Sezione di Milano, Via Celoria 16, 20133, Milano and LASA, Via F. Cervi 201, 20090 Segrate (MI), Italy
[2] DESY, Notkestrasse 85, 22603 Hamburg, Germany
[3] Università degli Studi di Milano, Via Festa del Perdono 7, 20100 Milano, Italy
[4] Istituto di Ricovero e Cura a Carattere Scientifico Ospedale San Raffaele, Via Olgettina 60, 20132 Milano, Italy
[5] Università di Ferrara, Via Saragat, 1 44122 Ferrara, Italy
[6] INFN - Sezione di Ferrara, Via Saragat, 1 44122 Ferrara, Italy
[7] Istituto Nazionale dei Tumori, Via Giacomo Venezian, 1 - 20133 Milano, Italy
[8] LAL, Univ. Paris-Sud, CNRS/IN2P3, Université Paris-Saclay, 91898 Orsay, France
[9] Politecnico di Milano, Piazza Leonardo da Vinci, 32 20133 Milano, Italy
[10] Università degli Studi di Roma Tor Vergata and INFN, Via della Ricerca Scientifica, 1 00133 Roma, Italy
[11] Istituto di Fotonica e Nanotecnologie, CNR, Piazza Leonardo da Vinci, 32 20133 Milano, Italy
[12] INFN - Sezione di Padova, Via Marzolo, 8 - 35131 Padova, Italy
[13] Elettra - Sincrotrone Trieste, 34149 Basovizza, Trieste, Italy
[14] INFN - Laboratori Nazionali di Frascati, Via Enrico Fermi, 40 00044 Frascati (RM), Italy
[15] European X-ray Free Electron Laser Facility GmbH, Holzkoppel, 4 - 22869 Schenefeld, Germany
[16] ARCNL, Advanced Research Center for Nano-Lithography, EUV Group, 106 Science Park, 1098xg Amsterdam, The Netherlands
[17] Università degli Studi di Napoli 'Federico II', Dipartimento di Fisica 'E. Pancini' and INFN Sez. Napoli, Via Cintia, 80126, Napoli, Italy
[18] Università degli Studi di Roma 'La Sapienza' and INFN, Piazzale Aldo Moro, 5 - 00185 Roma, Italy
[19] CERN - Accelerator & Technology Sector, Esplanade des Particules, 1 - 1217 Meyrin, Switzerland. On leave from Università Degli Studi di Milano.
[20] Faculty of Sciences, Mohammed V University, Rabat, Morocco
[21] Alma Mater Studiorum - Università di Bologna, Dipartimento di Fisica e Astronomia, via Irnerio, 46 40126 Bologna, Italy
[22] Istituto Nazionale dei Tumori, Via Giacomo Venezian, 1 - 20133, Milano, Italy and Università degli Studi diMilano, Dipartimento di Oncologia ed Emato-oncologia, Via S. Sofia, 9/1 - 20122 Milano, Italy
[23] ASST Grande Ospedale Metropolitano Niguarda, Piazza Ospedale Maggiore, 3 - 20162 Milano, Italy

Executive Summary published on NIM-A

Nuclear Physics

European Collaboration for the proposal of a Gamma-Beam System to the ELI-NP Project

Technical Design Report

EuroGammaS proposal for the ELI-NP Gamma beam System

With 73 tables and 230 figures

O. Adriani, S. Albergo, D. Alesini, M. Anania, D. Angal-Kalinin, P. Antici, A. Bacci, R. Bedogni, M. Bellaveglia, C. Biscari, N. Bliss, R. Boni, M. Boscolo, F. Broggi, P. Cardarelli, K. Cassou, M. Castellano, L. Catani, I. Chaikovska, E. Chiadroni, R. Chiche, A. Cianchi, J. Clarke, A. Clozza, M. Coppola, A. Courjaud, C. Curatolo, O. Dadoun, N. Delerue, C. De Martinis, G. Di Domenico, E. Di Pasquale, G. Di Pirro, A. Drago, F. Druon, K. Dupraz, F. Egal, A. Esposito, F. Falcoz, B. Fell, M. Ferrario, L. Ficcadenti, P. Fichot, A. Gallo, M. Gambaccini, G. Gatti, P. Georges, A. Ghigo, A. Goulden, G. Graziani, D. Guibout, O. Guilbaud, M. Hanna, J. Herbert, T. Hovsepian, E. Iarocci, P. Iorio, S. Jamison, S. Kazamias, F. Labaye, L. Lancia, F. Marcellini, A. Martens, C. Maroli, B. Martlew, M. Marziani, G. Mazzitelli, P. McIntosh, M. Migliorati, A. Mostacci, A. Mueller, V. Nardone, E. Pace, D.T. Palmer, L. Palumbo, A. Pelorosso, F.X. Perin, G. Passaleva, L. Pellegrino, V. Petrillo, M. Pittman, G. Riboulet, R. Ricci, C. Ronsivalle, D. Ros, A. Rossi, L. Serafini, M. Serio, F. Sgamma, R. Smith, S. Smith, V. Soskov, B. Spataro, M. Statera, A. Stecchi, A. Stella, A. Stocchi, S. Tocci, P. Tomassini, S. Tomassini, A. Tricomi, C. Vaccarezza, A. Variola, M. Veltri, S. Vescovi, F. Villa, F. Wang, E. Yildiz, F. Zomer

109 Authors, 327 pages
published today on ArXiv
http://arxiv.org/abs/1407.3669

Challenges of *electron-(optical)photon colliders* as *X/γ* beam Sources using Compton back-scattering

- **Need of *high peak brightness/high average current* electron beams (cmp. FEL's drivers) *fsec-class* synchronized and *μm-μrad-scale* aligned to *high peak/average power* laser beams**
- **Main goal for Nuclear Physics and Nuclear Photonics:**

  ***Spectral Densities* > 10^4 $N_{ph}/(s \cdot eV)$**

  photon energy range 1-20 MeV, *bandwidths* 10^{-3} class
- **Main goal for Medical Applications with *X*-rays: tunability in the 20-120 keV range, good mono-chromaticity (1-10 %), high flux (10^{11} min., 10^{12} for radio-imaging, 10^{13} for radio-therapy)**

- **Main goal for *MeV-class* $\gamma - \gamma$ and *TeV* γ - nucleon colliders:**
  ***Peak Brilliance* > 10^{21}** $N_{ph}/(s \cdot mm^2 \cdot mrad^2 \cdot 0.1\%)$ **$10^9 < N_{ph} < 10^{13}$**
  Source spot size μm-scale (low diffraction, few μrad)
  Tunability, Mono-chromaticity, Polarization (H,V,C)
- **Photon-Photon scattering (+ Breit-Wheeler: pair creation in vacuum) is becoming feasible with this new generation γ-beams: a γ-γ low energy collider**

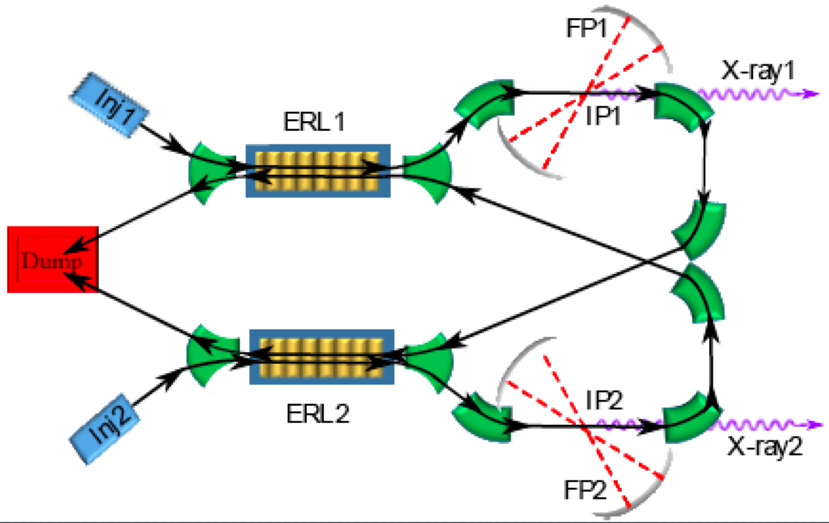

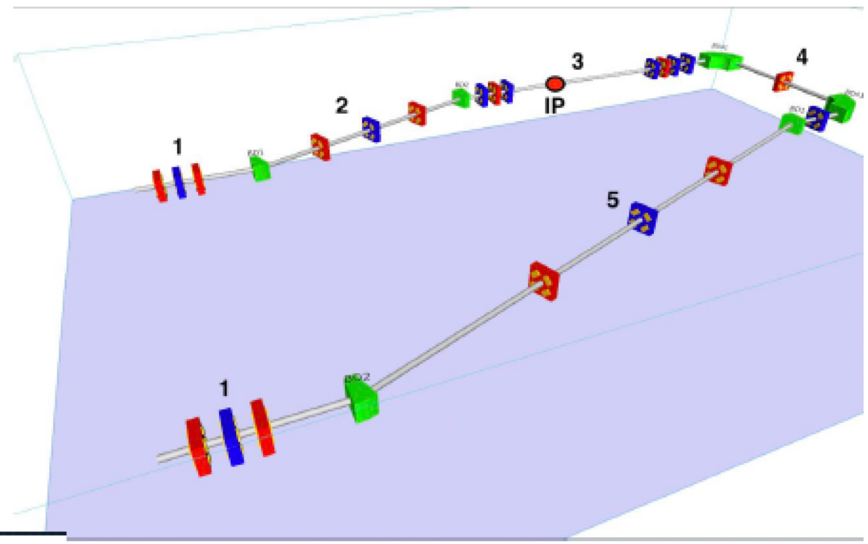

Physica Medica
European Journal of Medical Physics

Articles and Issues | For Authors | Journal Info | Editor's Choice | Virtual Issues | Society Info | EF

All Content | Search | Advanced Search

< Previous Article | August 2018 Volume 52, Supplement 1, Page 74 | Next Article >

[OA192] Kilovoltage rotational radiotherapy with the marix/brixs source for partial breast irradiation

Giovanni Mettivier, Illya Drebot, Alberto Bacci, Vittoria Petrillo, M. Rosetti, Andrea Rossi, Luca Serafini, Riccardo Calandrino, Mauro Cattaneo, Claudio Fiorini, Roberta Castriconi, Antonio Sarno, Francesca Di Lillo, Marica Masi, Paolo Russo

DOI: https://doi.org/10.1016/j.ejmp.2018.06.264

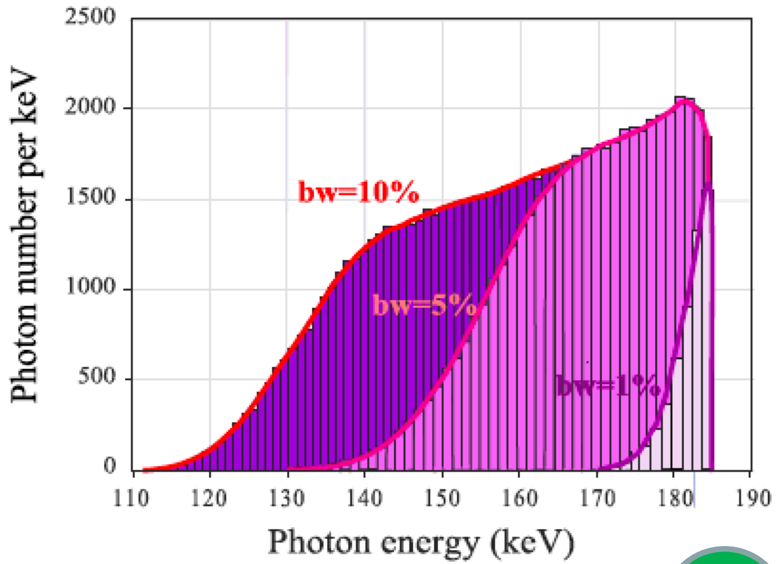

If the Physics of Linear Compton/Thomson back-scattering is well known….

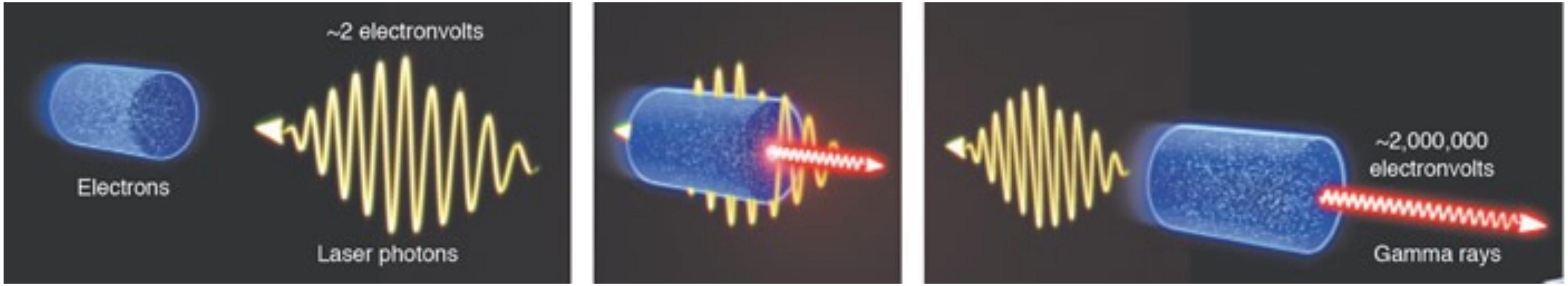

the Challenge of making a Compton Source running as an electron-photon Collider with maximum Luminosity, to achieve the requested Spectral Density, Brilliance, narrow Bandwidth of the generated *X/γ* ray beam, is a completely different issue/business !

Re-visiting the Physics of Compton back-scattering with an eye to effects impacting the quality and behavior of the photon (and electron) beam phase space distributions

Courtesy L. Palumbo

LINEAR (a_0<<1, single photon) THOMSON BACK-SCATTERING

$$\nu_X = \nu_L \frac{1-\beta\cos\alpha_L}{1-\beta\cos\theta} \approx \nu_L \frac{4\gamma^2}{1+\theta^2\gamma^2} \approx 4\gamma^2\nu_L$$

$$for\ \alpha_L = \pi\ (scatt.\ angle) \qquad and$$

$$\theta << 1 \quad or \quad \theta = 0\ (obs.\ angle)$$

e^- (1 GeV); λ_0=1μm, E_0=1.24 eV ⟶ λ_T=6 x10^{-8}μm, E_T=20 MeV

e^- (200 MeV); λ_0=1μm, E_0=1.24 eV ⟶ λ_T=1.56 x10^{-6}μm, E_T=800 KeV

e^- (29 MeV); λ_0=0.8μm, E_0=1.5 eV ⟶ λ_T=0.5 x10^{-4}μm, E_T=20 KeV

From the electron orbits and the Liénard-Wiechert potentials **in the far zone** one can write the expression of the electric field [Jackson..]:

$$\mathbf{E} = \frac{e}{c}\left[\frac{\mathbf{n}\times\left[(\mathbf{n}-\boldsymbol{\beta}(t'))\times\dot{\boldsymbol{\beta}}(t')\right]}{R(1-\mathbf{n}\cdot\boldsymbol{\beta}(t'))^{3}}\right]_{ret}$$

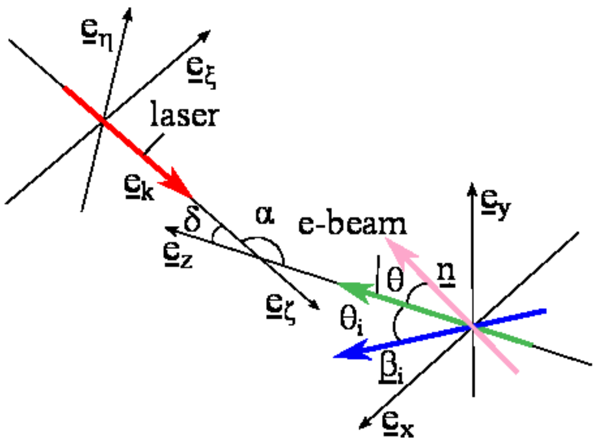

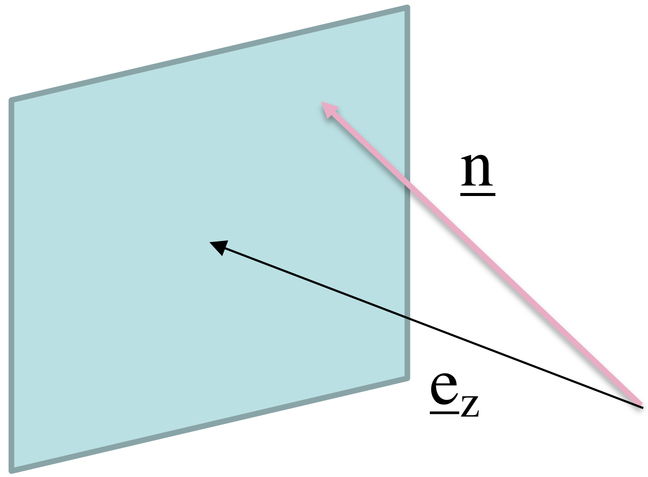

Courtesy V. Petrillo

From the motion equation of the electrons

$$\frac{d\mathbf{p}}{dt} = -e(\mathbf{E}_L + \boldsymbol{\beta} \times \mathbf{B}_L)$$

If **E** and **B=k**x**E** are electric and magnetic field of the incoming laser,

$$\dot{\boldsymbol{\beta}} = \frac{d\boldsymbol{\beta}}{dt} = -\frac{e}{mc\gamma}(\mathbf{E}_L(1-\boldsymbol{\beta}\cdot\mathbf{e}_k) + \boldsymbol{\beta}\cdot\mathbf{E}_L(\mathbf{k}-\boldsymbol{\beta}))$$

Courtesy V. Petrillo

Classical double differential spectrum

The double differential spectrum for **one electron** is:

$$\frac{d^2W_i}{d\omega d\Omega} = \frac{e^2}{4\pi^2 c}\left|\int_{-\infty}^{+\infty} dt e^{i\omega t}\,\frac{\mathbf{n}\times\left[(\mathbf{n}-\beta(t'))\times\dot{\beta}(t')\right]}{(1-\mathbf{n}\cdot\beta(t'))^3}\right|^2 = \hbar\omega\frac{\mathrm{d}^2\mathrm{N}_\mathrm{i}}{\mathrm{d}\omega\mathrm{d}\Omega}$$

And for all the beam:

$$\hbar\omega\frac{\mathrm{d}^2\mathrm{N}}{\mathrm{d}\omega\mathrm{d}\Omega} = \hbar\omega\sum_i\frac{\mathrm{d}^2\mathrm{N}_\mathrm{i}}{\mathrm{d}\omega\mathrm{d}\Omega}$$

$$\Psi \equiv \gamma\vartheta_M$$

$$N(\Psi) \cong \pi\alpha\Im N_e\left(\frac{cT}{\lambda}\right)a_0^2\Psi^2\,\frac{(1+\Psi^2+\frac{2}{3}\Psi^4)}{\left(1+\Psi^2\right)^3}$$

Full treatement of linear and nonlin. TS for a plane-wave laser pulse with analytical expression of the distributions in ***P. Tomassini et al***., Appl. Phys. B **80**, 419 (2005).

$$\Psi \equiv \gamma \vartheta_M$$

$$N(\Psi) \cong \pi \alpha \Im N_e \left(\frac{cT}{\lambda} \right) a_0^2 \Psi^2 \frac{(1+\Psi^2+\frac{2}{3}\Psi^4)}{\left(1+\Psi^2\right)^3}$$

$$a_0 = 4.3 \frac{\lambda}{w_0} \sqrt{\frac{U_L[J]}{\sigma_t[ps]}}$$

$a_0 \equiv e^2 A/(m_e c^2) = 8.5 \times 10^{-10} \sqrt{I \lambda_0^2}$, I being the peak intensity in W/cm^2 and λ_0 the wavelength in μm, the pulse

$$N_l a_0^2 \propto \frac{U_L}{w_0^2}$$

Total intensity and Stokes parameter $|E_x|^2-|E_y|^2$ on the screen at 1 m, γ=1200

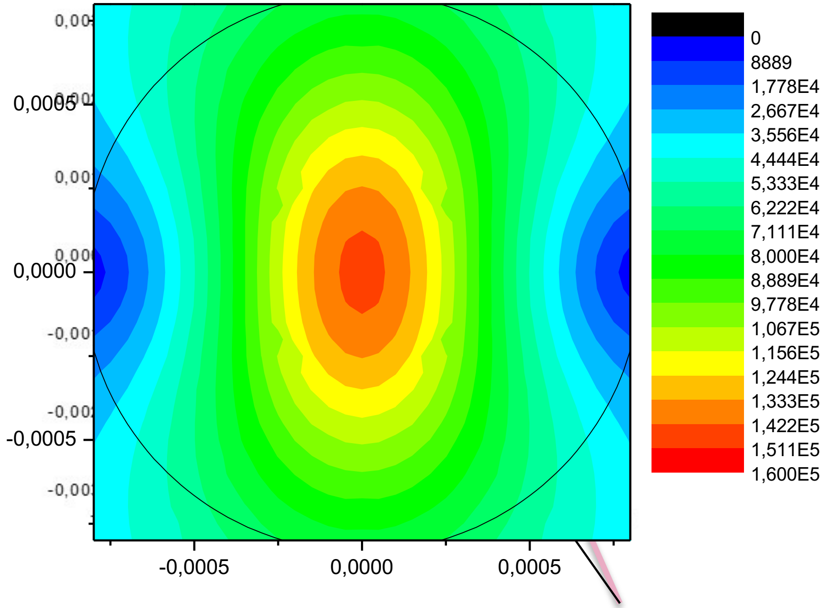

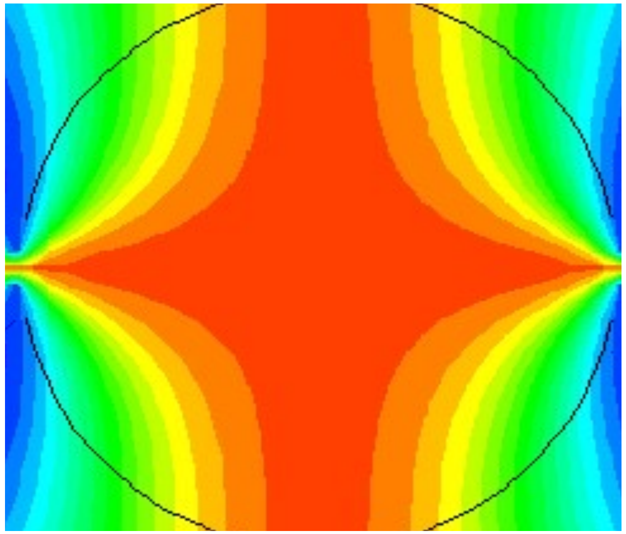

IEEE TRANSACTIONS ON PLASMA SCIENCE, VOL. 36, NO. 4, AUGUST 2008

Linear and Nonlinear Thomson Scattering for Advanced X-ray Sources in PLASMONX

Paolo Tomassini, A. Bacci, J. Cary, M. Ferrario, A. Giulietti, Danilo Giulietti, L. A. Gizzi, Luca Labate, L. Serafini, Vittoria Petrillo, and C. Vaccarezza

***Abstract*—Thomson scattering of laser pulses onto ultrarelativistic e-bunches is becoming an advanced source of tunable, quasi-monochromatic, and ultrashort X/gamma radiation. Sources aimed at reaching a high flux of scattered photons need to be driven by high-brightness e-beams, whereas extremely short (femtosecond scale or less) sources need to make femtosecond-long e-beams that collide with the laser pulses. In this paper, we explore the performance of the PLASMONX TS source in several operating regimes, including preliminary results on a source based on e-bunches produced by laser wakefield acceleration and controlled injection via density downramp.**

***Index Terms*—Compton scattering, Thomson scattering (TS), X-ray sources.**

I. Introduction

FUNDED by the Istituto Nazionale di Fisica Nucleare (INFN), the PLasma Acceleration at Sparc and MONOfield acceleration (LWFA) with internal/external injection or Thomson scattering (TS) physics and applications. TS X-ray sources are attracting strong attention because of their flexibility and potential compactness with respect to conventional synchrotron sources. A TS source driven by high-quality e-beams can be switched on in several operating modes, namely, the high-flux-moderate-monochromaticity mode (HFM2), the moderate-flux-monochromatic mode (MFM), and the short-and-monochromatic mode (SM). The HFM2 mode is suitable, e.g., for medical imaging, when high-flux sources are needed and a moderate monochromaticity is useful to improve the detection/dose performance. The MFM mode is useful for static probing when high monochromaticity and, possibly, tunability are needed (e.g., imaging with subtraction of images taken with different energies). The SM mode is finally u[...] pump-and-probe experiments, e.g., in physical chem[...]

the Compton process). If the electrons are ultrarelativistic, the scattered radiation looks frequency-upshifted and is mostly emitted forward with respect to the motion of particles in a small cone of aperture roughly given by the inverse of their Lorentz gamma.

The physics of TS is quite complex in the nonlinear regime, i.e., when the laser pulse strength $a0 = 8.5 \cdot 10^{-10}(I\lambda^2)^{1/2}$ approaches or exceeds unity. At intensities above the so-called "relativistic intensity" $I\lambda^2 = 10^{18}\ \mu\mathrm{m}^2 \cdot \mathrm{W/cm}^2$, the extremely intense electric field makes the electrons' quivering speed approach the light speed, making the magnetic field relevant for dynamics, thus generating a complex particle motion.

The computation in the far field of the scattered photons' distribution N_λ of pulsation ω can be performed in the classical regime provided that the energy of the electrons is far below tens of gigaelectronvolts, as it is the case for this paper, by using

$$\frac{d^2N_\gamma}{d\omega d\Omega} = \frac{\alpha}{4\pi^2}\omega\left|\vec{J}(\vec{n},\omega)\right|^2$$
$$\vec{J}(\vec{n},\omega) = \vec{n}\times\left(\vec{n}\times\int dt\vec{\beta}(t)e^{i\omega\left(t-\frac{\vec{n}\cdot\vec{r}(t)}{c}\right)}\right) \quad (1)$$

where r and β represent the particle position and speed, respectively, and $\vec{n}$ is the emitted photon unit versor. By taking the retarded effects into account, which are the nonlinear quivering and secular motion of each electron in the bunch due to pulse longitudinal ponderomotive forces, an analytical computation

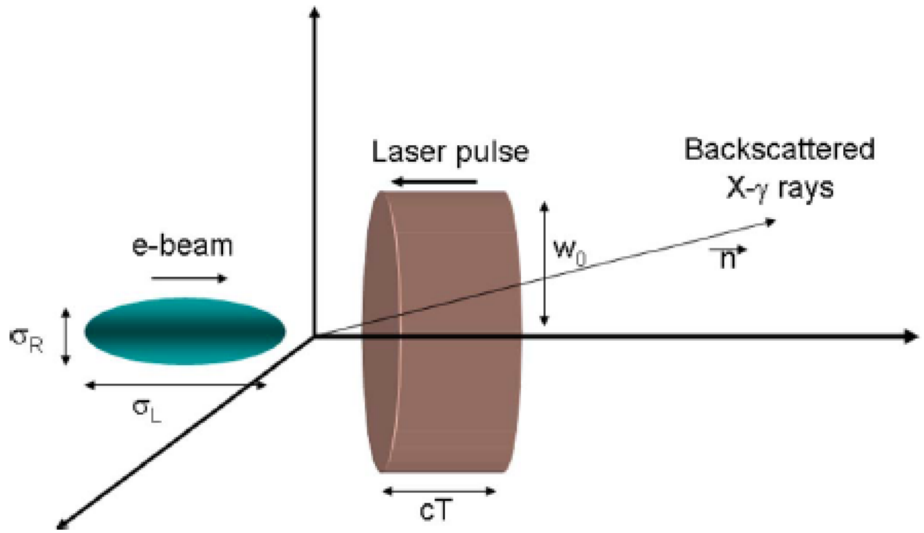

Fig. 1. Thomson backscattering geometry. The electron beam of longitudinal and transverse sizes σ_L and σ_R, respectively, is moving at a relativistic speed from left to right, colliding with a photon beam of waist size w_0 and duration T, thus emitting scattered radiation mainly in the direction of motion of the electron beam.

electron bunch parameters considered in this paper; see [4]). Considering that the analytical outcome sketched in (2) and (3) are valid only for the case of planar long flattop laser pulse, the code decomposes the pulse in a sequence of single cycles, with each cycle having its own phase shift and intensity. While the particle is moving along its secular path, it interacts with different cycles of the pulse, and the coherent summat[illegible] the radiation emitted in each cycle gives rise to the ra[illegible] emitted during the entire interaction.

Example

Quasi head-on collision of a 5 MeV electron ($\theta_e = 50$ mrad, $\phi_e = \pi/2$) on a flat-top pulse of normalized ampliude a_0=1.5, $\lambda = 1\mu$m and T = 20 fs

P. Tomassini et al., Appl. Phys. B 80, 419 (2005)

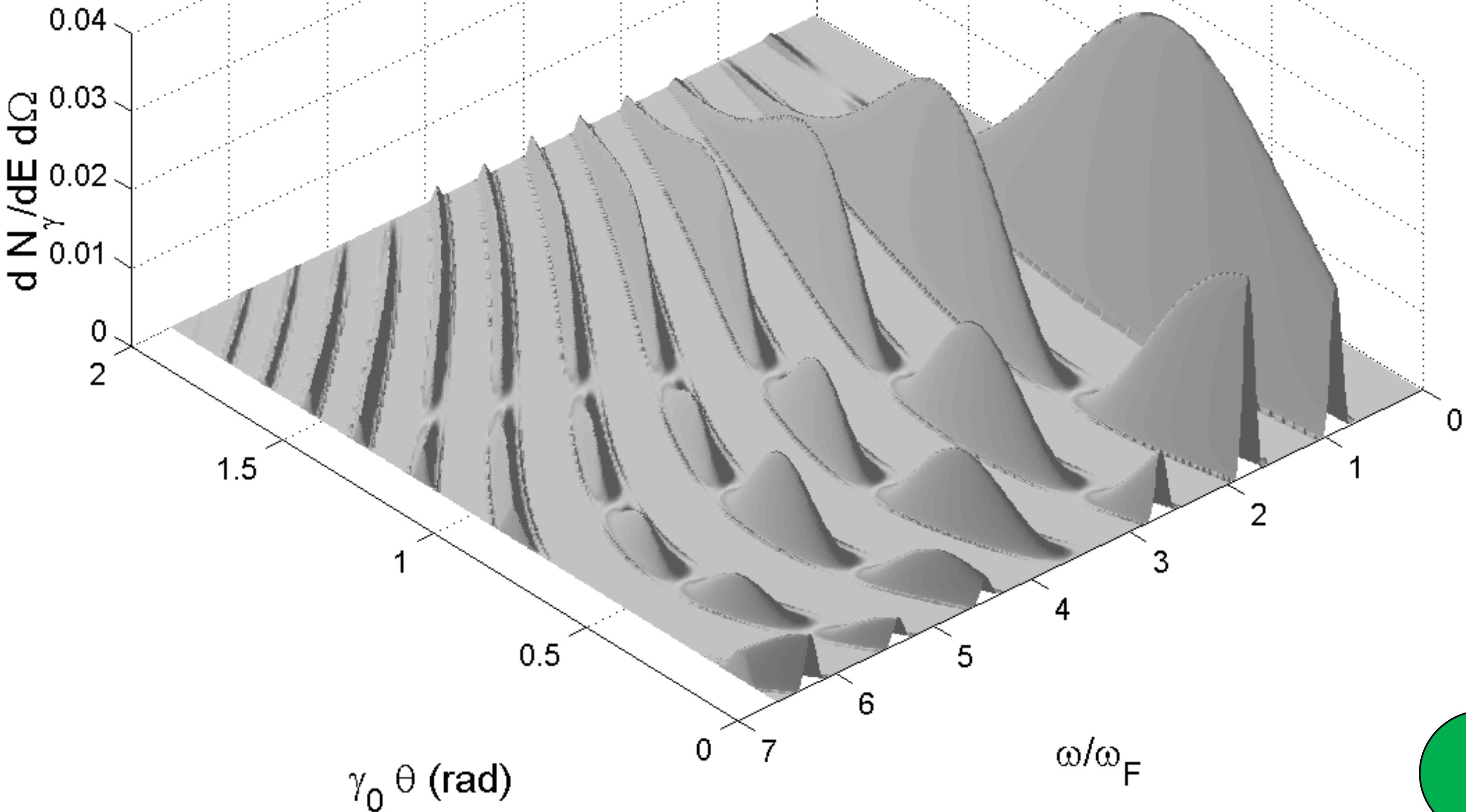

Compton Inverse Scattering Physics is clear: recall some basics

Quantum model

Laboratory ref. system

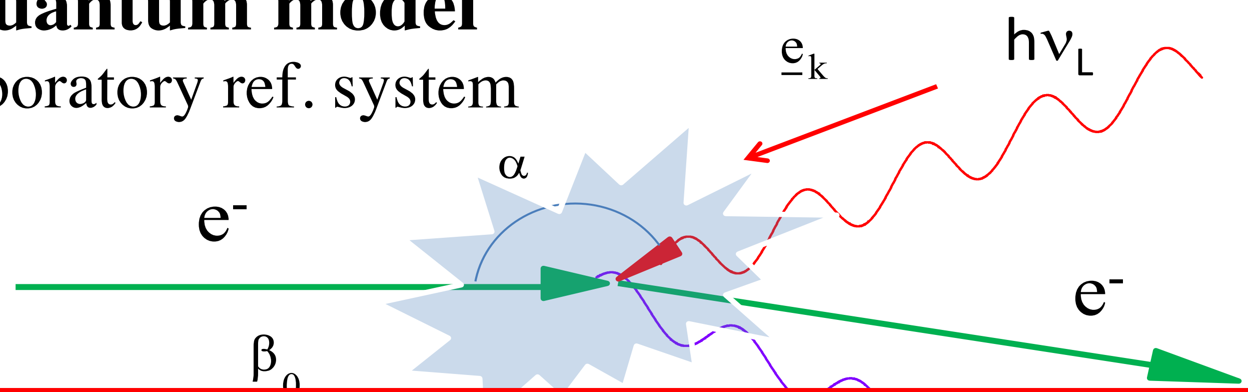

3 regimes: a) Elastic, Thomson b) Quasi-Elastic, Compton with Thomson cross-section c) Inelastic, Compton, recoil dominated

$$\begin{cases} mc^2(\gamma-\gamma_0) = -h(\nu-\nu_L) \\ mc(\underline{\beta}\gamma-\underline{\beta}_0\gamma_0) = -h(\underline{k}-\underline{k}_L)/2\pi \end{cases}$$

Energy and momentum conservation laws

γ_0:initial Lorentz factor

$$\nu = \nu_L \frac{1-\underline{e}_k\cdot\underline{\beta}_0}{1-\underline{n}\cdot\underline{\beta}_0 + \frac{h\nu_L}{mc^2\gamma_0}(1-\underline{e}_k\cdot\underline{n})}$$

$$\lambda = \lambda_L \frac{1-\underline{n}\cdot\underline{\beta}_0}{1-\underline{e}_k\cdot\underline{\beta}_0} + \frac{h}{mc\gamma_0}\frac{1-\underline{e}_k\cdot\underline{n}}{1-\underline{e}_k\cdot\underline{\beta}_0}$$

Petrillo V. and al., NIM A **693** (2012)
Sun C. and Wu Y. K., PRSTAB **14** (2011) 044701

Courtesy V. Petrillo

Quant… ns in the Cente… ematics)

ref.

n. ref.

$\ldots^{*}_{e} + \hbar\vec{k}^{*}_{h\nu} = \vec{0}$

Analytical description of photon beam phase spaces in Inverse Compton Scattering sources

C. Curatolo,[1] I. Drebot,[1] V. Petrillo,[1,2] and L. Serafini[1]

[1] *INFN-Milan, via Celoria 16, 20133 Milano, Italy*

[2] *Università degli Studi di Milano, via Celoria 16, 20133 Milano, Italy*

(Dated: 22 May 2017)

We revisit the description of inverse Compton scattering sources and the photon beams generated therein, emphasizing the behavior of their phase space density distributions and how they depend upon those of the two colliding beams of electrons and photons. Main objective is to provide practical formulas for bandwidth, spectral density, brilliance, which are valid in general for any value of the recoil factor, i.e. both in the Thomson regime of negligible electron recoil, and in the deep Compton recoil dominated region, which is of interest for gamma-gamma colliders and Compton Sources for the production of multi-GeV photon beams. We adopt a description based on the center of mass reference system of the electron-photon collision, in order to underline the role of the electron recoil and how it controls the relativistic Doppler/boost effect in various regimes. Using the center of mass reference frame greatly simplifies the treatment, allowing to derive simple formulas expressed in terms of rms momenta of the two colliding beams (emittance, energy spread, etc.) and the collimation angle in the laboratory system. Comparisons with Monte Carlo simulations of inverse Compton scattering in various scenarios are presented, showing very good agreement with the analytical formulas: in particular we find that the bandwidth dependence on the electron beam emittance, of paramount importance in Thomson regime, as it limits the amount of focusing imparted to the electron beam, becomes much less sensitive in deep Compton regime, allowing a stronger focusing of the electron beam to enhance luminosity without loss of mono-chromaticity. A similar effect occurs concerning the bandwidth dependence on the frequency spread of the incident photons: in deep recoil regime the bandwidth comes out to be much less dependent on the frequency spread. The set of formulas here derived are very helpful in designing inverse Compton sources in diverse regimes, giving a quite accurate first estimate in typical operational conditions for number of photons, bandwidth, spectral density and brilliance values - the typical figures of merit of such radiation sources.

I. INTRODUCTION

Inverse Compton Scattering sources (ICSs) are becoming increasingly attractive as radiation sources in photon energy regions either not covered by other high brilliance sources (FEL's, synchrotron light sources) or where compactness becomes an important figure of merit, like for advanced X-ray imaging applications to be implemented in university campus, hospitals, museums, etc., i.e. outside of research centers or large scale laboratories [1]. ICSs are becoming the γ-ray sources of reference in nuclear photonics, photo-nuclear [2, 3] and fundamental physics [4], thanks to superior performances in spectral densities achievable. Eventually they will be considered for very high energy photon generation (in the GeV to TeV range) since there are no other competing techniques at present, neither on the horizon, based on artificial tools at this high photon energy [5]. As a consequence, a flourishing of design activities is presently occurring in several laboratories [6–15] and companies [16–19], where ICSs are being conceived, designed and built to enable several domains of applications, and ranging from a few keV photon energy up to GeV's and beyond. Designs of ICSs are carried out considering several diverse schemes, ranging from high gradient room temperature pulsed RF Linacs [3, 20, 21] to CW ERL Super-conducting Linacs [22, 23] or storage rings [2, 24–27], as far as the electron beam generation is concerned, and from single pulse J-class amplified laser systems running at 100 Hz to optical cavities (e.g. Fabry-Perot) running at 100 MHz acting as photon storage rings for the optical photon beams, not to mention schemes based on FEL's to provide the colliding photon beam [22, 28, 29].

In order to assess the performances of a specific ICSs under design, detailed simulations of the electron-photon beam collision are typically carried out using Monte Carlo codes [30–32] able to model the linear and nonlinear electron-photon quantum interaction leading to Compton back-scattering events, taking into account in a complete fashion the space-time propagation of the two colliding beams through the interaction point region, including possible multiple scattering events occurring during the overlap of the two pulses. Only in case of negligible electron recoil, i.e. in the so called Thomson regime typical of low energy X-ray ICSs, classical electromagnetic numerical codes (e.g. TSST [33]), modelling the equivalent undulator radiation emitted by electrons wiggling in the electromagnetic field of the incoming laser pulse, allow to analyze particular situations such as the use of chirped [34], tilted [35] and twisted [36] lasers.

In the recent past some efforts have been developed to carry out analytical treatments of the beam-beam collision physics, embedding the single electron-photon collision from a quantum point of view within a rms distribution of the scattered photon beam [27, 37–43], or,

$electron\ 4-ve\ldots\ E_e^2/c^2 - m_e^2c^2\Big]$

$photon\ 4-vec\ldots\ {}_L/c\Big]$

Invariant Mass, Lorentz transformation from Lab to c.m. ref. system

$$Total\ 4-vector\ \mathbf{P} = \mathbf{P}_e + \mathbf{P}_{h\nu} = \left[E_e/c + h\nu_L/c, 0, 0, \sqrt{\frac{E_e^2}{c^2} - m_e^2 c^2} - h\nu_L/c \right]$$

$$Invariant\ Mass\ s \equiv c\mathbf{P} \bullet c\mathbf{P} = E_{tot}^{2*} = E_{cm}^2$$

$$\left(4-vector\ product\ \mathbf{P}_1 \bullet \mathbf{P}_2 \equiv \left[E_1 E_2 / c^2 - \vec{p}_1 \cdot \vec{p}_2 \right] \right)$$

$$E_{cm} \cong \sqrt{4 E_e h\nu_L + m_e^2 c^4} = m_e c^2 \sqrt{1 + \frac{4\gamma h\nu_L}{m_e c^2}} = m_e c^2 \sqrt{1 + \Delta}$$

$$e^-\ recoil\ factor\ \Delta \equiv \frac{4\gamma h\nu_L}{m_e c^2}$$

from $\vec{p}^{\,*}_{tot} = \vec{p}^{\,*}_e + \hbar\vec{k}^{\,*}_{h\nu} = \vec{0}$ $\Rightarrow$ $|\vec{p}^{\,*}_e| = \hbar|\vec{k}^{\,*}_{h\nu}|$

and $E_{cm} = E^*_e + h\nu^* = m_e c^2\sqrt{1+\Delta}$

$$\begin{pmatrix} E^{*}_e = m_e^2 c^4 + |\vec{p}^{\,*}_e|^2 c^2 \\ h\nu^* = \hbar|\vec{k}^{\,*}_{h\nu}|c \end{pmatrix}$$

$\Downarrow$

$$E^*_e = m_e c^2 \frac{2+\Delta}{2\sqrt{1+\Delta}}$$

$$h\nu^* = m_e c^2 \frac{\Delta}{2\sqrt{1+\Delta}} = \frac{2\gamma h\nu_L}{\sqrt{1+\Delta}}$$

$$|\vec{p}^{\,*}_e| = m_e c \frac{\Delta}{2\sqrt{1+\Delta}}$$

Holds before and after scattering (c.m ref. system!)

$$\begin{cases} E_{cm} \xrightarrow[\Delta\to 0]{} m_e c^2 \\ E_{cm} \xrightarrow[\Delta\to\infty]{} 2\sqrt{\gamma m_e c^2 h\nu_L} = 2\sqrt{E_e E_{h\nu}} \end{cases}$$

Δ=0 electron as relativ. mirror

Δ>>1 symmetric collider

$$\begin{cases} E_e^* \xrightarrow[\Delta\to 0]{} m_e c^2 \\ E_e^* \xrightarrow[\Delta\to\infty]{} m_e c^2 \dfrac{\sqrt{\Delta}}{2} = \sqrt{\gamma m_e c^2 h\nu_L} \end{cases}$$

$$\begin{cases} h\nu^* \xrightarrow[\Delta\to 0]{} m_e c^2 \dfrac{\Delta}{2} = 2\gamma h\nu_L \\ h\nu^* \xrightarrow[\Delta\to\infty]{} m_e c^2 \dfrac{\sqrt{\Delta}}{2} = \sqrt{\gamma m_e c^2 h\nu_L} \end{cases}$$

$$E_e^* \xrightarrow[\Delta\to\infty]{} h\nu^*$$

symm. collider

before scattering

$$\begin{pmatrix} \vec{p}^{\,*}_{eIN} = \left[0,0,p^*_e\right] \\ \hbar\vec{k}^*_{IN} = \left[0,0,-h\nu^*/c\right] \end{pmatrix}$$

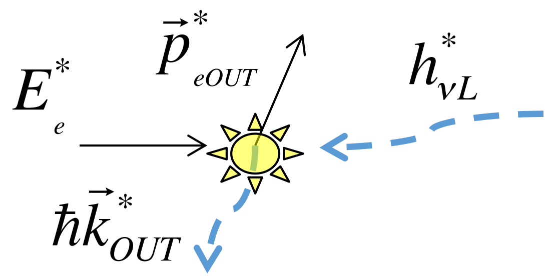

after scatt.

$$\begin{pmatrix} \vec{p}^{\,*}_{eOUT} = \left[p^*_e \sin\vartheta^* \cos\varphi^*, p^*_e \sin\vartheta^* \sin\varphi^*, p^*_e \cos\vartheta^*\right] \\ \hbar\vec{k}^*_{OUT} = \left[-p^*_e \sin\vartheta^* \cos\varphi^*, -p^*_e \sin\vartheta^* \sin\varphi^*, -p^*_e \cos\vartheta^*\right] \end{pmatrix}$$

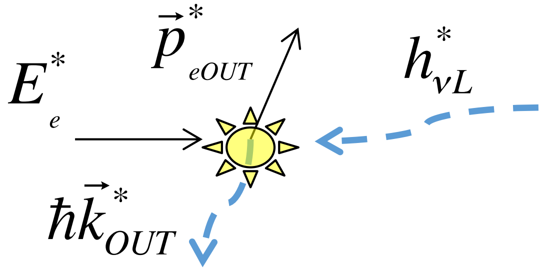

what is the probability of scattering at ϑ^*, φ?
Klein-Nishina differential cross-section

$$\frac{d\sigma}{d\theta' d\phi'} = r_e^2 \left(\frac{2}{2+\Delta(1-cos\theta')}\right)^2 \left(\frac{1+cos^2\theta'}{2}\right) \cdot \left(1 + \frac{\Delta^2(1-cos\theta')^2}{2(1+cos^2\theta')(2+\Delta(1-cos\theta'))}\right) sin\theta'$$

$\Delta \rightarrow 0$

$$\frac{d\sigma}{d\vartheta^* d\varphi^*} = r_e^2 \left(\frac{1+\cos^2\vartheta^*}{2}\right) \sin\vartheta^*$$

$$\vartheta^* = \vartheta' \sqrt{1+\Delta}$$

To transform to the Lab ref. system we need to compute γ_{cm}

$$\gamma_{cm} = \frac{E_{lab}}{E_{cm}} = \frac{E_e + h\nu_L}{m_e c^2 \sqrt{1+\Delta}} \cong \frac{\gamma}{\sqrt{1+\Delta}}$$

Then apply a Lorentz transformation

$$\begin{cases} E_{ph} = p^*_{ph}\gamma_{cm}\left(1 + \sqrt{1 - \frac{1}{\gamma^2_{cm}}}\cos\theta^*\right) \\ p_{phx} = p^*_{ph}\sin\theta^*\cos\phi^* \\ p_{phy} = p^*_{ph}\sin\theta^*\sin\phi^* \\ p_{phz} = p^*_{ph}\gamma_{cm}\left(\sqrt{1 - \frac{1}{\gamma^2_{cm}}} + \cos\theta^*\right) \end{cases}$$

$$\tan\vartheta = \frac{\sin\vartheta^*}{\gamma_{cm}\left(\beta_{cm}+\cos\vartheta^*\right)} \cong \frac{\sqrt{1+\Delta}\,\sin\vartheta^*}{\gamma\left(1+\cos\vartheta^*\right)}$$

$$\cos\vartheta^* \cong \frac{1-\gamma_{cm}^2\tan^2\vartheta}{1+\gamma_{cm}^2\tan^2\vartheta} = \frac{1+\Delta-\gamma^2\tan^2\vartheta}{1+\Delta+\gamma^2\tan^2\vartheta} \qquad if\ \ \beta_{cm}=1$$

general solution
see below

considering only $\vartheta \ll 1 \quad (\vartheta < 1/\gamma)$

$$E_{ph} = m_e c^2 \frac{\Delta\gamma}{2(1+\Delta)}\left[1+\sqrt{1-\frac{1+\Delta}{\gamma^2}\,\frac{1+\Delta-\gamma^2\vartheta^2}{1+\Delta+\gamma^2\vartheta^2}}\right]$$

$\gamma\vartheta < 1$

$$E_{ph} = m_e c^2 \frac{\Delta\gamma}{2(1+\Delta)}\left[2-\frac{1+\Delta}{2\gamma^2}-\frac{2\gamma^2\vartheta^2}{1+\Delta}\right]$$

$$\cos\vartheta^* = \frac{\sqrt{1+tan^2\vartheta}-\gamma_{cm}\sqrt{\gamma_{cm}^2-1}\,tan^2\vartheta}{1+\gamma_{cm}^2 tan^2\vartheta}$$

notation warning $h\nu_x = E_{ph}$

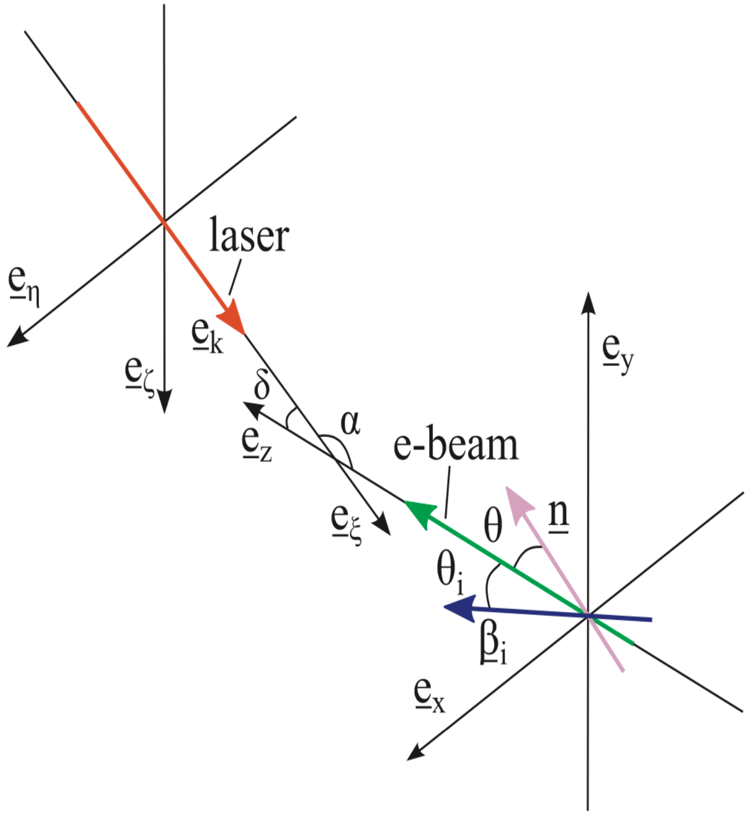

Fig. 1. Geometry of the laser–electron interaction. $\underline{e}_k$ is the unit vector of the laser wave vector, $\underline{\beta}_i$ is the electron normalized velocity, $\underline{n}$ is the scattered radiation direction, $\alpha=\pi-\delta$ is the angle between $\underline{e}_k$ and the axis of the electron beam $\langle\underline{\beta}_i\rangle=\underline{e}_z$, θ the angle between the electron beam axis and $\underline{n}$, and θ_i the angle between the i-th electron velocity $\underline{\beta}_i$ and the beam axis.

Lorentz factor given by

$$\gamma=\gamma_0-\frac{h}{mc^2}(\nu_p-\nu_0) \tag{5}$$

or

$$\gamma=\sqrt{1+\frac{\left(m\gamma_0 c\underline{\beta}_0+\frac{h\nu_0}{c}\underline{e}_k-\frac{h\nu_p}{c}\underline{n}\right)^2}{m^2c^2}}$$

where

$$\nu_p=\nu_0\frac{1-\underline{e}_k\cdot\underline{\beta}_0}{1-\underline{n}\cdot\underline{\beta}_0+\frac{h\nu_0}{mc^2\gamma_0}(1-\underline{n}\cdot\underline{e}_k)} \tag{6}$$

is the Compton frequency of the scattered photon. In these formulas, the index 0 refers to the coordinates before the scattering, $\underline{n}$ is the direction of the scattered photon and $\underline{e}_k$ is the unit vector of the direction of the incident photon of the laser.

A very useful expression is given by the wavelength:

$$\lambda_p=\lambda_0\frac{1-\underline{n}\cdot\underline{\beta}_0}{1-\underline{e}_k\cdot\underline{\beta}_0}+\frac{h}{mc\gamma_0}\frac{1-\underline{n}\cdot\underline{e}_k}{1-\underline{e}_k\cdot\underline{\beta}_0} \tag{7}$$

where the classic and quantum contributions appear clearly

$$E_{ph} = \frac{4\gamma^2 h\nu_L}{1+\Delta}\left[1 - \frac{1+\Delta}{4\gamma^2} - \frac{\gamma^2\vartheta^2}{1+\Delta}\right]$$

$$\gamma >> 1 \qquad (1+\Delta)/\gamma^2 << 1$$

$$f(\alpha) = \frac{1 - \cos\alpha}{2}$$

$$E_{ph} = 4\gamma^2 h\nu_L \frac{1 - \dfrac{\gamma^2\vartheta^2}{1+\Delta}}{1+\Delta} f(\alpha)$$

Deep Compton regime
(Δ>>1 recoil dominated)

$$E_{ph} \xrightarrow[\Delta\to\infty]{} \gamma mc^2 \left(1 - \frac{\gamma^2\vartheta^2}{\Delta}\right) f(\alpha)$$

Thomson regime Δ=0 no recoil

$$E_{ph} \xrightarrow[\Delta\to 0]{} 4\gamma^2 h\nu_L \left(1 - \gamma^2\vartheta^2\right) f(\alpha)$$

$$\Delta \equiv \frac{4\gamma h\nu_L}{m_e c^2}\left(\frac{1 - \cos\alpha}{2}\right)$$

Recap
(exact analytical formula, no approximations)

$$\Delta = \frac{4\gamma h\nu_L}{m_e c^2} \qquad \gamma_{cm} = \frac{\gamma}{\sqrt{1+\Delta}}$$

$$E_{ph} = \frac{2\gamma^2 h\nu_L}{1+\Delta}\left[1+\sqrt{1-\frac{1+\Delta}{\gamma^2}}\cos\vartheta^*\right]$$

$$\cos\vartheta^* = \frac{\sqrt{1+tan^2\vartheta}-\gamma_{cm}tan^2\vartheta\sqrt{\gamma_{cm}^2-1}}{1+\gamma_{cm}^2 tan^2\vartheta} \qquad if \quad \vartheta < \frac{\pi}{2}$$

$$\cos\vartheta^* = \frac{-\sqrt{1+tan^2\vartheta}-\gamma_{cm}tan^2\vartheta\sqrt{\gamma_{cm}^2-1}}{1+\gamma_{cm}^2 tan^2\vartheta} \qquad if \quad \vartheta > \frac{\pi}{2}$$

$$E_{ph-max} = \frac{4\gamma^2 h\nu_L}{1+\Delta} = 4\gamma_{cm}^2 h\nu_L$$

Recap
(exact analytical formula, example 250 MeV electrons against $h\nu_L$=1.2 eV photons)

$\gamma = 490. \quad \Delta = 0.0046 \quad \gamma_{cm} = 488.88$

$$E_{ph}(MeV) = \frac{1.1472}{2}\left[1 + \sqrt{1 - \frac{1+\Delta}{\gamma^2}}\cos\vartheta^*\right]$$

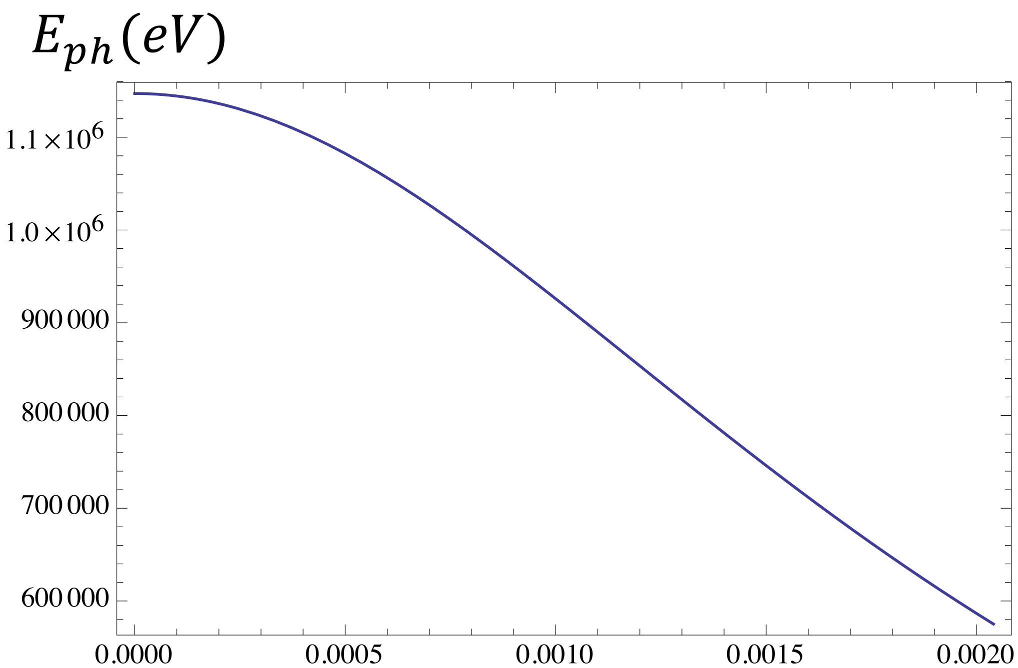

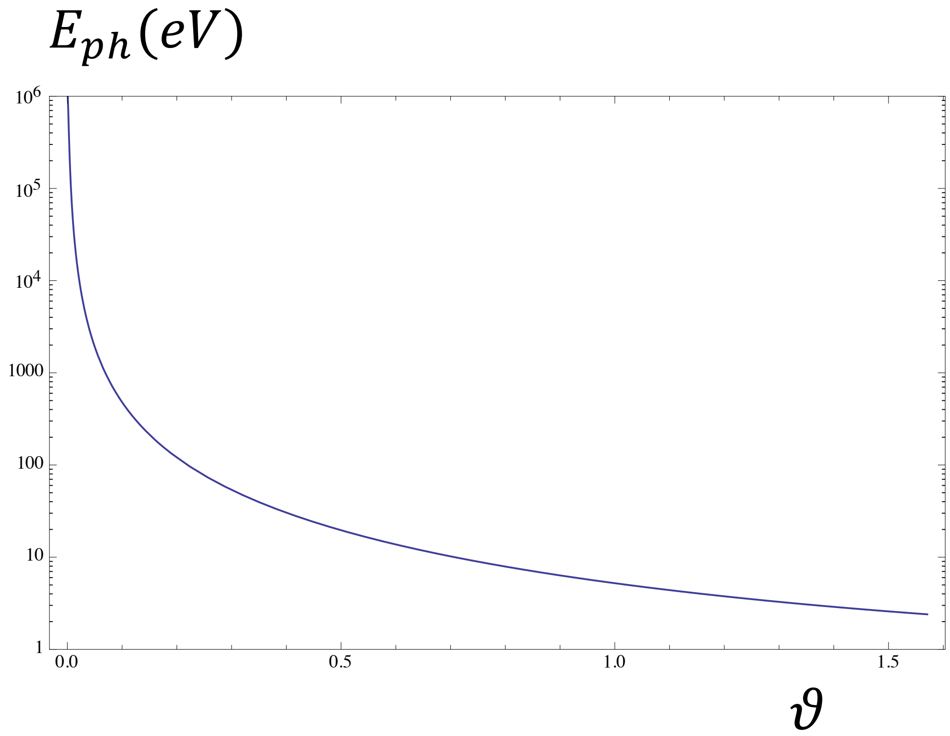

$\vartheta = 1/\gamma$

Recap (exact analytical formula, example 250 MeV electrons against $h\nu_L$=1.2 eV photons)

$\gamma = 490.$ $\Delta = 0.0046$ $\gamma_{cm} = 488.88$

$$E_{ph}(MeV) = \frac{1.1472}{2}\left[1 + \sqrt{1 - \frac{1+\Delta}{\gamma^2}}\cos\vartheta^*\right]$$

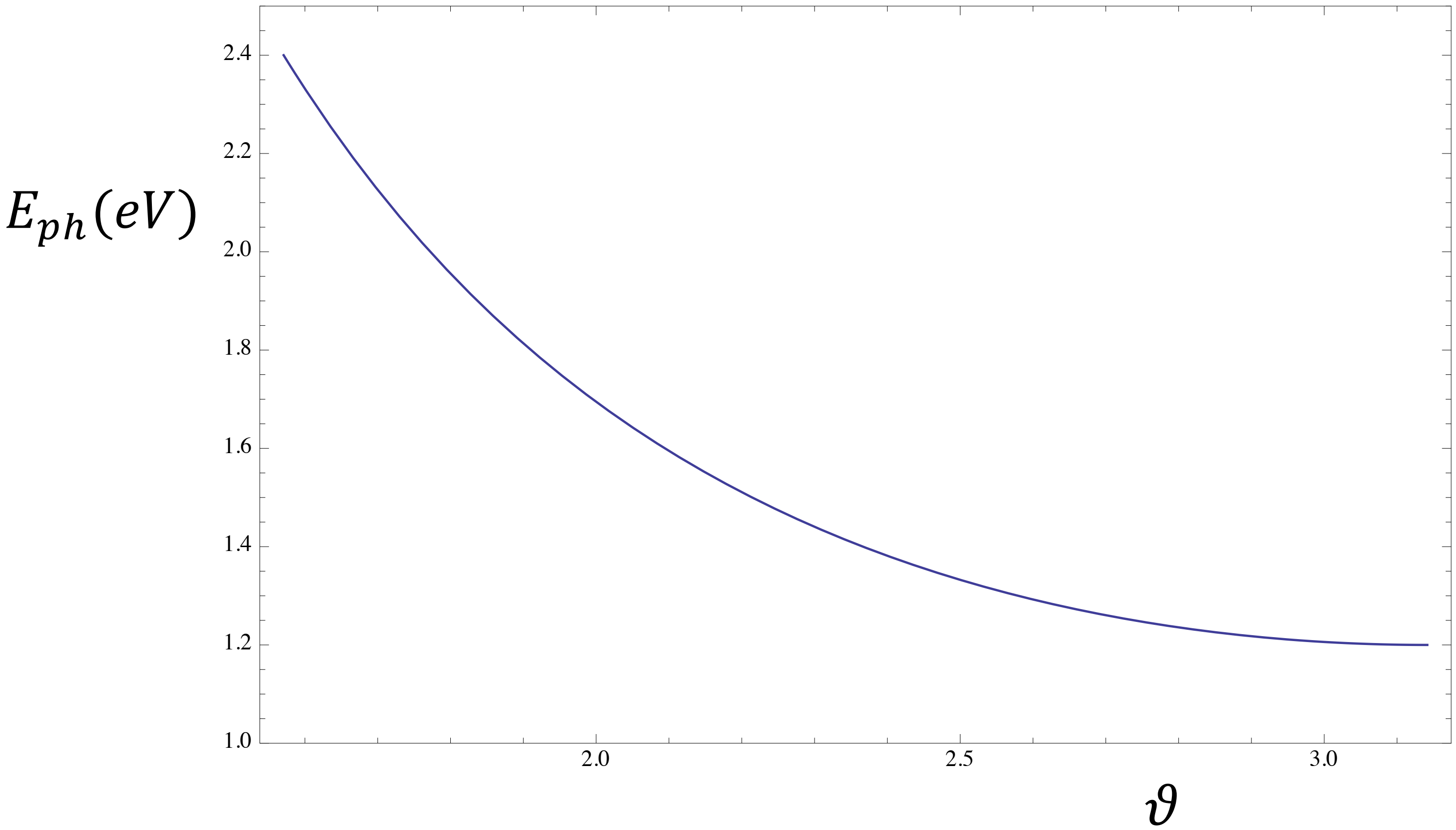

Single electron-photon spectra

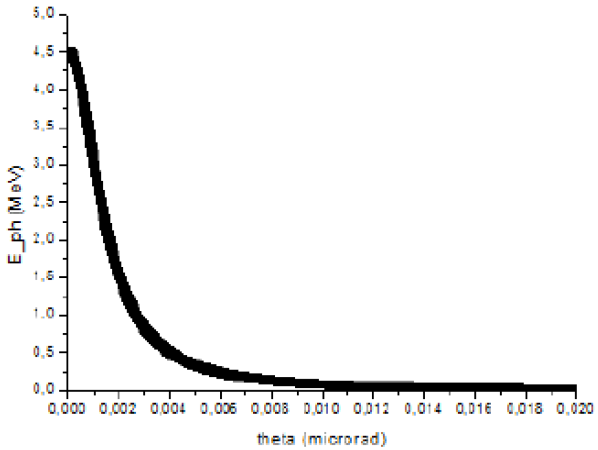

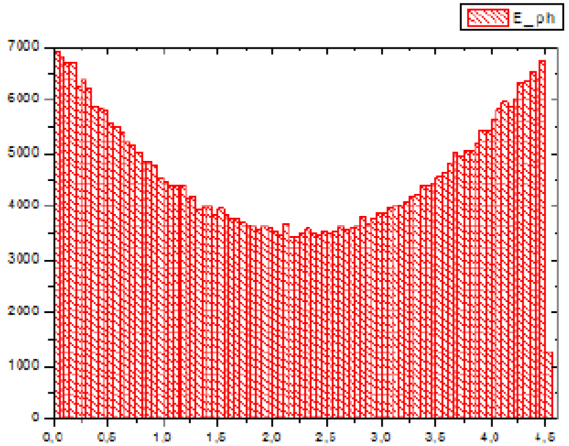

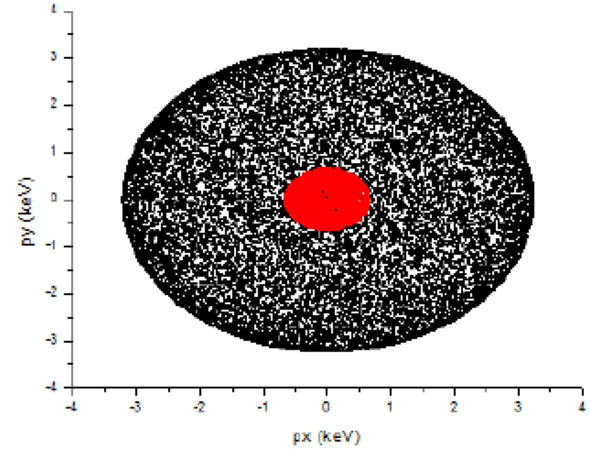

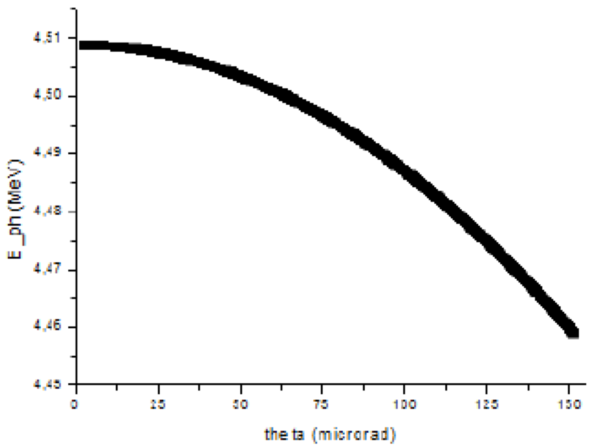

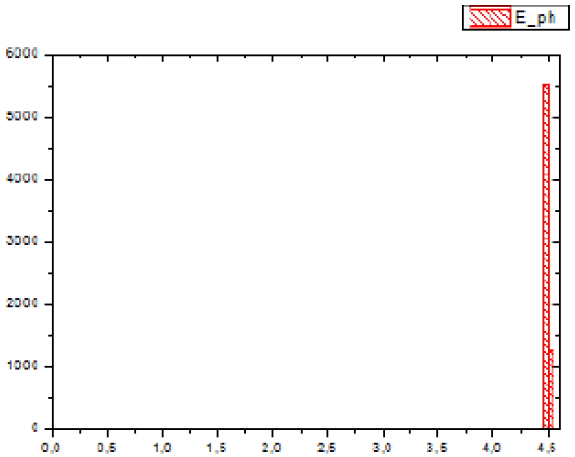

Energia elettroni 360 MeV
Energia fotoni 2.3 eV
Angolo alpha 0 gradi
Theta collimazione 151 microrad
Banda relativa 0.003

$$\gamma\vartheta = 0.11$$

What happens when we scatter beams of electron against beams of photons?

Electron beam emittance and energy spread spread out the c.m. propagation so to generate a "beam" of c.m. ref. frames

If the electron has not null transverse components respect to the z axis, the Lorentz transformations in a generic direction have to be used:

$$\begin{cases} E_{ph} = p^*_{ph}\gamma_{cm} + p^*_{phx}\gamma_{cm}\beta_x + p^*_{phy}\gamma_{cm}\beta_y + p^*_{phz}\gamma_{cm}\beta_z \\ p_{phx} = p^*_{ph}\gamma_{cm}\beta_x + p^*_{phx}\dfrac{1+\gamma^2_{cm}\beta^2_x}{1+\gamma_{cm}} + p^*_{phy}\dfrac{\gamma^2_{cm}\beta_x\beta_y}{1+\gamma_{cm}} + p^*_{phz}\dfrac{\gamma^2_{cm}\beta_x\beta_z}{1+\gamma_{cm}} \\ p_{phy} = p^*_{ph}\gamma_{cm}\beta_y + p^*_{phx}\dfrac{\gamma^2_{cm}\beta_x\beta_y}{1+\gamma_{cm}} + p^*_{phy}\dfrac{1+\gamma^2_{cm}\beta^2_y}{1+\gamma_{cm}} + p^*_{phz}\dfrac{\gamma^2_{cm}\beta_y\beta_z}{1+\gamma_{cm}} \\ p_{phz} = p^*_{ph}\gamma_{cm}\beta_z + p^*_{phx}\dfrac{\gamma^2_{cm}\beta_x\beta_z}{1+\gamma_{cm}} + p^*_{phy}\dfrac{\gamma^2_{cm}\beta_y\beta_z}{1+\gamma_{cm}} + p^*_{phz}\dfrac{1+\gamma^2_{cm}\beta^2_z}{1+\gamma_{cm}} \end{cases}$$

See C. Curatolo, PhD Thesis, Univ. of Milan, 2016 (and references therein)

Electron-photon Collider Spectra

The transverse momentum of the incoming electron beam is linked to the emittance by the relation

$$\sigma_{p_x} = \frac{\epsilon_{n,x} M_e}{\sigma_x}$$

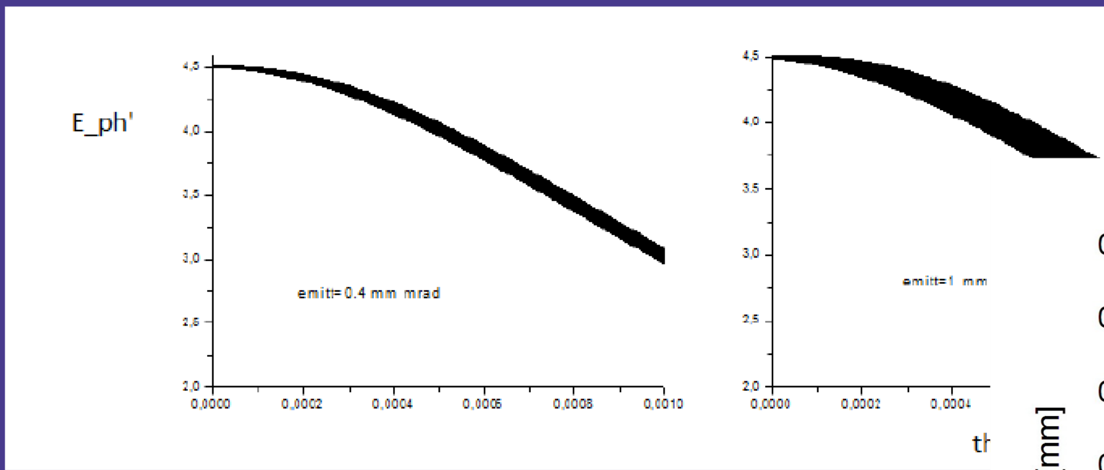

FIGURA : Energy of the emitted photons as a fun
different values of the electron beam emittance.

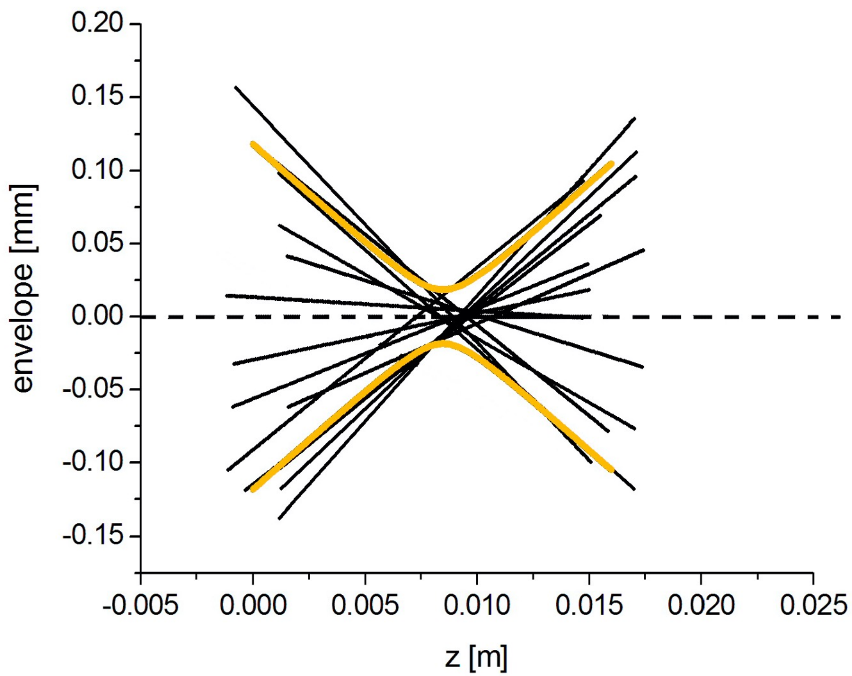

Recalling Compton differential cross-section

$$\frac{d\sigma}{d\theta' d\phi'} = r_e^2 \left(\frac{2}{2 + \Delta(1 - cos\theta')} \right)^2 \left(\frac{1 + cos^2\theta'}{2} \right) \cdot \left(1 + \frac{\Delta^2 (1 - cos\theta')^2}{2(1 + cos^2\theta')(2 + \Delta(1 - cos\theta'))} \right) sin\theta' \qquad (2.11)$$

total cross-section can be obtained from eq. (2.11) by integrating over θ' and ϕ'

$$\sigma_{tot} = 2\pi r_e^2 \frac{1}{\Delta} \left[\left(1 - \frac{4}{\Delta} - \frac{8}{\Delta^2} \right) \log(1 + \Delta) + \frac{1}{2} + \frac{8}{\Delta} - \frac{1}{2(1 + \Delta)^2} \right] \qquad (2.14)$$

and

$$\begin{cases} \lim_{\Delta \to 0} \sigma_{tot} = \frac{8\pi r_e^2}{3} (1 - \Delta) = \sigma_T (1 - \Delta) & \text{non-relativistic case} \\ \lim_{\Delta \to \infty} \sigma_{tot} = \frac{2\pi r_e^2}{\Delta} \left(\log \Delta + \frac{1}{2} \right) & \text{ultra-relativistic case.} \end{cases} \qquad (2.15)$$

$\sigma_T = 670\ mbarn$

For example, the recoil parameter Δ associated with the head-on scattering of an electron at $E_e = 400$ MeV and a photon with $h\nu_0 = 2.4047$ eV (these energies are in LAB) is given by

$$\Delta = \frac{2h\nu_0'}{mc^2} = \frac{4\gamma_i h\nu_0}{mc^2} = 7.37 \cdot 10^{-3}$$

$$E_{cm} = m_e c^2 \sqrt{1 + \Delta}$$

$$\Delta = \left(E_{cm} / m_e c^2 \right)^2 - 1$$

The Physics of Compton Inverse Scattering is quite straightforward

Quantum model

What are we missing by adopting the Quantum QED treatment of Compton back-scattering?

We re-construct the beam-beam back-scattering from single electron-photon scattering events by summing over the phase space density distributions of electrons and photons (treated incoherently!)

$mc^2(\gamma-\gamma_0)=-h(\nu-\nu_L)$

The coherent aspect (phase) of the laser e.m. field is lost… Multi-photon absorption/scattering phenomena are not taken into account (dressed electron model in e.m. field)

Linear QED treatment is good for low intensity (a_0<1) laser pulses

3 …

Thomson cross-section c) Inelastic, Compton, recoil dominated

Courtesy V. Petrillo – Univ. of Milan

Matching Laser Pulse Length and Focus Size

Laser pulse length matched to focus size (Rayleigh length).

Laser pulse too long for small focus size.

Laser pulse must be short compared to Rayleigh length so that whole pulse is focused simultaneously.

Laser may be shorter than Rayleigh length, but less than 0.5 ps is not practical, and could lead to non-linear effects not included in our spectral model.

courtesy of
D. Moncton

$$L = \frac{N_{el} N_{las}}{2\pi\left(\sigma_0^2 + w_0^2/4\right)} f$$

Electron Bunch Length Matched to Rayleigh Length

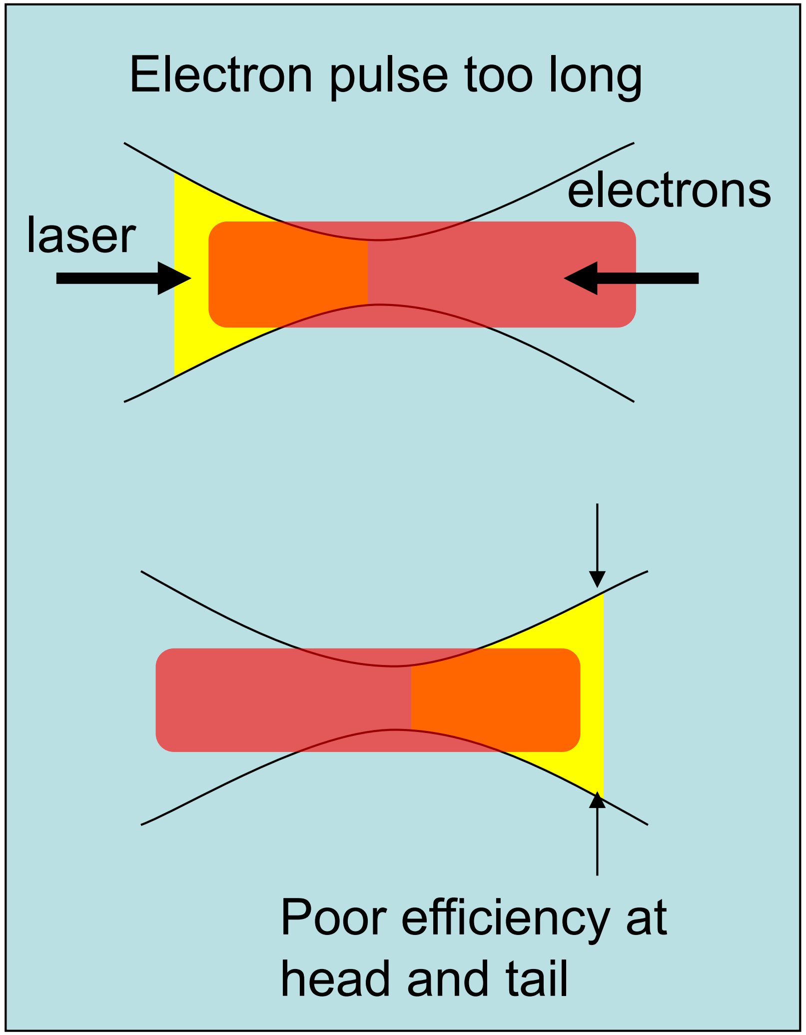

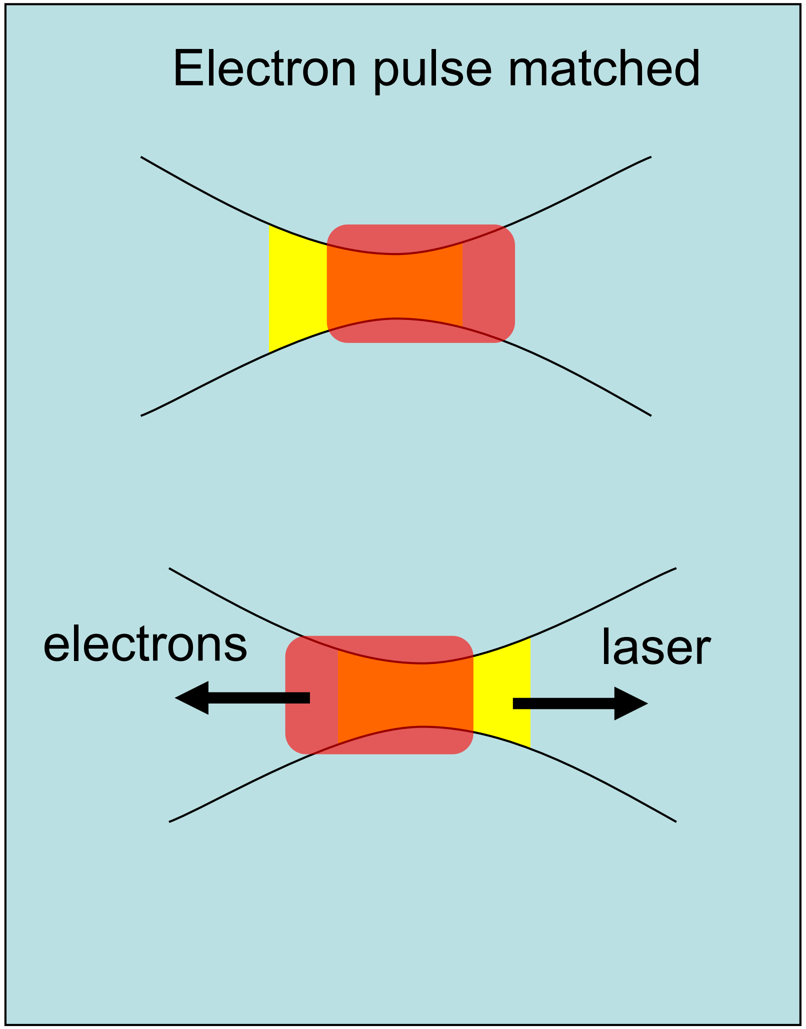

courtesy of D. Moncton

Bandwidth due to collection angle, laser and electron beam phase space distribution

$$\nu_X = \frac{4\gamma^2 \nu_L}{1+\Delta}\left(1 - \frac{\gamma^2\vartheta^2}{1+\Delta} - \frac{a_0^2}{2}\right) \qquad \Delta = 4\gamma\, h\nu / mc^2$$

$$\left.\frac{\delta\nu_X}{\nu_X}\right|_{\nu_L} = \frac{\partial\nu_X}{\partial\nu_L}\frac{\nu_L}{\nu_X}\frac{\delta\nu_L}{\nu_L} \;;\; \left.\frac{\delta\nu_X}{\nu_X}\right|_{\gamma} = \frac{\partial\nu_X}{\partial\gamma}\frac{\gamma}{\nu_X}\frac{\delta\gamma}{\gamma} \;;\; \left.\frac{\delta\nu_X}{\nu_X}\right|_{\vartheta} = \frac{1}{2}\frac{\partial^2\nu_X}{\partial\vartheta^2}\frac{\delta\vartheta^2}{\nu_X} \quad etc$$

angular spread due to scattering angle and angular spread due to single electron incoming angle (emittance) are treated symmetrically

$$\langle\gamma^2\theta^2\rangle \cong \langle\gamma^2\vartheta^2\rangle + \langle\gamma^2\vartheta_e^2\rangle \cong \gamma^2\vartheta_{rms}^2 + (\sigma_{p\perp}/mc)^2 \cong \gamma^2\vartheta_{rms}^2 + 2(\varepsilon_n/\sigma_x)^2$$

$$\frac{\delta\nu_X}{\nu_X} = \sqrt{\left(\left.\frac{\delta\nu_X}{\nu_X}\right|_{\nu_L}\right)^2 + \left(\left.\frac{\delta\nu_X}{\nu_X}\right|_{\gamma}\right)^2 + \left(\left.\frac{\delta\nu_X}{\nu_X}\right|_{\vartheta}\right)^2 + \ldots\ldots}$$

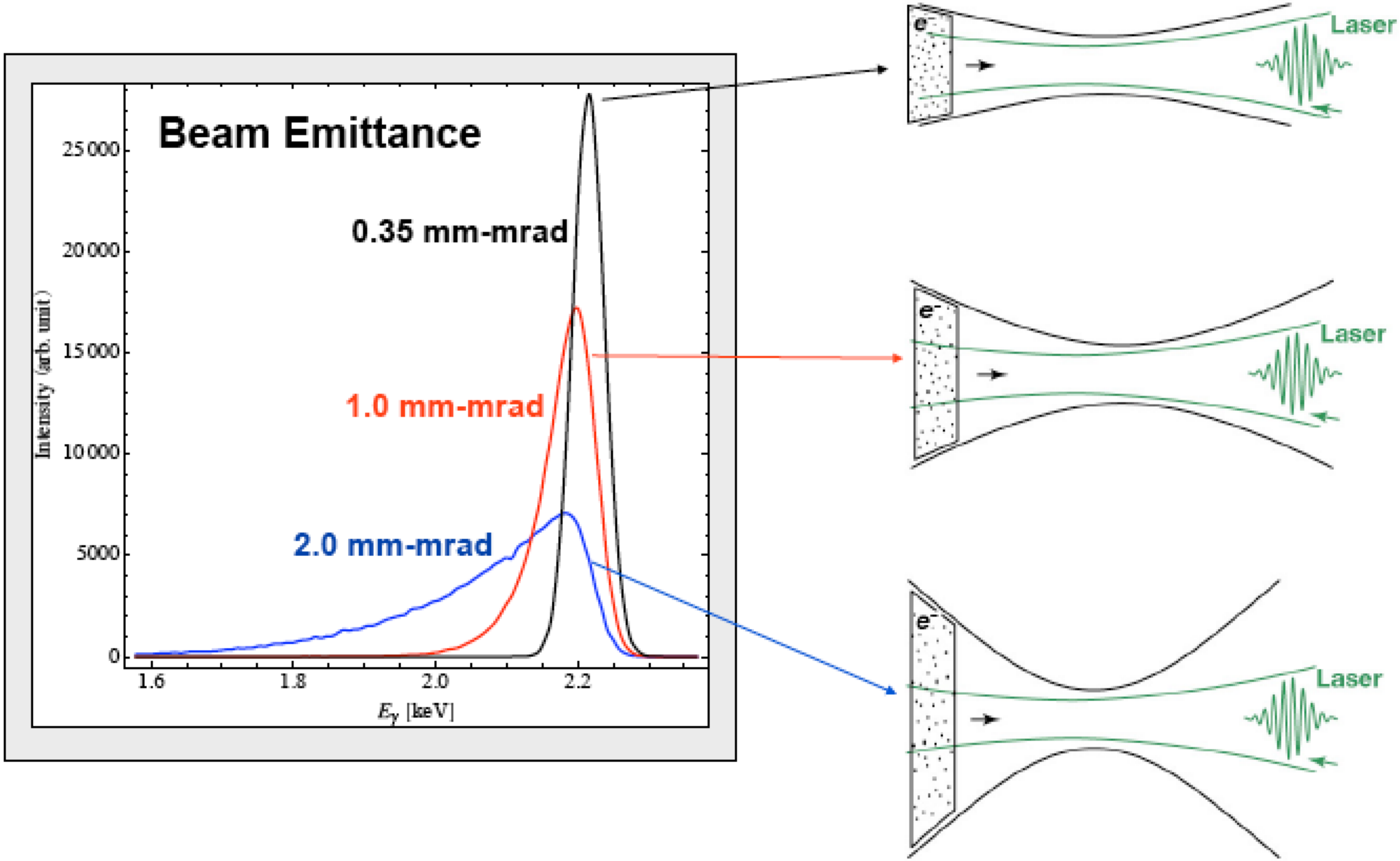

Courtesy C. Barty - LLNL

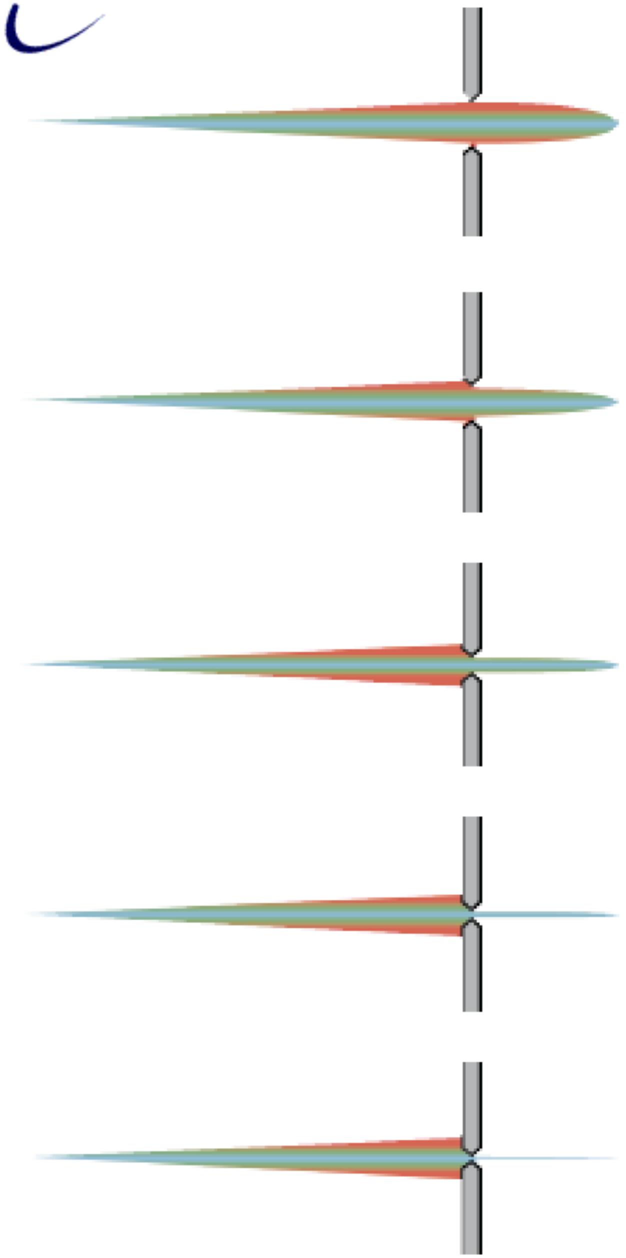

$$\Delta\theta \approx \frac{1}{\gamma} \; ; \; \Delta\nu_\gamma \approx 50\%$$

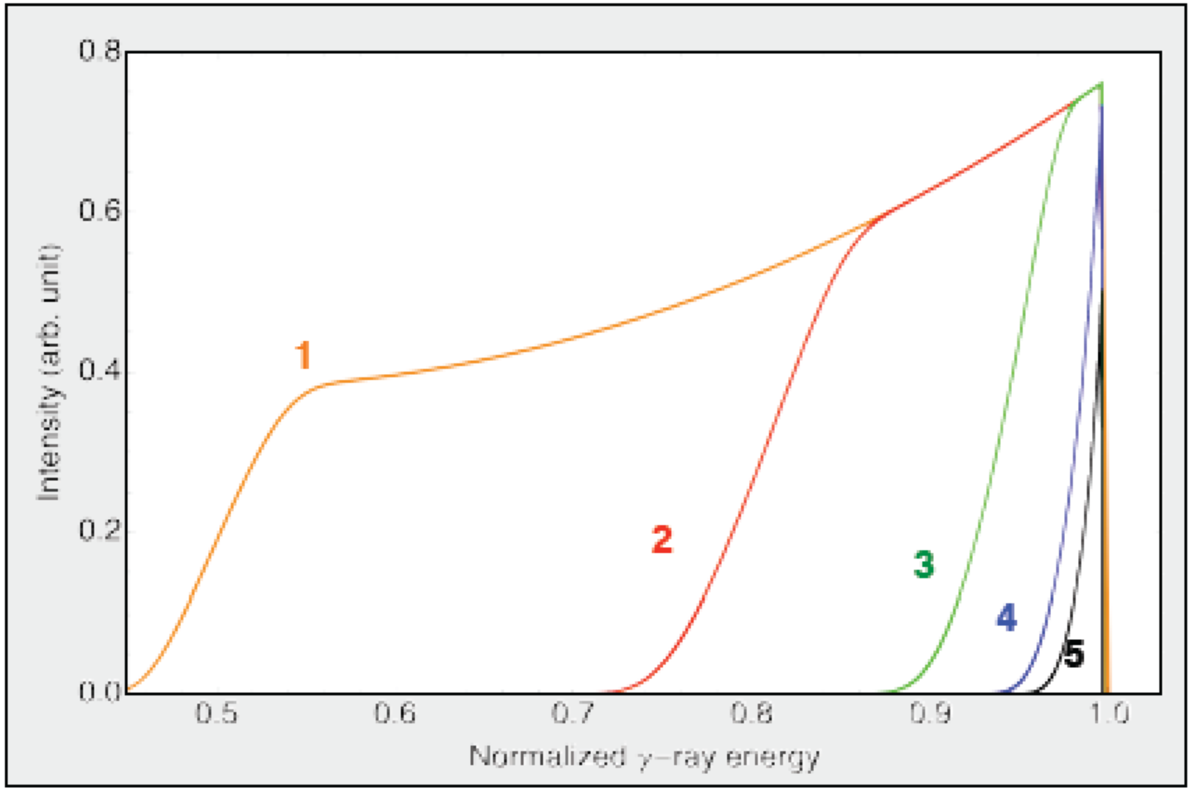

$$\Delta\theta \approx \sigma_{x'} = \frac{\varepsilon_n}{\gamma\sigma_x} \; ; \; \Delta\nu_\gamma \approx \left(\frac{\varepsilon_n^2}{\sigma_x^2}\right)$$

Courtesy C. Barty - LLNL

Spectral broadening due to ultra-focused beams:
Thomson Source classically described as a
Laser Syncrotron Light Source

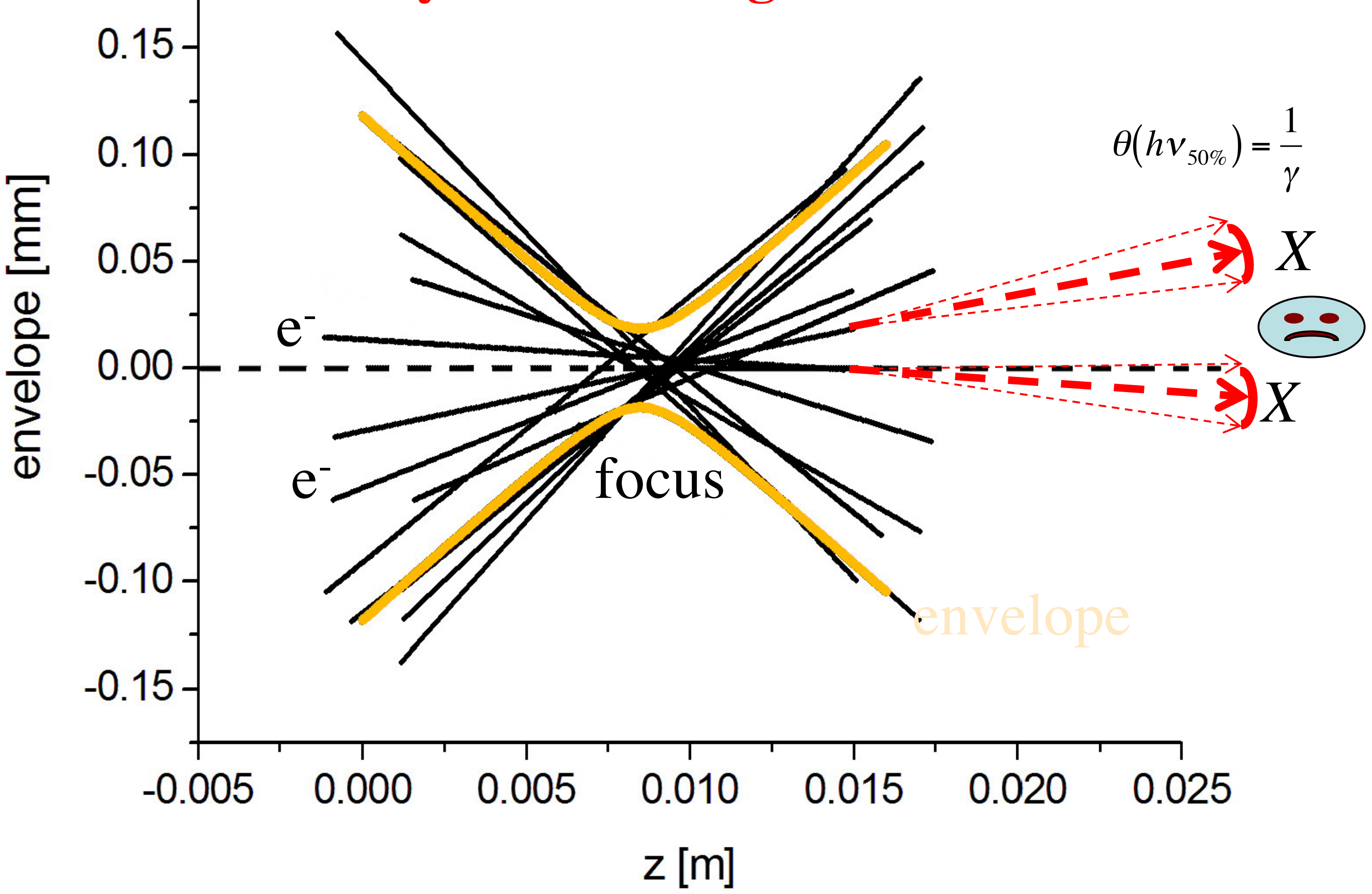

Scattering angle in Thomson limit (no recoil) is small, i.e. < $1/\gamma$

Spectral broadening due to ultra-focused beams:
Thomson Source classically described as a
Laser Syncrotron Light Source

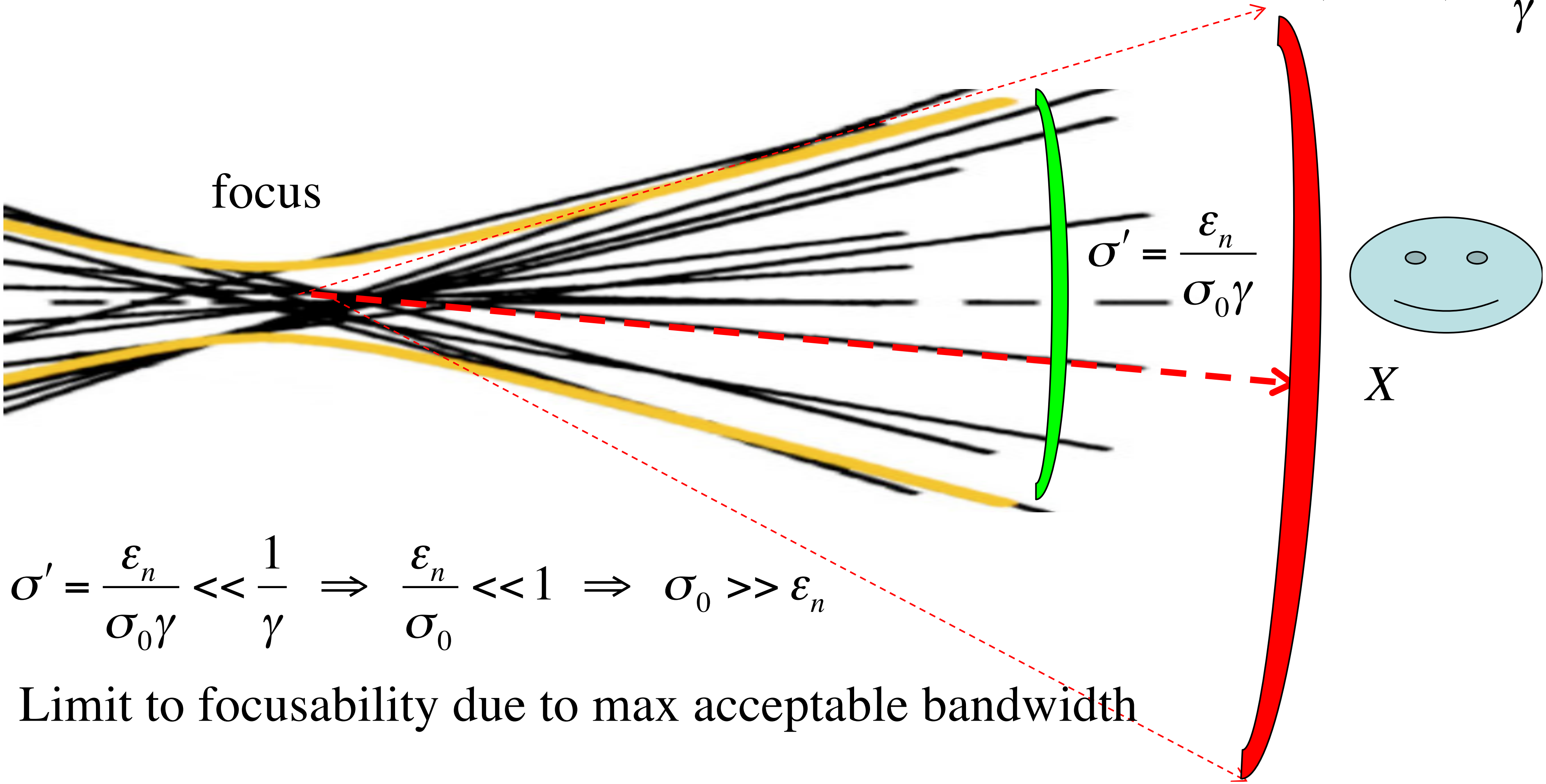

$$\sigma' = \frac{\varepsilon_n}{\sigma_0 \gamma} << \frac{1}{\gamma} \quad \Rightarrow \quad \frac{\varepsilon_n}{\sigma_0} << 1 \quad \Rightarrow \quad \sigma_0 >> \varepsilon_n$$

Limit to focusability due to max acceptable bandwidth

Petrillo-Serafini Formula* for ICS photon beam bandwidth

collimation

electron beam phase space

$$\frac{\delta\nu_\gamma}{\nu_\gamma} \cong \sqrt{\left[\left(\frac{\gamma^2\vartheta^2/\sqrt{12}}{1+\gamma^2\vartheta^2/2}+\frac{2\varepsilon_n^2/\sigma_x^2}{1+\sqrt{12}\,\varepsilon_n^2/\sigma_x^2}\right)\frac{1}{1+\Delta}\right]^2+\left(\frac{2+\Delta}{1+\Delta}\frac{\delta\gamma}{\gamma}\right)^2+\left(\frac{1}{1+\Delta}\frac{\delta\nu}{\nu}\right)^2+\left(\frac{M^2\lambda_L}{2\pi w_0}\right)^4+\left(\frac{a_0^2/3}{1+a_0^2/2}\right)^2}$$

laser beam phase space

laser collective effects

PHYSICAL REVIEW ACCELERATORS AND BEAMS **20,** 080701 (2017)

Analytical description of photon beam phase spaces in inverse Compton scattering sources

C. Curatolo,[1,*] I. Drebot,[1] V. Petrillo,[1,2] and L. Serafini[1]
[1]*INFN-Milan, via Celoria 16, 20133 Milano, Italy*
[2]*Università degli Studi di Milano, via Celoria 16, 20133 Milano, Italy*
(Received 9 March 2017; published 3 August 2017)

$\Delta E_{ph}/E_{ph}$ from the laser and the electron beam parameters, which are: γ the Lorentz factor, $\Delta\gamma/\gamma$ the relative energy spread, ϵ_n the normalized emittance and σ_x the rms spot size at interaction point of the electron beam, $\Delta E_L/E_L$ the laser bandwidth, λ_0 the laser wavelength, w_0 the laser focal spot size, M^2 the beam quality factor and the laser parameter a_0. We improve and generalize the formula described in Refs. [3, 36, 41, 45] by taking into to account the effect given by the electron recoil on the emitted radiation: the use of γ_{CM} instead then γ extends the validity of the equation to any recoil regime.
As in the above mentioned references, we consider a Gaussian phase space distribution for the electron beam and for the laser pulse while the resulting shape of the photon spectrum is determined by the energy-angle correlation described by Eqs. (6) and (11).
We define the acceptance angle as

$$\Psi = \gamma_{CM}\theta_{max} \tag{12}$$

and the term

$$\overline{P} = \gamma_{CM}\frac{\sqrt{2}\epsilon_x}{\sigma_x} = \frac{\sqrt{2}\epsilon_n}{\sigma_x\sqrt{1+X}} \tag{13}$$

where $\sqrt{2}\epsilon_n/\sigma_x$ represents the normalized rms transverse momentum of the electron beam which coincides with $\overline{P}$ at low recoil. Instead $\overline{P}$ is reduced by a factor $\gamma_{CM}/\gamma \simeq \sqrt{X}$ when the recoil is large. The relative bandwidth of the emitted radiation is given by

$$\frac{\Delta E_{ph}}{E_{ph}} \simeq \sqrt{\left[\frac{\Psi^2/\sqrt{12}}{1+\Psi^2} + \frac{\overline{P}^2}{1+\sqrt{12}\,\overline{P}^2}\right]^2 + \left[\left(\frac{2+X}{1+X}\right)\frac{\Delta\gamma}{\gamma}\right]^2 + \left(\frac{1}{1+X}\frac{\Delta E_L}{E_L}\right)^2 + \left(\frac{M^2\lambda_0}{2\pi w_0}\right)^4 + \left(\frac{a_0^2/3}{1+a_0^2/2}\right)^2} \tag{14}$$

length.
We note that Eq. (14) is based on a fourth order expansion in the acceptence angle Ψ: this approach limits the validity of the formula to angles $\Psi < 1$.
The number of scattered photons per second is given by

$$\mathcal{N} = \mathcal{L}\sigma = \frac{N_e N_L r}{2\pi\,(\sigma_x^2 + \sigma_L^2)}\,\sigma \tag{16}$$

where $\mathcal{L}$ is the luminosity,

$$\sigma = \frac{2\pi r_e^2}{X}\left[\frac{1}{2} + \frac{8}{X} - \frac{1}{2(1+X)^2} + \left(1 - \frac{4}{X} - \frac{8}{X^2}\right)\log(1+X)\right] \tag{17}$$

is the total unpolarized Compton cross section [49], N_e, N_L are the number of incoming electrons and photons, r is the repetition rate of the collisions, and σ_x, $\sigma_L = w_0/2$ are the rms spot size radius at the interaction point of the electron and photon beams respectively. The value of σ varies between the classical limit $X \to 0$ and the ultra-relativistic limit $X \to \infty$ as presented in Eq. (18) where $\sigma_T = 0.67$ barn represents the total Thomson cross section [50].

$$\mathcal{N} = 4.2 \cdot 10^8 \frac{\sigma\, U_L(J)\, Q(pC)\, r}{\sigma_T\, E_L(eV)\, (\sigma_x^2(\mu m) + \sigma_L^2(\mu m))}. \tag{19}$$

By using the Compton differential cross section [49] in the approximation $\Psi < 1$, we obtain the analytical expression to estimate $\mathcal{N}^\Psi$, the number of photons in acceptance angle Ψ, and the spectral density S:

$$\mathcal{N}^\Psi = 6.25 \cdot 10^8 \frac{U_L(J)\, Q(pC)\, r}{E_L(eV)\, (\sigma_x^2(\mu m) + \sigma_L^2(\mu m))} \cdot \frac{\left(1 + \sqrt[3]{X}\,\Psi^2/3\right)\Psi^2}{(1 + (1+X/2)\Psi^2)\,(1+\Psi^2)}, \tag{20}$$

$$S = \frac{\mathcal{N}^\Psi}{\sqrt{2\,\pi}\, 4\, E_L \gamma_{CM}^2 \frac{\Delta E_{ph}}{E_{ph}}}. \tag{21}$$

The rms source spot size is

$$\sigma_s = \frac{\sigma_x\, \sigma_L}{\sqrt{\sigma_x^2 + \sigma_L^2}} \tag{22}$$

and the emittance of the emitted radiation is

$$\epsilon_\gamma = \sigma_s \frac{\theta_{max}}{\sqrt[4]{12}\, \sqrt[9]{1+X}}. \tag{23}$$

INFN

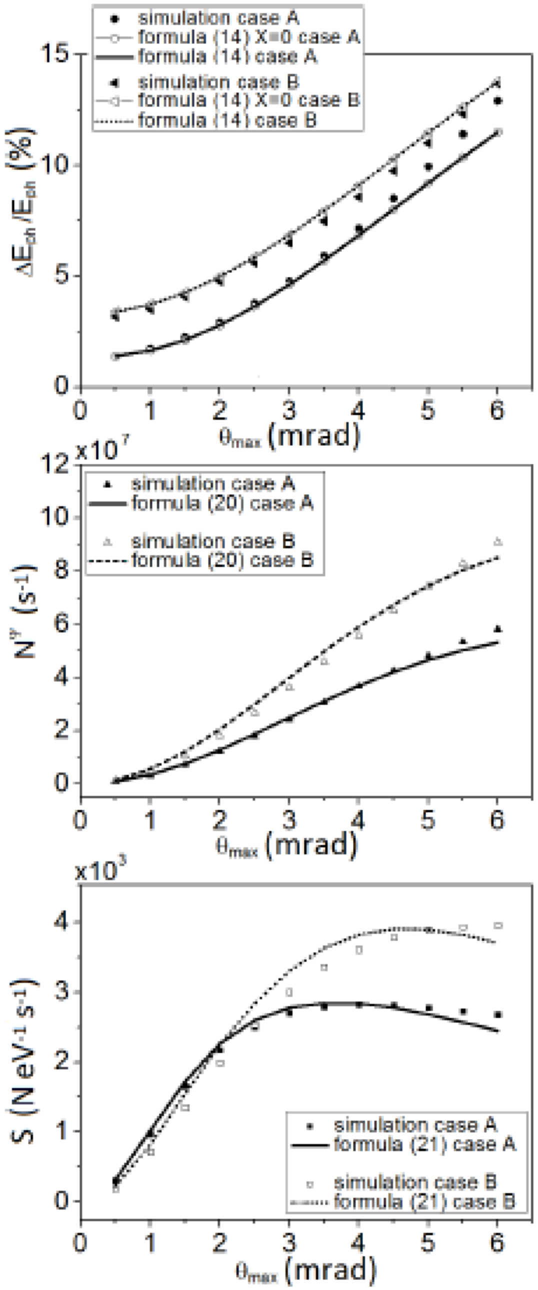

Figure 1. Cases A and B: $\Delta E_{ph}/E_{ph}$ (%) from CAIN simulation vs formula (14) without and with X correction, N^{Ψ} (s^{-1}) number of photons from CAIN simulation vs formula (20), S (N eV^{-1} s^{-1}) spectral density per shot ($r = 1$) from CAIN simulation vs formula (21) as a function of θ_{max} (mrad).

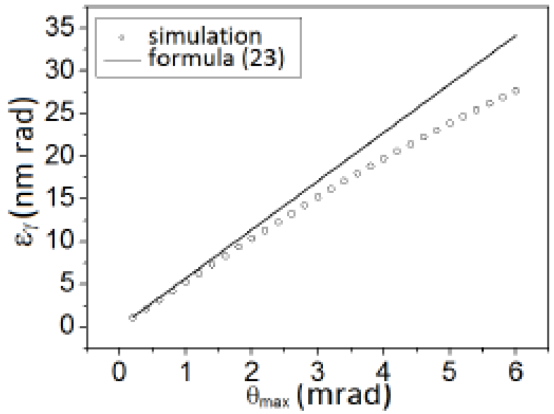

Figure 2. Case A: ϵ_{γ} (nm rad) value from CAIN simulation vs formula (23) as a function of θ_{max} (mrad).

and the emittance of the emitted radiation is

$$\epsilon_\gamma = \sigma_s \frac{\theta_{max}}{\sqrt[4]{12}\,\sqrt[9]{1+X}}. \quad (23)$$

The peak brilliance is defined as

$$B^{peak} = \frac{\mathcal{N}^\Psi}{(2\pi)^3\,\epsilon_\gamma^2\,\sigma_t^\gamma\,\frac{\Delta E_{ph}}{E_{ph}}\,[0.1\%]\,r} \quad (24)$$

with σ_t^γ the rms duration value of the emitted γ photons. The average brilliance on one second is instead given by

$$B^{ave} = \frac{\mathcal{N}^\Psi}{(2\pi)^{\frac{5}{2}}\,\epsilon_\gamma^2\,\frac{\Delta E_{ph}}{E_{ph}}\,[0.1\%]}. \quad (25)$$

X-ray flux N_X^{bw} in photons/sec within rms bandwidth *bw*

Case A: head-on collision STAR-like

U_L energy of colliding laser pulse, Q electron bunch charge, f_{RF} rep rate of electron bunches, σ_x electron beam spot size at collision

$$N_X^{bw} = 5.8 \cdot 10^8 \frac{U_L[J]Q[pC]f_{RF}}{\sigma_x^2[\mu m^2]} bw$$

$$U_L = 1\ J, Q = 1\ nC, f_{RF} = 100\ Hz, \sigma_x = 15\ \mu m, bw = 0.1 \Rightarrow N_X^{bw} = 2.6 \cdot 10^{10}$$

$$U_L = 0.4\ J, Q = 1\ nC, f_{RF} = 3.2\ kHz, \sigma_x = 15\ \mu m, bw = 0.1 \Rightarrow N_X^{bw} = 3.3 \cdot 10^{11}$$

Case B: BriXS-like with F-P optical cavity

P_{FP} power stored in Fabry-Perot cavity, $\langle I_e \rangle$ average electron beam current

$$N_X^{bw} = 1.4 \cdot 10^{17} \frac{P_{FP}[MW]\langle I_e \rangle [mA]}{f_{FP}[MHz]\sigma_x^2[\mu m^2]} bw$$

$$P_{FP} = 1\ MW, \langle I_e \rangle = 1\ mA, f_{FP} = 100\ MHz, \sigma_x = 20\ \mu m, bw = 0.1 \Rightarrow N_X^{bw} = 3.5 \cdot 10^{12}$$

$$P_{FP} = 1\ MW, \langle I_e \rangle = 100\ mA, f_{FP} = 100\ MHz, \sigma_x = 12\ \mu m, bw = 0.1 \Rightarrow N_X^{bw} = 10^{15}$$

Efficiency of Compton Sources in converting electron beam energy into radiation beam energy

energy of photons in collimation angle

number of photons per shot in collimation angle

electron beam total energy

$$\eta^{\Psi} \simeq \frac{4\gamma_{CM}^2 E_L}{N_e E_e}\frac{N^{\Psi}}{r} \simeq \frac{4\gamma_{CM}^2 E_L}{N_e E_e}\left(\frac{6.25\cdot 10^8 U_L(J) Q(pC)}{E_L(eV)\left(\sigma_x^2(\mu m)+\sigma_L^2(\mu m)\right)}\frac{\left(1+\sqrt[3]{X}\Psi^2/3\right)\Psi^2}{\left(1+(1+X/2)\Psi^2\right)\left(1+\Psi^2\right)}\right)$$

$$= \frac{7.82\cdot 10^{-4}\,\gamma U_L(J)}{\left(\sigma_x^2(\mu m)+\sigma_L^2(\mu m)\right)}\frac{\Psi^2}{\left(1+\Psi^2\right)^2} = \frac{3.38\cdot 10^{-5}\gamma\, a_0^2\, \sigma_t(ps)}{\lambda_0^2(\mu m)}\frac{\Psi^2}{\left(1+\Psi^2\right)^2}$$

if $X \ll 1 \Rightarrow$
$\gamma_{CM} \simeq \gamma,\ \Psi \simeq \gamma\theta_{max}$

$\sigma_x = \sigma_L,\ w_0 = 2\sigma_L$
$a_0 = 6.8\frac{\lambda_0}{w_0}\sqrt{\frac{U_L(J)}{\sigma_t(ps)}}$

Ex: TABLE I. Interaction parameters for STAR. $\sigma_L = 15\ \mu$m, $\sigma_t = 1$ ps and σ_{p_x} electron beam rms transverse momentum (keV).

Case	Q (nC)	E_e (MeV)	$\Delta\gamma/\gamma$ (10^{-3})	ϵ_n (μm rad)	σ_{p_x} (keV)	σ_x (μm)	λ_0 (μm)	U_L (J)
A	1	65	5	1	34	15	1	0.2
				$X = 0.00123$				

$$\eta^{\Psi\,SIM} \simeq \frac{3.67\cdot 10^7\cdot 4\cdot 127.2^2\cdot 1.239}{6.24\cdot 10^9\cdot 65\cdot 10^6} = 7.25\cdot 10^{-6}$$

$$\eta^{\Psi\,FOR} \simeq \frac{7.82\cdot 10^{-4}\cdot 0.2\cdot 127.2^3\cdot 16\cdot 10^{-6}}{2\cdot 15^2\cdot\left(1+127.2^2\cdot 16\cdot 10^{-6}\right)^2} = 7.22\cdot 10^{-6}$$

ELI-NP-GBS eta-psi=1.2*10^-5

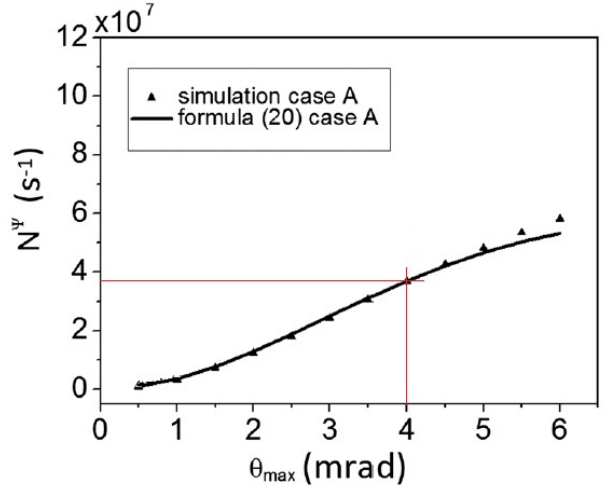

Inverse Compton Sources, Overview, Theory, Main Technological Challenges – Photonic Colliders

Luca Serafini – INFN-Milan and University of Milan

4 Lecture Outline

- **Overview of Projects/Proposal for ICS' and Applications**
- **Classical e.m. and Linear Quantum Theory of Inverse Compton Sources (ICS) and paradigms for ICS**
- **Photon-Photon Colliders at low energy for Breit-Wheeler and photon-photon scattering experiments**
- **Hadron-Photon Colliders as muon photo-cathodes for TeV photons, neutrino and pion/muon low emittance beam generation**

Total cross section of various $\gamma-\gamma$ or e-γ interactions

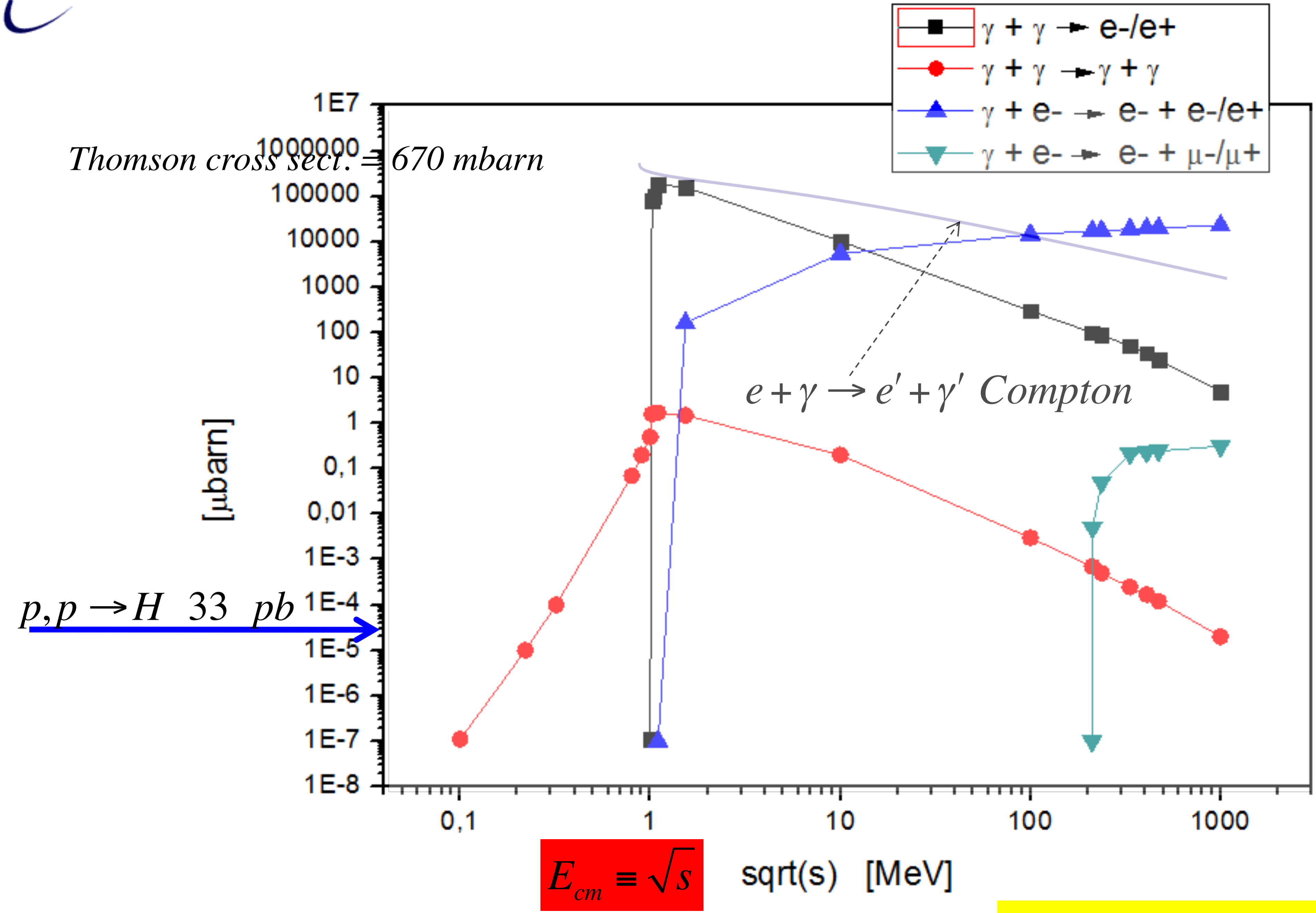

Courtesy C. Curatolo

CONCLUSIONS on e-gamma colliders

- Compton Sources are opening an era of high brilliance photon beams spanning from keV to TeV energy with unprecedented phase space density features
- Medical Applications are being enabled by compact Thomson Sources that can be located and operated inside Hospitals
- Nuclear Photonics is beginning an era of research and discovery enabled by MeV-class Compton back-scattered photon beams
- MeV-class invariant mass photon-photon colliders are now conceivable by exploiting the potentialities of advanced Compton Sources – basic energy physics oriented

Existing and planned Thomson sources

	Type	Energy [KeV]	Flux (@ 10% bandwidth)	Source size (µm)
*PLEIADES (LLNL) [11,12]	Linac	10-100	10^7 (10 Hz)	18
*Vanderbilt [13,14]	Linac	15-50	10^8 (few Hz)	30
*SLAC [15]	Linac	20-85		
*Waseda University [16,17]	Linac	0.25-0.5	$2.5\ 10^4$ (5 Hz)	
*AIST, Japan [18]	Linac	10-40	10^6	30
*Tsinguha University [19]	Linac	4.6	$1.7\ 10^4$	
*LUCX (KEK) [20]	Linac	33	$5\ 10^4$ (12.5 Hz)	80
+ UTNL, Japan [21,22]	Linac	10-40	10^9	
MIT project [23]	Linac	3-30	$3\ 10^{12}$ (100 MHz)	2
MXI systems [24]	Linac	8-100	10^9 (10Hz)	
SPARC –PLASMONX [25]	Linac	20-380	$2\ 10^8$ -$2\ 10^{10}$	0.5-13
Quantum Beam (KEK) [26,27]	Linac		10^{13}	3
*TERAS (AIST) [28]	Storage ring	1-40	$5\ 10^4$	2
*Lyncean Tech [29,30,31]	Storage ring	7-35	~ 10^{12}	30
Kharkov (SNC KIPT) [32]	Storage ring	10-500	$2.6\ 10^{13}$ (25 MHz)	35
TTX (THU China) [33,34]	Storage ring	20-80	$2\ 10^{12}$	35
ThomX France [35]	Storage ring	50	10^{13} (25 MHz)	70

Table 3: Compact Compton X ray sources. Symbols * and + refers respectively to machines in operation and to machines in construction.

STAR (Calabria) Linac 20-100 10^{11} (100 Hz) 18

From **THOMX** Conceptual Design Report, A.Variola, A.Loulergue, F.Zomer, LAL RT 09/28, SOLEIL/SOU-RA-2678, 2010

$$Peak\ \ Brilliance\ \ B_\gamma \equiv \frac{N_\gamma^{bw}}{\varepsilon_\gamma^2 \dfrac{\Delta\nu_\gamma}{\nu_\gamma}\sigma_t}$$

(10)

$$B_\gamma = 5.6 \cdot 10^{19} \frac{\gamma^2 U_L[J]Q[pC]}{h\nu[eV]\dfrac{\Delta\nu_\gamma}{\nu_\gamma}\sigma_0^2 w_0^2 \sigma_t}$$

$$correction\ \ factor\ \ for\ \ collision\ \ angle\ \ \phi$$

(11)

$$\delta_\phi = \frac{1}{\sqrt{1 + \dfrac{\phi^2\left(\sigma_{z-el}^2 + c^2\sigma_t^2\right)}{4\left(\sigma_0^2 + \dfrac{w_0^2}{4}\right)}}}$$

Brilliance of Lasers and X-ray sources

ELI

BELLA

$$N_{ph} = 10^{19} - 10^{20}$$

$$\sigma_t = 10 - 20 \quad fs$$

$$B = \frac{N_{ph}}{\sqrt{2\pi}\sigma_t \left(M^2 \lambda\right)^2 \frac{\Delta\lambda}{\lambda}}$$

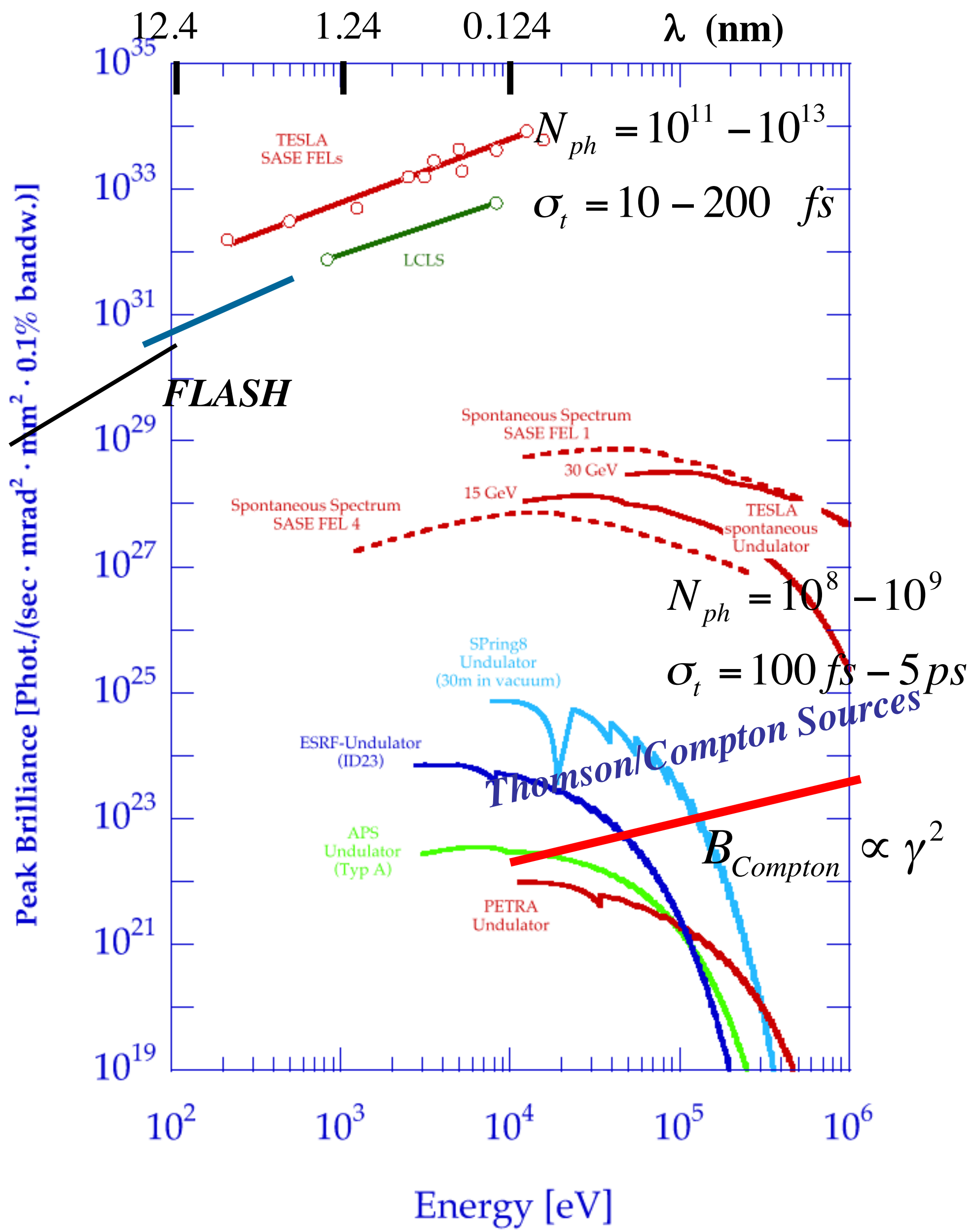

Outstanding X/γ photon beams for Exotic Colliders

Unsurpassable by any other technology/source for energies > 1 MeV

The peak brilliance of an optimized MEGa-ray source is both revolutionary and transformative

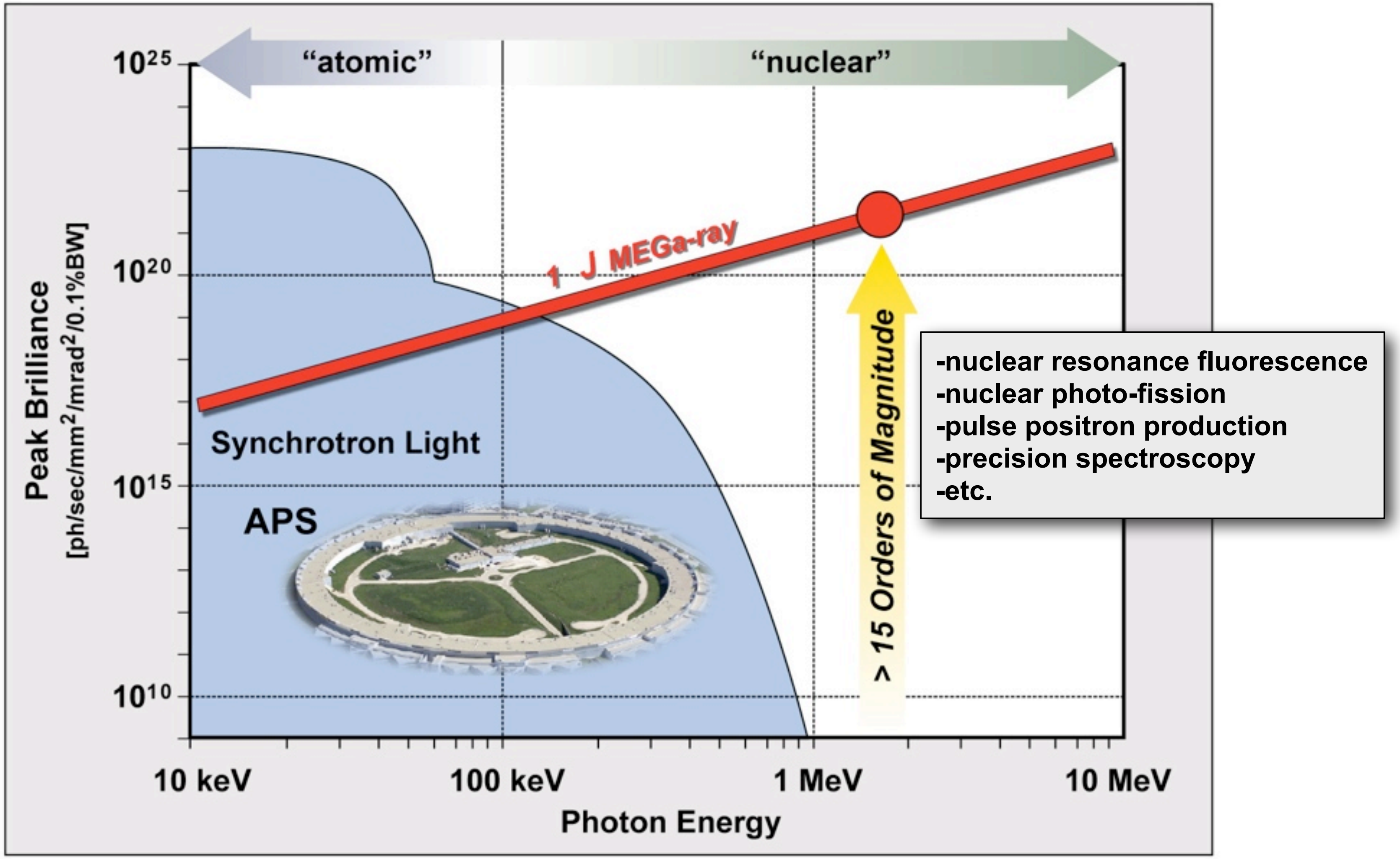

Courtesy C. Barty - LLNL

ELI-NP γ beam: the quest for narrow bandwidths (from 10^{-2} down to 10^{-3})

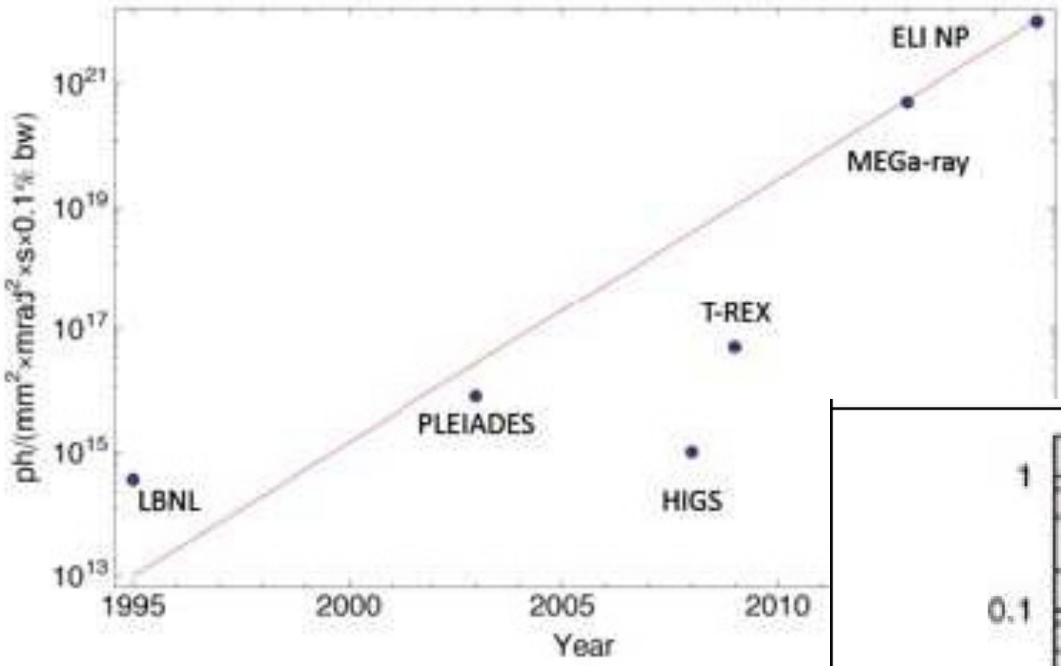

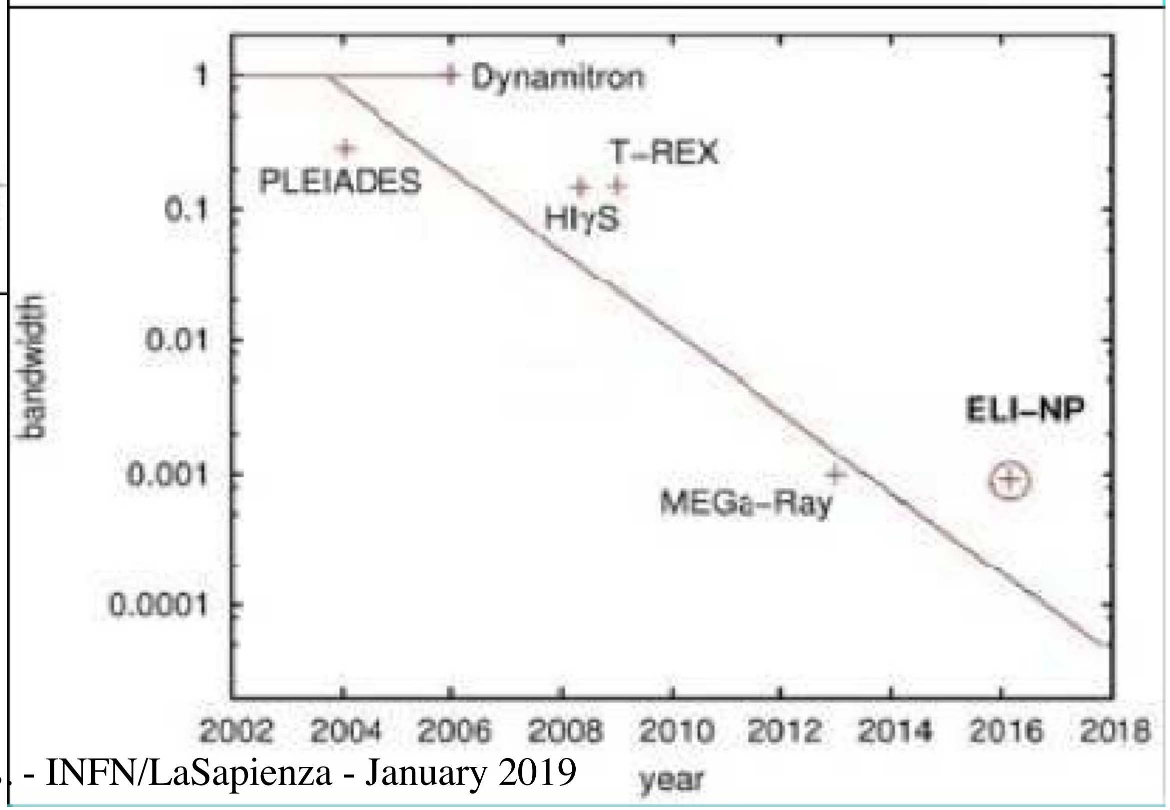

Courtesy V. Zamfir – ELI-NP

ELI-NP GBS (Extreme Light Infrastrucutre Gamma Beam System) Main Parameters

$$\gamma - ray \quad 1-20 \quad MeV \ ; \ rms \quad Bandwidth \quad 3.-5.\ 10^{-3}$$

$$Spectral \quad Density: \quad 10^{3}-10^{4} \quad photons/s\cdot eV$$

$$needs \quad 3.10^{5} \quad photons/pulse \ @ \ 3 \quad kHz \quad rep \quad rate$$

$$rms \quad divergence \quad 30 < \quad 300 \quad \mu rad$$

$$linear \quad or \quad circular \quad polarization \quad > \quad 95\%$$

outstanding electron beam @ 750 MeV with high phase space density
(all values are projected, not slice! cmp. FEL's)

$$Q = 250\,pC \ ; \ \varepsilon_{n} = 4.10^{-7}\,m\cdot rad \ ; \ \Delta\gamma/\gamma = 5\cdot 10^{-4}$$

Back-scattering a high quality *J-class* ps laser pulse

$$U_{L} = 400 \quad mJ \ ; \ M^{2} = 1.2 \ ; \ \frac{\Delta\nu}{\nu} = 5\cdot 10^{-4}$$

not sustainable by RF, Laser!

PHYSICAL REVIEW SPECIAL TOPICS - ACCELERATORS AND BEAMS **17,** 033501 (2014)

Design and optimization of a highly efficient optical multipass system for γ-ray beam production from electron laser beam Compton scattering

K. Dupraz,* K. Cassou, N. Delerue, P. Fichot, A. Martens, A. Stocchi, A. Variola, and F. Zomer
LAL, Université Paris-Sud, CNRS/IN2P3, Orsay, Bâtiment 200, BP 34, 91898 Orsay cedex, France

A. Courjaud and E. Mottay
Amplitude Systèmes, 6 allée du Doyen Georges Brus, 33600 Pessac, France

F. Druon
Laboratoire Charles Fabry de l'Institut d'Optique, UMR 8501 CNRS, Université Paris Sud, 91127 Palaiseau, France

G. Gatti and A. Ghigo
INFN-LNF, Via Enrico Fermi 40, 00044 Frascati Rome, Italy

T. Hovsepian, J. Y. Riou, and F. Wang
Alsyom, Parc des Algorithmes, Bâtiment Aristote, 9 Avenue du Marais, 95100 Argenteuil, France

A. C. Mueller
National Institute for Nuclear and Particle Physics, CNRS, 3 rue Michel-Ange, 75016 Paris, France

L. Palumbo
Universita di Roma La Sapienza, Dipartimento Energetica, Via Antonio Scarpa, 14-00161 Rome, Italy

L. Serafini and P. Tomassini
INFN-MI, Via Celoria 16, 20133 Milano, Italy
(Received 31 December 2013; published 26 March 2014)

A new kind of nonresonant optical recirculator, dedicated to the production of γ rays by means of Compton backscattering, is described. This novel instrument, inspired by optical multipass systems, has its design focused on high flux and very small spectral bandwidth of the γ-ray beam. It has been developed to fulfill the project specifications of the European Extreme Light Infrastructure "Nuclear Pillar," i.e., the Gamma Beam System. Our system allows a single high power laser pulse to recirculate 32 times synchronized on the radio frequency driving accelerating cavities for the electron beam. Namely, the polarization of the laser beam and crossing angle between laser and electrons are preserved all along the 32 passes. Moreover, optical aberrations are kept at a negligible level. The general tools developed for designing, optimizing, and aligning the system are described. A detailed simulation demonstrates the high efficiency of the device.

INFN

Low emittance pion beams generation from bright photons and relativistic protons

L. Serafini, C. Curatolo and V. Petrillo
INFN-Milan and Università degli Studi di Milano, via Celoria 16, 20133 Milano, Italy
(Dated: July 11th, 2015)

Present availability of high brilliance photon beams as those produced by X-ray Free Electron Lasers in combination with intense TeV proton beams typical of the Large Hadron Collider makes it possible to conceive the generation of pion beams via photo-production in a highly relativistic Lorentz boosted frame: the main advantage is the low emittance attainable and a TeV-class energy for the generated pions, that may be an interesting option for the production of low emittance muon and neutrino beams. We will describe the kinematics of the two classes of dominant events, i.e. the pion photo-production and the electron/positron pair production, neglecting other small cross-section possible events like Compton and muon pair production. Based on the phase space distributions of the pion and muon beams we will analyze the pion beam brightness achievable in three examples, based on advanced high efficiency high repetition rate FELs coupled to LHC or Future Circular Collider (FCC) proton beams, together with the study of a possible small scale demonstrator based on a Compton Source coupled to a Super Proton Synchrotron (SPS) proton beam.

[physics.acc-ph] 7 Aug 2015

I. INTRODUCTION

One of the main challenges of present muon collider design studies is the capture/cooling stage of muons after generation by intense GeV-class proton beams impinging on solid targets: this mechanism produces pions further decaying into muons and neutrinos. As extensively analyzed in Ref. [1, 2], the large emittance of the generated pion beams, which is mapped into the muon beam, is mainly given by the mm-size beam source at the target (i.e. the proton beam focal spot size) and by Coulomb scattering of protons and pions propagating through the target itself, inducing large transverse momenta which in

Their combined capability of producing ultra-high phase space density particle beams is the base of our strategy for generating low emittance pion, muon and neutrino beams, using collisions between two counter-propagating beams of highly relativistic protons and ultra-high intensity photons. The extremely high luminosity achievable by such a collider (10^{38} cm^{-2}s^{-1}) can compensate for the low efficiency of the pion photo-production which has a total cross section of $\simeq 220$ μbarn with 300 MeV photons, much smaller than GeV-proton based pion production ($\simeq 20$ mbarn).

There are two crucial aspects in such a collision scheme. The first is the much higher energy of the X-ray

Download PDF | Export | Search ScienceDirect | Advanced search

Article outline Show full outline

Figures and tables

Table 1

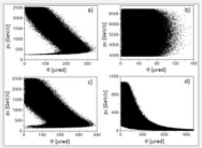

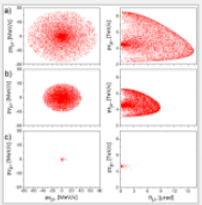

ELSEVIER

Nuclear Instruments and Methods in Physics Research Section A: Accelerators, Spectrometers, Detectors and Associated Equipment

Available online 2 September 2016

In Press, Accepted Manuscript — Note to users

Phase space analysis of secondary beams generated in hadron-photon collisions

C. Curatolo, F. Broggi, L. Serafini

Show more

http://dx.doi.org/10.1016/j.nima.2016.09.002

Abstract

Present availability of high brilliance photon beams in combination with intense TeV hadron beams makes it possible to conceive the generation of low emittance TeV-class energy pion/muon beams via photoproduction in a highly relativistic Lorentz boosted frame. We analyze the secondary beams brightness achievable by the coupling of

High Recoil of 12 keV photons scattering off 7 GeV electrons

$$\Sigma_{TH} = 670 \ mbarn \ 0-recoil$$

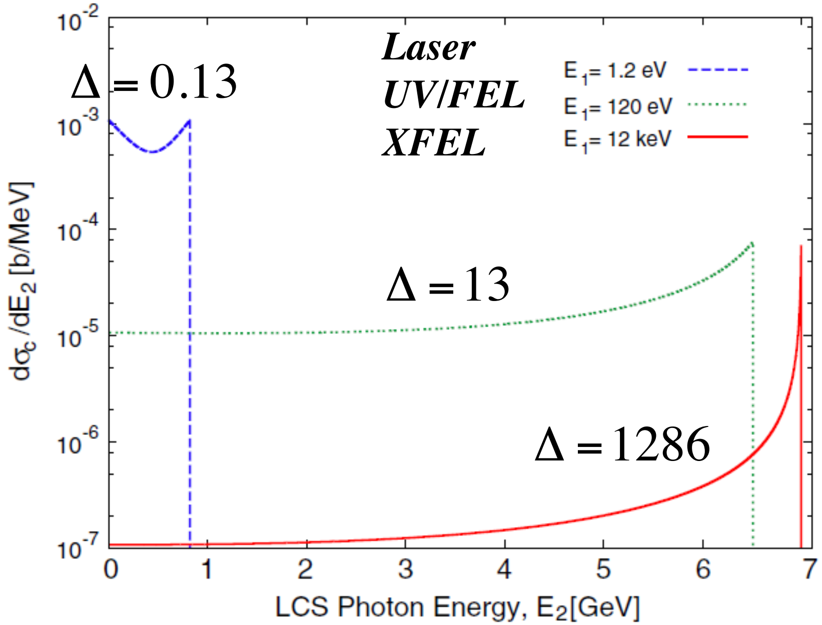

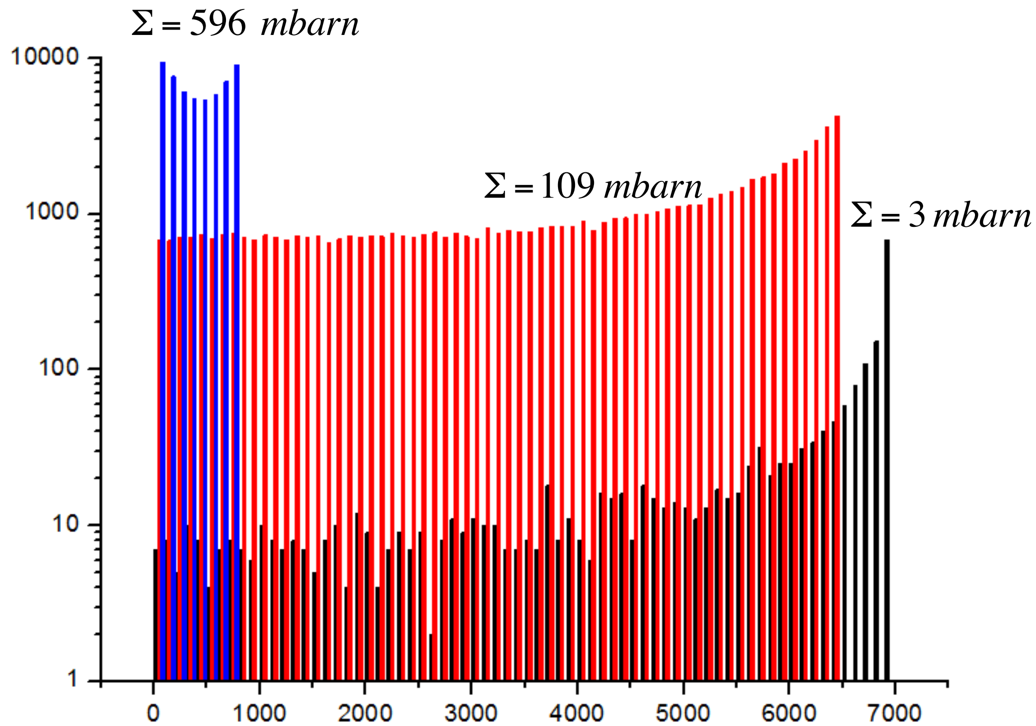

- Compare stationary and moving oscillators →
- Angle-dependent Doppler shift
- Compare non-relativistic, stationary oscillator and moving relativistic oscillator
- “Projector” effect: relativistic charged particle radiates in a narrow forward cone
- $\gamma=E/E_0$, relative particle energy = ratio of full energy to the rest energy (0.511 MeV for electrons)

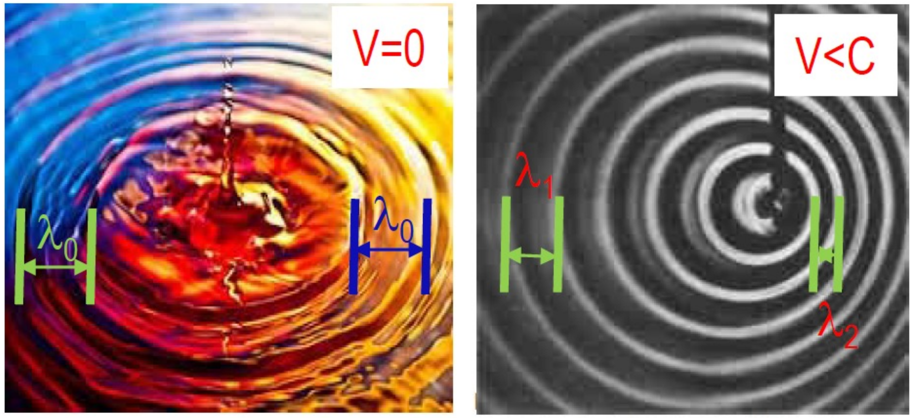

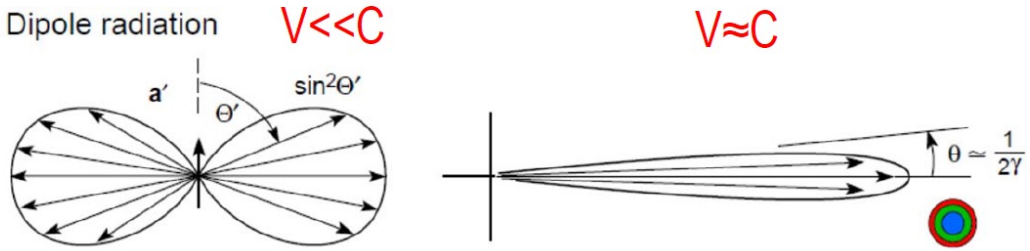

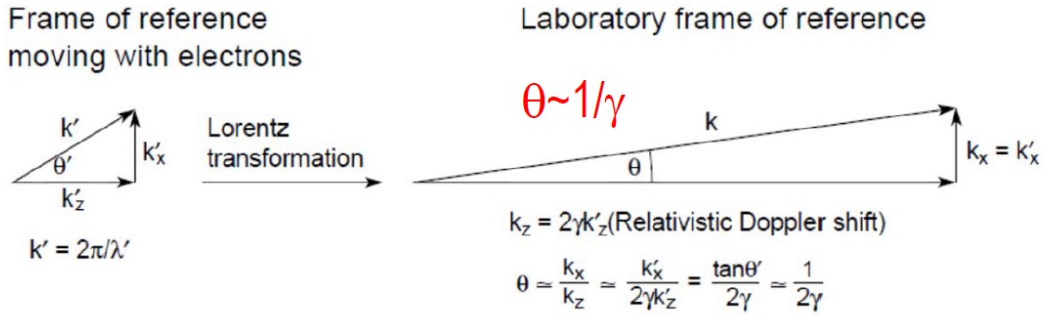

Radiation is emitted into a narrow cone

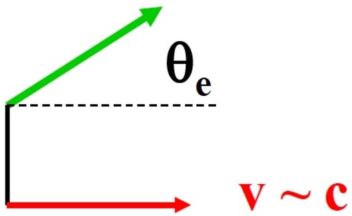

$$\theta = \frac{1}{\gamma} \cdot \theta_e$$

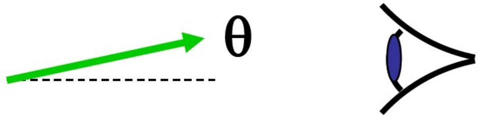

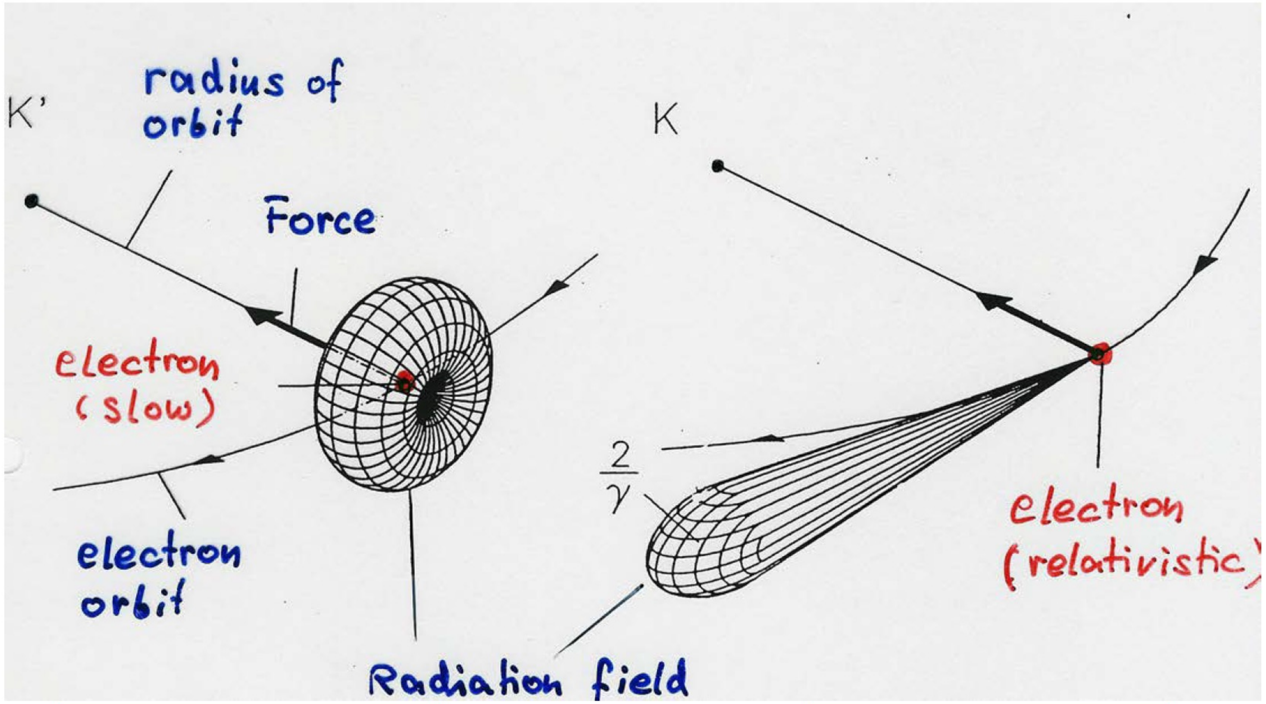

v << c

v ≈ c

courtesy of L. Rivkin - PSI

Critical energy

The energy at which the SR is higher is the critical energy, which is obtained from the critical frequency

$$\varepsilon_c = \hbar\omega_c = C_c \frac{E^3}{\rho} \qquad C_c = \frac{3\hbar c}{2(mc^2)^3}$$

For electrons we can write

$$\varepsilon_c(keV) = 2.2183 \frac{E^3(GeV^3)}{\rho(m)} = 0.66503 E^2(GeV^2) B(T)$$

The higher the bending field the higher the SR photon critical energy

The SR spectrum in a circular accelerator is made up of harmonics of the particle revolution frequency up and beyond the critical frequency, not much separated and with beamline spread, so that the spectrum appears continuous.

Synchrotron radiation emission as a function of beam energy

Dependence of the frequency distribution of the energy radiated via synchrotron emission on the electron beam energy (same ρ)

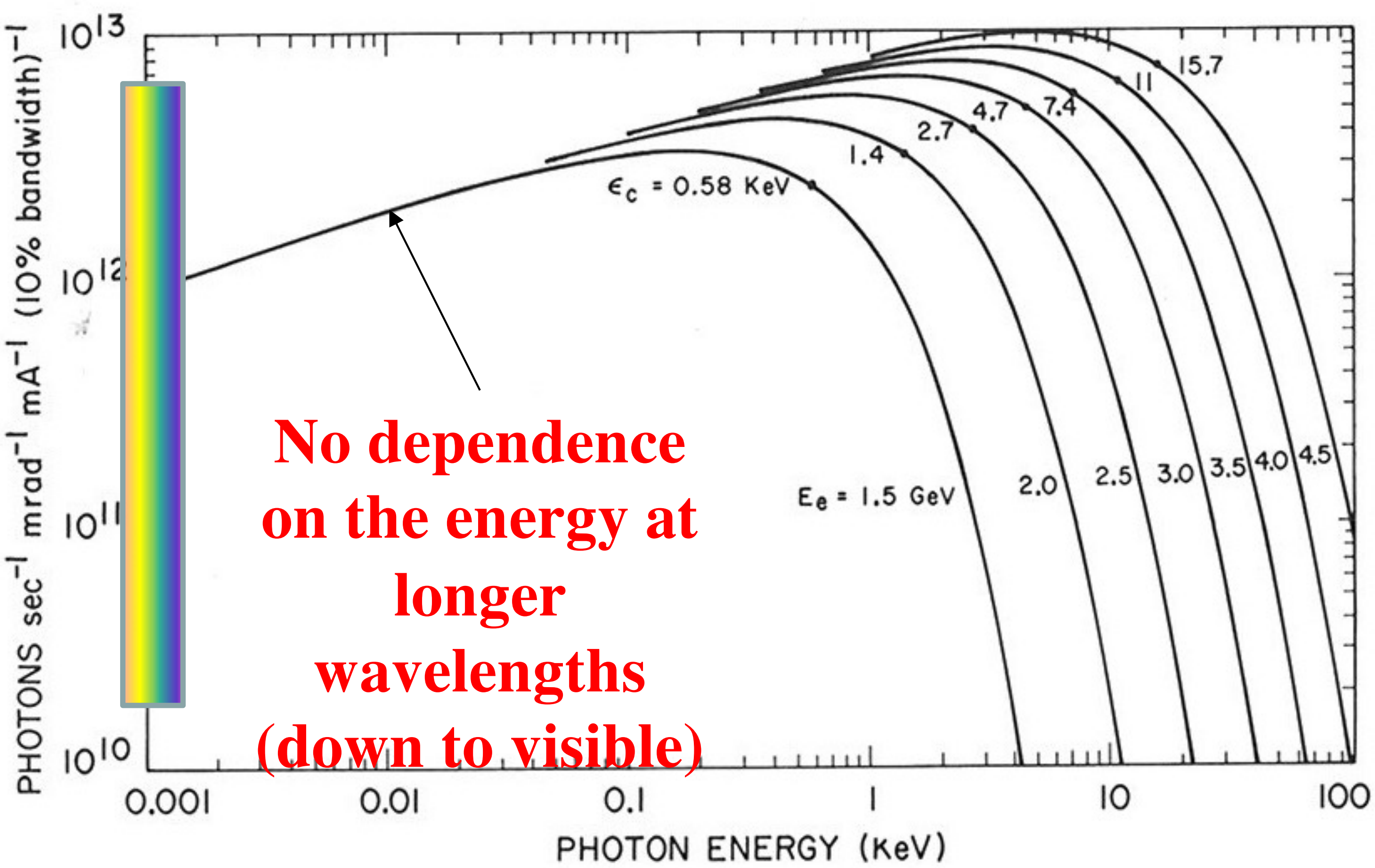

FEL resonance condition

$$\lambda_R = \lambda_w \frac{\left(1 + a_w{}^2\right)}{2\gamma^2}$$

(magnetostatic undulator)

Example : for λ_R=*1A*, λ_w=*2cm, E=7 GeV*

$$a_w = 0.93\lambda_w[cm]B_w[T]$$

Violation of Energy-Momentum Conservation !!

$$\lambda_R = \lambda \frac{\left(1 + a_0^2/2\right)}{4\gamma^2}$$

(electromagnetic undulator)

Example : for λ_R=*1A, h*ν*=12 keV,* λ*=0.8*μ*m, E=25MeV*

Example : for *h*ν*=10 MeV,* λ*=0.4*μ*m, E=530 MeV*

L. Serafini et al., Proceedings of the SPIE, Volume 6634, article id. 66341G (2007)

$$a_0 \propto \frac{\lambda[\mu m]\sqrt{P[TW]}}{R_0[\mu m]}$$

laser power

laser spot size